ABSTRACT

Title of Document: FUNDAMENTALS OF EXCESS ELECTRON TRANSPORT IN BIOLOGICALLY RELEVANT SYSTEMS

Amethist Shajary Finch
Doctor of Philosophy, 2008

Directed By: Professor Steven E. Rokita
Department of Chemistry and Biochemistry

Thymine dimers are premutagenic lesions that form via ultraviolet irradiation of DNA. While the distribution of thymine dimers is non-random, it is also not yet predictable. Thymine dimer accumulation is likely to be controlled by both its formation and reversion. Formation of thymine dimers occurs via direct excitation of thymine residues, while the reversion is governed by both direct and indirect photochemical processes. The Rokita lab previously determined that charge transport from surrounding DNA sequences affect the accumulation of UV-induced thymine dimers in DNA.

This dissertation focuses on the variable efficiency of both direct and indirect pathways affecting thymine dimer distribution. Thymine dimer accumulation is dependent upon sequence and conformation. The conformational dependence was used to study the kinetic versus thermodynamic control of thymine dimer accumulation in natural systems. In this system, no difference was observed in the accumulation of thymine dimer in free vs. constrained DNA. Therefore, the anticipated studies on the

reversibility of thymine dimer formation still await a suitable system that does respond to DNA conformation.

A model system was also used to concurrently investigate the effect of local sequence on thymine dimer accumulation. Excess electron transport in DNA is also important in modulating the overall accumulation of thymine dimers. The parameters affecting excess electron transport were investigated with a model system based on electron transfer from an aromatic amine to bromouridine. Electrons injected into duplex DNA by the aromatic amine migrate through the stacked nucleotides to the bromouridine acceptor covalently attached to the DNA. Modifications of the intervening nucleotide sequence previously allowed for the study of distance dependence, sequence dependence, and directionality of excess electron transfer reactions.

This system was used here to determine if a polaron type mechanism was operative in excess electron transport in analogy to such observations in hole transfer. At least for the systems examined in this work, a polaron type mechanism does not appear operative for excess electron transfer. In order to determine if excess electron transport efficiency is dependent on the reduction potential of the aromatic amine, the redox potentials of a variety aromatic amine were determined. These aromatic amines differed by the addition of electron donating groups and π conjugation. Preliminary studies in this final model system with an aromatic amine of strong reduction potential showed no difference in excess electron transport when compared to the aromatic amine with a weaker reduction potential.

FUNDAMENTALS OF EXCESS ELECTRON TRANSPORT IN BIOLOGICALLY RELEVANT SYSTEMS

By

Amethist Shajary Finch

Dissertation submitted to the Faculty of the Graduate School of the
University of Maryland, College Park, in partial fulfillment
of the requirements for the degree of
Doctor of Philosophy
2008

Advisory Committee:
Professor Steven E. Rokita, Chair
Assistant Professor T. Ashton Cropp
Professor Daniel E. Falvey
Associate Professor Douglas A. Julin
Associate Professor David C. Straney

Dedication

For Michael and Parker Finch

Acknowledgements

I would first like to thank Professor Rokita for everything he has done for me while I have been at the University of Maryland. This dissertation would not have been possible without his all of his suggestions and his guidance over the years. Most importantly I would like to thank him for his patience, his positive outlook, and his kindness. He is by far the best mentor that any graduate student could ask for. Additionally, I would like to extend a special thanks to Miss Liliana Rokita, who joined the Rokita lab at the same time as I did. I believe that her presence has played a great role in granting patience and understanding to Professor Rokita.

Thank you to my committee, Professors Falvey, Julin, Cropp and Straney. I appreciate your thoughts and comments and more importantly I appreciate the scientific guidance that you have given me over the years. A special thanks to Dr. Cropp for stepping in at the last minute, your generosity is greatly appreciated.

I owe special thanks to the Laboratory of Dr. William Davis, and more importantly to his former graduate student Dr. Chad C. Bjorklund who provided me with the Widom 601 modified DNA and reconstituted nucleosomes. The final experiments would not have been possible without their generosity and for their help I am forever grateful.

I am deeply indebted to Dr. James Sumner and the Army Research Labs in Adelphi, MD. First, thank you to Dr. Sumner for his advice and

expertise with the electrochemistry apparatus and experiments and more importantly for being a wonderful DOD mentor. Second, thank you to all the scientists at the Army Research labs for the useful discussions and more importantly for allowing me to drink as much coffee as needed (with a new baby in the house this was no small matter).

Also, I would not have had the opportunity to become an expert electrode polisher without the funding from the Department of Defense SMART fellowship. While the funding was a bonus, I am most thankful for the research opportunities and collaborations the fellowship made possible. A special thanks to Dr. Nicholas Fell for giving me the opportunity to do more research after I graduate!

I would be remiss if I did not thank all the staff of the department of chemistry. Thank you to all that have helped me solve any paperwork problems that I may have had over the years, there were many, so many thanks are in order! Thank you to Taryn Faulkner for all the conversations, help and advice that you have given me, you are truly a wonderful person.

Thank you to all the other research labs in Wing 5, the members of the Kahn, Julin, and Cropp Labs especially. Special thanks to the Julin lab for use of their phosphorimaging plates, seven day exposure times would not have been possible without your generosity. Thanks to Kahn lab for use of their FPLC, gel pourer, speedvac and space in the -80 °C.

Thanks to all the members of the Rokita Lab past and present. Thanks to Dr. Takeo Ito for helping me when I started in the lab and for answering all

my e-mail questions even after he was gone. Thank you to all the postdocs that have been in the lab, I have learned something from each and every one of you. I wish all the graduate and undergraduate students much love and success in whatever their future endeavors are.

Jim Watson, thank you for all the things you have taught me and for constantly making me laugh, the lab was not the same after you graduated.

Emily Weinert, you are a good friend and will always be welcome wherever I am.

Neil Campbell, thank you for all of the synthesis and help with everything that I ever asked, no matter what anyone says I don't think you are a grumpy old man! For everything you have done, I owe you and Susannah many many dinners!

Patrick McTamney, thanks for the reading and corrections, I don't just owe you a beer, I owe you a case!

Jen Adler, I have truly enjoyed the time we have shared in the Rokita lab! Thank you for the help and I wish you the best in science and life!

Wendy Heiserman, thank you for teaching me that it is possible for me to run more than a mile and for encouraging me to do more than I ever thought possible. You are a great friend, Baltimore 2008 here we come!

To my friends, Tammy, Kevin and their beautiful baby girl Caitlin, thank you for being such wonderful friends and for always inquiring about the state of my dissertation. We miss you guys, MOVE BACK!!!!

Finally, my family: Thank you to my parents for being the best role models that anyone could ask for and for making sure that I had all the opportunities in life made available to me. I appreciate everything that you do for me more than you could ever possibly know. Thank you to my brother for always keeping me grounded and reminding me not to take myself so seriously.

Most importantly I am thankful to my husband Mike and my son Parker. Mike has been patient with me over the years and has put up with my neurosis over all the hurdles and frustrations that are associated with research and pursuing a higher education. Mike has willingly made sacrifices so I could achieve my goals and for that I cannot thank him enough. Thank you for always making me laugh, I would not have been able to keep a smile on my face without you. Also, thank you to my son Parker for teaching me patience and for showing me what unconditional love really is.

This dissertation would not exist without the love and support of my friends and family. Thank you!

Table of Contents

List of Abbreviations

1,1DMDN	N1,N1-dimethyldiaminonapthalene
1,5DMDN	N1,N5-dimethyldiaminonapthalene
1AN	1-aminoanthracene
2AN	2-aminoanthracene
5S DNA	154 base pair NPS from *Xenopus borealis* 5s RNA sequence
A	adenine
AA	aromatic amine
AP	apurinic
APS	ammonium persulfate
ATP	adenosine triphosphate
BCA	bicinchoninic acid protein assay
^{Br}U	5-bromo-2′-deoxyuridine
BER	base excision repair
C	cytosine
CPD	cyclopyrimidine dimer
CT	charge transfer
C^T	cytosine thymine dimer
DAN	1,5-diaminonapthalene
DNA	deoxyribonucleic acid
dNTP	deoxyribonucleotides: dATP, dCTP, dGTP and dTTP
dpDAN	N-(4-Aminooxybutyl)-1-5-diaminonaphthalene

dpTMDN	N-(4-Aminooxybutyl)-N,N′,N′-trimethyl-1-5-diaminonaphthalene
DPM	disintegrations per minute
EDTA	ethylenediaminetetraacetic acid
EET	excess electron transport
EndoIV	T4 endonuclease IV
EndoV	T4 endonuclease V
ESI MS	electrospray mass spectrometry
FADH	flavin adenine dinucleotide
FPLC	fast protein liquid chromatography
G	guanine
HOMO	highest occupied molecular orbital
HPLC	high performance liquid chromatography
HT	hole transport
KPi	potassium phosphate buffer, pH 7
LUMO	lowest unoccupied molecular orbital
MALDI-MS	matrix assisted laser desorption/ionization mass spectrometry
MWCO	molecular weight cut off
MMDN	monomethyldiaminonapthalene
MN	micrococcal nuclease
NaPi	sodium phosphate buffer, pH 7
NCP	nucleosome core particle
NER	nucleotide excision repair

NMR	nuclear magnetic resonance
NPS	nucleosome positioning sequence
PAGE	polyacrylamine gel electrophoresis
PCNA	proliferating cell nuclear antigen
PCR	polymerase chain reaction
pGEM	plasmid GEM
prDAN	N-(4'-bromobutyloxy)-5-norbornene-2,3-dicarboximide-1-5-diaminonapthalene
prTMDN	N-(4'-bromobutyloxy)-5-norbornene-2,3-dicarboximide-N,N',N'-trimethyl-1-5-diaminonapthalene
pXP	plasmid XP
PMSF	phenylmethanesulphonylfluoride
RCF	relative centrifugal force
RFC	replication factor C
RPM	revolutions per minute
SBX	sucrose bromophenol blue xylene cyanol
SDS	sodium dodecyl sulfate
T	thymine
T^C	thymine cytosine dimer
T^T	thymine thymine dimer
T4 Pol	T4 DNA polymerase
TBE	tris, boric acid, EDTA pH 8.0 buffer
TEMED	N,N,N',N'-tetramethylethylenediamine
TLC	thin layer chromatography

TMDN	N1,N1,N6,N6-tetramethyldiaminonapthalene
TriMDN	trimethyldiaminonapthalene
UV	ultraviolet
UVrA	ultraviolet radiation A (320 – 400 nm)
UVrB	ultraviolet radiation B (280 – 320 nm)
UVrC	ultraviolet radiation C (190 – 280 nm)
W601	Widom 601NPS
XP	Xeroderma Pigmentosum

List of Tables

Chapter 1

None

Chapter 2

Chapter 3

Chapter 4

None

Appendix I

None

Appendix II

None

List of Figures

Chapter 1

Chapter 2

Chapter 3

Appendix I

Appendix II

List of Equations

Chapter 1

None

Chapter 2

Chapter 3

Chapter 4

None

Appendix I

None

Appendix II

None

Chapter 1

Background and Significance

1.1 Introduction to Photodamage caused by UV light

The primary source of energy for life on earth is the sun. In photosynthesis, light energy is converted to chemical energy which is stored as adenosine triphosphate (ATP), and subsequently stored in chemical bonds of carbohydrates like sugars and starch.[1] These chemicals in turn provide food for herbivores and subsequently carnivores. While the sun has the capacity to give life, it has many properties which can damage life, one being ultraviolet light.

In 1877, Downes and Blunt reported to the Royal Society of London that sunlight killed bacteria.[2] This affect was chiefly associated with the short wavelength (Ultraviolet, UV) component of radiation. Subsequently in 1928, Frederick Gates noticed that wavelengths of light most effective at killing bacteria were also the ones that were best absorbed by nucleic acids.[3] Since then scientists have been studying the effect of UV light on DNA and the photoproducts formed by UV absorption.

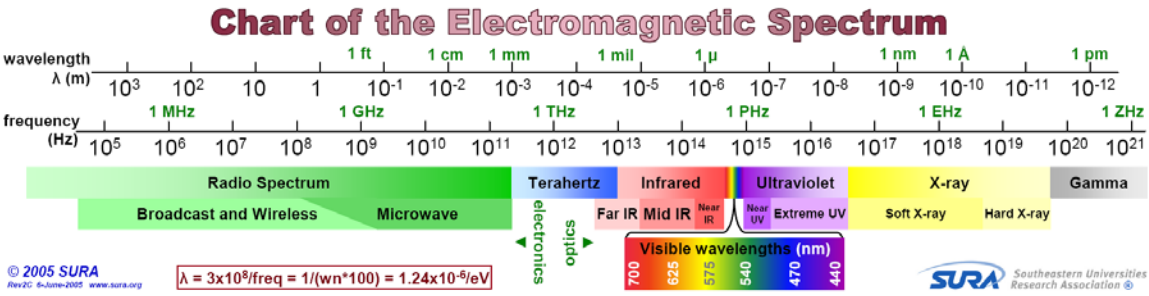

Figure 1.1: Electromagnetic spectrum: UV portion of spectrum ranges from 190 - 400 nm.[4]

The UV region of the electromagnetic spectrum (Figure 1.1)[4] can be broken down into three different ranges uvA (320-400 nm), uvB (280-320

nm), and uvC (190-280 nm).[5,6] The longer wavelengths of uvA light (greater than 320 nm) seem to be ineffective at cellular damage. Thus, the majority of DNA damage results from a narrow region in the UV spectrum which corresponds to uvB radiation. Wavelengths in the 290 nm region are 1000-10,000 times more effective at thymine dimer (T^T) production, single and double strand breaks in DNA, DNA mutation, cell death, production of skin erythema, and skin cancer than the other wavelengths of UV light.[7,8] DNA also absorbs in the region corresponding to uvC radiation, however uvC is completely filtered out by the ozone layer so there are negligible amounts of damage from this area of the UV spectrum.[9]

The ozone layer of the atmosphere is one of the major reasons there are not more occurrences of skin cancer. Ozone has an absorption spectrum almost identical to DNA and acts to filter the harmful rays.[5,10] Since the ozone layer is slowly being depleted,[11] understanding the formation and repair of mutagenic photoproducts has become critical. Calculations predict that with every 1 % decrease in the level of ozone, there will be a 4 % increase in the rate of skin cancer.[12-14] More specifically, with the current amount of ozone one hour of sun exposure causes seven cyclopyrimidine dimers (CPD, the most common photolesion) per cell per hour of exposure. Studies have shown that if the ozone decreases by as much as 50 %, the same amount of CPD would be produced in 10 minutes and in the complete absence of ozone the time would be reduced to only 10 seconds.[15-17]

1.2 The Chemistry and Biochemistry of Cyclobutane Pyrimidine Dimers

Just as sunlight is necessary for life, DNA is also necessary for life since it is the carrier of genetic material. Therefore, in order to understand the ways that UV radiation affects CPD formation in DNA, it is first necessary to understand the structure and conformation of DNA and the nucleotides involved in photoproduct formation. Figure 1.2 illustrates the four naturally occurring bases found in DNA, two purines adenine (**A**) and guanine (**G**), and two pyrimidines thymine (**T**) and cytosine (**C**). Under physiological conditions these bases form Watson-Crick base pairs with **A** forming two hydrogen bonds with **T** and **G** forming three hydrogen bonds with **C** (Figure 1.3).[18]

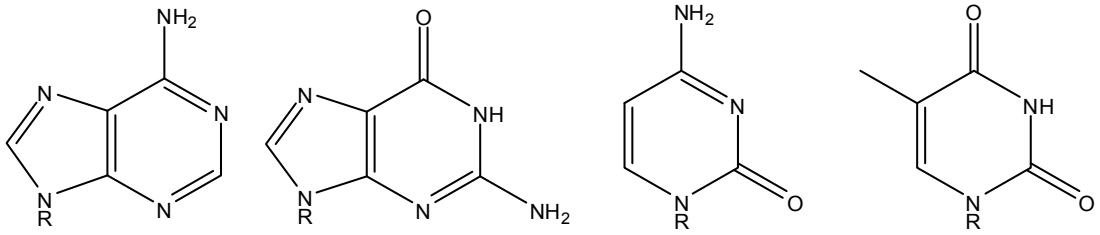

Adenine (**A**) Guanine (**G**) Cytosine (**C**) Thymine (**T**)

Figure 1.2: The naturally occurring DNA bases. R = sugar and phosphate group joined by ester bonds in DNA.

While purines are relatively stable to UV light, pyrimidines are unstable to UV light.[19] Upon exposure of DNA to UV light adjacent pyrimidines form four possible CPD's (C^C, C^T, T^C and T^T). Specifically T^T appears to be the major photoleasion that leads to mutations which can ultimately lead to cancer.[20-22]

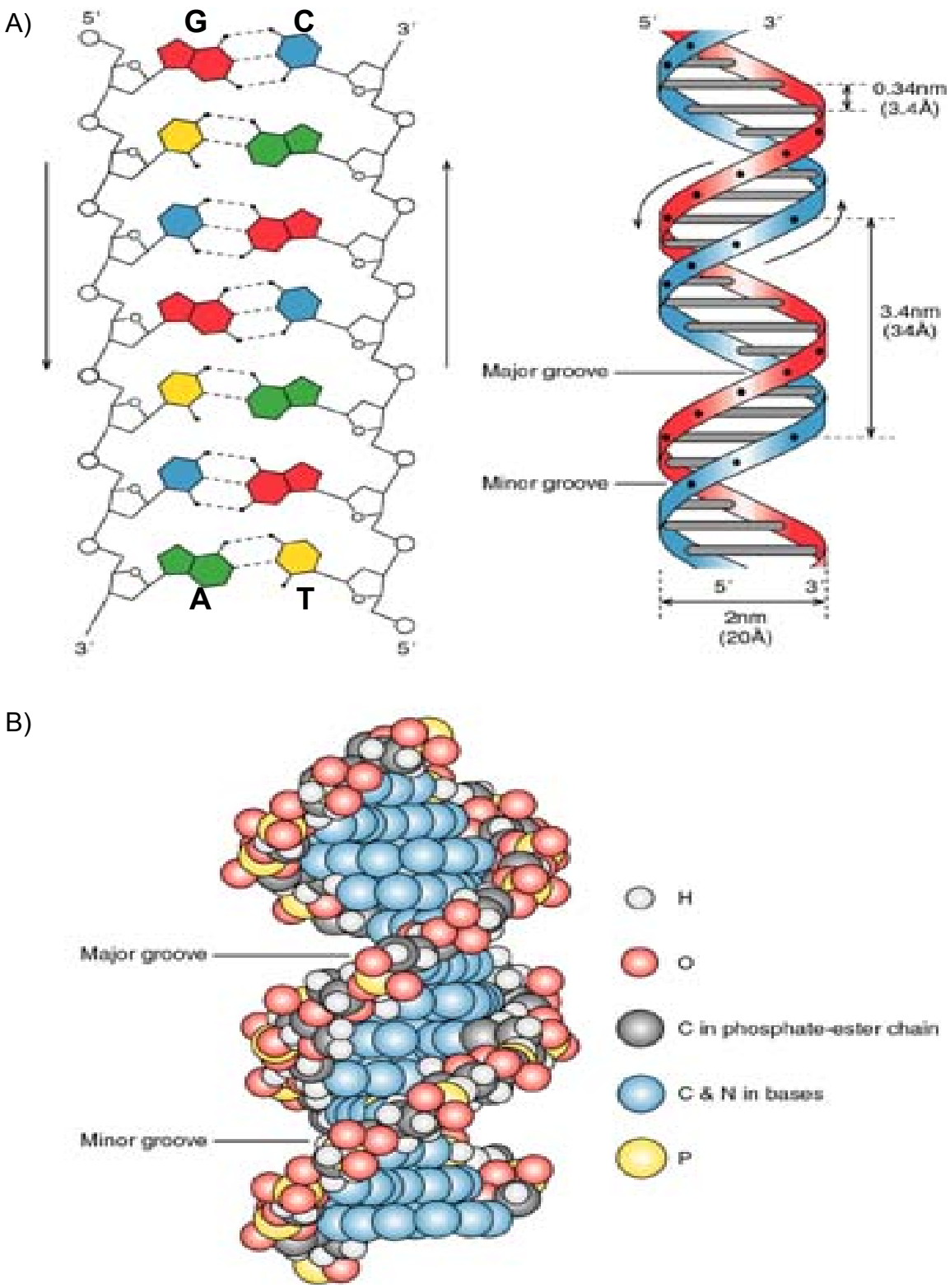

Figure 1.3: A) Watson Crick base pairing, B) Double helical form of DNA (taken from reference 23).[23]

Types of Dimers

The first report of CPD formation was published in 1961 by S.Y. Wang.[24] Wang noted that the proximity of the bases in DNA (Figure 1.3) might allow interaction between two adjacent **T** residues on the same chain to form T^T. Once formed, T^T formation does not allow for hydrogen bonding and the double helix (Figure 1.3) form of DNA is destabilized when hydrogen bonding is disrupted.[18,23] This disruption and destabilization allows the double stranded DNA (dsDNA) to unwind. Although the linkage of two **T**'s to form a cyclobutane ring can form four possible stereoisomers, only the cis-syn T^T is formed in dsDNA.[19] In addition to T^T two other isomers are formed by direct irradiation of adjacent **T**'s. The 6-4 and Dewar T^T are minor photoproducts and form < 10 % of total CPD (Figure1.4).[19] While T^T are premutagenic lesions, nature has a variety of processes dedicated to detecting and repairing damage in DNA.

Thymine Dimer Repair

In 1964 a paper on the first formal demonstration of excision repair of T^T was published.[25] Since then numerous papers have been published on the repair of T^T in both prokaryotes and eukaryotes.[26,27] These mechanisms allow removal of the damaged DNA bases, and use the undamaged strand as a template.[28] T^T formation blocks replication because most polymerases are not able to bypass the DNA damage, therefore the T^T must be repaired for replication to continue.[20,28-30] The importance of these repair systems is

highlighted by hereditary diseases such as Xeroderma Pigmentosum (XP) and Cockayne Syndrome in which the repair systems are compromised and lead to a reduction or elimination of DNA repair processes.[31-33] The deficiency in the repair systems of individuals with these diseases makes them susceptible to the DNA damage caused by UV light and many die at an early age from malignant skin tumors.[10,18,32-35]

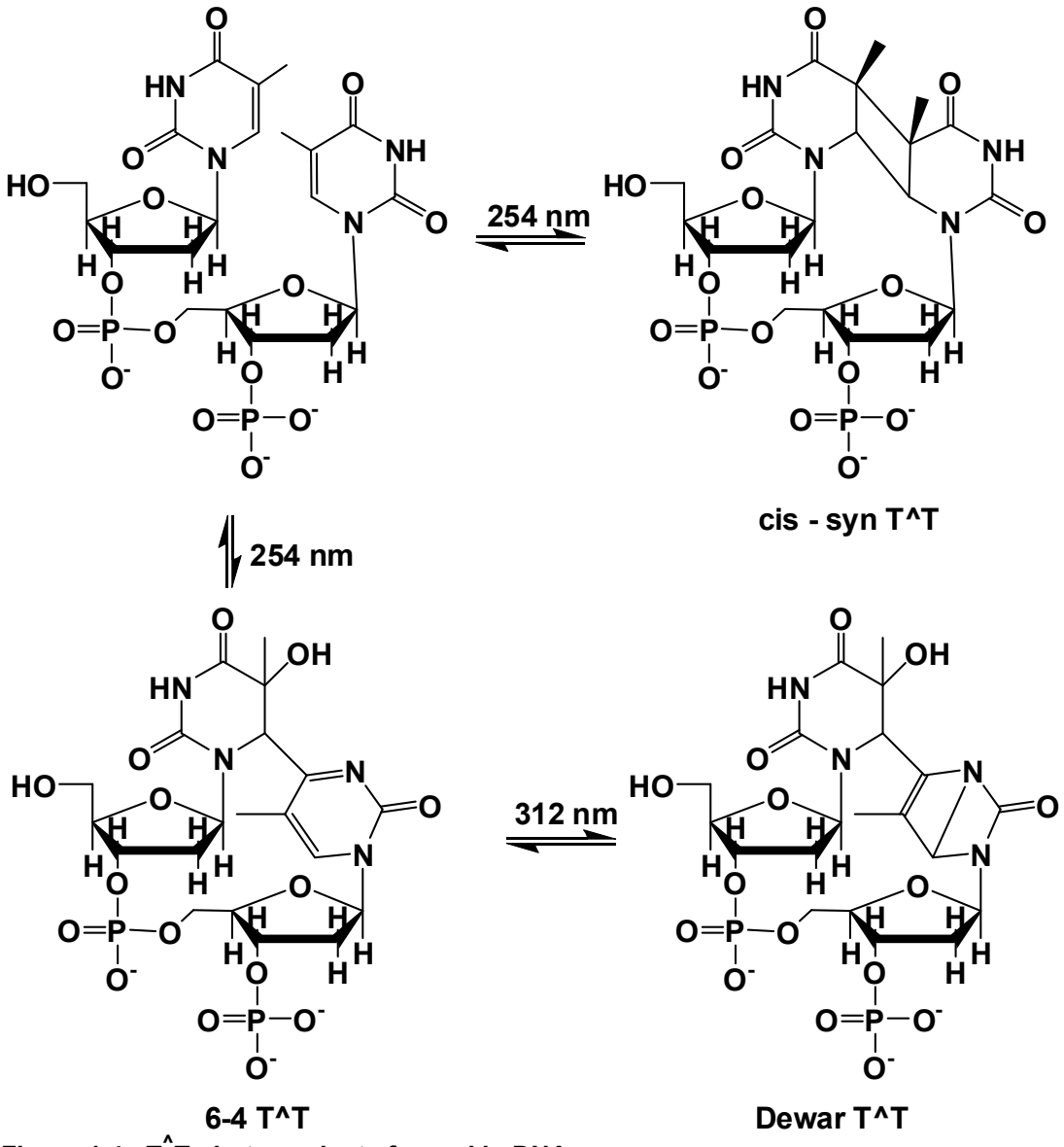

Figure 1.4: T^T photoproducts formed in DNA.

The inability of many DNA polymerases to replicate past T^T requires cells to have a method to either bypass or repair the sites of DNA damage. Prokaryotes have two polymerases (Pol Eta & Pol Zeta) that act as lesion bypass polymerases.[36] These polymerases allow for replication to continue by bypassing and not repairing the damaged bases. Pol eta allows for error free replication because it is able to replicate opposite T^T and inserts **A**'s. Pol zeta, however, is also able to replicate opposite T^T, but it is mutagenic and does not always place an **A** opposite **T**.[37] These processes allow the cell to continue replication, but can be mutagenic. This type of repair is especially important in cells that undergo rapid cell division (i.e. skin cells) and are susceptible to T^T formation from UV light.

In addition to the lesion bypass polymerases, another repair enzyme is T4 endonuclease V (EndoV) which is a 16 kd protein that specifically recognizes cis-syn T^T caused by UV irradiation. EndoV is part of the base excision repair pathway (BER).[29,38] As its name implies, the initial step in the BER pathway involves the removal of a damaged DNA base (Figure 1.5). Endo V has both DNA glycosylase and apurinic (AP) lyase activity. EndoV first cleaves the glycosyl bond of the 5' end of the T^T and then the endonuclease cleaves the phosphodiester bond at the resulting apurinic site. This causes a break in the DNA backbone. The resulting gap is repaired by DNA polymerase and the nick is closed by DNA ligase. While this enzyme is useful for T^T repair; plants, insects, mammals and other eukaryotes rely on other repair mechanisms for the removal of DNA damage.

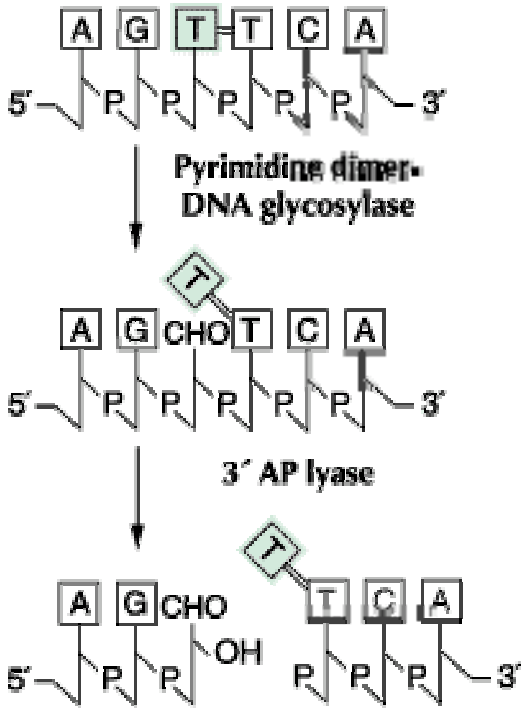

Figure 1.5: EndoV two step mechanism for removal of T^T (adapted from reference 20).

As mentioned previously, T^T formation slightly perturbs the double helical structure and disrupts base pairing in DNA. As a result, replication is blocked until the T^T is repaired. In addition to the pathways mentioned above, the major T^T repair pathway for both prokaryotes and eukaryotes is the nucleotide excision repair (NER) pathway (Figure 1.6). In prokaryotic cells the NER pathway consists of three enzymes named Uvr ABC. A cartoon diagram of the mechanism of this pathway is illustrated in Figure 1.6.

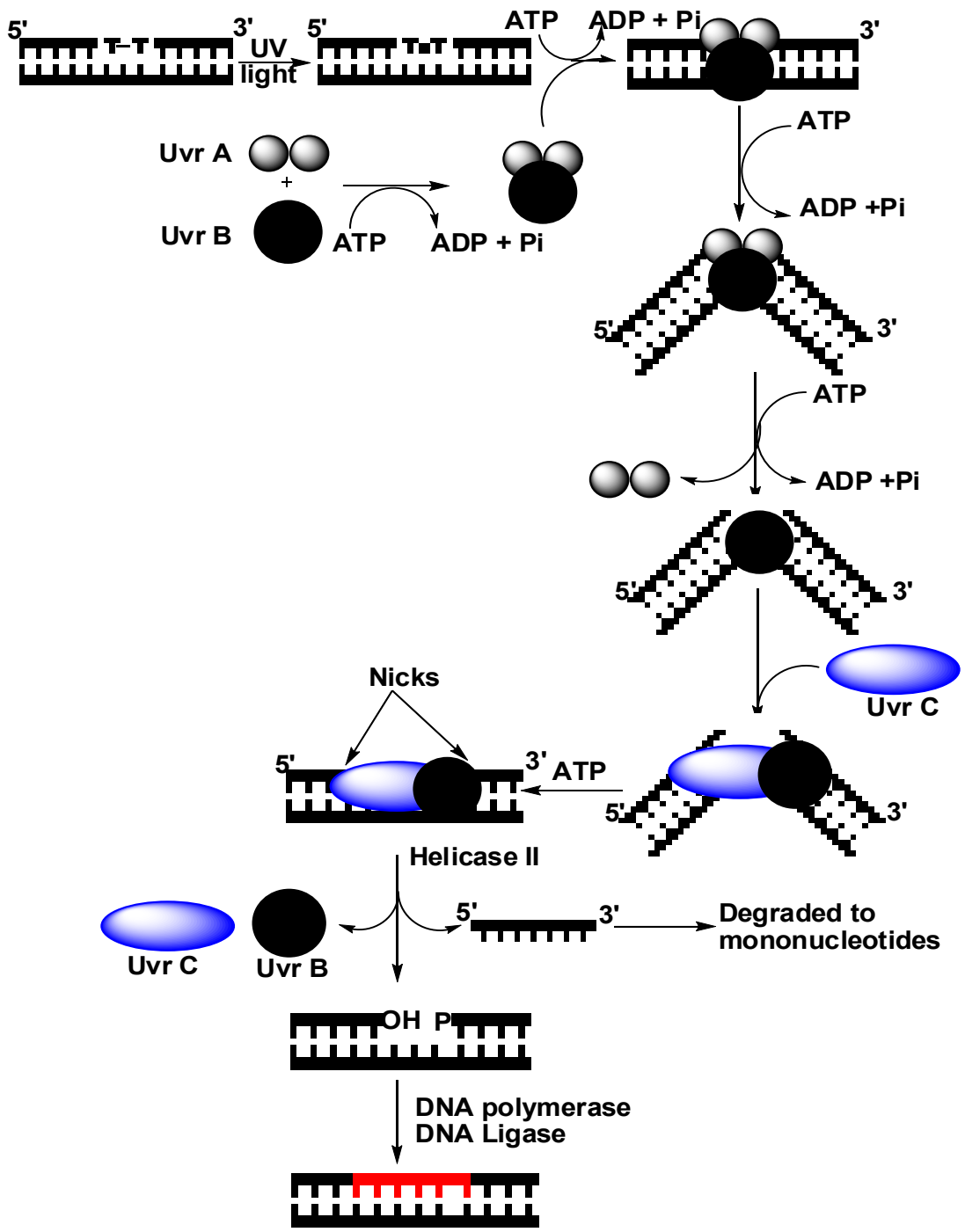

Figure 1.6: NER pathway for removal of damaged DNA site (adapted from reference 1).

Once a damaged site is found the Uvr AB complex binds and causes a conformational change in the DNA. The conformational change results in the

DNA helix denaturing and kinking by 130°. Uvr A dissociates and then uvr C endonuclease binds and cuts the damaged strand on both 5' and 3' ends, excising a piece of DNA that is 12-13 nucleotides in prokaryotes and 27-29 nucleotides in eukaryotes.[28] After this excision process the uvr BC complex dissociates and the excised piece of DNA is degraded into mononucleotides. DNA polymerase (DNA polymerase I in prokaryotes or DNA polymerase δ or ε and PCNA/RFC in eukaryotes) binds and fills the resulting gap using the undamaged strand as template. Finally the sugar-phosphate backbone is covalently closed by DNA ligase.[28,30,39,40] A similar, yet slightly more complex process exists for eukaryotes.

Perhaps one of the most interesting T^T repair pathways that exists in prokaryotic and eukaryotic cells is that conducted by photolyase.[41-43] DNA photolyase enzymes use blue or near-UV sunlight to drive cleavage of the CPD's cyclobutane ring (Figure 1.7). There are two classes of photolyases which differ in their chromophores. The chromophores are methenyltetrahydrofolate (antenna pigment) in the folate class of photolyases or 8-hydroxy-7,8-deazariboflavin in the deazaflavin class of photolyases.

Crystal structures of both classes of photolyases (most recently of the photolyase with a T^T analog) have been published.[44-47] The T^T bound crystal structure shows that the first step of T^T repair involves flipping the T^T away from the double helix and into the enzyme active site. Research has suggested that the second step involves an electron which is transferred from either directly from a reduced flavin ($FADH^-$) or by energy transfer from a

second chromaphore to the $FADH^{-}$.[48] The excited state FADH (FADH*) then transfers an electron to the T^T to induce splitting of the cyclobutane ring. Finally, the radical anion is then transferred back to the FADH completing the catalytic cycle. However the exact mechanism of electron transfer from FADH* to T^T has yet to be elucidated. The proximity of the **A** to the T^T in the crystal structure of T^T bound photolyase suggests that the electron migrates through the **A** to reach the T^T. Although this mechanism proceeds via electron injection from an enzyme, some research has shown that T^T reversal can also occur through donation of an electron through the DNA base stack from surrounding **G**'s.[49] Model systems that probe charge transfer (CT) through DNA can perhaps probe the mechanism of this reaction.[50-53]

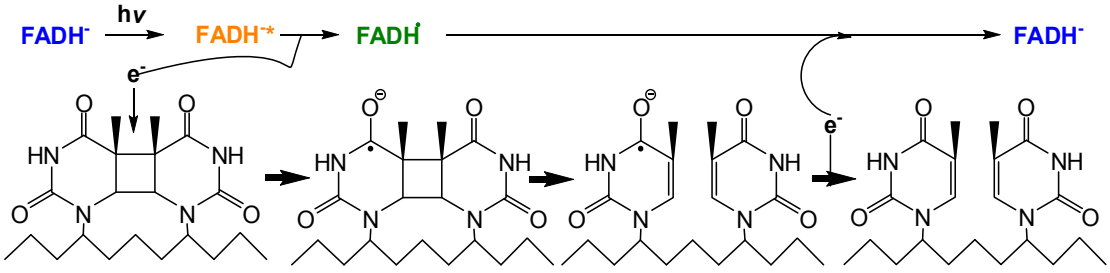

Figure 1.7: Photolyase pathway for repair employs electron transfer from flavin cofactor to reverse T^T formation.

Although these various repair systems exist, T^T and more generally CPD can still ultimately lead to mutations and skin cancer.[10,33,54,55] Studies have shown that CPD formation and repair varies with nucleotide sequence,[49,56-58] DNA conformation[59-62] and protein dependent bending of DNA.[63-66] For example, CPD are removed approximately 5 times more slowly than the 6-4 photoproducts, and there are conflicting theories on what causes the different rates.[54,59,67-72] One theory is that CPD causes only a small

distortion to the DNA double helix and is therefore more difficult to be detected by repair enzymes.[73] This difference in repair rates is one cause for the mutagenic properties of CPD. If the repair enzymes become saturated with 6-4 photoproducts, competitive inhibition of CPD repair occurs due to all available repair enzymes being bound.[74] In addition to the repair efficiency, replication by error prone polymerases allow for CPD bypass that lead to mutations that ultimately cause skin cancer. One example of a carcinogenic CPD induced mutation is in the p53 protein which acts as a tumor suppressor in healthy cells.[75] Once mutated, this protein becomes inactive and is unable to inhibit oncogenesis.[76] Many studies have been conducted that indicate CPD (specifically the most common form the cis-syn T^T) as the cause of DNA mutations leading to cancer development. In order to understand the repair efficiency and mechanism of T^T formation it is critical to look at the factors that affect the variability of T^T formation.

Variablility of T^T Formation.

Despite a variety of studies regarding T^T formation and repair in DNA, most do not address the reversibility of the cycloaddition reaction. T^T are reversible through either direct excitation or local charge transport from surrounding bases and the intrinsic levels of T^T accumulation are directly dependent on the rates of the forward and reverse reaction of T^T formation. These rates in turn are dependent on DNA sequence, conformation, and

directionality. Therefore in order to elucidate the possible mechanism it is necessary to understand all the factors that affect T^T accumulation.

T^T formation is catalyzed by the direct excitation of **T** monomer, but the reversion reaction by UV light is catalyzed by two possible mechanisms:

1.2 Direct excitation (Figure 1.8A)[77,78]

1.3 Indirect excitation (Figure 1.8B)[79-81]

a. CT from adjacent base

b. CT from photoexcited compound

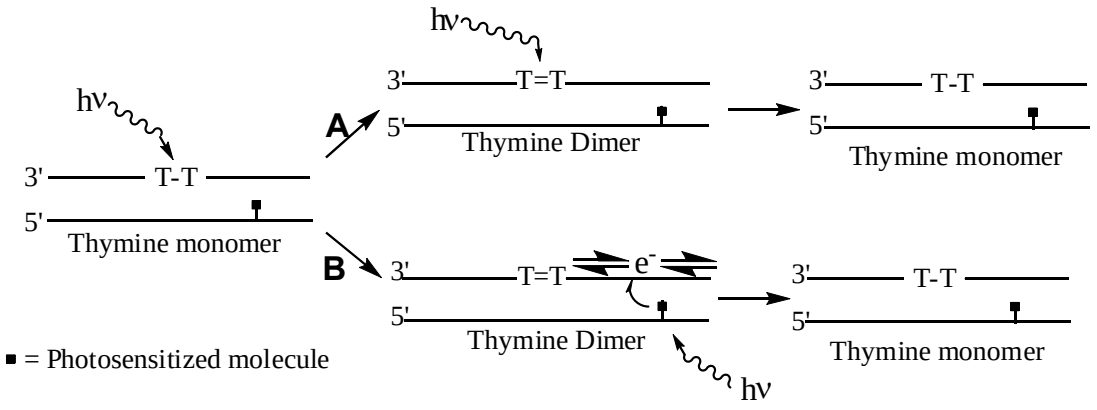

Figure 1.8: T^T formation occurs by direct excitation of adjacent T monomers, however reversal may occur via two pathways. A) Direct excitation of T^T or B) excitation of a either a DNA base or photosensitive compound and electron transfer to repair T^T.

In the direct excitation mechanism (Figure 1.8A) formation and reversion of the T^T cycloaddition can be controlled using different wavelengths of UV light. Thymine monomer has an absorbance maximum at 270 nm and the absorbance decreases upon T^T formation (Figure 1.9).[19] Formation of T^T does not reach 100 % with white light due to the photostationary state where the forward dimerization reaction is in

pseudoequilibrium with the reverse monomerization reaction.[19] Complete reversal of T^T formation is possible by irradiation at 240 nm. The monomerization reaction is driven by the steric repulsion between the methyl groups and the cyclobutane ring strain. While the determinants of T^T accumulation and variability are in part determined by the direct excitation mechanism, T^T reversal can also occur via an indirect electron transfer mechanism (Figure 1.8B). The indirect method of T^T reversal can occur by an antenna effect which is dependent on the surrounding DNA sequence or excess electron transport (EET), which is covered in the next section.

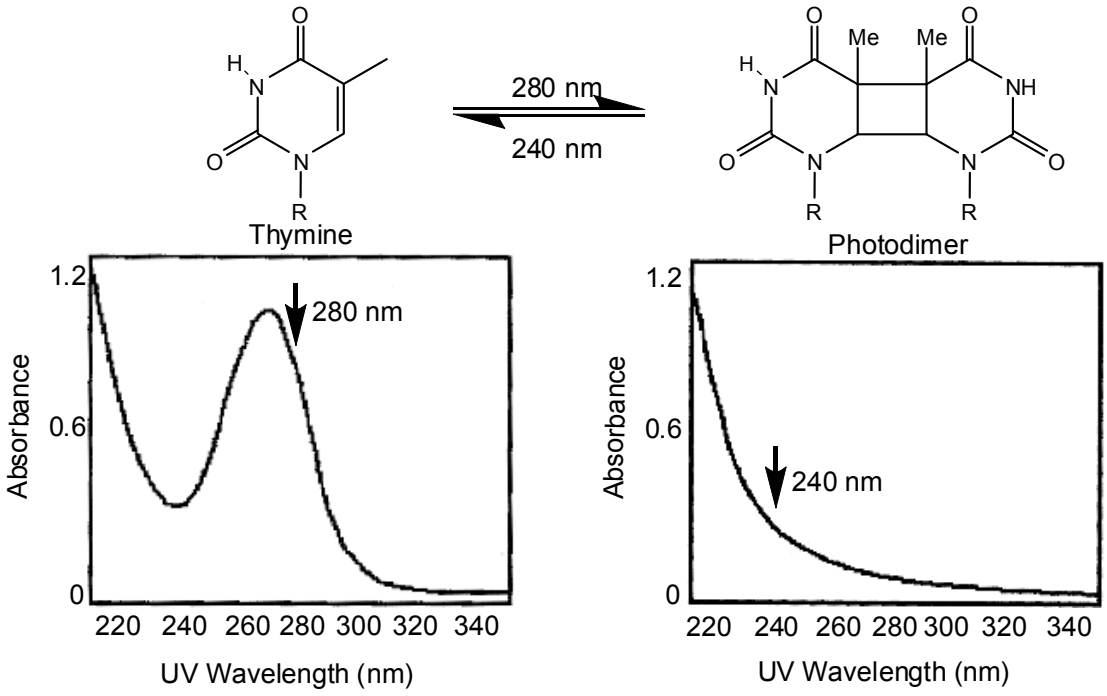

Figure 1.9: T^T formation can be modulated using different wavelengths of UV light (adapted from reference 19).

Understanding the effects of DNA sequence on formation and reversion of T^T may explain why T^T are the site of photoproduct formation but do not always lead to mutation. This suggests that the sequence on

either side of the photoproduct can alter the reaction rates.[54] Specifically, long tracts of **A**-**T** sequences are "hot spots" for cis-syn T^T formation.[82] The Rokita lab has previously shown that CPD formation may be promoted by local, directional electron transfer from a 5' guanosine embedded in duplex DNA.[83] For example, the total amounts of T^T formation in oligonucleotide sequence **GTTX**, where **X** represents any purine, was compared to oligonucleotide sequence **ATTX** and was found to have an average photostationary state of 3 % vs 10 % respectively. Data analysis suggests this difference is due to the rate of the reverse reaction and not the forward reaction. Specifically, CPD photostationary levels are determined primarily by the base 5' of T^T.[49] Although local sequence effects change the amount of total T^T formation, a detailed mechanism of CT in DNA is necessary to understand effects of reversibility on the overall T^T formation reaction.

Studying the sequences that facilitate CT in DNA may give mechanistic insight to the factors which affect T^T formation and repair mechanisms. In addition to T^T formation and reversion, understanding the mechanism of CT in DNA is important since it has been implicated in aging, several different cancers, and diseases such as arteriosclerosis. In order to understand what facilitates T^T formation, a model system is needed to identify what factors facilitate CT in biological systems.

1.3 Charge Transfer in Biological Systems

Electron transfer in DNA has been the subject of increasing scrutiny over the last 40 years, when it was first suggested that DNA could possibly

transport charge.[84] The efficiency and stability of biological processes are of interest to researchers because they have been optimized over many millennia. This coupled with the implications of CT described in the previous section are reasons that recent research has lead to a push towards the use of biologically inspired devices for real world applications.[85-87] One such example is the study of electron transport through DNA for synthesis of conductors,[88-90] sensors,[91,92] DNA based wires[88,93,94] and nanoelectronic devices.[95] The versatility of DNA allows for development of systems with different specificity and transport capabilities. DNA is an ideal candidate for mechanistic studies due to its well understood structure that has been extensively characterized under a variety of conditions.[96,97] DNA is capable of self sorting which allows for ordered complex network formation.[98] Most importantly it is relatively inexpensive, easy to synthesize, and is readily modified with a variety of different functional groups.

There are two complementary methods of charge transport in DNA: hole transfer (HT) and excess electron transfer (EET).[99] While these two processes both involve electron transport, they differ in the molecular orbital in which the electron travels (Figure 1.10). While EET has only recently been the focus of research, over the last 20 years widespread studies have been conducted on HT resulting in a solid understanding of the mechanistic fundamentals and DNA sequence requirements necessary for HT.[100]

Hole Transfer

HT is initiated by excitation of an electron acceptor by UV radiation creating an electron deficiency which results in the movement of a positive charge through the highest occupied molecular orbital of DNA. Several different mechanisms including superexchange,[101-103] hopping[101,104] and polaron[104-107] mechanisms have been used to describe HT. HT via superexchange mechanism is limited to short distances (< 10 Å) and occurs on a very fast time scale.[108-111] Long distance transfer (> 10 Å) occurs via hopping and polaron mediated mechanisms.[104,112-114] One common factor in these mechanisms is that guanine acts as the intermediate charge carrier.[115,116] Among the four DNA bases, guanine is the most easily oxidized.[117] A true picture of HT must take into account a combination of these different mechanisms as well as effects from variations in DNA sequence and hole injector strength. These combined factors affect the efficiency and observed rate of HT.

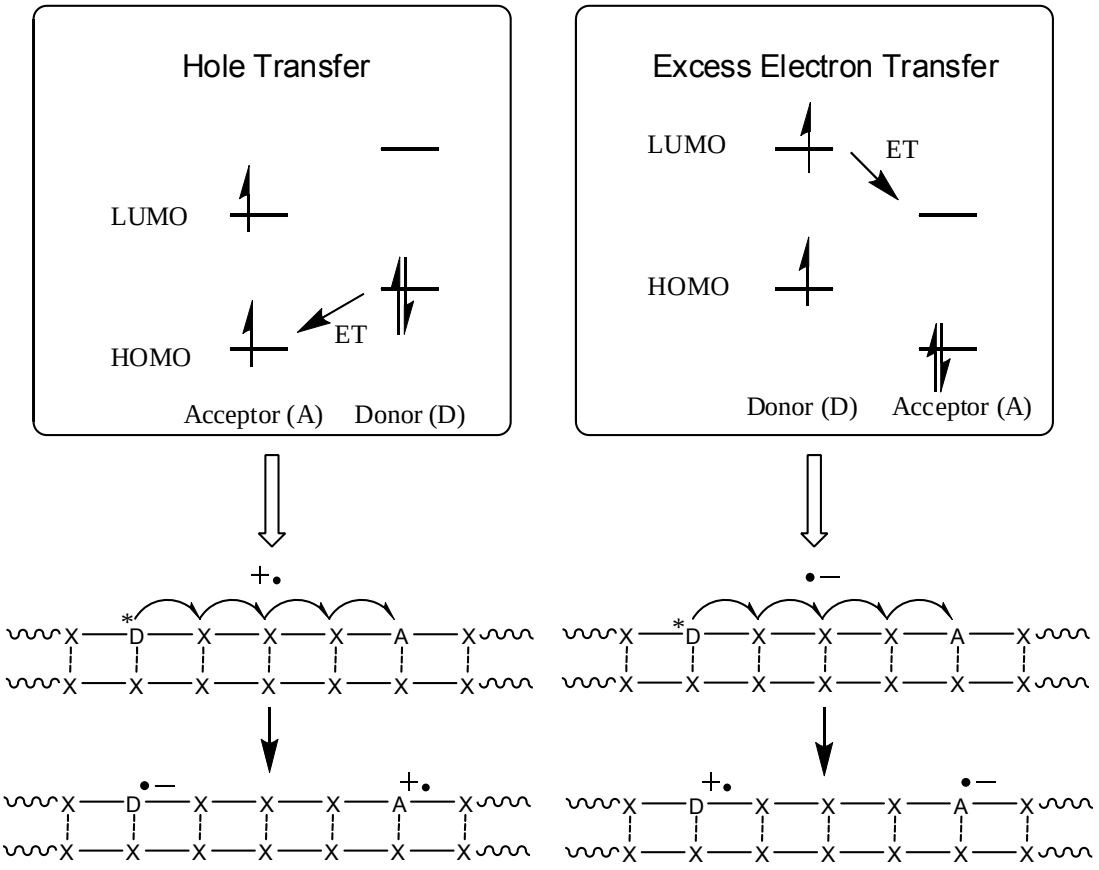

Figure 1.10: Differences in orbital control between HT and EET. HT is a HOMO mediated process, while EET is a LUMO mediated process.[118]

A number of sensitizers (acceptors) have been used to study HT in DNA.[99,119,120] The sensitizers vary from metal-based rhodium and ruthenium complexes used by Barton and coworkers[121] to small organic compounds like the anthraquinone derivatives used by Schuster and coworkers.[120] Figure 1.11 illustrates just a few of the most common types sensitizers used for HT. In addition to differing in structural properties, redox potentials, and wavelengths absorbed, these systems also differ in efficiency of HT (for a review see reference 99).[99]

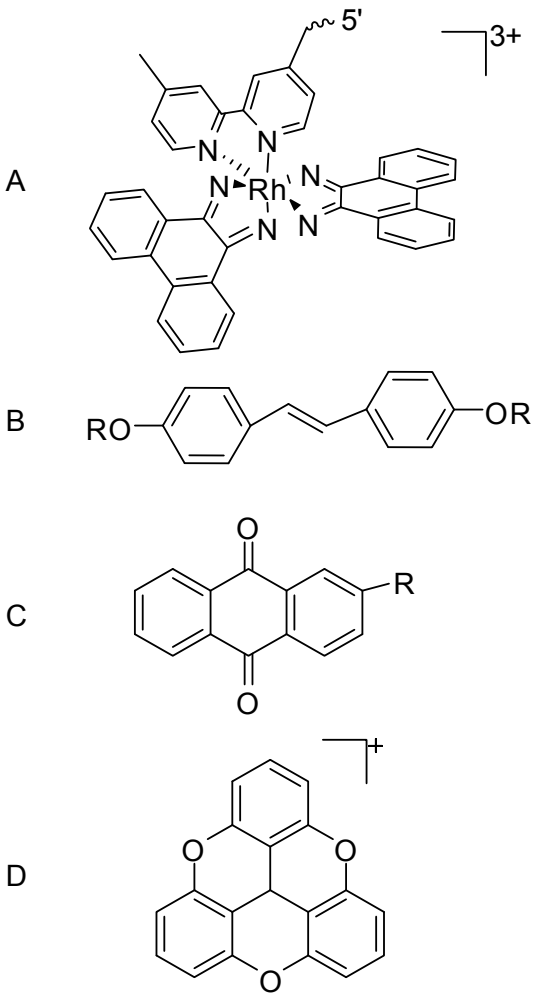

Figure 1.11: Examples of sensitizers used to initiate HT studies. (A) Ruthenium complex,[121] (B) stilbene diether hairpin,[122] (C) anthraquinone derivative,[114] (D) trioxatriangulenium ion[123]

The sensitizers are covalently linked to the DNA in a variety of ways. Figure 1.12 illustrates the types of DNA modifications used to study HT and EET. HT can be photoinitiated by direct excitation of the sensitizer which oxidatively removes an electron from the DNA. The positive charge (or hole) is eventually trapped by **G** and the resulting oxidation product is detected via HPLC or densitometry methods. In addition to **G**, another trap for the study of DNA mediated HT is repair of T^T. Excited state oxidants are able to initiate

long range (19 – 26 Å) repair of T^T by removal of an electron, however this method does not work with every sensitizer.[52] The differences in sensitizer efficiency were postulated to either be due to the inherent nature of the oxidants or because of the differences in measured quantum yields.[124] While these traps have been used to experimentally demonstrate that long range HT (> 200 Å) is possible, the distance of HT is highly dependent on DNA sequence and HT is severely impeded by DNA mismatches. This has lead research in the field to focus on the modification of DNA complexes to increase mismatch sensitivity and range of HT.[125] For example, Barton and coworkers use both tethered[126] and nontethered[127] DNA intercalators to detect a DNA base pair mismatch.

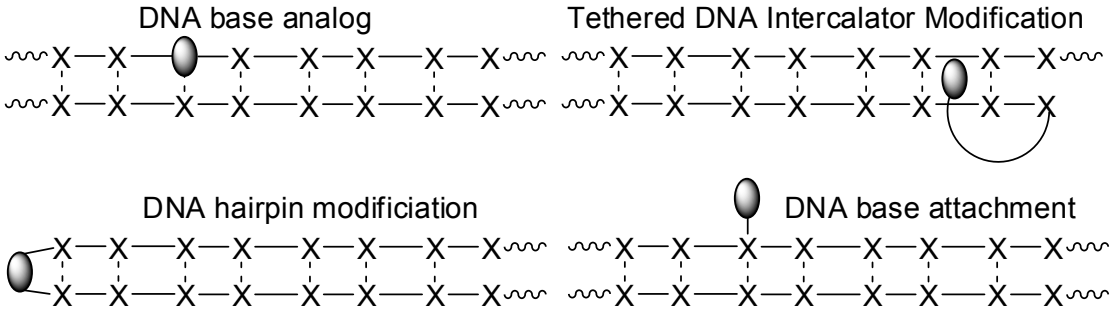

Figure 1.12: Various DNA modification strategies used for CT studies. Oval represents initial electron donor/acceptor for HT and EET.

Excess Electron Transfer

In contrast to HT, very little is known about EET which involves movement of an electron through the lowest unoccupied molecular orbital (LUMO) of DNA base pairs.[128-132] Studies by the Rokita lab show electrons are injected into the DNA base stack from electron donating groups covalently attached to the DNA.[133] These electrons travel between donors and

acceptors using π-stacking to facilitate electron transfer. Unlike HT where **G** is the charge carrier, **T** is suggested to be the intermediate charge carrier for EET.[119] This theory is based on the relative reduction potentials of the DNA bases, **T** > **C** >> **A** > **G**.[53,134]

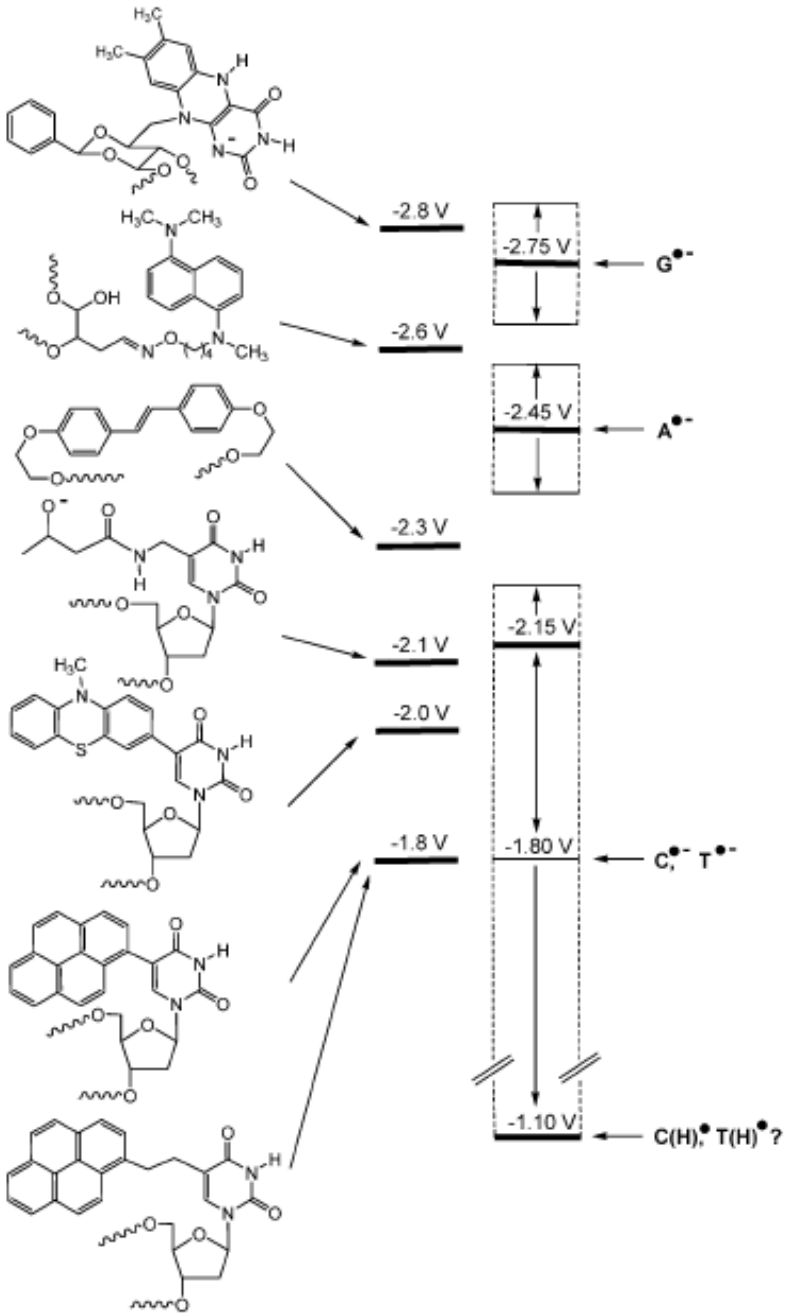

Figure 1.13: Donors used for EET studies in DNA in order of reduction potential in comparison with DNA base reduction potentials (taken from reference 99).

Model systems for EET use a variety of electron donors (Figure 1.13) to photochemically inject electrons into DNA. While the donors differ in structure, the main difference is in their reduction potentials and ability to reduce the DNA bases. To date, two traps have been used for detection of the radical anion (Figure 1.14).

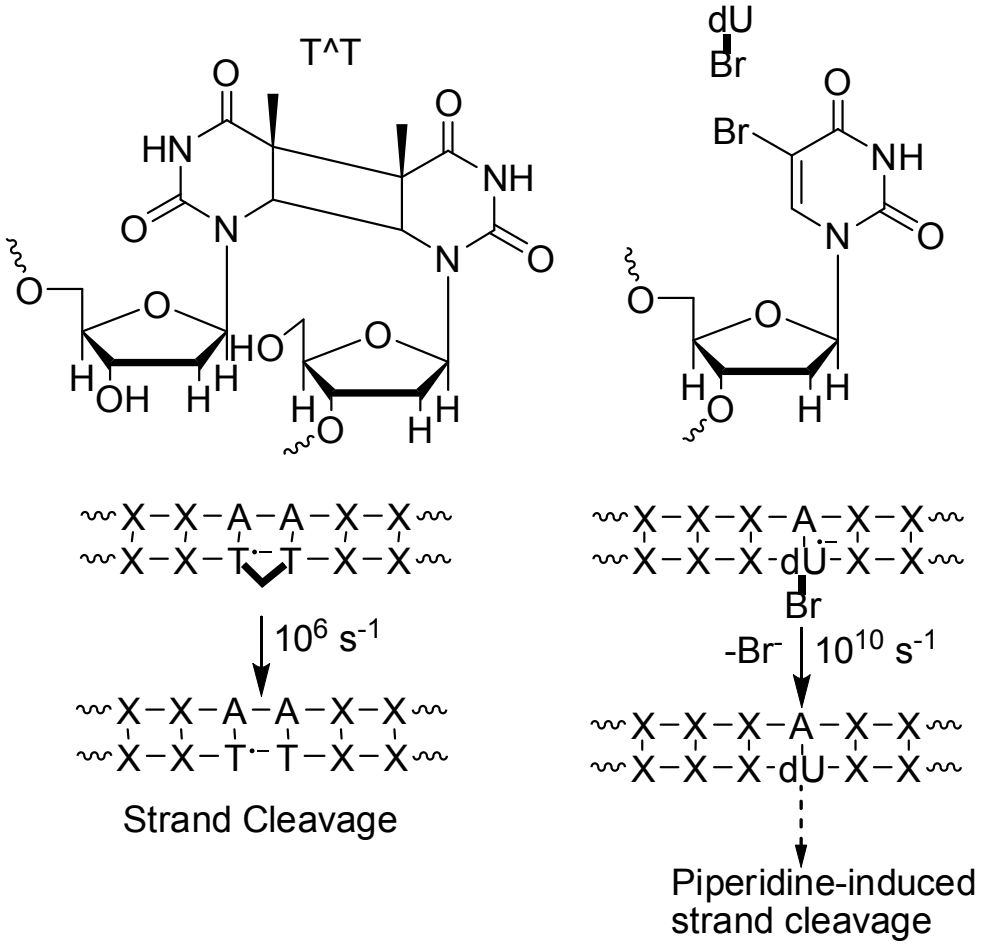

Figure 1.14: Traps used for EET studies (adapted from reference 99).

The first trap is a T^T which lacks a phosphodiester bridge and leads to strand cleavage upon cleavage of its cyclobutane ring by EET.[131,132,135] The second is the 5-bromo-2-deoxyuridine (^{Br}U) which upon EET leads to abasic site formation and subsequent strand cleavage after hot piperidine

treatment.[130,133] Cleavage is detected typically either by gel electrophoresis or by HPLC coupled techniques.[136] The major difference between these two traps is the time scale for detection of EET. The T^T splits at a rate of 10^6 s^{-1} [52,53] whereas the ^{Br}U reaction is much faster at 10^{10} s^{-1}.[137] These differences in cleavage rates lead to discrepancies in reported characteristics of EET. Therefore additional studies are needed to look at the affect of the electron traps and electron donors on the efficiency and observed rates of EET.

Since EET is a relatively new field of study, initial experiments have focused on designing model systems for characterization of EET. An ideal model system will have flexibility in the donor, acceptor, and DNA sequences used for initial studies on EET. Compilation of data from many different systems is needed to determine the fundamentals necessary to facilitate EET in biological systems.

1.4 Specific Aims

The long term goals of this project are to study the reversibility of T^T formation and the affect of EET on T^T repair. My research focused on using two different biological systems to probe the fundamentals of T^T reversibility in DNA.

(1) The nucleosome system was used to study the kinetics of T^T reversibility with a physiologically relevant model. The periodicity of T^T formation of irradiated nucleosomal DNA makes it an ideal candidate for study. T^T formation is distributed statistically in free duplex DNA of

heterogeneous sequence and modulated in nucleosomal DNA of heterogeneous sequence. A single DNA sequence was used to create a homogenous population of NCP in order to determine the irradiation time necessary to convert between the varied populations of T^T.

(2) The second system explores fundamentals of EET in a more abstract way. The criteria that allow for efficient long range transport of electrons were tested by using a DNA based model system containing an electron donor and an electron sink. The model system tests the ability of a DNA sequence to facilitate and promote EET and ultimately allows for examination of the effect of delocalized charge on T-tracts. Additionally, the reduction potentials of a variety of donors are examined using electrochemical techniques.

Chapter 2

Reversibility of T^T in a Biologically Relevant System

2.1 Higher Order DNA Structures

Most charge transfer (CT) studies have focused on B form DNA, however the majority of DNA in biological systems exists in higher order structures called chromatin. The chromatin can be broken down into the individual nucleosome structure (Figure 2.1). Therefore in order to understand the biological effects of UV irradiation and subsequent CT with DNA, it is necessary to look at the effects of UV irradiation in the naturally occurring assembly of DNA. Histone proteins, which make up the protein portion of the nucleosome core particle (NCP), have a common conserved structure that is found in all eukaryotes and are among the most highly conserved of all known proteins.[18] Figure 2.1 illustrates the levels of packing DNA around octameric histone core.[138]

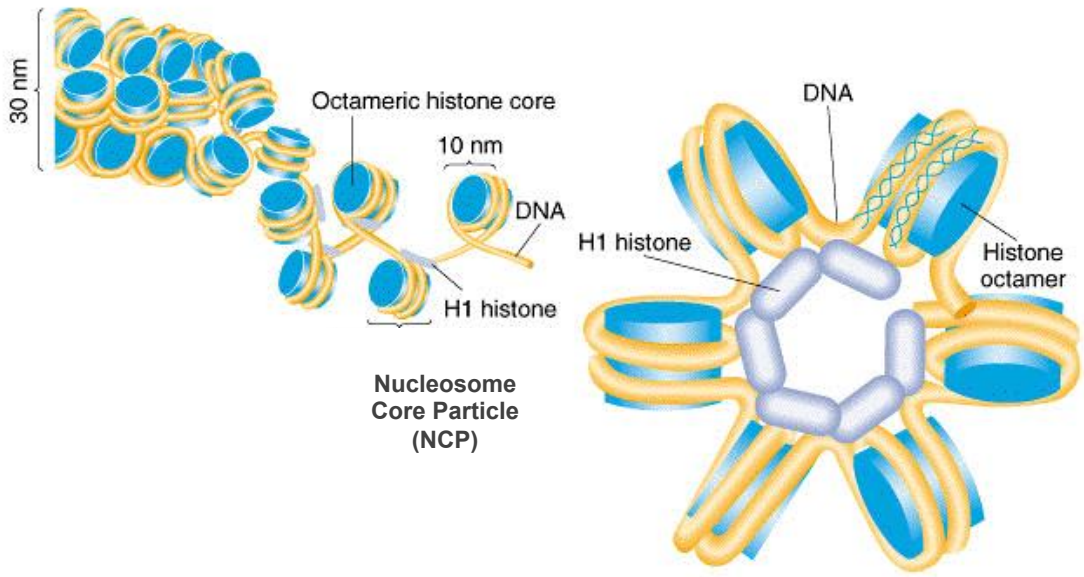

Figure 2.1: Levels of DNA packing from the 30 nm filament to individual NCP.[138]

Nucleosome Structure

The NCP contains 146 base pairs of DNA which wraps in a 1.75 left-handed superhelix of distorted B form DNA with an average pitch of 28 Å around the outside of the histone octamer.[23] The histone octamer contains two copies of each histone protein H2A, H2B, H3, and H4 (Figure 2.2).[139,140] The H1/H5 histone protein is found in higher order eukaryotes and is thought to help in packaging of the structures to make the 30 nm filament (Figure 2.1).[18] Packing of the nucleosome allows DNA to become more compact and also provides some protection to the phosphodiester backbone since it becomes inaccessible to the medium.[141]

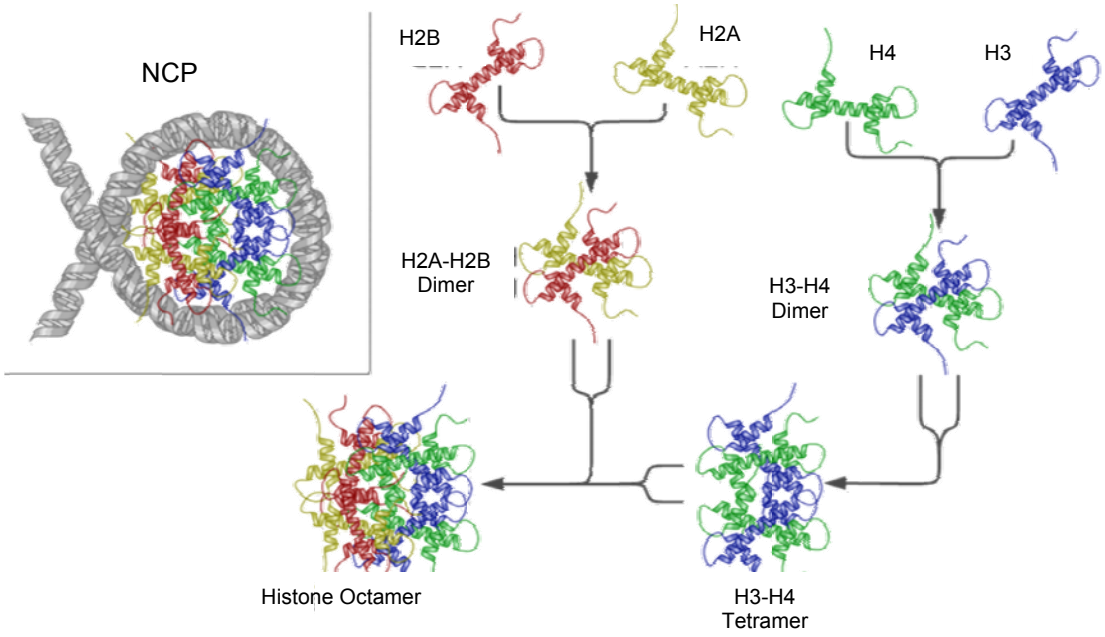

Figure 2.2: Individual histones forming the octamer of the nucleosome core.[142]

Nucleosomal DNA curvature seems to play a considerable role in the frequency of photoproduct formation in the nucleosome core of DNA.[65] Unfolding of the nucleosome core changes the distribution of UV

photoproducts in DNA.[65] In fact, photoproduct distribution seems to be highly modulated in nucleosomal DNA (Figure 2.3c). Cyclopyrimidine dimers (CPD) appear to orient away from the histone surface and specifically T^T favor bending away from the major groove. Upon irradiation with ultraviolet light, T^T formation occurs every 10.3 base pairs.[63,66,143] More importantly, DNA irradiated without NCP gave a random pattern of photoproduct distribution.[63,64,66,143] These findings suggest that either structural features of the histone-DNA interactions or the bending forces CPD formation in DNA to particular sites as a result of UV light. Therefore the structurally based differences in photoproduct formation can be used to vary the photoproduct distribution by changing the conformation of the DNA.

In 1992 Pehrson & Cohen tested the effect of DNA curvature on T^T formation by preparing a 108 base oligonucleotide bound at each end by a lambda repressor. Binding of DNA by the lambda repressor causes a DNA loop to form (Figure 2.3A).[62] They discovered that T^T distribution in the random sequence occurs approximately every 10 base pairs, the same as seen with nucleosomes (Figure 2.3B). The lambda repressor only binds the DNA at two regions and there are no T^T formation sites in the binding region. Therefore, the structure must control the reactivity of the DNA. These studies show that in addition to the sequence effects described in Chapter 1, DNA bending and rotation may determine the distribution of CPD in nucleosomal DNA.

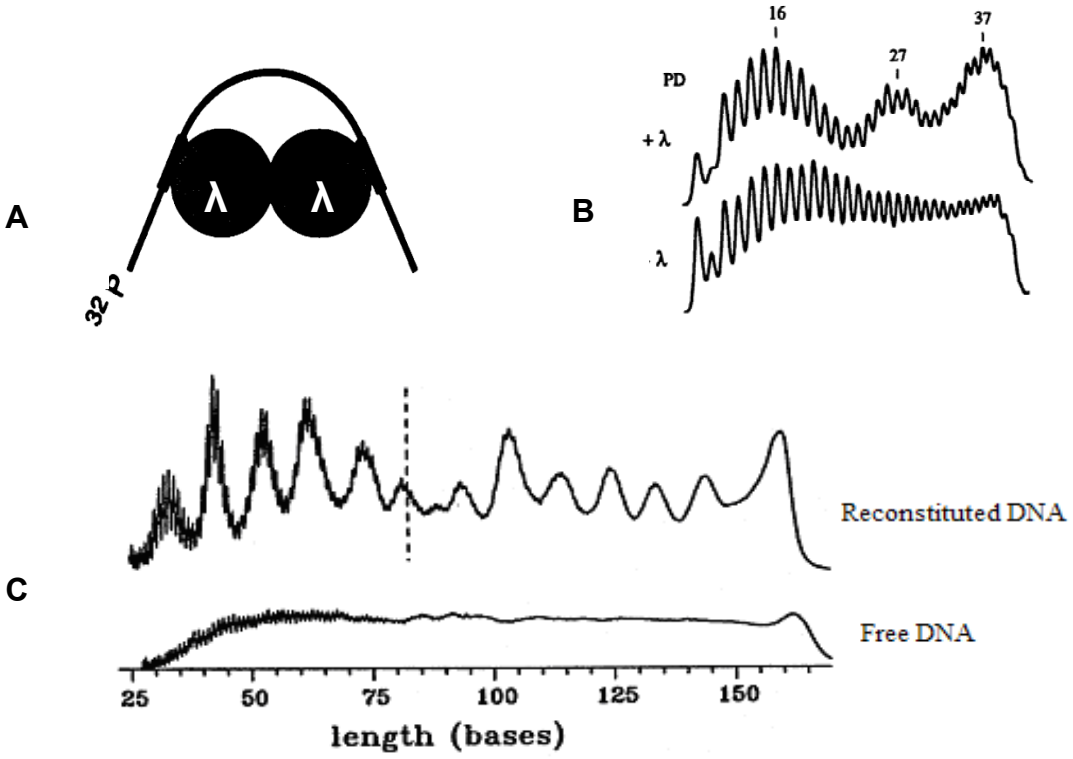

Figure 2.3: Modulation of T^T formation by structure. (A) Lambda repressor with random DNA, image taken from reference 62. (B) CPD formation with lamdba repressor shows periodicity, image taken from reference 62. (C) CPD formation on free and reconstituted DNA. Free DNA shows a random distribution of CPD formation and nucleosomal DNA shows highly modulated CPD formation at approximately every 10.3 base pairs, image taken from reference 65.

The NCP and the lambda repressor experiments illustrate that conformation is important in T^T formation. As mentioned in chapter 1, DNA sequence and the reversibility of T^T formation also play an important role in the overall distribution of T^T. It is possible to induce one state (modulated) of T^T formation and then convert to another (random) by utilizing the varied distributions of T^T formation. The relaxation between the two states of T^T formation will allow for studies to be conducted on the time of relaxation between the two states of T^T formation. The ultimate goal of these experiments is to determine the rates of reversibility of T^T in DNA.

2.2 Experimental

Materials

PAGE purified oligonucleotide primers were purchased from IDT DNA (Coralville, IA) and Gibco Bioresearch Labs (Carlsbad, California). 10 µL aliquots of 50 pmol/µL of DNA primer samples were flash frozen with liquid nitrogen (N_2) and stored at -20 ˚C. 30 % washed pooled chicken blood in Alsevers buffer was purchased from Lampire Biological Laboratories, Pipersville, PA. Blood was aliquoted into 12.5 mL samples, frozen with liquid N_2, and stored at -80 ˚C. Plasmid XP 10 (pXP 10) with *Xenopus borealis* 5s RNA gene insert was obtained from the laboratory of the late Dr. A. Wolffe.[144] Lyophilized histones from calf thymus (type IIA) were purchased from Sigma and stored at 4 ˚C. Plasmid GEM (pGEM) with 601 positioning insert was obtained from the laboratory of Dr. J. Widom, Northwestern University, Evanston, Illinois. Nuclesomes reconstituted with 5′ radiolabeled Widom 601 positioning sequence were obtained from the laboratory of Dr. W. Davis, Washington State University, Pullman, Washington. All PAGE gels were scanned using a Molecular Dynamics Storm 860 phosphorimager (Sunnyvale, CA). Image processing was conducted using Molecular Dynamics ImageQuant v.5.2 (Sunnyvale, CA). All aqueous solutions were prepared with distilled deionized water (Barnstead NANOpure II purifier, ≥ 17.8 MΩ·cm). All chemicals were purchased from Fisher Scientific or Aldrich and were enzymatic grade or the highest grade available.

General Methods

PCR of 5s DNA from Plasmid. A mixture of pXP 10 (1 pg/μL), primers (50 pmol each, forward (+) 5'–AAT TCG AGC TCG CCC GGG GAT CCG-3' and reverse (-) 5'-ACT AAC CAG GCC CGA CCC TGC TTC-3'), 2 mM deoxynucleotide triphosphate (dNTP, MBI Fermentas), 1.4 units Vent DNA polymerase (New England Biolabs), 1X thermopol buffer (10 mM KCl, 20 mM Tris-HCl, (pH 8.8), 10 mM $(NH_4)_2SO_2$, 2 mm $MgSO_4$, and 0.1 % Triton X-100) was combined in a final volume of 100 μL. The plasmid template was amplified by using the following PCR protocol. The sample was heated for 5 minutes at 90 ˚C and then 25 cycles (94 ˚C for 30 seconds for denaturation and 72 ˚C for 1 minute for annealing and extension of primers) on an Eppendorf Mastercycler 5330 with lid heated to 110 ˚C. Samples not analyzed immediately were quenched with 5 mM EDTA and stored at -20 ˚C.

PCR of Widom 601 NPS from Plasmid. A mixture of pGEM (1 pg/ μL), primers (50 pmol each, forward (+) 5'- CTG GAG AAT CCC GGT GCC G -3' and reverse (-) 5'- ACA GGA TGT ATA TAT CTG ACA CG -3'), 2 mM dNTP (MBI Fermentas), 1.4 units Vent DNA polymerase (New England Biolabs), 1X thermopol buffer (10 mM KCl, 20 mM Tris-HCl, (pH 8.8), 10 mM $(NH_4)_2SO_2$, 2 mM $MgSO_4$, and 0.1 % Triton X-100) were combined in a final volume of 100 μL. The plasmid template was amplified by running 5 minutes at 90 ˚C and then 25 cycles (94 ˚C for 30 seconds and 50 ˚C for 1 minute) on an Eppendorf Mastercycler 5330 with lid heated to 110 ˚C. Samples not analyzed immediately were quenched with 5 mM EDTA and stored at -20 ˚C.

Agarose Gel Purification of PCR Products.[145] A solution of 0.5x TBE (44.5 mM tris, 44.5 mM boric acid, 1 mM EDTA, pH 8.0) was used to make 30 – 300 mL of 1 % agarose gel solution (SeaKem HGT Agarose, Cambrex Bio Science). SBX loading dye (20 µL) which is comprised of 0.25 % bromophenol blue, 0.25 % xylene cyanol, 40 % w/v sucrose, and 5 mM EDTA was added to 100 µL PCR samples. Sample (60 µL) was loaded into each well of the agarose gel and a 100 base pair ladder (MBI Fermentas) was used for reference. Agarose gel was run for 80 minutes at 120 volts. Spectroline EF-140C transilluminator was used to shine on gel placed on TLC plate with fluorescent indicator in order to detect DNA bands. Bands corresponding to 5s DNA or W601 DNA were excised. QIAquick gel extraction kit (Qiagen Inc.) was used to recover sample from excised agarose gel slice.

5' - [^{32}P]- labeling. 60 pmol of (-) primer was incubated for 45 minutes at 37 ˚C with 4 µL γ - [^{32}P] – ATP (Amersham 10 µCi/µL), 10 units T4 polynucleotide kinase (New England Biolabs), and 2.5 µL of T4 polynucleotide kinase buffer (70 mM Tris-HCL, 10 mM $MgCl_2$, 5 mM dithiothreitol). Sample was diluted to a final volume of 25 µL with ddH_2O. In order to remove excess salt and ATP, the mixture was spun through a prewashed (3 times with 400 µL ddH_20 and spin down for 2 minutes at 1000 relative centrifugal force (rcf)) P6 Micro Bio-Spin column (Biorad) for four minutes at 1000 rcf. Radioactivity of the resulting mixture was measured by

adding 1 µL of sample to approximately 1 mL of scintillation fluid (Fisher ScintiSafe Plus 50 %) using a Packard 1600TR Liquid Scintillation Analyzer.

PCR of 5s DNA with (-) Primer Labeled. A solution of 50 pmol (-) radiolabeled primer, 50 pmol (+) primer, 25 ng template (reverse strand sequence[146] of 154 base pair 5s DNA 5'-ACT AAC CAG GCC CGA CCC TGC TTG GCT TCC GAG ATC AGA CGA TAT CGG GCA CTT TCA GGG TGG TAT GGC CGT AGG CGA GCA CAA GGC TGA CTT TTC CTC CCC TTG TGC TGC CTT CTG GGG GGG GCC CAG CCG GAT CCC CGG GCG AGC TCG AAT T-3') was combined with 2 mM dNTP mix, 1.4 units Vent DNA polymerase (New England Biolabs), 1X thermopol buffer (10 mM KCl, 20 mM Tris-HCl, (pH 8.8), 10 mM $(NH_4)_2SO_2$, 2 mM $MgSO_4$, and 0.1 % Triton X-100) and brought to a final volume of 100 µL with ddH_2O. The plasmid template was amplified by using the following PCR program: 5 minutes at 90 ˚C and then 25 cycles (94 ˚C for 30 seconds and 72 ˚C for 1 minute) on an Eppendorf Mastercycler 5330 with lid heated to 110 ˚C. Samples not analyzed immediately were combined with 5 mM EDTA to quench reaction and stored at -20 ˚C.

Native and Denaturing Polyacrylamide Gel Electrophoresis (PAGE). Native gels (8 %) were prepared by combining 10 ml of a 40 % acrylamide (19:1 acrylamide:bis-acrylamide) solution, 5 mL 5X TBE (54 g Tris, 27.5 g boric acid, 23.8 mL 0.42 M EDTA (pH 8.0), ddH_20 to 1 L) with 35 mL of ddH_2O. TEMED (35 µL) and APS (300 µL) were added and were cast between two glass plates (19.5 cm (L) x 2 mm (W) x 20 cm (H)) using 1.5 mm

spacers. The wells were washed with 0.5X TBE prior to loading DNA samples (60 µL) in loading dye (0.05 % bromophenol blue, 0.05 % xylene cyanol, 5 % sucrose) and the gel was run at 4 °C in a cold box at 175 volts for 1 hour and 45 minutes. The gel was placed on a molecular dynamics phosphorimaging screen for 30 minutes and screen was developed using a Storm phosphorimager and quantified using Molecular Dynamics ImageQuant v.5.2 software. The radioactive band corresponding to 5s or W601 DNA was excised with a razor blade and DNA was removed via electroelution. The denaturing gel (8 %) stock solution was prepared by combining 420 g urea, 200 mL 5x TBE, and 200 ml 40 % acrylamide (19:1 acrylamide:bis-acrylamide) solution to a final volume of 1 L with ddH_2O. 6x denaturing loading dye was prepared containing 0.05 % bromophenol blue, 0.05 % xylene cyanol, 8 M urea, 40 % w/v sucrose. PAGE was conducted for 1 - 2 hours at 45 - 65 watts using 1X TBE as the buffer solution with an aluminum plate clamped to the glass plates to distribute heat evenly.

Electroelution of Radiolabeled DNA.[145] The following changes were made from the protocol outlined in reference 145 in order to optimize the conditions for DNA removal from the gel slice. The gel was electroeluted at 4 ˚C at 175 volts for 1.5 hours. The original protocol called for running electroelution for 2 hours at room temperature at 75 volts. Current was reversed for 5 minutes to remove any sample adhering to dialysis tubing. The original protocol called for current reversal for 1 minute at 75 volts. The elutent was removed from the dialysis bag and then treated with butanol

concentration, chloroform-phenol extraction, ethanol precipitation, and lyophilization as described below.

Butanol Concentration of Radiolabeled DNA. Equal volumes of butanol and DNA solution were combined, vortexed, and then centrifuged at 14,000 × g for 1 minute at room temperature. The top layer (organic) was discarded and the DNA was further purified via chloroform-phenol extraction.

Chloroform-Phenol Protein Extraction of Radiolabeled DNA. Equal volumes of phenol-chloroform and DNA solution were combined, vortexed, and then centrifuged at 14,000 × g for 1 minute at room temperature. The bottom layer (organic) was discarded and the DNA was precipitated with ethanol as described below.

Ethanol Precipitation of Radiolabeled DNA. Sodium acetate (0.1 volume, 3 M, pH 5.5) and 100 % ethanol (2.5 volumes, -20 ˚C) were added to DNA samples. The mixture was vortexed and stored at -80 °C for 1 hour and then centrifuged for 20 minutes at 4 °C at 14, 000 × g to pellet the precipitated DNA. The supernatant was carefully discarded in order not to disturb the pellet. The pellet was washed with 200 µL of 80 % ethanol (-20 ˚C) and the tube was centrifuged for 6 minutes at 4 °C at 14,000 × g. The supernatant was discarded and the pellet was dried under high vacuum in a speedvac. 20 – 100 µL ddH_2O was added to the sample and a scintillation count was taken to determine the amount of sample needed for subsequent reactions.

Photochemistry. Radiolabeled free DNA and NCP reconstituted DNA samples were irradiated in a 10 µL solution containing 200 kdpm of labeled

DNA, 10 mM potassium phosphate (pH 7.0), and 100 mM NaCl. Samples were irradiated using a 6035 Hg (Argon) Oriel Instruments Pencil Lamp (for light stabilization, the pen lamp was turned on 30 minutes prior to irradiation) samples are irradiated for 0 – 60 minutes. The low pressure Hg(Ar) pencil lamp was chosen because it is insensitive to temperature, has a constant average intensity and most importantly approximately 74 % of its irradiance is at 254 nm.[147] The height of the pen lamp was varied from 6 – 11 cm which changess the light flux from 0.16 – 0.016 mW/cm^2. After irradiation, samples were treated with T4 endonuclease V, piperidine, or T4 polymerase as described below. For reconstituted DNA samples, chloroform-phenol extraction was necessary before the treatment in order to remove histones which interfere with analysis.

T4 Endonuclease V Reaction. 10 µL of 12X Endo V Buffer (100 mM Tris-HCl (pH 7.5), 100 mM NaCl, 120 mM EDTA in 25 mL ddH_2O), 3 µL T4 endonuclease V (EpiCentre), and 7 µL ddH_2O were combined to make the working endo V reaction mixture. Endo V mix (2 µL) was added to 10 µL irradiated samples and incubated at 37 ˚C ≥ 5 hours.

Piperidine Treatment. 30 µL of 1 M piperidine was added to lyophilized DNA samples and incubated in a water bath at 90 ˚C for 30 minutes. Samples were then centrifuged at 14,000 × g for 1 minute, lyophilized in a speedvac, and after samples were dried, 20 µL of ddH_2O was added and samples were lyophilized again. This step was repeated to remove remaining piperidine since it interferes with gel electrophoresis.

T4 DNA Polymerase Reaction. Photoirradiated DNA samples were lyophilized and dissolved in 1 μL of BSA (New England Biolabs 100X stock included with T4 DNA polymerase) and 50 μL of T4 digestion buffer (33 mM tris-acetate (pH 7.8), 10 mM $Mg(OAc)_2$, 66 mM KOAc, and 0.5 mM dithiothreitol) and then denatured by placing in a 90 ˚C bath for 5 minutes. Samples were placed on ice (5 minutes) and 3 units of T4 polymerase (New England Biolabs) was added to each sample. Samples were then incubated in a 37 ˚C bath for 2 hours and reaction was terminated by heating to 65 ˚C for 10 minutes. The samples were then subject to chloroform-phenol extraction, ethanol precipitation, and lyophilization.

Nucleosome Preparation.[148,149] All buffers and solutions were autoclaved or sterile filtered before use. Chicken blood was thawed on ice at 4 ˚C ≤ 12 hours. 12.5 mL of chicken blood was added to 48 mL of chilled solution 1 (250 mL solution containing 0.14 M NaCl, 15 mM sodium citrate, and 9.8 mM Tris-HCl (pH 7.5)) containing 300 μL of 50 mM phenylmethylsulphonyl fluoride ((PMSF) in isopropanol) and 300 μL pepstatin (1 mg/mL in absolute ethanol). The sample was centrifuged (Beckman Avanti J25-I) at 2000 × g in Beckman JLA 10.500 rotor for 5 minutes. The supernatant was removed using a glass pasteur pipette and house vacuum with a trap to prevent any suction of chicken blood sample into vaccum line. The pellet was resuspended in 60 mL solution 1 containing PMSF and pepstatin and centrifuged at 2000 × g and remove supernatant, this step was repeated two times. The pellet was resuspended in 20 mL of

solution 2 (15 mM NaCl, 60 mM KCl, 340 mM sucrose, 15 mM Tris-HCl (pH 7.5), 0.5 mM spermidine, 0.15 mM spermine, 0.32 mL 2-mercaptoethanol in 200 mL ddH_2O) containing 100 µL PMSF and 200 µL pepstatin (per 20 mL volume)). NP-40 (detergent) was added to a final concentration of 0.01 – 1 % (amount needed varies with quantity and quality of cells). In order to determine the optimal amount of detergent needed, several different concentrations of detergent were tested in a trial NCP preparation. The cells were then lysed on ice for 10 minutes. Lysate was filtered through 5 layers of cheesecloth. The suspension was centrifuged at 2600 × g for 5 minutes prior to aspiration of the supernatant. The pellet was resuspended in 20 mL of solution 2 containing PMSF and pepstatin, centrifuged at 2600 × g for 5 minutes and then the supernatant was removed by aspiration. This step was repeated 3 times. The pellet was resuspended in 1 mL of solution 2 containing PMSF and pepstatin and transferred to an eppendorf tube. UV absorbance (Hewlett Packard HP8453 UV-Visible spectrophotometer) was determined at 260 nM by suspending 1 µL of sample in 1 mL of 0.1 M NaOH (blank with 0.1 M NaOH). The sample pellet was then digested with micrococcal nuclease (MN) at 55 units of enzyme (Worthington 10 U/µL stock solution) per 67 A_{260} units of nuclei in 2 mM $CaCl_2$ and 30 mM Tris-HCl (pH 7.5) for 10 minutes at 30 ˚C. The reaction was quenched by addition of 5 mM EDTA (pH 8.0) and sample was centrifuged at 5900 × g for 20 minutes and the supernatant was discarded. The pellet was resuspended in nuclear lysis buffer (0.25 mM EDTA, 15 mM Tris-HCl (pH 7.5), 0.25 mM PMSF, 1.0 mM

benzamidine-HCl (prepared fresh), 5 μg/mL pepstatin, in 1 mL ddH_2O) at half the original digestion volume. The sample and resin mixture was incubated on ice for one hour and centrifuged at 5900 × g for 20 minutes to extract the solubilized chromatin in the supernatant. The pellet was discarded. The concentration of NaCl in the collected supernatant was slowly increased to 0.35 M. This solution was added to an aqueous suspension of Bio-Rad's AG 50W-X2 cation exchange resin (prewashed with 15 mL of 1 M NaOH, 3 × 15 mL ddH_2O, 15 mL 1 M HCl, 3 × 15 mL ddH_2O, 1 M NaOH, 3 × 15 mL ddH_2O) at concentration of 0.7 mg / A_{260} nuclei. The sample was stirred on ice for 90 minutes and the supernatant was collected from the resin and centrifuged at 500 × g for 5 minutes to remove residual resin. The supernatant was dialyzed using 25 Kda SpectraPor 7 dialysis tubing against 25 mM NaCl and 10 mM Tris-HCl (pH 7.5) in a total volume of 800 mL overnight at 4 ˚C in a QuixSep spin dialysis button (Membrane Filtration Products Inc., Seguin, Texas). The sample was stored at 4 ˚C and for long term storage 1 mM dithiothreitol was added.

Determination of Nucleosome Purity.[150] Denaturing SDS discontinuous gel (Laemmli method) was run as described.

BCA Assay. Protein concentration was determined by BCA Protein Assay Kit (Pierce) using the manufacturers protocol.

Reconstitution of Nucleosome.[151,152] 70 μg of chicken nucleosome protein (determined by BCA Assay) was combined with, 1 M NaCl, 10 mM potassium phosphate pH 7, 0.5 μg ^{32}P – labeled 5s DNA (see equations,

constants, and conversion factors below for DNA concentration calculation) prepared from PCR of radiolabeled primer in a final volume of 200 µL using autoclaved ddH_2O in an eppendorf tube placed on ice.

Equation 2.1: Radioactive decay calculation used to determine concentration of DNA based on radioactivity of DNA sample. Where for ^{32}P A_0=3000 ci/mol and $t^{1/2}$=14.3 days, and t=time in days. In order to convert the number Ci to dpm, the conversion factor 1 Ci = 2.2 × 10^{12} dpm is used. DPM is measured by scintillation counter and finally pmol can be converted to pg by using the conversion factor pg=(pmol × number of base pairs × 660 pg/pmol).

$$A = A^0 e^{-\lambda t}$$

$$\lambda = 0.693/t^{1/2}$$

Sample was incubated for 30 minutes at 4 ˚C in an ice-water bath and then transferred into a dialysis cell with a 25 KDa MWCO SpectraPor 7 membrane. Sample was dialyzed in a 600 mL beaker at 4 ˚C containing 250 mL of 10 mM potassium phosphate (pH 7) and 1 M NaCl for 20 minutes. 50 mL of 10 mM potassium phosphate (pH 7) was added every 20 minutes until final solution volume is 500 mL (0.5 M NaCl). Dialysis sample was placed in another buffer solution of 10 mM potassium phosphate (pH 7) 0.46 M NaCl in a 600 mL beaker and 50 mL of 10 mM potassium phosphate (pH 7) was added every 20 minutes until final solution volume is 500 mL (0.22 M NaCl). Dialysis sample was placed in final buffer solution containing 10 mM potassium phosphate (pH 7.0) and 0.1 M NaCl repeat addition of 10 mM potassium phosphate (pH 7) until buffer volume was 500 mL (.05 M NaCl). Once the final concentration of 10 mM potassium phosphate buffer and 50 mM NaCl was reached the sample was dialyzed overnight at 4 ˚C. A

scintillation count was taken of the sample in order to determine sample concentration (using equations 2.1). In order to ensure DNA was all similarly positioned around nucleosome (5s DNA experiments) sample was placed in 37 ˚C bath for two hours.[153] Analysis of the NCP reconstituted sample was performed via native PAGE to determine efficiency of reconstitution.

Analysis of 5s and W601 NCP Reconstitution.[145] Native gel (6 %) was prepared using 1 mL 10X tris-glycine buffer (0.25 M Tris, glycine (1.92 M), dd$H_2$0 to 1 L, pH 8.8) diluted to 10 mL with ddH_2O and the gel was cast on a Bio-Rad MiniProtean3 apparatus (10 well, 1.5 mm thick gel). Protein samples (20 µL) in loading dye (0.05 % bromophenol blue, 0.05 % xylene cyanol, 5 % sucrose) were loaded and run at 175 volts for 55 minutes in a cold box at 4 °C. The gel was placed on a molecular dynamics phosphorimaging screen overnight and screen was developed using Storm phosphorimager and quantified using molecular dynamics Image Quant 5.2 software.

Calf Histone Reconstitution.[153] Calf histones were obtained from Sigma-Aldrich in lyophilized form and were stored at – 20 °C until ready for use. Reconstitution procedure was followed as outlined in reference 153, the only change from the published procedure was that 10 times more 2-mercaptoethanol was used in the dialysis buffers.

Histone protein removal.[145] Equal volumes of chloroform-phenol-isoamyl alcohol (25:24:1) and reconstituted W601 DNA samples were combined and vortexed. Samples were then placed in a 90 °C bath for 5

minutes, vortexed again, spun down in a centrifuge and then placed on ice. Separation of organic and aqueous phases was completed using 5 prime phase lock gel tubes, using the protocol provided with the tubes. Aqueous layer was then dried in speedvac. 10 – 20 µL ddH_2O was added to dried samples for subsequent analysis by PAGE.

A+G Reaction.[145] A solution of 300 kdpm of dsDNA, 1.0 µL of 1.0 M piperidine-formate (pH 2.0), and 1.0 µL calf thymus DNA (1 mg/mL) was prepared in a final volume of 40 µL. Samples were incubated at 42 ˚C for 10 minutes and lyophilized in speedvac until dry. 25 µL of ddH_2O was added and again lyophilized in speedvac. 10 – 20 µL ddH_2O was added to dried samples for subsequent analysis by PAGE gel.

T Reaction.[145] A solution of 300 kdpm of dsDNA, 1 µL $KMnO_4$ (20 mM freshly prepared), 2 mM EDTA, 5 mM potassium phosphate buffer (pH 7.0) was prepared to a final volume of 40 µL. Samples were incubated at 60 ˚C for 20 minutes and reaction was quenched by addition of 20 mM Na_2SO_3. The sample was then subject to chloroform-phenol extraction, ethanol precipitation, lyophilization, and piperidine treatment.

2.3 Results and Discussion

5s DNA

The initial aim of the study was to use a well characterized system with a defined sequence to study thymine dimer (T^T) formation and reversion.

This was achieved by using the 5s DNA positioning sequence. There are a few benefits associated with the 5s sequence. This sequence exhibits especially strong positioning about the octameric histone core.[154] Through DNA footprinting conducted in various research labs, precise positioning of the T's with respect to the histone core has been determined (Figure 2.4).[65,155,156] The second benefit is that 5s DNA positioning around nucleosome is independent of temperature and salt concentration under the reaction conditions used for photochemistry experiments.[155,157] The efficiency of T^T formation can therefore be directly correlated to positioning on NCP. In addition to the benefits outlined above, the 5s DNA sequence was readily available and already in use in the Rokita laboratory.

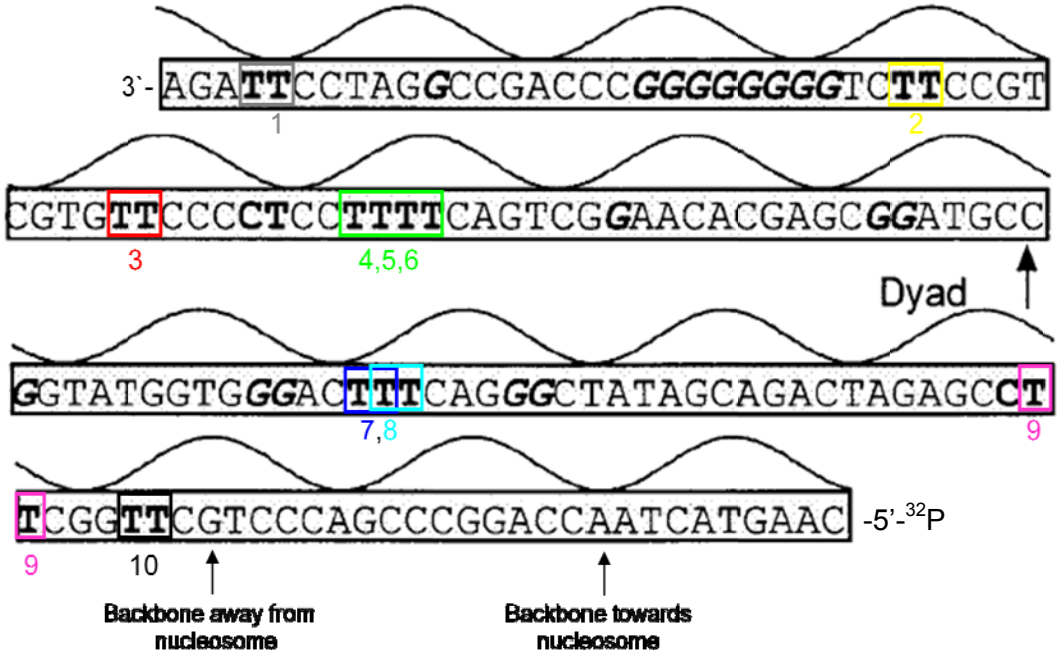

Figure 2.4: Sequence of 154 base pair 5s DNA.[65] Numbers correspond to the bands shown on the gels representing the sites of T^T formation. The color coding of the individual T^T's corresponds to the color show on subsequent graphs to ease reference back to sequence. ^{32}P Denotes location of radiolabel.

The sequence of 5s DNA is illustrated in Figure 2.4. The possible sites for T^T formation are numbered 1 through 10 and are color coded in order to simplify identification of each T^T site on graphs comparing the sites of T^T formation. Each site was individually characterized to determine T^T formation over time and total percentage of T^T formation. After characterization of each T^T in free 5s DNA, studies were conducted on NCP reconstituted 5s DNA samples.

Figure 2.5 illustrates the basic steps of the experiments designed to study the rates of T^T formation and reversion. The first step (Figure 2.5A) was to study the photochemistry of the 5s DNA free in solution. The irradiation of free 5s DNA was expected to give a random distribution of T^T formation in solution. Irradiation times were optimized based on the criteria of clear and distinguishable T^T formation, in addition to minimizing background photochemical oxidation reactions. The second step (Figure 2.5B) was to determine distribution of T^T formation in 5s DNA reconstituted onto nucleosomes. The final step (Figure 2.5C) was to irradiate DNA initially reconstituted and then remove the protein and determine the rate at which the population of T^T changes from a modulated to a random distribution.

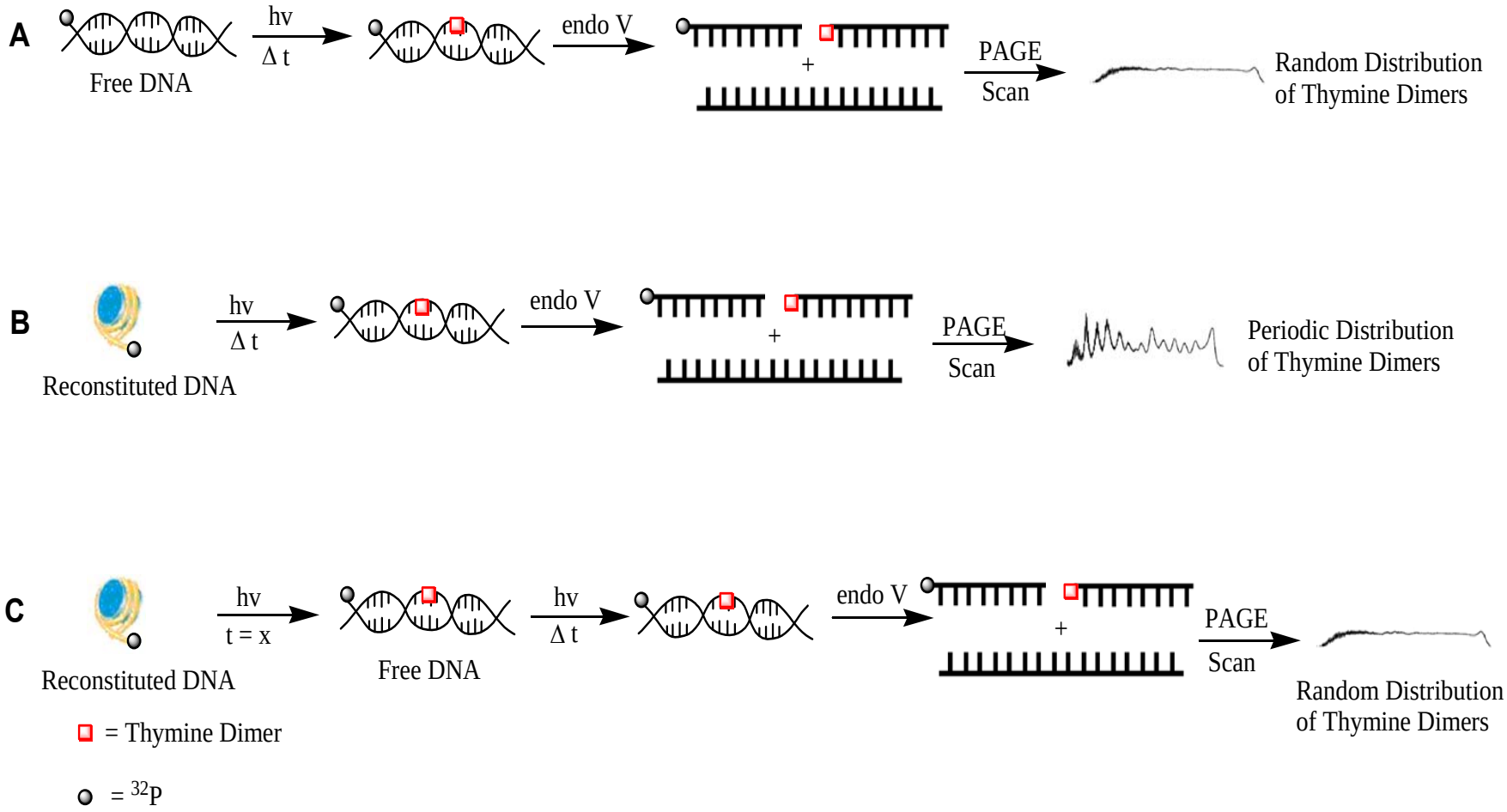

Figure 2.5: Schematic diagram of assay used for T^T photostationary state studies. (A) Irradiation of free DNA to give random distribution of T^T. (B) Irradiation of NCP reconstituted DNA to give varied distribution of T^T formation. (C) Irradiation of NCP reconstituted DNA for a static time point (x) and then removal of the NCP and irradiation of the free DNA over a variety of time points to look at the redistribution of T^T formation from varied to random.

For initial experiments, the 5s DNA was radiolabeled at the 5' end of the reverse PCR strand (Figure 2.4) because this strand contains the majority of the T^T sites in the 5s DNA template. DNA was then irradiated for 0 to 60 minutes and either subject to endoV, piperidine, or T4 polymerase (T4 pol) treatment. As mentioned in chapter 1, endoV treatment is specific for cis-syn T^T, therefore this was the major method of experimental detection of T^T formation. The piperidine treatment was used to ensure that there was not an excess of background oxidation reactions which would decrease the amount of T^T formation observed. Piperidine is sensitive to oxidative damage and abasic sites and results in DNA strand cleavage.[158] Finally, as an alternative to endoV treatment, T4 pol treatment was used to visualize CPD formation. T4 pol has a 3'-5' exonuclease activity that will fully digest undamaged DNA, however is unable to digest DNA with photochemical damage sites such as CPD's.[143]

After treatment to induce strand cleavage, samples were separated by polyacrylamide gel electrophoresis (PAGE) and subject to autoradiography for band visualization. In order to determine error in the experimental conditions, all photochemistry experiments were run in duplicate. In order to minimize experimental error all samples were prepared simultaneously and then aliquoted into separate microcentrifuge tubes for various time points in the photochemistry experiments.

Preliminary irradiation times were tested to give a broad range of T^T formation and to observe if differences between initial T^T formation rates and

photostationary rates could be determined. For each set of experiments the first (0 minutes) and last time point (30 or 60 minutes) were treated with hot piperidine to ensure that DNA was not damaged before irradiation and that damage was not extensive after irradiation. Figure 2.6 illustrates that after initial analysis, 60 minute time point for photoirradiation was excluded due to excessive background cleavage when treated with hot piperidine. Graphical analysis of the time course of total T^T formation illustrates that the 60 minute time point (Figure I.1) shows decreased total percent T^T cleavage compared with the 20 and 30 minute time points. This decrease was possibly due to multiple damage sites and oxidative damage caused by the prolonged exposure to irradiation. In order to focus on T^T equilibration, it was necessary to reduce other forms of DNA damage. Therefore, latter experiments were conducted from 0 to 30 minutes.

Endo V treatment of free 5s DNA gave a maximum of 6 or 7 bands when analyzed by PAGE. Since there are 10 possible T^T, the next step was to correlate the gel bands to the template sequence. Maxam-Gilbert[145] chemical sequencing (Figure I.2 and Figure I.3) was used to correlate cleavage bands with position of T^T in the 5s DNA sequence. The following is a characteristic gel (Figure 2.6) with the T^T locations color coded and labeled with numbered arrows which correspond to the sequence labels.

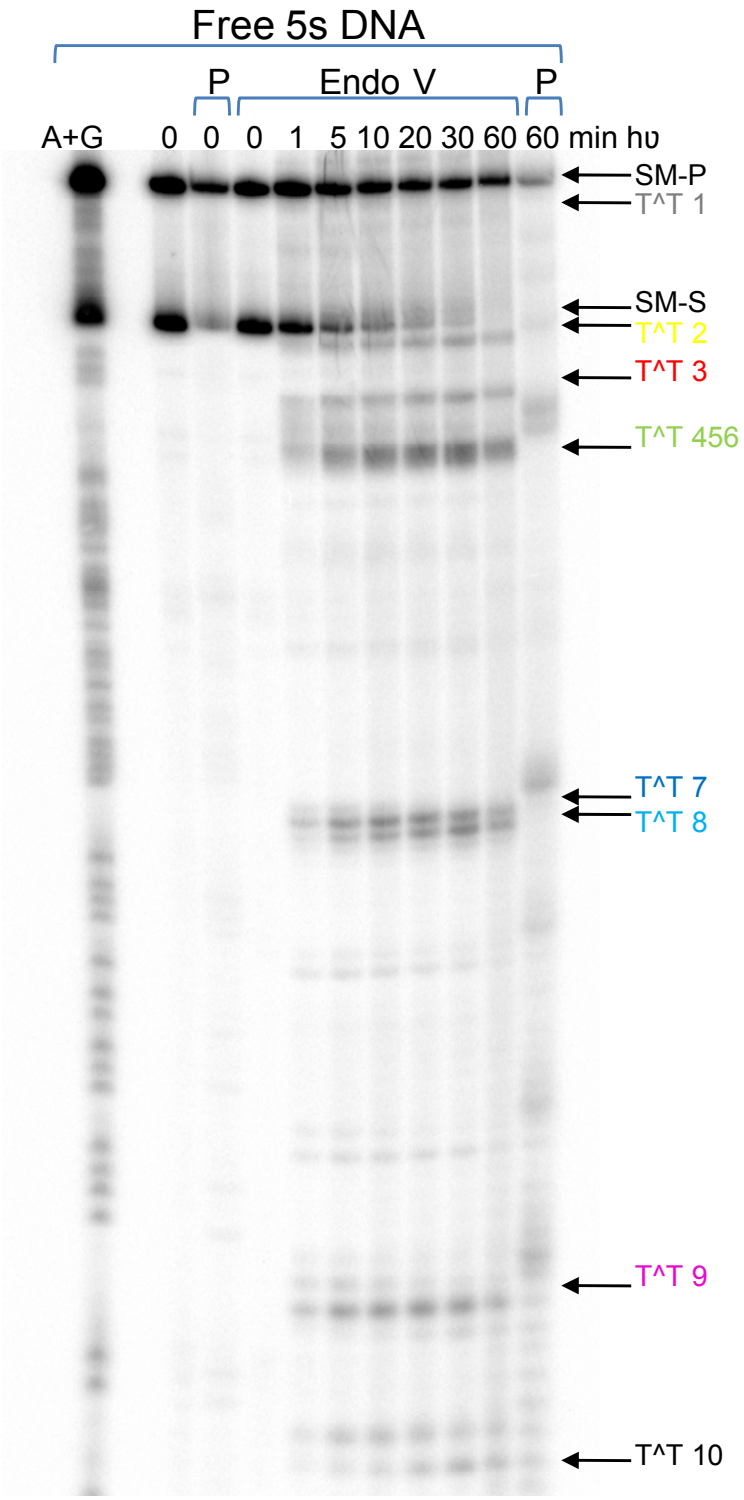

Figure 2.6: Autoradiogram of an 8 % denaturing PAGE gel showing T^T formation in free 5s DNA with increasing irradiation times upon treatment with endoV. A+G lane is Maxam-Gilbert sequencing reaction, P=piperidine, SM-P=starting material –primary band, SM-S=starting material – secondary band and T^T cleavage bands are color coded and numbered for reference.

The preliminary experiments gave a few additional crucial pieces of information, in addition to illustrating that the 60 minute time point needed to be excluded due to excess background cleavage. After 1 minute of irradiation there was a significant amount (10 %) of total T^T formation and by the 5 minute irradiation point there was 35 % of total T^T formation. These data suggest that shorter time points were necessary to determine the initial rates of T^T formation. The second was that the amount of total T^T formation levels off after 10 minutes (Figure I.1), suggesting that a photostationary state between T^T monomerization and T^T dimerization has been reached.

An increased number of time points between 0 and 10 minutes were tested in order to determine the initial rates of T^T formation. Figure 2.7 illustrates that the initial rates of T^T formation can be determined using data from 20 seconds to 10 minutes of irradiation time. The 10 second time point does not vary significantly from the 0 second time point. Therefore, all subsequent irradiations included 15, 30, and 45 second time points and were conducted to a maximum of 30 minutes. These shorter time points were necessary to extract initial rates and the time points greater than 10 minutes were needed to determine the photostationary quantities from gels.

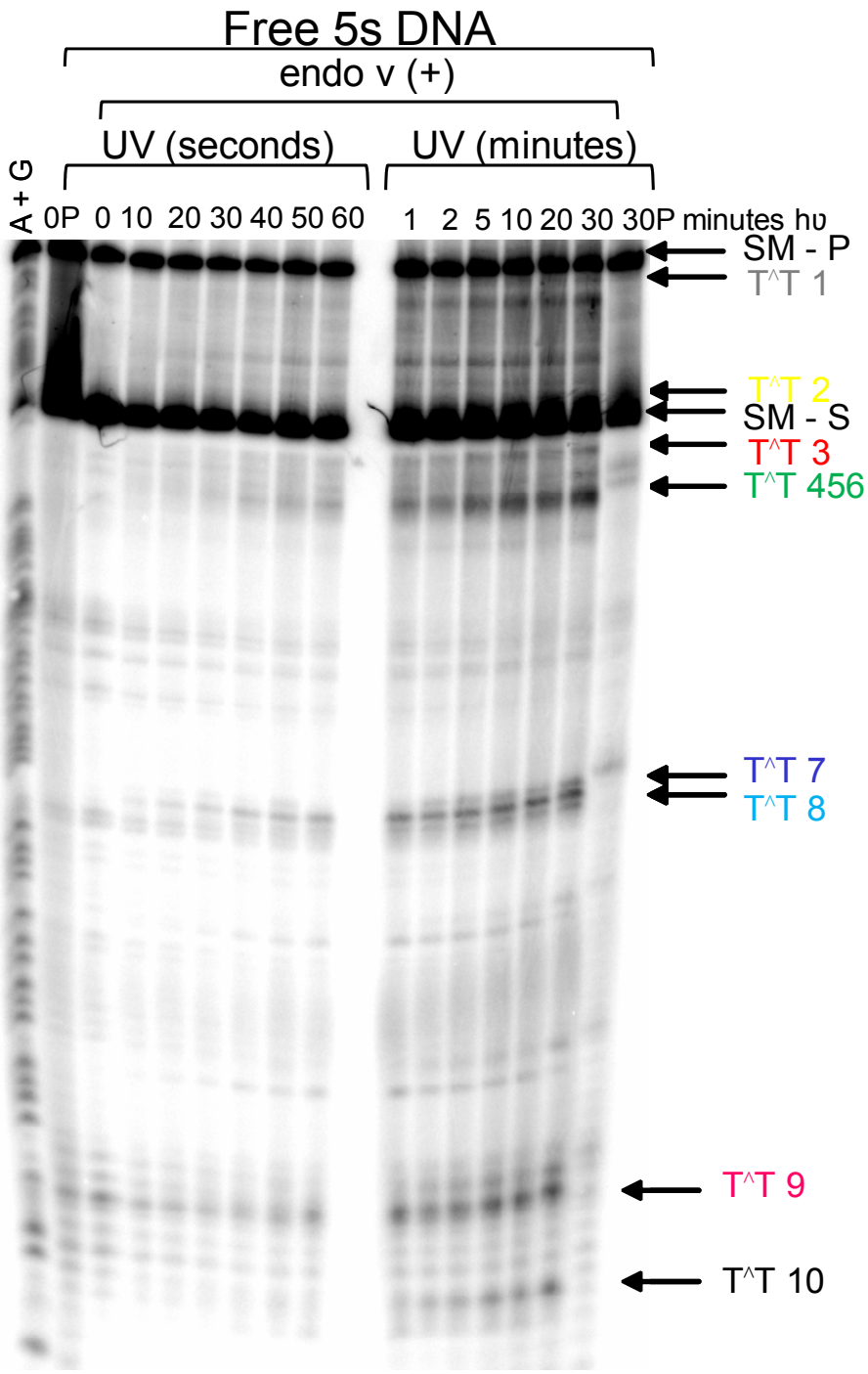

Figure 2.7: Autoradiogram of 8 % denaturing PAGE gel showing T^T formation in free 5s DNA with increasing irradiation times upon treatment with endoV. A+G lane is Maxam-Gilbert sequencing lane, P stands from hot piperidine treatment, SM-P is starting material primary band, SM-S is starting material secondary band and T^T are color coded and highlighted with arrows.

Before further studies were conducted it was necessary to determine the cause of the two starting material bands. The top band is attributed to be full length primary 5s DNA (SM-P in Figure 2.7) that is denatured and the bottom band is assumed to be a full length 5s DNA secondary structure (SM-S in Figure 2.7). Despite the fact that samples were denatured with 8 M urea loading buffer, heated to 90 °C and run on a denaturing page 7 M urea PAGE the second band was always present. M-fold calculations (Figure I.4) suggest that there is a stable secondary structure with a ΔG of -31 kcal/mol and a melting temperature of 69 °C.[159] The secondary structure of 5s RNA is documented in the literature and is well conserved between different classes of organisms.[160]

Exhaustive conditions were attempted to denature the secondary structure. This included using different types and combinations of denaturing loading buffers and gels (formamide as well as urea). Additionally, increased incubation at 90 °C and keeping the samples in a heating block until they were loaded onto the gels was also attempted. Finally, gels were run at the maximum wattage of 65 W in order to increase the running temperature in an attempt to ensure complete denaturation of 5s DNA during electrophoresis. All these efforts were unsuccessful at eliminating the secondary structure band as determined by presence of both bands on PAGE gels. Therefore experiments continued with the knowledge that it would be difficult to resolve T^T 1 due to its proximity to the starting material and T^T 2 due to its proximity with the secondary structure band.

The goal for this first set of experiments was to look at T^T formation in free 5s DNA, to obtain reproducible data, and determine time points for photostationary experiments. The data from seven to nine independent determinations have been compiled in the following graphs. The first graph (Figure 2.8) shows the amount of total T^T formation over time. Initial T^T formation appears to be linear for irradiation up to 10 minutes, with increased time (10 to 60 minutes) T^T formation appears to level off suggesting a photostationary state. The data was consistent with what was observed with preliminary reactions with 5s DNA. This suggests that the data was reproducible and 7 to 9 trials were performed to determine the error in the reaction conditions.

Analysis of the gel (Figure 2.7) shows that some of the T^T are not visualized or resolvable from one another. As mentioned previously, T^T 1 runs close to the SM-P band and T^T 2 runs close to the SM-S band, and therefore are not always resolvable e with endoV. T^T 3, 7, 8, 9, and 10 are easily quantifiable and T^T 4, 5, and 6 run together. Many attempts were made to resolve T^T 4, 5 and 6 by sequentially loading the samples on PAGE gel (run gel 30 – 60 minutes then load another lane and run normal time), but were unsuccessful (Figure I.5). As evident from the sequence, T^T 7 and 8 cannot form simultaneously because there are only three adjacent T's and two are needed to form a T^T. From the gel it is possible to see that T^T 7 forms more quickly than T^T 8, but from the sequence it was not evident why this occurs.

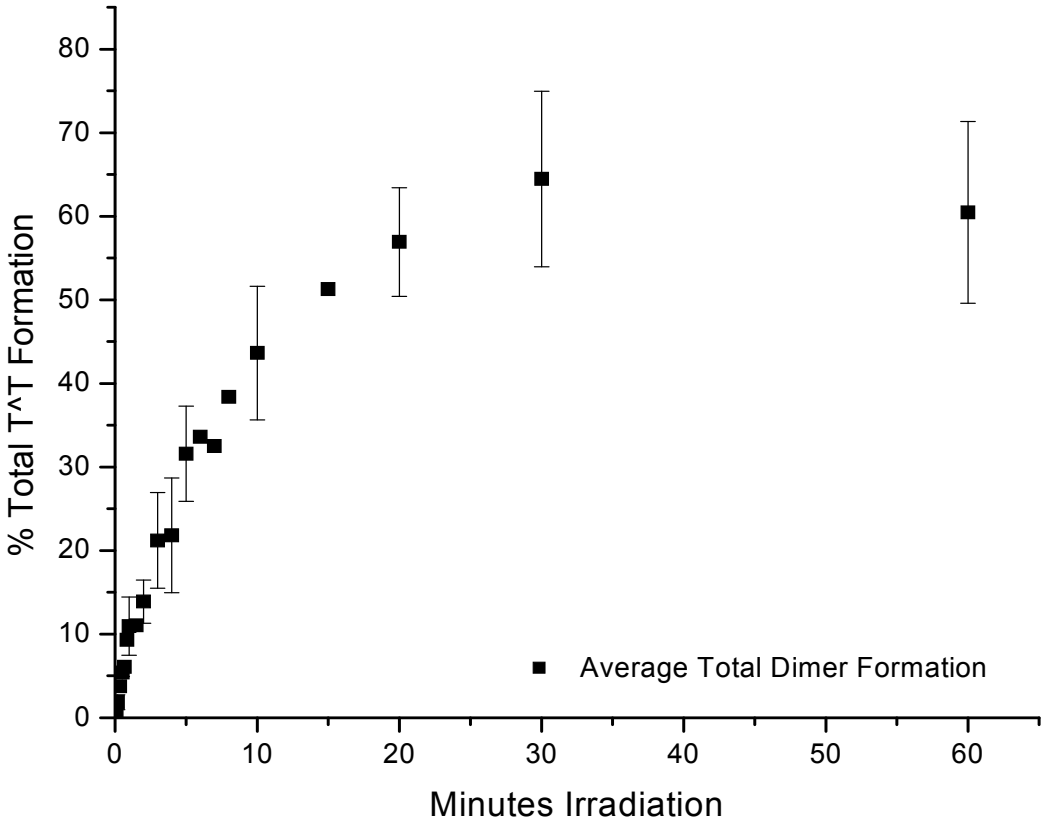

Figure 2.8: Total T^T formation in free 5s DNA. Yields were calculated from the total intensity of strand cleavage from T^T relative to total sample per time point as determined by denaturing 8 % gel electrophoresis. Each time point represents an average value from no less than 5 independent experiments and the indicated uncertainty represents the standard deviation from the average.

The second graph (Figure 2.9) illustrates the relative amount of individual T^T's. The photostationary formation of each individual T^T appears to be very similar and range between 4 – 8 %. The only exception being T^T 4, 5, 6 which is due to the fact that the calculation for T^T 4, 5, 6 is for the formation of three possible T^T. They are shown as one point because individual T^T points are unresolvable. As mentioned above, T^T 1 is not illustrated due to lack of detectability. While T^T 2 is illustrated on the graph, the earliest detection via endo V treatment is after 5 minutes. This is due to the decrease in starting material bands and increase in T^T bands, so the

determination of initial rates of T^T 2 formation were not possible using endo V. In order to obtain data from all T^T in 5s DNA sequence, it was necessary to use a technique that was able to resolve both T^T 1 and 2 from the starting material bands.

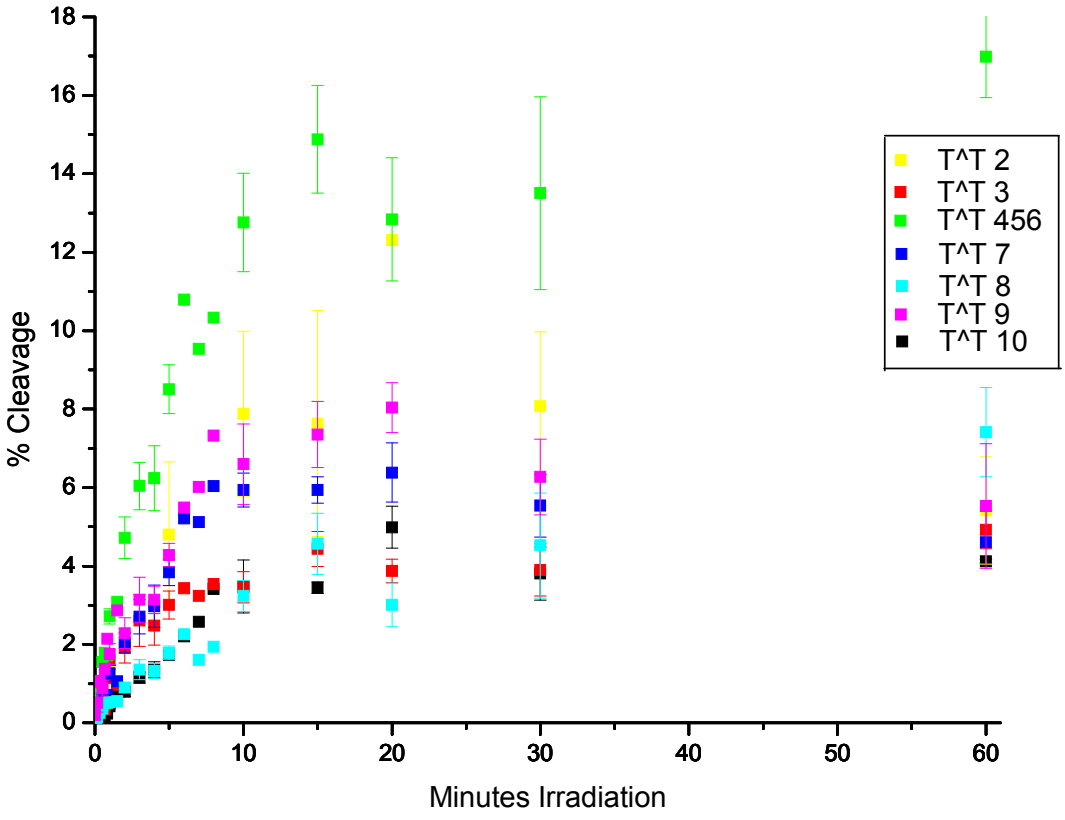

Figure 2.9: Percent individual T^T formation in free 5s DNA over time. Yields were calculated from the intensity of strand cleavage from each individual T^T relative to total sample per time point as determined by denaturing 8 % PAGE. Each time point represents an average value from no less than 5 independent experiments and the indicated uncertainty represents the standard deviation from the average.

While the endo V reaction is specific for cis-syn T^T, another method of T^T detection is cleavage by T4 Polymerase (T4 pol). Under the reaction conditions only the 3' – 5' exonuclease of the polymerase is active due to lack of deoxynucleotide triphospates (dNTP's).[161] Therefore, the nuclease removes nucleotides from the 3' end until it reaches a damage site that it is

unable to bypass. Undamaged DNA will be fully digested, while damaged DNA will remain intact after the site of damage. Figure 2.10 is a schematic comparison highlighting the differences between endoV and T4 pol.

Figure 2.10: Schematic comparison of endoV vs. T4pol cleavage. Red boxes represent sites of DNA damage.

Figure 2.11 illustrates T4pol treatment on irradiated 5s DNA. There are a few noticeable differences between the T4 pol and endoV treatment. The first difference was that there are more cleavage bands in the T4pol reaction due to lack of its specificity for only T^T. The extra bands were not characterized and, by location in 5s DNA sequence, photoproducts such as the 6-4, C^T or T^C dimers appear to form as mentioned in Chapter 1.

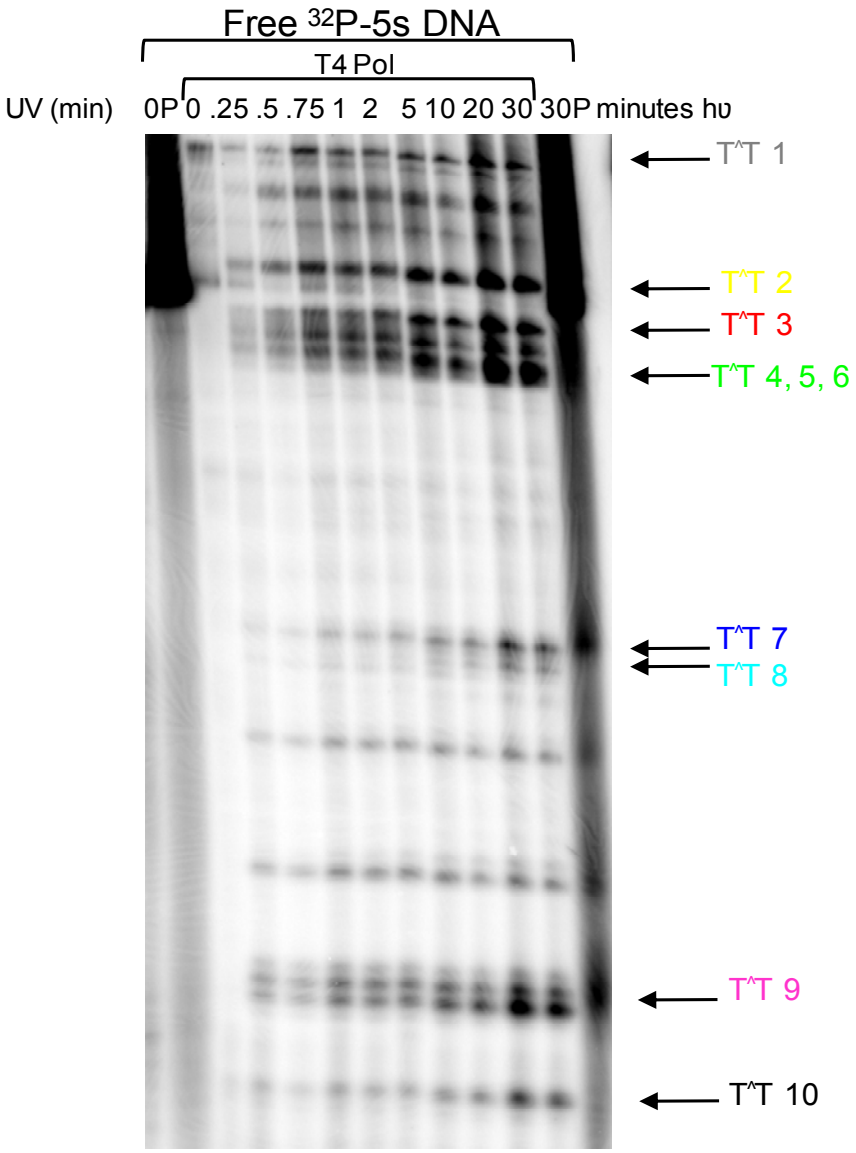

Figure 2.11: Autoradiogram of an 8 % denaturing PAGE gel showing cleavage products from T4 pol treatment of free 5s DNA after photoirradiation. Lanes are normalized to 10 kdpm to allow for comparison between lanes. P = piperidine treatment.

The second difference between endoV and T4 pol was that upon T4 pol treatment T^T 1 is separate from the 5s primary structure (SM-P) band. This is mainly due to the fact that a majority of the starting material was digested because there was no damage present. Finally, the secondary structure band (SM-S) has been eliminated. Therefore, T^T 2 can be

identified. Again this was due to the fact that the undamaged product is fully digested by the T4 pol. Figure 2.11 illustrates that T4 pol is a complementary method for T^T visualization and Figure 2.12 shows the amounts of individual T^T cleavage by T4 pol. The range of individual T^T formation at the photostationary state varies between 1 – 14 % which is larger than the range of 4 % – 13 % identified with endoV. However, the majority of photostationary levels between T^T formation in endoV vs. T4 pol is within experimental error of one another (Figure I.6 thru Figure I.14). The only notable differences are the increase in T^T 3 and the decrease in T^T 7 and T^T 8 with T4 pol treatment, however it is not apparent what causes these variations

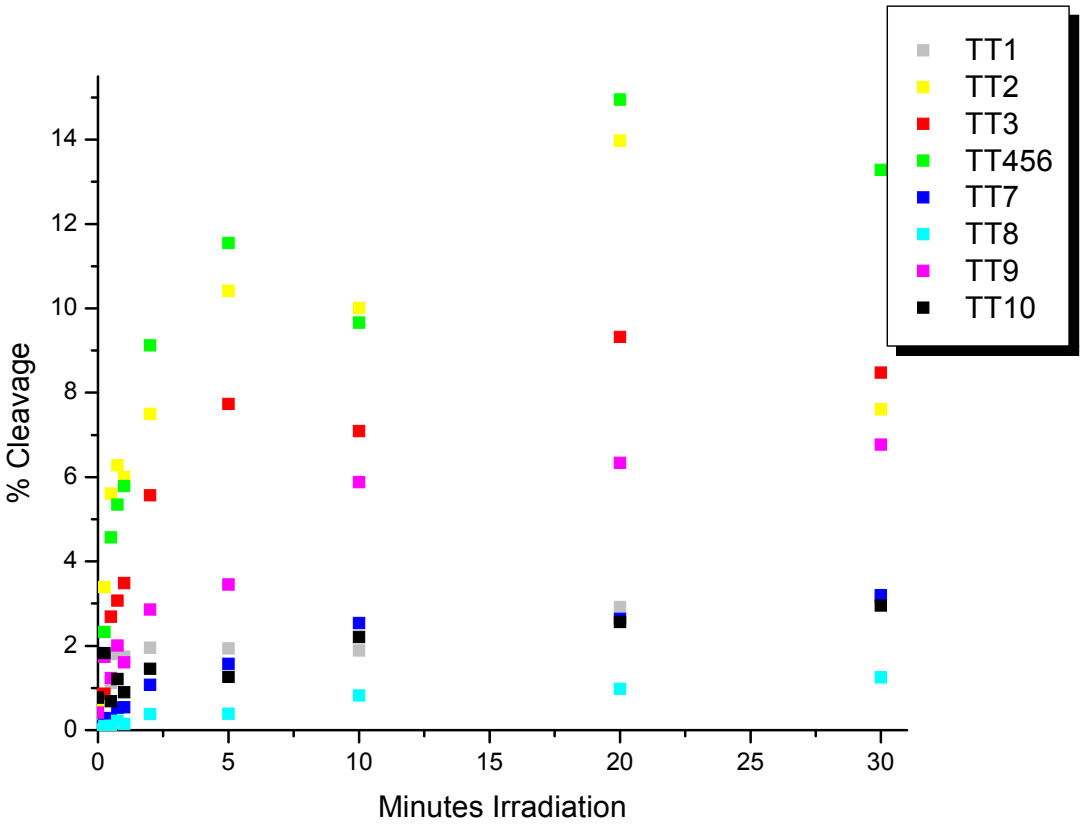

Figure 2.12: Individual T^T cleavage by T4 pol in photoirradiated 5s DNA. Yields for percent cleavage were calculated from the individual intensity of each T^T with respect to the total intensity per sample as determined by 8 % denaturing gel electrophoresis.

Before studies on reconstituted DNA were begun, an important control reaction was necessary to illustrate that an excess of nucleosome protein in solution did not affect overall T^T formation. The reconstitution of 5s DNA involves a large excess of NCP and the comparison of T^T accumulation in free vs. NCP reconstituted DNA would be more complex if nucleosomes free in solution affected overall T^T formation. The presence of NCP in solution may affect the photon absorbance of the free 5s DNA causing either a diminishment or enhancement of T^T formation based on the reaction occurring. Photochemistry experiments were conducted on free 5s DNA and free 5s DNA with a 1000 fold molar excess of NCP present in solution in order to compare the samples and these experiment was repeated 5 times. Figure 2.13 illustrates that NCP in solution appear to slightly enhance T^T formation in the photostationary state, for a representative PAGE gel please see Appendix Figure I.15. Although there was a slight enhancement of the average total T^T formation in the sample with NCP in solution, the difference was not significant when the error bars were taken into account. Figure 2.14 is an enlargement of the 0 to 5 minute region of the graph (Figure 2.13) and is used to illustrate that in this region there is no difference in the total amount of T^T formation. Since NCP in solution do not affect T^T formation, NCP concentration does not have to be normalized between samples in order to compare results and experiments on reconstituted DNA can begin.

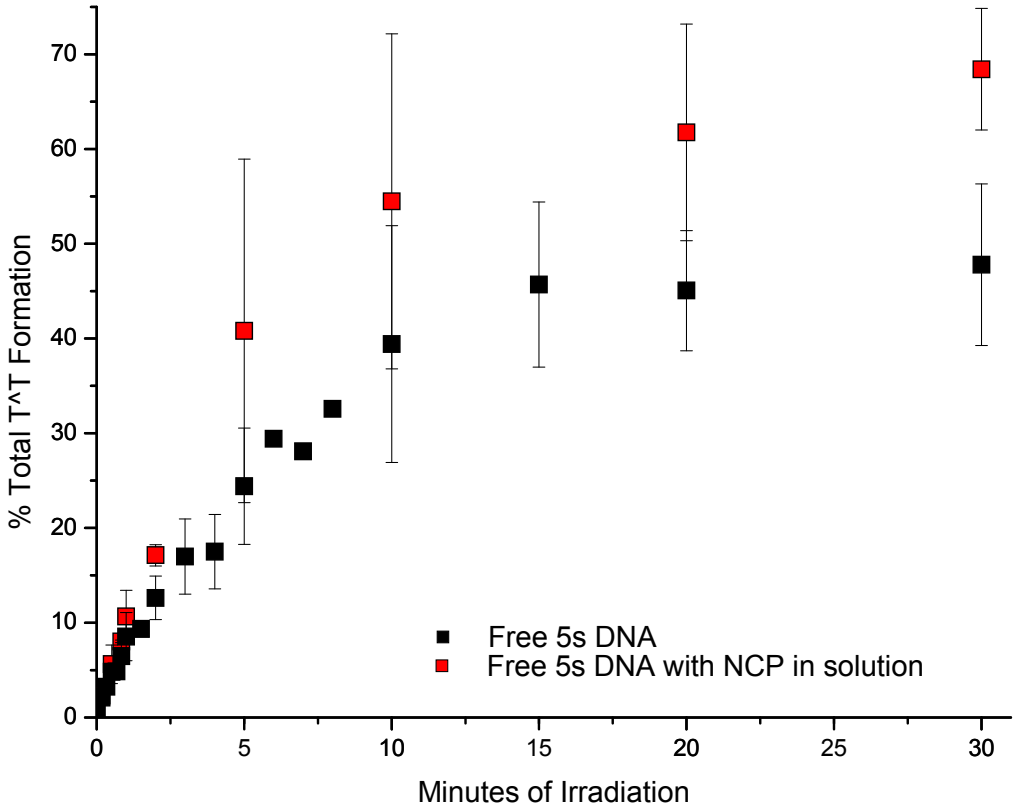

Figure 2.13: Total T^T formation in free 5s DNA and 5s DNA with NCP in solution. Yields for percent cleavage were calculated from the total intensity of T^T with respect to the total intensity per sample as determined by 8 % denaturing gel electrophoresis. Black squares represent photoirradiation of free 5s DNA and red squares represent photoirradiation of free 5s DNA with 1000 fold molar excess of NCP in solution. Each time point represents an average value from no less than 5 independent experiments and the indicated uncertainty represents the standard deviation from the average.

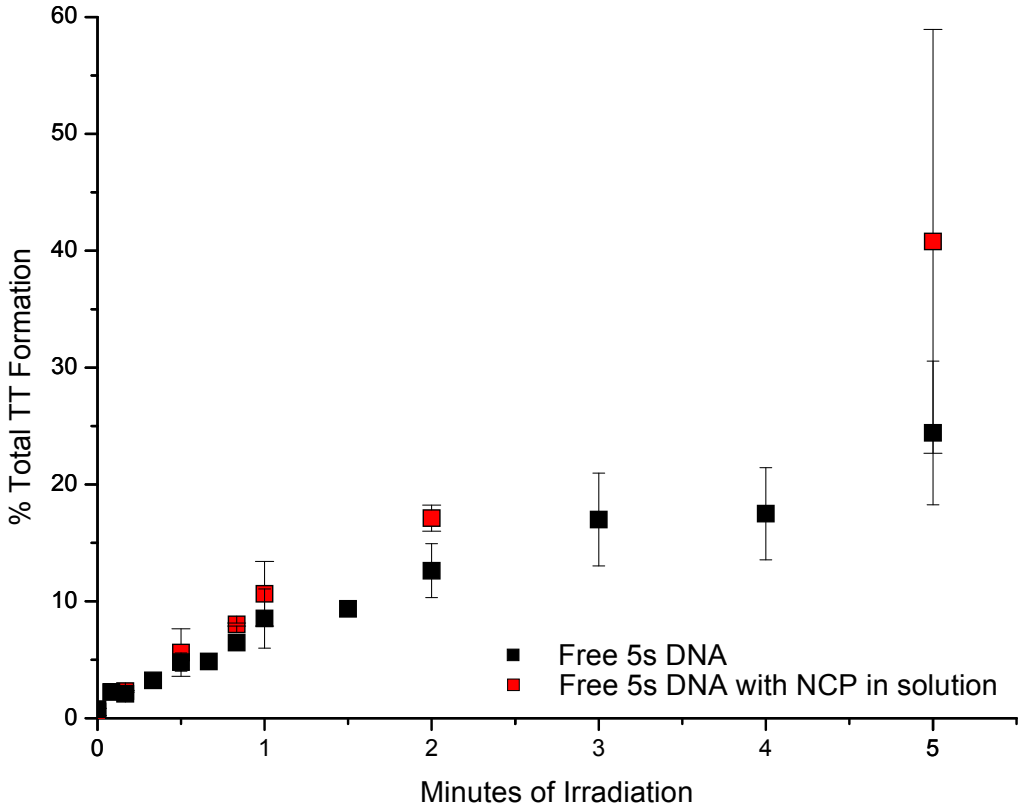

Figure 2.14: Total T^T formation in Free 5s DNA and Free 5s DNA with NCP in solution with focus on the initial rates of T^T formation. Yields for percent cleavage were calculated from the total intensity of T^T with respect to the total intensity per sample as determined by 8 % denaturing gel electrophoresis. Black squares represent photoirradiation of free 5s DNA and red squares represent photoirradiation of free 5s DNA with 1000 fold molar excess of NCP in solution. Each time point represents an average value from no less than 5 independent experiments and the indicated uncertainty represents the standard deviation from the average.

Photochemistry of Reconstituted 5s DNA.

Chicken blood nuclei are a common source of NCP. They provide large quantities of NCP's which is important because reconstitution protocols require a large excess of NCP present in solution. There are many NCP preparation protocols that are well cited in the literature.[153,162,163] However, obtaining NCP using these procedures proved to be problematic due to

variations in blood from the supplier. These variations include storage and handling of the blood after removal from the chicken and even the type of chicken used to obtain the blood can affect purification. Initial attempts at purification were unsuccessful due to low yields of soluble protein and thus did not provide any usable NCP. A variety of experimental conditions (a few of which are outlined below) were tested in order to determine the cause of the low yielding NCP purifications.

All solutions for the NCP preparation were freshly prepared, autoclaved, and checked to ensure the correct pH. However the NCP preparation was very low yielding and therefore unsuccessful, as determined by lack of histone protein bands in SDS PAGE analysis. By SDS PAGE all the protein appeared to be in the pellet and not the soluble portion of the sample (Figure 2.15). NCP would not be present in the supernatant and would remain in the pellet without digestion by micrococcal nuclease (MN). The MN digests the nuclear envelope to release the chromatin and further digests the chromatin to give individual nucleosomes.[164-166] Fresh micrococcal nuclease (MN) was purchased and the sample pellet from the previous NCP preparation was redigested with MN. Again, the preparation was unsuccessful and no protein bands were visible by SDS page analysis of the supernatant. The MN sample was tested and determined to be active because it digested plasmid DNA. The final variable tested was the concentration of detergent (NP-40). Various NP-40 concentrations (0.01 – 1 %) and incubation times (30 – 120 minutes) were tested. The proper

concentration was determined by running a NCP purification and aliquoting the pellet into a few different sample tubes and varying the NP-40 concentration in each sample. Once the correct concentration was determined this concentration was used for the remainder of the blood in the shipment. Each blood shipment needed to be individually tested as described above with various detergent concentrations (.01 – 1 %) in order to determine correct concentration for successful NCP preparation.

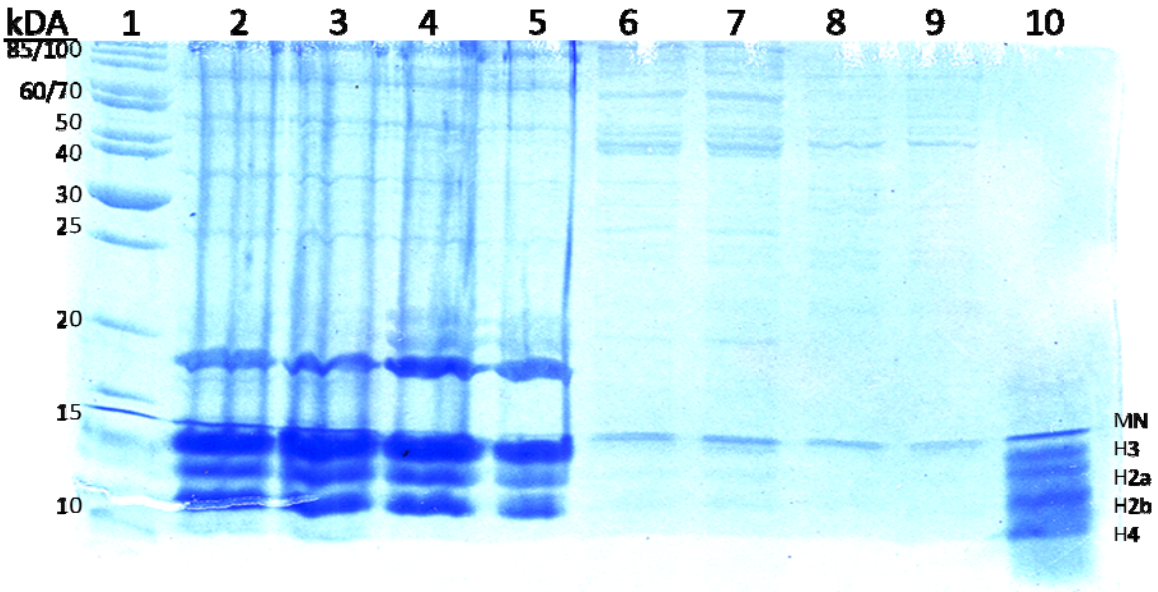

Figure 2.15: SDS PAGE gel showing aliquots from various NCP purification steps. 10 µL sample were loaded into each well. Protein ladder (Lane 1). Pellet after MN treatment (Lane 2,3), pellet after NP-40 treatment (Lane 5,6), supernatant after a series of washes and certrifugation step (Lane 6,7), NCP before resin (Lane 8), NCP before dialysis (Lane 9), NCP control (Lane 10).

The gel below (Figure 2.16) shows fractions from the various steps of a successful NCP purification. All four bands need to be of equal concentration to ensure that the NCP was intact and that there was no protein degradation. SDS PAGE band assignments of individual histone proteins were made

based on molecular weight. NCP can be safely stored for up to 4 months at 4 ˚C until reconstitution.

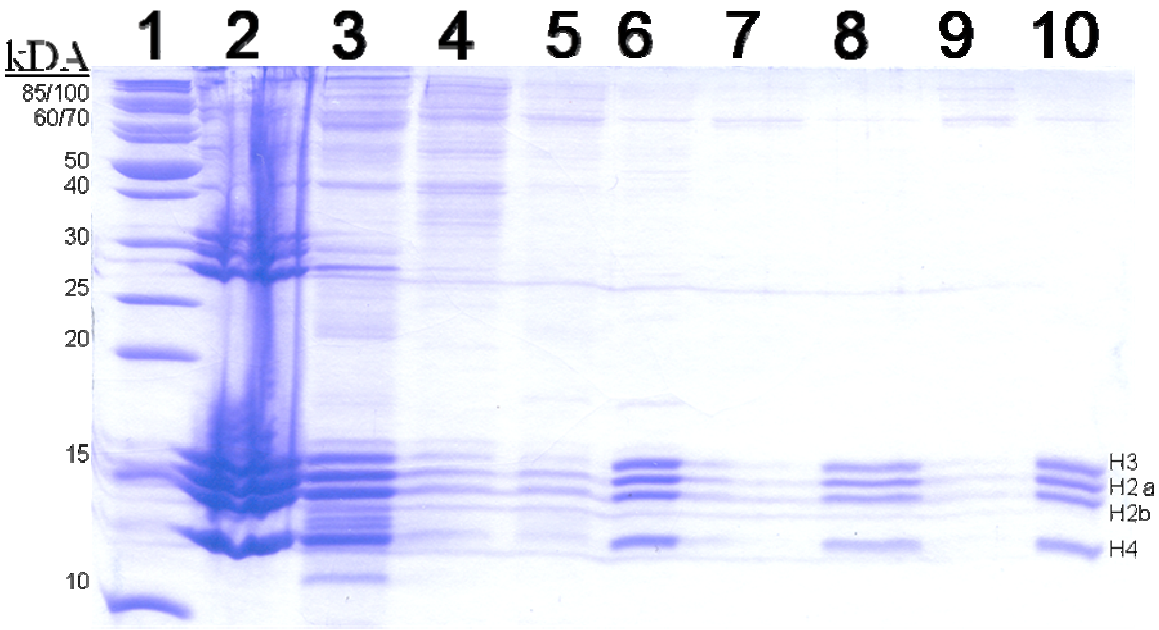

Figure 2.16: Discontinuous SDS page gel showing aliquots from the various purification steps involved in purification of NCP from chicken blood nuclei. 10 µL of sample were loaded in to each well. Protein ladder (Lane 1), pellet after micrococcal nuclease treatment and NP-40 treatment (Lane 2), supernatant after a series of washes and centrifugation steps (Lane 3, 4, 5), histones before resin tretment (Lane 6), empty (Lane 7), histones before dialysis (Lane 8), empty (Lane 9), final product (Lane 10). Each band in lane 10 corresponds to one of the four histone proteins as labeled and in a successful nucleosome preparation each band is of equal intensity.

A variety of different proportions of DNA to nucleosome were tested to determine optimal conditions for high reconstitution efficiency. In general the reconstitution was conducted by initial dialysis at high salt concentrations to disrupt DNA – histone interactions allowing for exchange with the more stable 5s DNA positioning sequence. Followed by dialysis with a decreasing salt gradient in order to return to biological conditions and provide stable NCP's. Reconstitution efficiency was determined by native PAGE gel electrophoresis as shown in Figure 2.17, with maximum reconstitution at ~ 75 %. It was determined that DNA needs to be added in a ratio of 1 : 1000 mole with

respect to nucleosome for best results. Decreased ratio leads to exponential decrease in the amount of reconstituted DNA and an increased ratio does not increase the percentage of reconstitution. For optimal results, reconstitution efficiency needs to be increased to > 95 %. This high degree of reconstitution efficiency was necessary in order to decrease the chance that the differences in T^T formation will be detectable above background from the unreconstituted sample in the experiment. Increased efficiency of reconstitution will decrease experimental background.

Figure 2.17: Autoradiogram of 8 % native PAGE gel highlighting reconstitution efficiency. Lanes each contain 10 kdpm of sample. Free 5s DNA (Lane 1), empty (Lane 2), NCP reconstitution time zero (Lane 3), NCP reconstitution before dialysis (Lane 4), NCP reconstitution after dialysis (Lane 5).

Reconstituted DNA (70 – 80 % purity) was irradiated in the same manner as free DNA. Initial time points from 0 to 30 minutes were chosen based on experiments with free DNA. Figure 2.18 is an example of a gel with both free and NCP reconstituted 5s DNA samples run simultaneously. This allowed for direct comparison between time points because the amount of radioactivity in the lanes was normalized to 10 kdpm per lane.

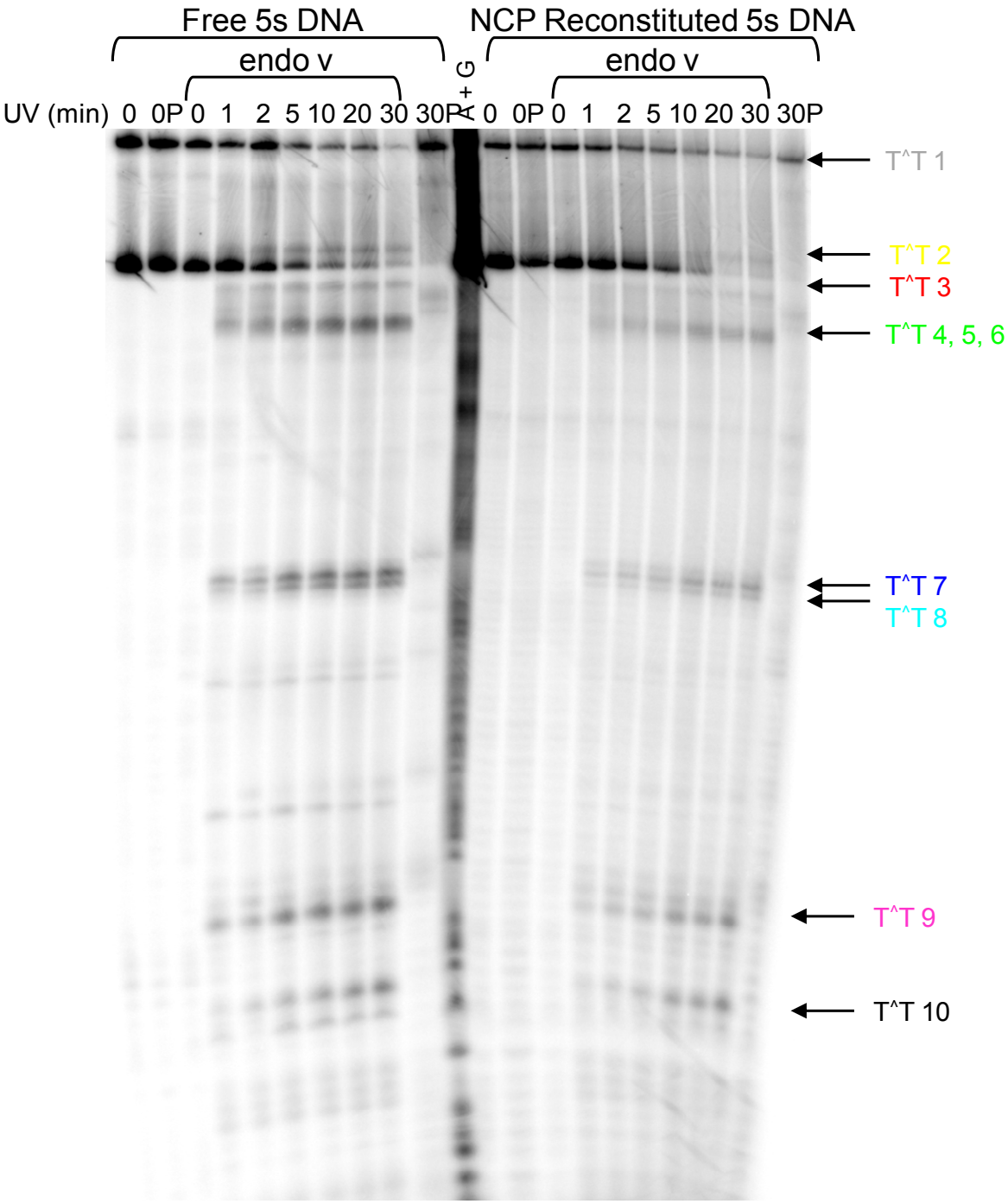

Figure 2.18: Autoradiogram of 8 % denaturing PAGE gels showing T^T cleavage in free vs. NCP reconstituted 5s DNA upon treatment with endoV with increasing irradiation times. Piperidine treatment labeled as P, and Maxam-Gilbert sequencing lane labeled as A+G. The lanes are normalized to 100 kdpm per lane to allow for direct comparison between free 5s and NCP reconstituted 5s DNA T^T are numbered and highlighted with arrows.

The most noticeable difference between the two samples was that the reconstituted sample appears to have a decreased amount of T^T formation. T^T 2 and 3 in the reconstituted samples, at first glance, do not seem to be discernable from background. However, upon analysis there was no discernable difference between the formation of any of the resolvable T^T's. Figure 2.19 illustrates the overall amount of T^T formation in free 5s DNA, free 5s DNA with NCP in solution and NCP reconstituted 5s DNA

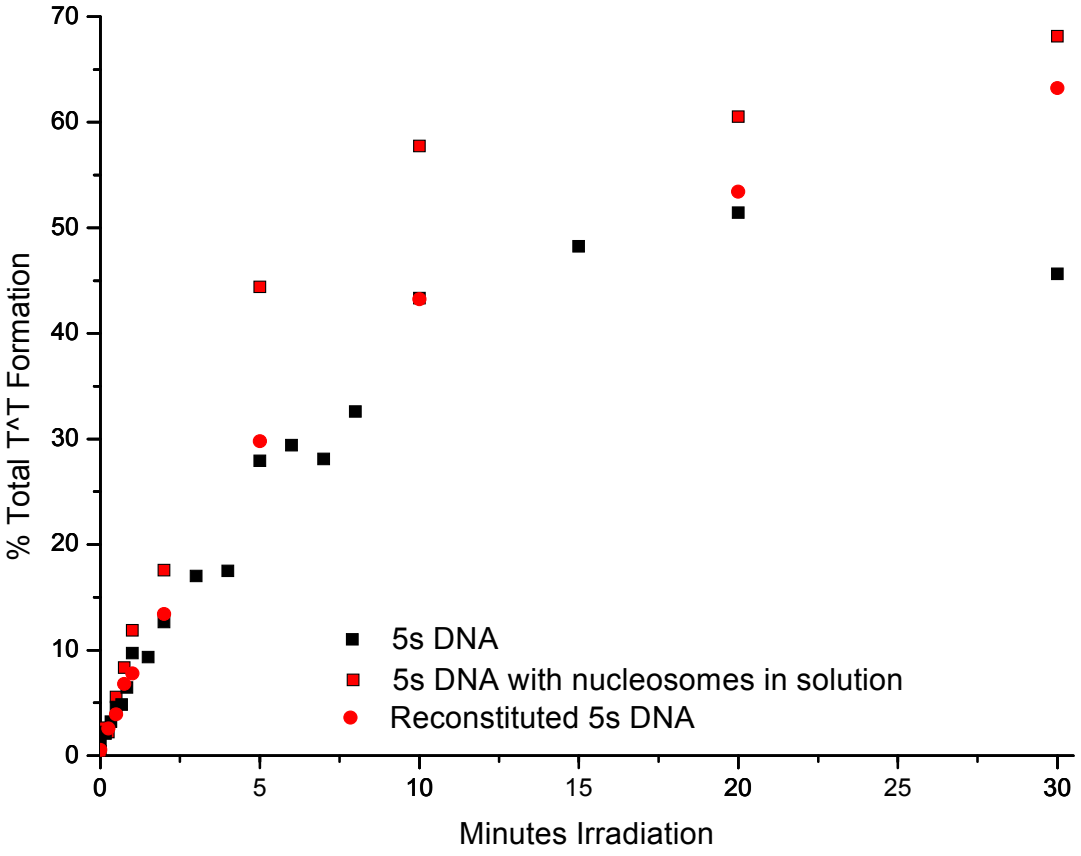

Figure 2.19: Total percent T^T formation in free vs. NCP reconstituted 5s DNA. Yields for percent total cleavage were calculated from the total intensity of T^T with respect to the total intensity per sample as determined by 8 % denaturing gel electrophoresis. Each time point represents an average value from no less than 3 independent experiments where the black squares represent photoirradiation of free 5s DNA, the red squares represent photoirradiation of free 5s DNA with 1000 fold molar excess of NCP in solution, and the red circles represent NCP reconstituted 5s DNA.

Each T^T was individually analyzed (Figure I.16 thru Figure I.22) and formation of each T^T in free versus reconstituted 5s DNA was within experimental error of each other. T^T 2, 3, and 6 have different orientation with respect to the nucleosome core, when compared to the other T^T (Figure 2.4). The T^T 2, 3, and 6 were expected to give decreased distributions of T^T formation due to the backbone of the DNA being positioned away from the NCP at these locations, however this was not the case. T^T 2 is not resolvable from background in the reconstituted sample and T^T 3 does not show decreased formation in comparison to free DNA sample. T^T 6 cannot be resolved from T^T 4 and 5, but the overall amount of T^T 4, 5, and 6 formation does not change, which suggests that formation of T^T 6 did not change. Finally, comparison of total T^T formation in free and reconstituted DNA shows little difference in the samples (Figure 2.19).

Summary and Conclusion – 5s DNA Sequence

No great difference in T^T formation between free 5s DNA and NCP reconstituted 5s DNA could be detected. These findings can be attributed to two things, the first was that the majority of detectable T^T on 5s DNA have similar orientations around the NCP (Figure 2.4) and the second was that only 75 % of the DNA was reconstituted. Differences in T^T formation may not be resolvable over background thus, research is needed with DNA that has a higher percent reconstitution to reduce the amount of overall error in the calculations. Higher reconstitution efficiency will help determine if the lack of

difference in T^T accumulation was due to reconstitution efficiency or was a result of sequence content. Without a significant difference between T^T formation in free and NCP reconstituted 5s DNA the time required for redistribution of T^T could not be determined.

Widom 601 Nucleosome Positioning Sequence

Due to the lack of observable difference between T^T formation in free and reconstituted 5s DNA, studies began with the Widom 601 (W601) nucleosome positioning sequence (NPS). As shown in Table 2.1[167] the W601 NPS binds more tightly to NCP's than with 5s DNA. By utilizing the tighter binding of this DNA sequence it may be possible to achieve higher reconstitution efficiency and lower background from unreconstituted DNA sample. The W601 sequence was obtained from the Widom lab as an insert into the pGEM-3z vector system (Figure I.23).

Table 2.1: Binding affinity of Widom lab DNA sequences vs. 5s DNA.[167-169]

Clone no.	ΔΔG (kcal mol $^{-1}$) Relative to 5S DNA
601	-2.9 ± 0.33
603	-2.7 ± 0.31
607	-2.5 ± .032
611	-2.5 ± .032
612	-2.1 ± 0.48
613	-2.3 ± 0.31
618	-2.3 ± 0.31

Figure 2.20 illustrates the sequence of the W601 NPS. The positioning sequence consists of 147 base pair dsDNA with 6 possible sites for T^T

formation as highlighted. The dyad axis of symmetry is shown by an arrow. The relative position of the T^T with respect to the backbone was also determined to ensure that T^T would be in varying positions for T^T studies. The different orientations should give different rates of T^T formation in NCP reconstituted vs. free W601 DNA. Since there are varying T^T positions, the next step is to use PCR to radiolabel the W601 insert from the plasmid.

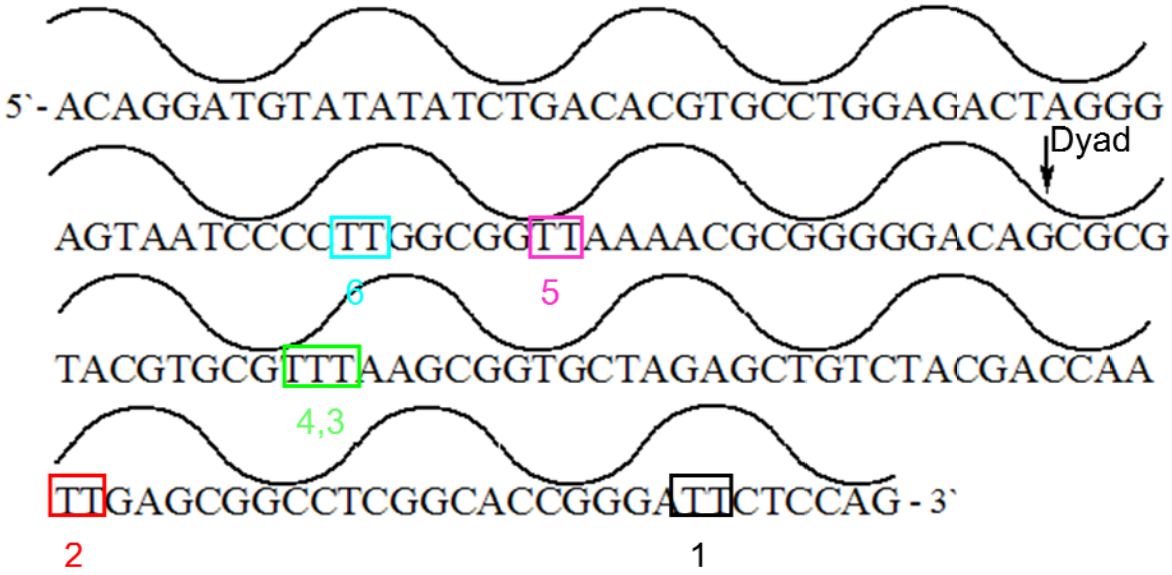

Figure 2.20: W601 NPS with sites of possible T^T formation highlighted and numbered. As with the 5s DNA, the valleys indicate DNA backbone towards the NCP and the hills indicate backbone away from NCP. T^T 1 and T^T 6 appear to have different orientations with respect to the NCP as compared with T^T 2 – 5.

The 5′ radiolabeled W601 was irradiated from 0 – 30 minutes and the T^T cleavage bands were visualized using gel electrophoresis and autoradiography (Figure 2.21). T^T 1 and 2 were not individually resolvable using endoV. T^T 1 is only 6 base pairs from the radiolabeled 5′ end therefore it runs close to the starting material band which is why it is hard to detect. However, it is not evident why T^T 2 does not appear as a cleavage band. One possible explanation is that irradiation times are too long, so

multiple T^T are forming in each strand. This would cause a greater increase in the T^T further down in the sequence and a reduction in T^T closer to the 3′ end. In contrast with T^T formation in 5s DNA, T^T formation in W601 is not detectable in time points less than 2 minutes. Another possible explanation is that T^T does not form at position 2 in the sequence. Since there are other T^T in the W601 sequence with NCP orientations similar to T^T 2 band, the fact this band is not resolvable is a relatively minor issue. The lack of T^T 2 formation can be focused on once photochemistry experiments were underway, NCP preparation experiments were conducted in the interim.

As mentioned earlier in this chapter, the NCP preparation proved to be problematic. Numerous attempts were made to purify intact histone octamer, but were unsuccessful. In addition to the preparation of NCP's from whole and pooled chicken blood, an attempt was made to form the octameric histone core using lyophilized calf histones. While this approach,provided viable NCP's as determined by SDS PAGE gel electrophoresis, the NCP's did not prove to be stable for long term storage. The samples were degraded upon storage for one month in 50 % glycerol at – 20 °C, as determined by SDS PAGE analysis. At this point it was decided that the most logical, time and cost effective approach was to collaborate with another laboratory that was using W601 reconstituted NCP's for their experiments.

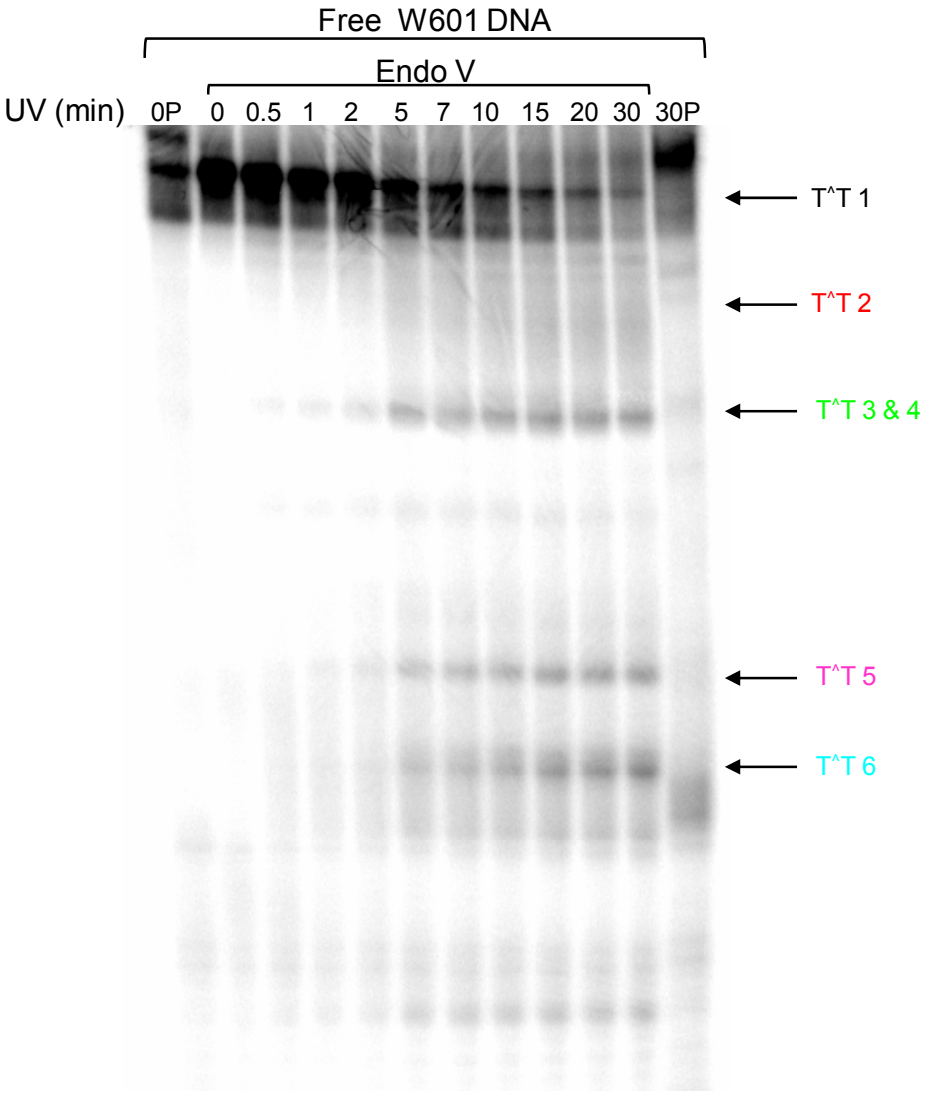

Figure 2.21: Autoradiogram of 8 % denaturing PAGE gel showing T^T cleavage in free of W601 upon cleavage with endoV with increasing irradiation times. T^T are numbered and highlighted with arrows. The lanes are normalized (100 kdpm) to allow for direct comparison between irradiation time points.

Luckily, we were able to contact and collaborate with Dr. William Davis at Washington State University. They provided 5'-^{32}P-labeled and reconstituted W601 for the remaining experiments. Additionally, they provided a modified free dsW601 which is 162 bp in length and was produced by PCR using a W601 containing plasmid. The sequence differs from the one

used previously in that one strand was modified by a C5-amino link (Figure 2.22). This amine modification allowed for select radiolabeling of the complementary strand of the dsDNA. An added bonus to this modification was its extension by a few base pairs to the end of the DNA strand which moves T^T 1 further from the 3' end giving a greater chance that it will be resolved from the starting material by denaturing gel electrophoresis.

NH_2-$(CH_2)_5$-P-5'-TAT ACG CGG CCG CC<u>C</u> TGG AGA ATC CCG GTG CCG AGG

CCG CTC AAT TGG TCG TAG ACA GCT CTA GCA CCG CTT AAA CGC ACG TAC

GCG <u>C</u>TG TCC CCC GCG TTT TAA CCG CCA AGG GGA TTA CTC CCT AGT

CTC CAG GCA CGT GTC AGA TAT ATA CAT CCT G<u>T</u>G-3'

Figure 2.22: W601 NPS DNA sequence obtained from the laboratory of Dr. William Davis, WSU. First underlined C (from 5'-end) = residue at NCP entrance, Second underlined C = residue at dyad axis of reconstituted NCPs, Underlined T = residue at exit of NCP. The complementary strand (Figure 2.18) is radiolabeled for photochemistry experiments.

Before photochemistry experiments were conducted it was necessary to determine that the sample was still fully reconstituted W601 after the shipment and that the sample irradiation did not affect the percent reconstitution. Autoradiogram anaylsis of Native PAGE (Figure I.24) of free vs. NCP reconstituted W601 shows that the sample is > 99 % reconstituted before and after 30 minutes of photochemistry under the same conditions used for all the photochemistry experiments. Therefore, photochemistry experiments can begin without further hesitation.

Since the reconstituted W601 samples were radiolabeled prior to shipment, the first experiments were conducted on the reconstituted samples.

Initially samples were irradiated between 0 through 30 minutes as previously described for the free 5s DNA and the 147bp W601. After analysis two things were apparent. The first was that the sample was not very radioactive therefore samples would have to be exposed on the phosphorimaging screens for 5 – 7 days before analysis. The second was that even after only 15 second irradiation times, the majority of the DNA had T^T damage. In fact, after 1 minute there is so much damage to the DNA the amount of T^T decreases and after 10 minutes there are no discernable T^T bands. Figure 2.23 illustrates that after 1 minute the overall amount of T^T formation decreases and by 10 minutes approximately 90 % of the sample was decomposed. The same effect was seen for samples of free W601 that was irradiated.

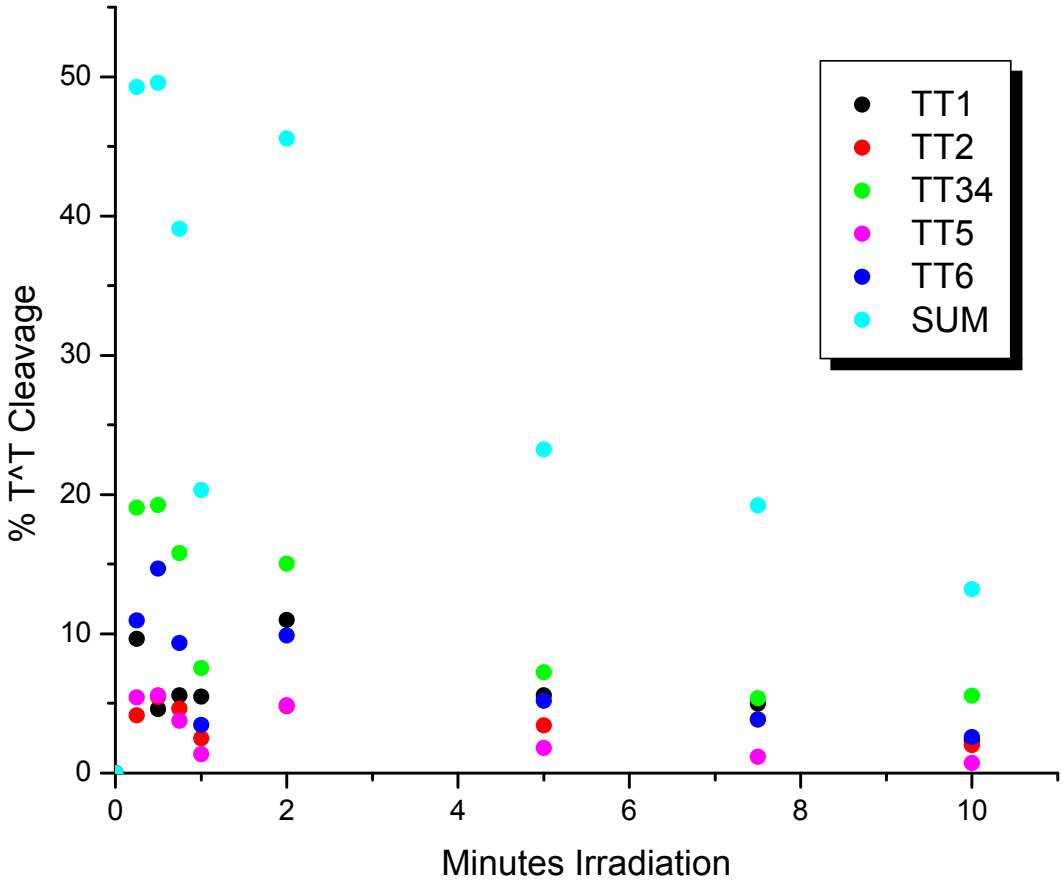

Figure 2.23: Individual and total percent T^T formation in NCP reconstituted W601 DNA as determined by cleavage with EndoV. Samples were irradiated at 10 cm pen height and yields for percent T^T cleavage were calculated from the total intensity of T^T with respect to the total intensity per sample as determined by 8 % denaturing gel electrophoresis.

The pen lamp height was increased to 30 cm in order to decrease the intensity of the light on the sample. Figure 2.24 illustrates that increasing the distance between the samples and the light source does diminish the rate of T^T formation. T^T formation appears to increase until 20 minutes and then decrease by 30 minutes. This decrease was due to multiple sites of T^T and other damage formation on each DNA strand. Therefore future irradiation times did not exceed 20 minutes and experiments on the free W601sequence could continue.

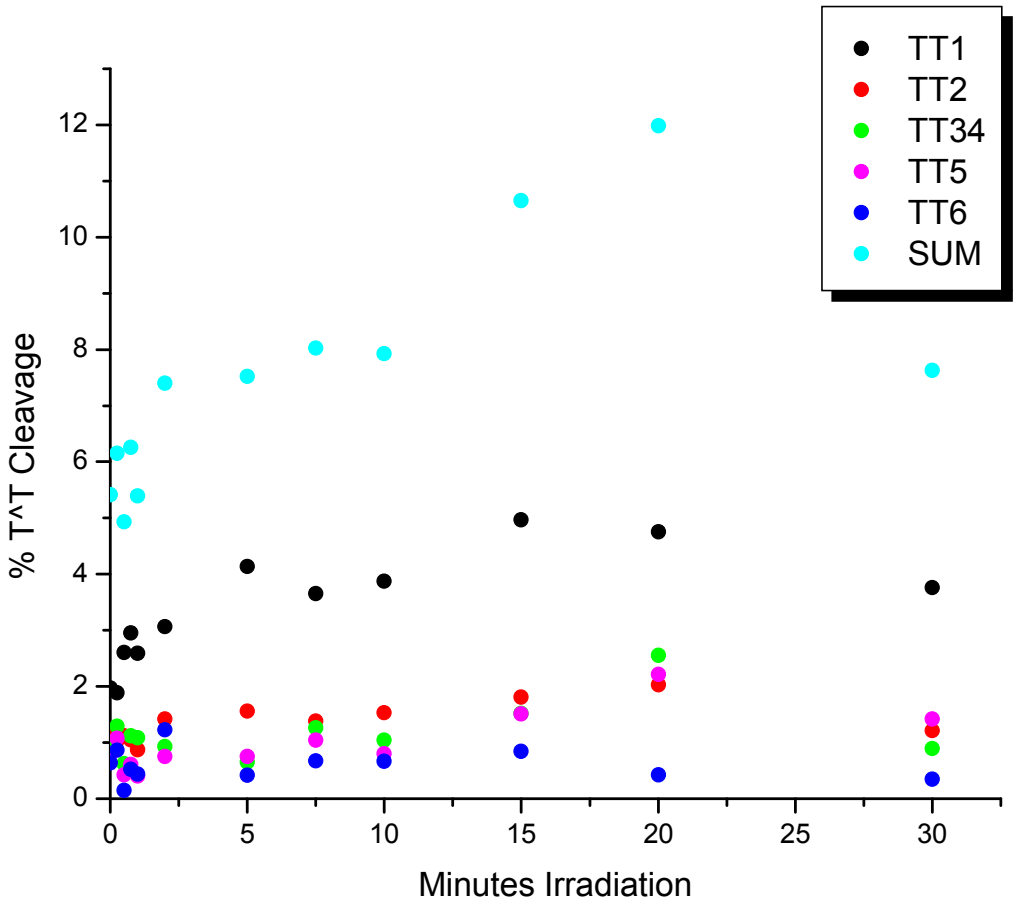

Figure 2.24: Individual and total percent T^T formation in NCP reconstituted W601 DNA as determined by cleavage with EndoV. Samples were irradiated at 30 cm pen height and yields for percent T^T cleavage were calculated from the total intensity of T^T with respect to the total intensity per sample as determined by 8 % denaturing gel electrophoresis.

While increasing the distance between the lamp and the sample decreased the amount of photoproduct formation in the reconstituted sample, the same effect was not seen for the free W601 DNA sample. Figure 2.25 illustrates that varying the pen lamp height did not affect the amount of photoproduct formation and after 10 minutes > 70 % of the starting material was consumed. These results suggest that the irradiation times and lamp intensity needs to be decreased further in order to obtain initial rate data from the free W601 experiments. Before multiple experiments were conducted to

address the differences in photoproduct formation, which have not been observed in previous experiments, it was decided to compare the photostationary states of the T^T in free vs. reconstituted W601. While the initial rates of T^T formation is of interest, a difference in T^T formation due to conformation should be detectable in the photostationary region.

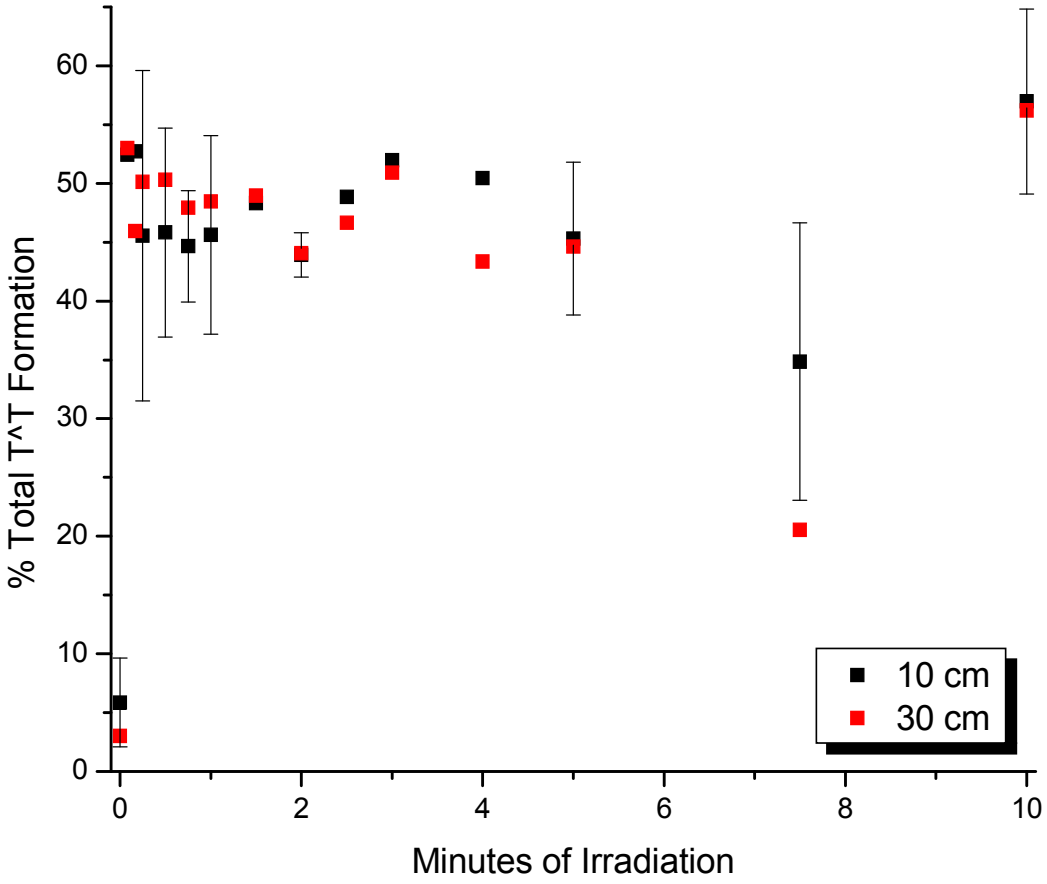

Figure 2.25: Total percent T^T formation in free W601 as detected by endoV treatment. Samples were irradiated at 10 cm (black squares) and 30 cm (red squares) pen height and yields for percent T^T cleavage were calculated from the total intensity of T^T with respect to the total intensity per sample as determined by 8 % denaturing gel electrophoresis. Time points including error are average values from no less than 3 independent experiments and the error bars repents the standard deviation.

Data for the formation of each individual T^T was compiled and compared (Figure 2.26). Despite > 99 % reconstitution there was no apparent difference between the initial or photostationary states of T^T

formation in free W601 vs. reconstituted. This result was disappointing, yet not entirely surprising. The TT's that are being compared must have exactly different orientations with respect to the NCP. In other words, T^T's need to be exactly 5 bp apart to see the maximum difference in T^T formation. If T^T spacing is in between then there will be an intermediate effect, which may fall within the experimental error of the experiment. Therefore, while it was disappointing that there was no difference seen between free and reconstituted DNA, another method must be developed to study the rates of T^T formation and reversion.

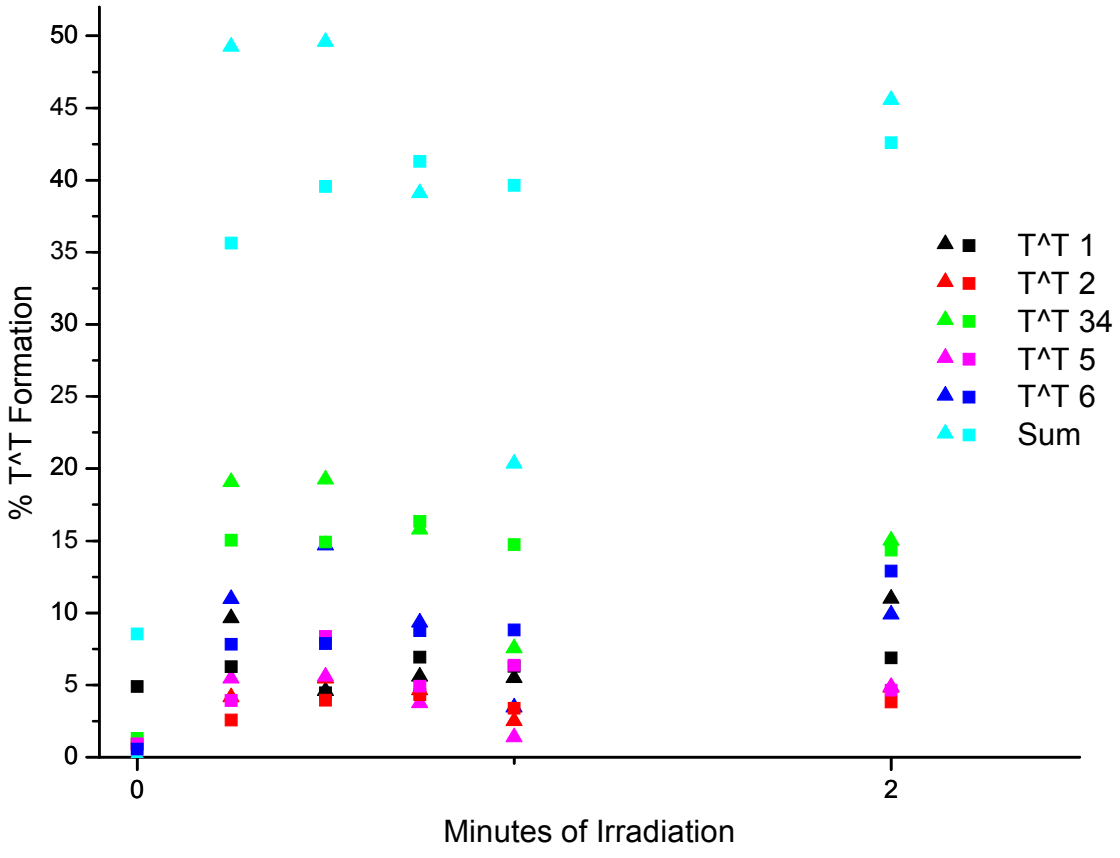

Figure 2.26: Percent individual and total T^T formation in free (squares) and NCP reconstituted (triangles) W601 DNA over time. Yields were calculated from the intensity of strand cleavage from each individual T^T relative to total sample per time point as determined by denaturing 8 % PAGE.

Summary and Conclusion

The 5s DNA NCP was the initial system used for these experiments. Reconstitution efficiency was achieved with maximum efficiency of 75 % reconstitution of 5s DNA. This degree of reconstitution did not show any variability in the accumulation of T^T in either the initial rates or the total percent accumulation of each individual T^T. It was hypothesized that the lack of difference between free and reconstituted 5s DNA may be a result of the entire sample not being reconstituted into NCP. This led to studies with the W601 NPS which has a higher affinity for the nucleosome than 5s DNA. The W601 was obtained fully reconstituted (100 %) and radiolabeled and it was determined that samples remained reconstituted under the photochemistry conditions. Unfortunately, the studies with W601 also did not show any variability in T^T formation when comparing free vs. NCP reconstituted W601. In order to achieve maximum variation in T^T formation, the T^T need to be in directly opposite orientations with respect to the NCP. This would require the T^T to be separated by multiples of 5 bp. Upon sequence analysis it appears that the differences in T^T orientation in W601 were either not significant enough to allow for detection or that these high affinity sequences did not exhibit variations in T^T accumulation.

Although the rates of T^T reversion were not determined by either 5s or W601 DNA sequences, it is possible to modify this experiment for success. Introducing T^T's spaced to optimize backbone orientation is one simple modification that may allow for different T^T distributions. This can be

accomplished by site directed mutagenesis of the 5s or W601 sequences. While this would be a relatively easy experiment, changing the sequences will change and possibly diminish their binding affinity to the NCP. Reduced binding would afford the same problems that were seen with the 5s sequence, therefore this method is not practical. Future experiments with this system need to ensure that T^T are properly spaced to allow maximize of the variations in T^T formation. This may be accomplished by using hetergenous DNA sequences as outlined in the literature and possible solutions will be discussed in the final chapter.

In addition to DNA structure and positioning affecting T^T distribution, nearest neighbors within the individual sequences can play a role on the levels of T^T.[49] These nearest neighbor effects on T^T accumulation are possibly due to EET from the surrounding DNA bases and also deserve further consideration.

Chapter 3

Fundamentals of Excess Electron Transport

As mentioned in Chapter 1, the variability of T^T formation is in part due to direct and indirect electron transport that affect the T^T reversion reaction (Figure 1.8). Since numerous intrinsic and extrinsic factors possibly influence this electron transport, a model system was used to focus on the effects of nucleotide sequence. This model system is used to compare the rates of EET in DNA of defined sequences and to determine the possible effect of electron donation from surrounding DNA bases on T^T accumulation. Initial sequences were designed to test if a polaron type mechanism is operative in EET through DNA transport and were designed based on analogus sequences used for HT.

3.1 Charge Transfer (CT) Mechanisms

Hole Transport (HT)

In Chapter 1 the two mechanisms that have been used to describe HT were introducted. The first mechanism is operative over very short distances (2 – 3 base pairs) and occurs as a superexchange mechanism (Figure 3.1).[102,122,171-174] The second mechanism used to describe HT occurs over long distances (> 200 Å) and can be described via a hopping type mechanism (Figure 3.2).[88,119,132,173,175,176] This hopping mechanism can further be broken down into two classes. The first class of hopping describes HT over short steps that combine together for long-range transfer. This multi-step hopping mechanism consist of the radical cation localizing on **G** and tunneling through

bridges composed of **A/T** base pairs until it is oxidatively trapped at a **G** (Figure 3.2). The second class of hopping mechanism is thought to occur via a polaron type model (Figure 3.3).[104,112,114] In the polaron model, a structural distortion of the DNA stabilizes and delocalizes the radical cation over several adjacent **G**'s.

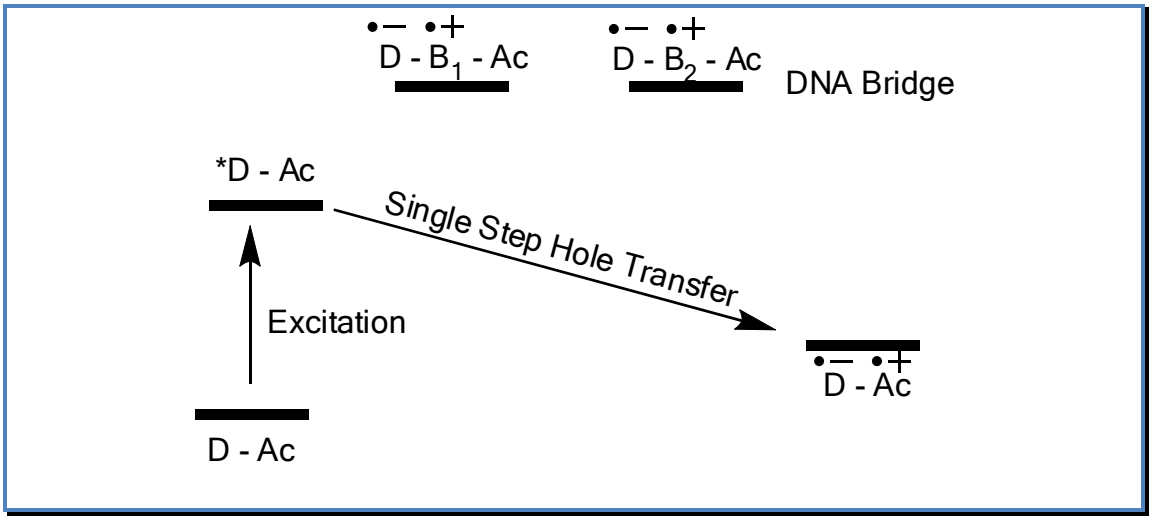

Figure 3.1: Superexchange mechanism of HT ((D = donor, Ac = acceptor, B= DNA bases) adapted from reference 118).

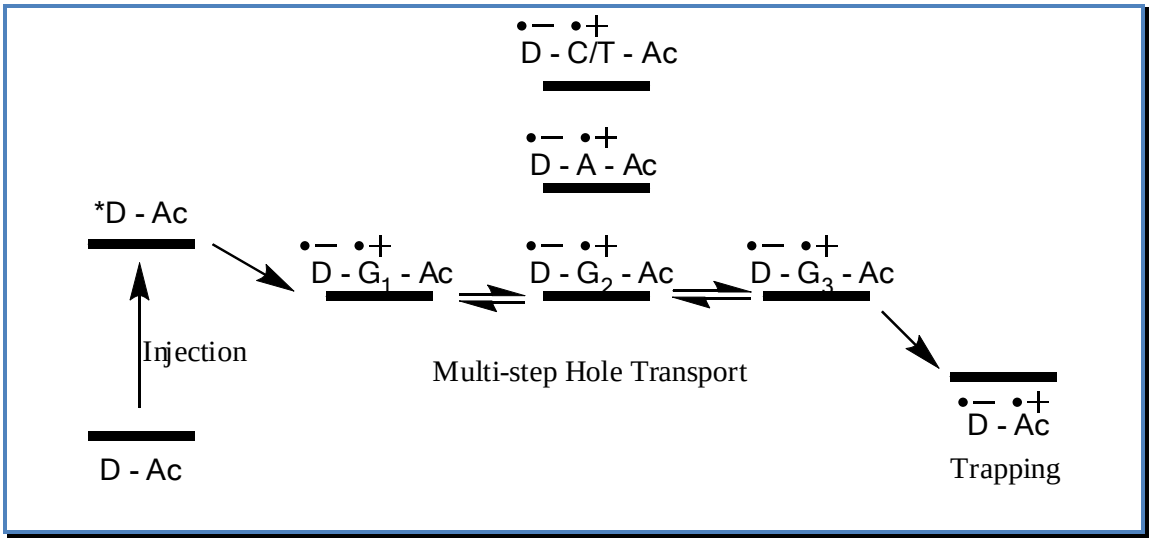

Figure 3.2: Multi-step hopping mechanism of HT ((D = donor, Ac = acceptor) adapted from reference 118).

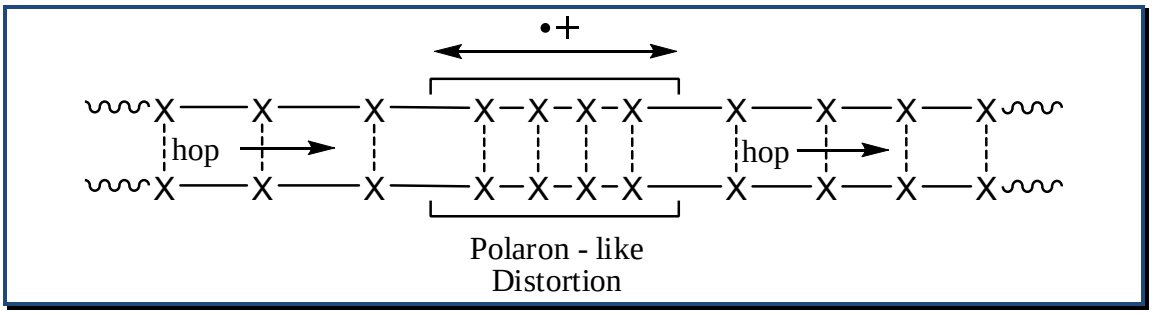

Figure 3.3: Polaron-like hopping mechanism of HT (adapted from reference 118).

The polaron allows for the delocalization of the radical cation which stabilzes this state relative to a localized equivalent (for a background on polarons see reference 106).[106] The polaron model relies on distortion of DNA structure upon electron injection that allows for a local distortion to increase electronic overlap between bases.[107] **G** acts as the resting site for the radical cation in the polaron model because it has the lowest ionization potential of all the DNA bases.[134] This ability to stabilize a radical cation increases in $(\mathbf{G})_n$ sequences (n=1-3).[177] Insertion of a **T** into an all purine sequence will create a barrier to radical cation migration. The height of the barrier depends on the DNA sequence surrounding the **T**, with **ATA** having the largest barrier to HT.[104] This large barrier results in a slowing of transport so that the rate of trapping the radical cation with water occurs faster than hopping. For example, long range transport via the polaron mechanism has been detected by oxidative trapping of the hole and is possible using sequences with repeats of **AGGA**.[177,178] Figure 3.4 illustrates the affect of sequence on polarons and the barriers to HT.[104] In the black curve, the radical cation is delocalized and stabilized in polarons. Radical cation delocalization stabilizes it and results in a high barrier ($\Delta G^{\neq}$) at the **ATA**

sequence. In these sequences, trapping of the radical cation by water occurs much faster than this barrier can be crossed. For the blue curve, the same **AAGGAA** polaron is identified however, there are no thymines that create a high barrier for hopping from one polaron to the next, which occurs faster than trapping by water. The red curve represents an intermediate case where the polaron is assumed to be the **GGA** sequence, which is less delocalized and therefore higher in energy than **AAGGAA**. Consequently, the barrier introduced by the **ATA** sequence is lower than for black curve and the rate of crossing this barrier is comparable with reaction of the radical cation with water

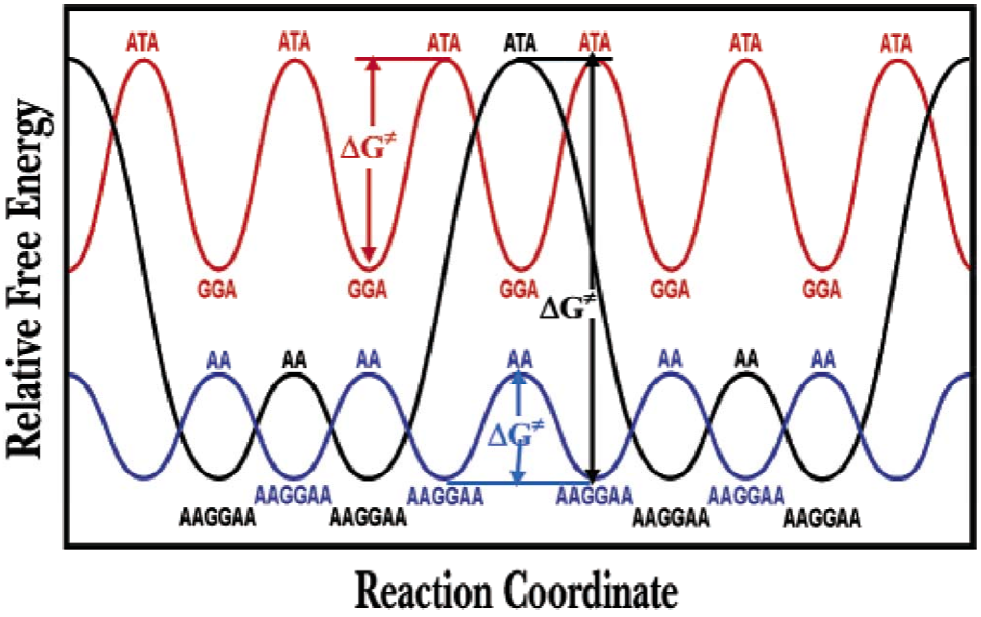

Figure 3.4: Reaction coordinate diagram illustrating the sequence effects in charge transport in DNA. Blue and red curves illustrate the ability of a polaron to stabilize and propagate of HT, whereas the black curve illustrates a case where the polaron stabilizes the charge and the crossing barrier to HT either slower or comparable to trapping with water (image taken from reference 104).

The numerous studies conducted on HT have led to a general consensus that the mechanism of HT in DNA is a combination of the

superexchange and hopping mechanisms. The mechanism of HT varies with sequence and by rational design, sequences that facilitate HT long range transport can be created.

Excess Electron Transport Mechanism

The complementary process of EET is also thought to occur via hopping of excess electrons through DNA however, the sequences that facilitate EET have yet to be determined. In order to establish if a polaron type mechanism is consistent with EET, studies with a model system are essential. The model system used by the Rokita lab employs an aromatic amine (AA) to induce electron transfer to bromouridine (^{Br}U) (Figure 3.5).[130,133] The AA is believed to intercalate into the abasic site and is photochemically excited at wavelengths (> 330 nm) not absorbed by DNA. Subsequent injection of an electron into the bases of DNA ultimately leads to electron trapping by ^{Br}U, debromination, strand cleavage, and detection of EET. Once the electron is injected into the base stack, there are many possible outcomes. Two of these outcomes are illustrated in Figure 3.5. The first is that the electron can be quenched by the ^{Br}U and the second back electron transfer and to reform with the AA. The rate of EET to the ^{Br}U is affected by these competing mechanisms and the sequences that affect these require idenficiation. Additionally, other mechanisms and side reactions may affect the observed cleavage and need to be explored. This model system allows for identification of the fundamentals of EET including the

possibility of a polaron type mechanism and the effect of intervening sequence on EET.

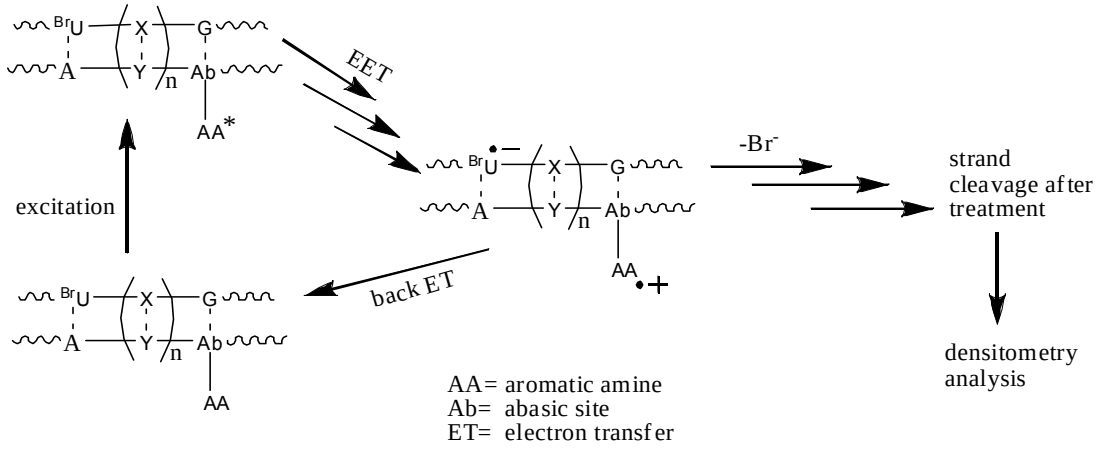

Figure 3.5: Model system used by Rokita lab for studies on EET.[133]

EET Donors

The model system employed by the Rokita lab also allows for studies to be conducted on the affect of donor strength on the observed mechanism for EET. The versatility of this system allows for a variety of modifications in order to directly determine what factors influence the mechanism of EET. One such modification is of the electron donor, the efficiency of electron injection into the surrounding DNA may greatly affect observed EET. The origin criteria for donor selection included ease of preparation, ability to be conjugated to DNA abasic site, and an excitation wavelength well resolved from the maximum of DNA. Preliminary experiments in the lab were conducted using an oligonucleotide conjugated N,N,N′,N′–tetramethyl-1,5-diaminonapthalene (TMDN) as the AA. TMDN was chosen for the reasons stated above, as well as having an excited state oxidation potential(E_{ox}*) of -

3.06 V allowing it to donate an electron to any of the four nucleotides.[179] Furthermore, the planar aromatic ring structure of TMDN should allow for intercalation into the DNA abasic site leading to efficient EET to surrounding nucleobases. Most importantly, TMDN has an absorption maximum (> 300 nm) well shifted away from that of DNA (< 300 nm) allowing for direct excitation of TMDN without excitation of the DNA. TMDN that was not conjugated to the abasic site also proved capable of promoting EET however, a trial study using the unligated and unmethylated naphthalene (1,5-diaminonapthalene (DAN)), demonstrated that DAN was more efficient than TMDN at promoting EET.[179] These results illustrated that more studies were needed about the effect of the donor on EET as well as the effect of DNA sequence on the transfer. More specifically, it is necessary to determine if changes in the E_{ox}* of the AA are the cause of differences in observed EET.

3.2 Experimental

Materials

All chemicals were purchased from Fisher Scientific or Aldrich and were enzymatic grade or the highest grade available. 5-bromo-2′-deoxyuridine (^{Br}U) oligonucleotides are purchased from IDT DNA (Coralville, IA). Oligonucleotides containing abasic sites are purchased from TriLink Biotechnologies (San Diego, CA). All aqueous solutions are prepared with distilled deionized water (Barnstead NANOpure II purifier, ≥17.8 MΩ·cm).

DNA concentration was determined using a Hewlett Packard 8453 UV-vis spectrophotometer. Preparative and analytical HPLC were performed using a JASCO dual pump PU980 and a JASCO multi wavelength detector MD 1510 using a Varian Microsorb MV column (300 Å, 5C18 250 x 4.6 mm). Photoirradiation was conducted using a high pressure 1000 Watt Xe-arc lamp (LH151, Oriel Instruments) powered with a LPS255HR power supply (1000 W) through a 335 nm cut-off filter glass (WG335, Schott).

Methods

Oligonucleotide Purification.[145] Oligonucleotides with the ^{Br}U were purified by denaturing (7 M urea) polyacrylamide gel electrophoresis and a crush and soak extraction overnight into 50 mM NaOAc and 1 mM EDTA (pH 5.2) at 37 ˚C. The mixture was filtered through a Corning Costar Spin-X (Lowell, MA) centrifuge tube (0.45 μm), precipitated by addition of 0.1 volumes of 3 M NaOAc (pH 5.5) and 2.5 times volume of absolute ethanol, dried in a Savant Speed Vac (Waltham, MA), and redissolved in water.

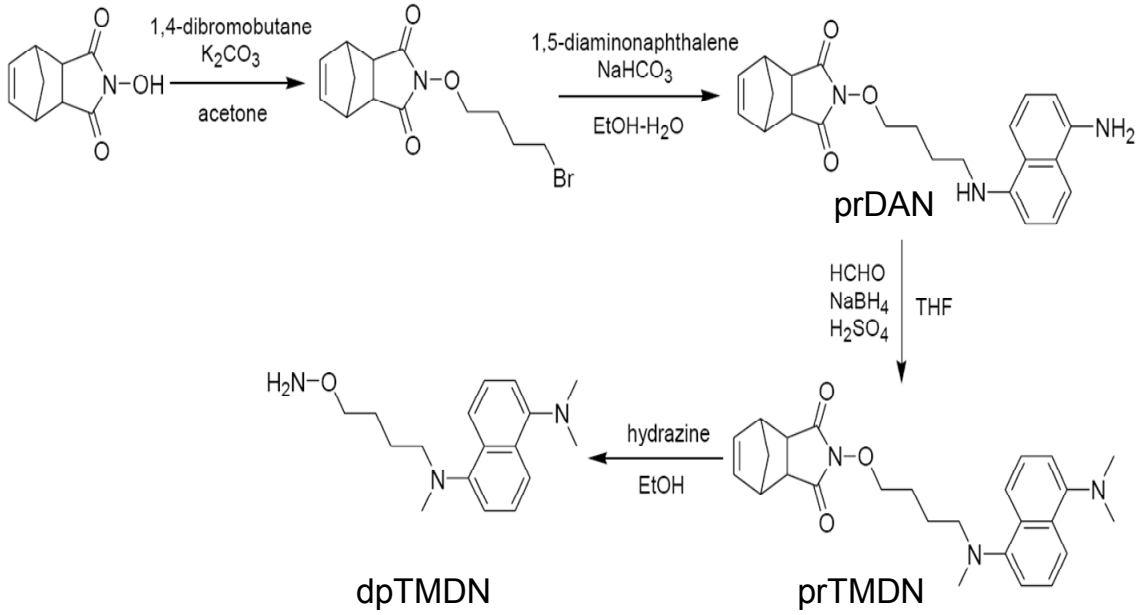

Figure 3.6: Synthetic scheme for preparation of deprotected TMDN (dpTMDN).[133]

N-(4-Aminooxybutyl)-N,N',N'-trimethyl-1-5-diaminonaphthalene (dpTMDN). Anhydrous hydrazine (5 mg Aldrich, 2 mL ampules under Argon) was added to a solution of N-(4'-bromobutyloxy)-5-norbornene-2,3-dicarboximide-N,N',N'-trimethyl-1-5-diaminonapthalene (prTMDN (34 mg, 0.04 mmol)) in 95 % ethanol (1.5 mL). The prTMDN material was synthesized by Neil Campbell following a literature procedure (Figure 3.6).[133] The reaction was refluxed under N_2 for 2.5 hours and then evaporated to dryness. The residue was redissolved in approximately 1 mL of ethyl acetate and purified via silica gel flash chromatography (hexanes-ethyl acetate 1:0 to 1:1, 15 % gradient). The desired product was obtained as colorless syrup in 95 % yield (12 mg). ^{1}H NMR data was in agreement with published literature.[133] Mass spectral analysis (ESI+) m/z calculated for $C_{17}H_{25}N_{3O}$ [M+H] 288.2086 found 288.21959.

N-(4-Aminooxybutyl)-1-5-diaminonaphthalene (dpDAN). Hydrazine monohydrate (100 µL Aldrich, 98 % reagent grade, N_2H_4 64-65 %) was added to a solution of N-(4'-bromobutyloxy)-5-norbornene-2,3-dicarboximide-1-5-diaminonapthalene (25 mg) in 95 % ethanol (5 mL). The reaction was refluxed under N_2 overnight and then evaporated to dryness. The residue was redissolved in approximately 1 mL of ethyl acetate and purified via silica gel flash chromatography (hexanes-ethyl acetate 1:0 to 1:1, 15 % gradient). The desired product was obtained as clear pink syrup in 90 % yield (10 mg) and this was immediately dissolved in HPLC grade acetonitrile (25 mM) and used for subsequent conjugation to oligonucleotides.

dpTMDN Oligonucleotide Conjugation.[133] Abasic site containing oligonucleotides (120 µM) and 2 mM sodium periodate in 100 mM sodium acetate (pH 5.0, 40 µL) were combined and incubated for 30 minutes at 4 °C in the dark. After incubation, the salts were by passage through a prewashed (3 times with 400 µL ddH_20 and spin down for 2 minutes at 1000 rcf) P6 Micro Bio-Spin column (Biorad) for four minutes at 1000 rcf. The solution was then incubated with dpTMDN (25 mM, 20 µL) in HPLC grade acetonitrile at room temperature for 1 hour. The excess dpTMDN was removed by passage through a prewashed (3 times with 400 µL ddH_20 and spin down for 2 minutes at 1000 rcf) P6 Micro Bio-Spin column (Biorad) for four minutes at 1000 rcf.

dpDAN Oligonucleotide Conjugation. Abasic site containing oligonucleotides (120 µM) and 2 mM sodium periodate in 100 mM sodium acetate (pH 5.0, 40 µL) were combined and incubated for 30 min at 4 °C

(dark). After incubation salts were removed using a prewashed (3 times with 400 µL ddH_20 and spin down for 2 minutes at 1000 rcf) P6 Micro Bio-Spin column (Biorad) for four minutes at 1000 rcf. The solution was then incubated with 25 mM dpDAN in HPLC grade acetonitrile (50 µL) at 37 °C for 1 hour. The excess dpDAN was removed by passage through a prewashed (3 times with 400 µL ddH_20 and spin down for 2 minutes at 1000 rcf) Biorad Micro Biospin P6 Column for four minutes at 1000 rcf. Mass spectral analysis (MALDI+) m/z calculated for Chemical Formula: $C_{193}H_{245}N_{81}O_{122}P_{18}$ [M+H] 6206.09, found 6206.

Oligonucleotide Conjugate Purification. Oligonucleotides containing dpTMDN or dpDAN conjugated to abasic site were purified by reverse phase HPLC (C-18) using a gradient of 10 % acetonitrile in 50 mM triethylamine acetate buffer (pH 5.0) to 30 % acetonitrile in 35 mM triethylamine acetate over 15 min (1 mL/min). Material corresponding with DAN or TMDN oligonucleotide conjugate (as determined by absorbance at 260 nm and 330 nm with a 260/330 ratio of 40) was collected and dried in a Speedvac (Savant) overnight. Dried samples were redissolved in distilled deionized water and concentration was determined by UV-Vis spectrometry based on the molar extinction coefficients provided for the oligonucleotides by the manufacturer (Trilink Biotechnologies) and range from 180 -190 OD/µmole depending on the sequence. A_{260} of donor was not used in calculation.

Labeling Oligonucleotide with a 5' - [^{32}P]. A 25 µL solution containing 1 µL ^{Br}U oligonucleotides (5 mM stock solution) were incubated for 30 - 60 minutes at 37 ˚C with 4 µL γ - [^{32}P] – ATP (Amersham 10 µCi/µL), 10 units T4 polynucleotide kinase (New England Biolabs), and 2.5 µL of T4 polynucleotide kinase buffer (70 mM Tris-HCL, 10 mM $MgCl_2$, 5 mM dithiothreitol) according to suppliers standard protocol. After incubation, 5 µL ddH_2O was added to make a total volume of 30 µL. Excess salt and ATP were removed by passage through a prewashed (3 times with 400 µL ddH_20 and spin down for 2 minutes at 1000 rcf) P6 Micro Bio-Spin column (Biorad, Hercules, CA) for four minutes at 1000 rcf. Radioactivity of the resulting oligonucleotide was measured by adding 1 µL of sample to approximately 1 mL of scintillation fluid (Fisher ScintiSafe Plus 50 %) and measured dpm with a Packard 1600TR Liquid Scintillation Analyzer.

Preparation of Double Stranded DNA. The ^{Br}U containing oligonucleotide (1.5 µM) was incubated with complementary 2.0 µM TMDN/DAN conjugated oligonucleotide and 100 kdpm/sample of radiolabeled ^{Br}U containing oligonucleotide in a solution of 10 mM sodium phosphate buffer (pH 7.0) and 100 mM NaCl. The mixture was placed in a 90 °C bath and cooled slowly to room temperature to allow for proper annealing.

Aerobic Photochemistry. Samples of radiolabeled double stranded conjugated TMDN/DAN (20 µL) in microcentrifuge tubes were photoirradiated at 10 °C with a 1000 Watt Xenon arc lamp using 330 nM UV cutoff filter (Figure 3.7). Distance between sample and light was varied to allow for a

constant flux of 2.0 mW/cm^2 measured using a model UVX digital radiometer (UVP of San Gabriel, CA). After irradiation samples were either treated with piperidine or endonuclease IV.

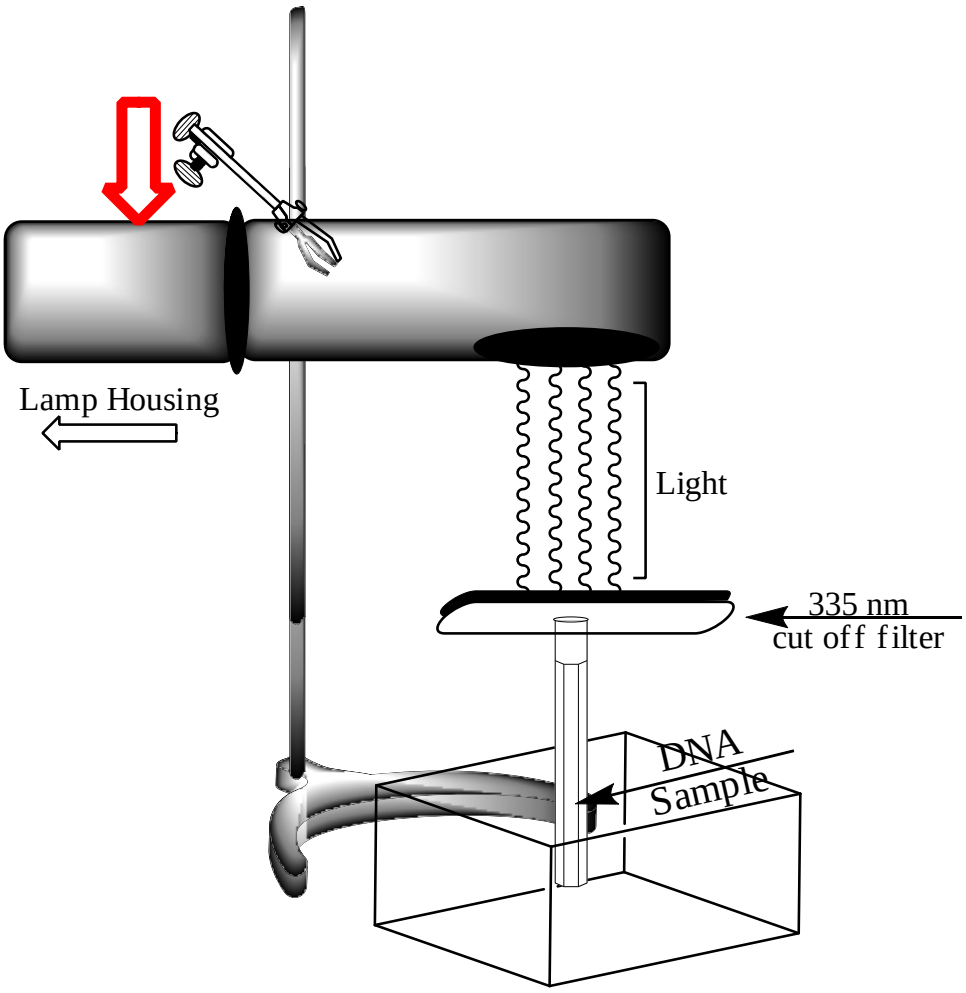

Figure 3.7: Cartoon illustration of photochemistry apparatus. Red arrow indicates where the glove bag was attached to the photochemistry apparatus, everything to the right of the red arrow was inside the glove bag.

Anaerobic Photochemistry. All solutions and buffers were bubbled with N_2 for at least 30 minutes prior to sample preparation and irradiation. Samples were irradiated as described in the aerobic photochemistry experiments, with the exception that samples were irradiated under N_2

atmosphere in a glove bag that was purged with N_2 five times prior to photoirradiation.

Piperidine Treatment. Photoirradiated samples were dried in a speedvac and resuspended in 30 µL of 10 % piperidine and then were incubated at 90 °C for 30 minutes. After incubation, samples were dried in the speedvac overnight. ddH_20 (30 µL) was added to the dried samples and then samples were vortexed, spun down, and dried in the speedvac again to remove any residual piperidine.

Endonuclease IV (endo IV) Treatment. Endo IV reaction mixture (0.5 uL endo IV, 1 µL of 10X NEB Buffer 3 (50 mM Tris-HCl, 100 mM NaCl, 10 mM MgCl2, 1 mM dithiothreitol, pH 7.9) and 8.5 µL ddH2O) was added to 10 µL photochemistry samples based on the manufacturer's protocol (New England Biolabs). Samples were then incubated overnight at 37 °C.

Maxam-Gilbert A+G Lane Sequencing Reaction.[145] Double stranded DNA (10 µL) was combined with 2 µL calf thymus DNA (1 mg/mL, Sigma-Aldrich) and 3 µL 10 % formic acid. Sample was incubated 15 – 20 minutes at 60 °C and then dried in the speedvac. Samples were then treated with hot piperidine as described previously.

PAGE analysis. DNA samples were diluted to a volume of 20 µL with ddH_2O and combined with 6 µL of 6X denaturing loading buffer (8 M urea, 40 % sucrose, 0.05 % bromophenol blue, 0.05 % xylene cyanol, in 1X TBE). Samples were then heated to 90 °C and loaded (8 µL) on a 20 % denaturing PAGE gel (19:1 acrylamide:bis-acrylamide) containing 7 M urea that had

been pre-run for 30 minutes. PAGE gel was run for 90 – 120 minutes (based on dye migration) at 65 watts. The gel was exposed to a phosphorimaging screen overnight and then analyzed using a Molecular Dynamics Storm PhosphorImager (Sunnyvale, CA) with Image Quant (IQ) v5.2 software.

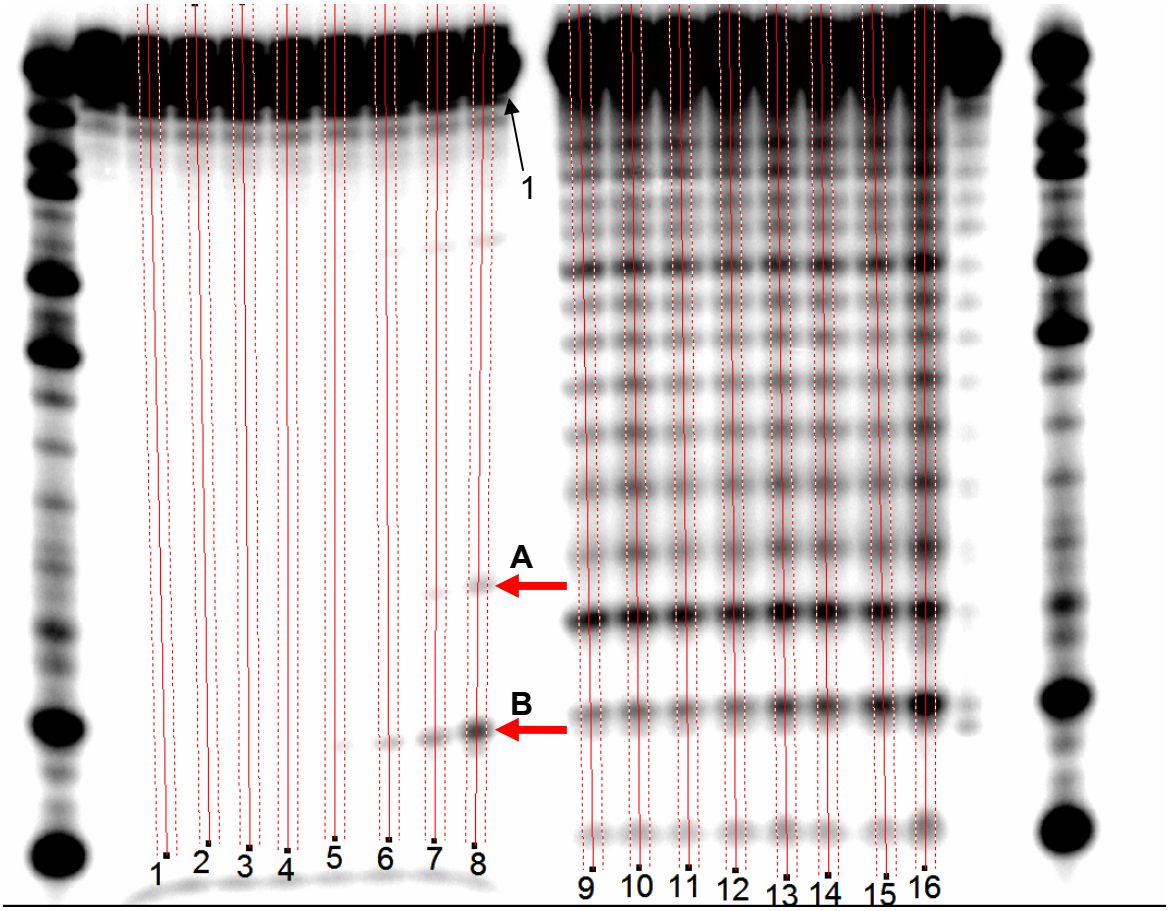

Figure 3.8: Example autoradiograph of a 20 % denaturing polyacrylamide gel showing cleavage products of 5′-^{32}P double stranded DNA after photolysis. Lanes were integrated using a line width of 16 pixels. Lanes 1 – 8 were treated with endo IV and lanes 9 – 16 were treated with piperidine. Red arrows (A and B) indicate photochemical cleavage bands and black arrow (1) indicates starting material.

Data Analysis. Gel image was created by the Storm phosphorimager and individual lanes were as illustrated in Figure 3.8. Each lane in Figure 3.8 corresponds to one time point in a photochemistry experiment. The width of the lines was set to 16 pixels in order to fit the individual lanes without overlap

between lanes. Each individual line designates a region to be converted into an area graph using the IQ graph tool (Figure 3.9). Then the peak finder tool was used to find the peaks on the graph and the background noise is set to 0.01 pixels in order to ensure all peaks are detected. Once the graph was created the peaks were correlated to the DNA sequence using the Maxam-Gilbert sequencing lane. Individual peaks were designated using the peak picking tool and then converted to an area report using Microsoft excel. In this case peaks 1, A and B were selected for further processing. Table 3.1 is an example of an area report created the using data of Figure 3.8 and the graph of Figure 3.9. The area report includes percent cleavage (percent product relative to total material per lane) for each band of the gel. This data was then transferred into Microccal OriginPro v.7.0 for graphical analysis of data.

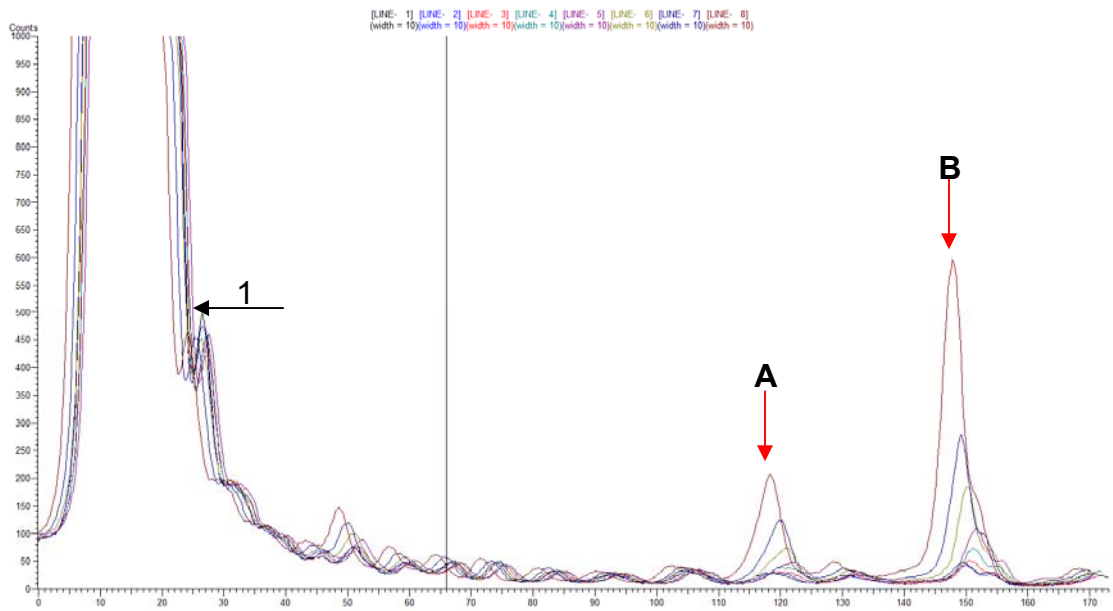

Figure 3.9: Densitometry plot created using data from lanes 1 – 8 of Figure 3.8. Arrows indicate peaks that correspond with photochemical cleavage bands in Figure 3.8.

Table 3.1: DNA cleavage (%) data obtained from area densitometry plot (Figure 3.9). Blue box highlights irradiation time points, yellow rows indicate photochemical cleavage band data (endo IV) and red boxes highlight DNA cleavage (%).

0 minutes hυ			
Peak #	Area	Height	**PERCENT**
1	1606084	99992	99.789
Peak A	768.23	21.163	0.048
Peak B	1277.039	39.748	0.079
0.5 minutes hυ			
Peak #	Area	Height	**PERCENT**
1	1545823	99990.54	99.824
Peak A	704.625	20.872	0.046
Peak B	1200.37	37.217	0.078
1 minutes hυ			
Peak #	Area	Height	**PERCENT**
1	1490894	99994.27	99.782
Peak A	956.293	25.398	0.064
Peak B	1469.775	46.026	0.098
2 minutes hυ			
Peak #	Area	Height	**PERCENT**
1	1493455	99993.1	99.684
Peak A	1193.067	33.575	0.08
Peak B	2174.063	66.151	0.145
5 minutes hυ			
Peak #	Area	Height	**PERCENT**
1	1509455	99989.86	99.662
Peak A	1263.71	38.905	0.083
Peak B	3040.318	103.165	0.201
10 minutes hυ			
Peak #	Area	Height	**PERCENT**
1	1511733	99992.65	99.49
Peak A	2023.462	66.492	0.133
Peak B	4659.314	177.1	0.307
15 minutes hυ			
Peak #	Area	Height	**PERCENT**
1	1462817	99986.73	99.209
Peak A	3018.16	114.704	0.205
Peak B	7049.507	270.133	0.478
30 minutes hυ			
Peak #	Area	Height	**PERCENT**
1	1465755	99990.35	98.472
Peak A	5288.696	198.609	0.355
Peak B	15213.12	587.632	1.022

AC Voltammetry.[180] Measurements were carried out using a CH Instruments 660A electrochemical workstation (Austin, TX) courtesy of the Army Research Labs, Adelphi, MD. AC voltammetry experiments were run in a three component electrode cell with a platinum working, platinum wire counter and saturated calomel reference electrode. Phosphate buffered saline pH 7.4 (PBS, Sigma) was used as the electrolyte. One tablet PBS was dissolved in 200 mL ddH_2O to make a working solution of 10 mM potassium phosphate, 137 mM NaCl and 2.7 mM KCl. Solutions of aromatic amines (500 mM) were prepared in HPLC grade acetonitrile. Aromatic amine (AA) solutions (10 µL) were then mixed with 10 mL PBS to final AA concentration of 500 µM in 0.1 % acetonitrile. The following parameters were set for on the AC voltammetry workstation for all experiments:

Init E (V) = 0
Final E (V) = 0.7
Incr E (V) = 0.004
Amplitude (V) = 0.025
Frequency (Hz) = 10
Sample Period (sec) = 1
Quiet Time (sec) = 2
Sensitivity (A/V) = 1e-5

E_{ox} was determined by the taking the apex of the peak resulting from the AC voltammetry scan.

Electrode Polishing. Platinum electrodes were soaked in 1 M NaOH for 10 minutes and then rinsed with ddH_2O. Electrodes were then soaked in 1 M Nitric acid for 10 minutes and rinsed with ddH_2O. Electrodes were then polished with 1.0 micron alumina in a figure eight pattern turning the electrode after 10 repetitions to diminish swirling on electrode surface. Electrodes were

then rinsed with ddH_2O, sonicated in soapy water for 5 minutes, and finally sonicated for 5 minutes in ddH_2O. The polishing process was repeated with 0.3 micron and 0.05 micron alumina. Electrodes were finally observed under a microscope to ensure a mirror finish and an absence of major scratches on electrode surface before their use in AC voltammetry experiments.

3.3 Results and Discussion

If a polaron type mechanism controls EET, **T**'s should work in tandem to stabilize an excess electron since the **T**'s have the highest reduction potential of the DNA bases. Our system was designed to vary the size of **T** tracts between the electron donor and acceptor in order to reveal if a polaron type mechanism is in effect. An **A** was used to divide $(\mathbf{T})_n$ from the neighboring donor as a barrier for EET in the initial studies because it has a much lower reduction potential than **T**. The relative reduction potential of the DNA bases is as follows **T**(**U**) ≈ **C** >> **A** > **G**, highlighting that **C** and **T** are the most easily reduced of the DNA bases and that **G** is the most difficult to reduce.[99] Figure 3.10 are sample reaction coordinate diagrams modified from HT studies and illustrate the basis of the sequence design for the polaron studies.

In Figure 3.10 radical anion delocalization in the $(\mathbf{T})_n$ sequences stabilizes the anion and results in a barrier at the **TAT** sequences (Figure 3.10 A, B, and C) and an even higher barrier at the **TGT** sequence (Figure 3.10 D). For the green curve (Figure 3.10 A) the four **T** residues adjacent to

the acceptor (^{Br}U) act as the polaron. In these types of sequences there should not be a high barrier to EET therefore EET should occur faster than other trapping mechanisms. Sequences illustrated by the blue and gray curves (Figure 2.10 B and C) should have an intermediate amount of transport relative to the green curve. This is based on the hypothesis that decreasing the number of **T**'s adjacent to the acceptor (^{Br}U) will decrease the stabilizing effect of the polaron. In these sequences, the rate of crossing the **A** barrier may be comparable or slower than the various trapping mechanisms. For the red curve (Figure 2.10 D), the (**T**)$_4$ polaron is identified however, there is a higher barrier to EET that is created by a **G** inserted into the sequence. This high barrier may slow or prevent EET because in these sequences radical recombination or other trapping mechanisms may occur faster than the **TGT** barrier can be crossed.

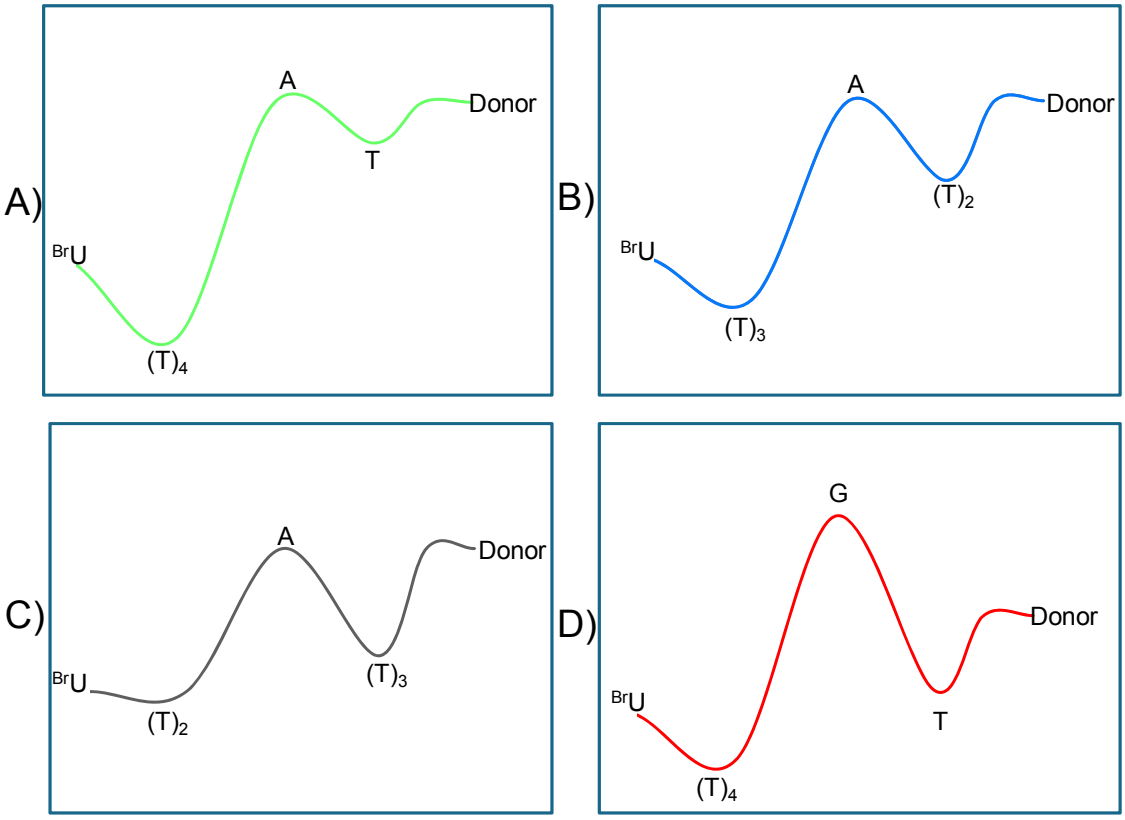

Figure 3.10: Reaction coordinate diagrams illustrating the hypothesized sequence effects for EET in DNA. Sequences illustrated in diagram A should promote EET followed by B, C and D.

Delocalization of EET by T-tracts: Polaron-Type Mechanism

In all sequences studied (Table 3.2) the donor and acceptor are separated by seven base pairs that differ only by the placement of one base pair. ASF001 has four **T** residues adjacent to the ^{Br}U and the TMDN donor was separated by an **A** placed one base pair from this polaron site. Based on polaron mechanism for HT, ASF001 was hypothesized to be the most effective at EET followed by ASF002 and ASF003. ASF004 would give an intermediate amount of cleavage because there was no **A** barrier to back electron transport. By placing the **A** adjacent to the donor and the acceptor,

ASF005 and ASF006 were designed to test the effectiveness of **A** as a barrier to EET. The ASF101 sequence was designed to test the affect of increasing the barrier height on EET since the **A** is changed to a **G**, which as mentioned previously has a lower reduction potential than **A**.

Table 3.2: DNA sequences used for polaron studies. (*) denotes location of radiolabel, bases red highlight sequence variation, Green N denotes site of conjugation with aromatic amine, and ^{Br}U is highlighted in blue.

DNA SEQUENCE	NAME
*5′ – GCCG^{Br}UTTTTATGTTGGCGC – 3′ 3′ – CGGC A AAAATANAACCGCG – 5′	ASF001
*5′ – GCCG^{Br}UTTTATTGTTGGCGC – 3′ 3′ – CGGC A AAATAANAACCGCG – 5′	ASF002
*5′ – GCCG^{Br}UTTATTTGTGGCGC – 3′ 3′ – CGGC A AATAAANACCGCG – 5′	ASF003
*5′ – GCCG^{Br}UTTTTTTGTTGGCGC – 3′ 3′ – CGGC A AAAAAANAACCGCG – 5′	ASF004
*5′ – GCCG^{Br}UATTTTTGTTGGCGC – 3′ 3′ – CGGC A TAAAAANAACCGCG – 5′	ASF005
*5′ – GCCG^{Br}UTTTTTAGTTGGCGC – 3′ 3′ – CGGC A AAAAATNAACCGCG – 5′	ASF006
*5′ – GCCG^{Br}UTTTTGTGTTGGCGC – 3′ 3′ – CGGC A AAAACANAACCGCG – 5′	ASF101

Before photochemistry experiments were conducted, the donor-oligo conjugate required preparation by deprotection (Figure 3.11) and conjugation of dpTMDN to the abasic site. dpTMDN was chosen as the donor because its

conjugation had been conducted previously in the lab and its properties as a donor were well documented.[130,133,179] However, results of this reactions had been erratic.[133] The reaction would work at times with > 95 % yields and at other times the starting material would remain inert. The original procedure used anhydrous hydrazine and anhydrous ethanol. A literature search was conducted to determine what reaction conditions had been used previously for similar deprotection reactions.[181,182] None of the earlier literature suggested excluding water from the reaction. By comparing the reaction under anhydrous and hydrous conditions it was determine that the success of the reaction was dependant on the presence of water. If 5 % water was present in the reaction, then the reaction proceeded with > 90 % yield. If care was taken to exclude all water from this reaction, then it would not go to completion. Therefore, reaction conditions now use 95 % ethanol as opposed to anhydrous and the reaction has been successful ever since.

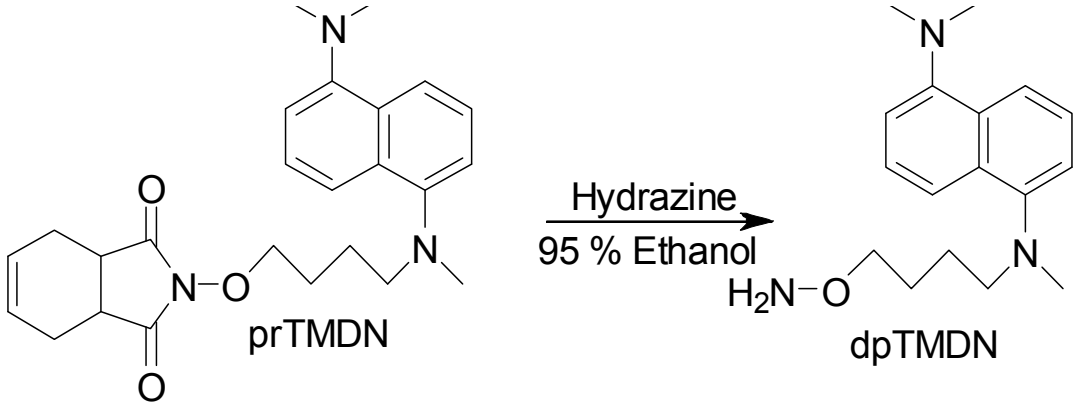

Figure 3.11: Deprotection of prTMDN.

ASF001 was the first sequence conjugated with dpTMDN since it was expected to be the sequence that would best facilitate EET. As mentioned

previously, this hypothesis was based on information from the complementary process of HT. As illustrated in Figure 3.10 it was hypothesized that the ASF001 sequence would be the most favorable for EET because it includes a $(\mathbf{T})_4$ polaron adjacent to the ^{Br}U. Figure 3.12 illustrates photochemical cleavage by EET in ASF001. As evident from this figure, there is a lot of non specific background cleavage (as evident from the multiple bands present in lanes 11-19) as a result of the piperidine treatment. Lanes 2-9 illustrate that without piperidine treatment there are little or no cleavage bands. These samples without piperidine were run as a control to illustrate that even after 30 minutes of photoirradiation spontaneous backbone cleavage was not occurring. If direct excitation of the DNA was occurring, as opposed to EET from the donor, cleavage would occur without piperidine treatment. The right hand side of the gel (lanes 11-19) illustrates cleavage detected in the photochemistry samples after hot piperidine treatment. ^{Br}U is base labile therefore, there is background ^{Br}U cleavage as well as some nonspecific cleavage throughout the sequence upon piperidine treatment. This cleavage of ^{Br}U is UV independent and is caused by the intrinsic lability of the ^{Br}U to piperidine treatment.[183] The high degree of background cleavage with piperidine led to a search for another method of detection.

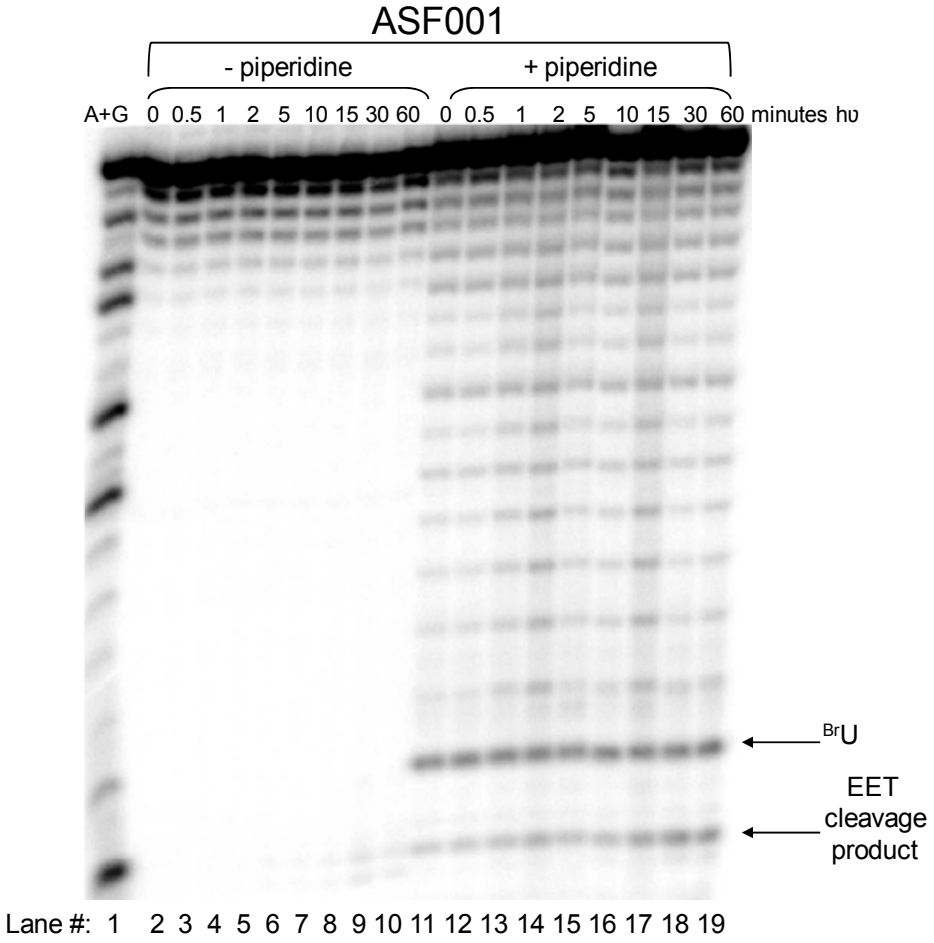

Figure 3.12: Autoradiogram of a 20 % denaturing polyacrylamide gel showing photochemical cleavage of ASF001 upon photoirradiation. Samples are normalized to 100 kdpm per lane. Lane 1 is a Maxam-Gilbert sequencing lane, Lanes 2-10 are not treated with hot piperidine and Lanes 11-19 are treated with hot piperidine. UV-independent strand scission after hot piperidine treatment is marked as the ^{Br}U band.

The ultimate product formed by 1 electron reduction of ^{Br}U is an abasic site on its 5′ side (Figure 3.13). [184,185] This abasic site is sensitive to piperidine, but another possible method of detection involves the use of an enzyme that cleaves DNA at abasic sites. One example of an enzyme that recognizes and specifically cleaves at such sites in endonuclease IV (endo IV).[186] Endo IV cleaves at abasic sites at the first phosphodiester bond that is 5′ to the lesion leaving a hydroxyl group at the 3′ terminus and a deoxyribose 5′-phosphate at the 5′ terminus.[187] Additionally, the enzyme also has a 3′-

diesterease activity and can release phosphoglycoaldehyde, intact deoxyribose 5-phosphate and phosphate from the 3′ end of DNA.[188]

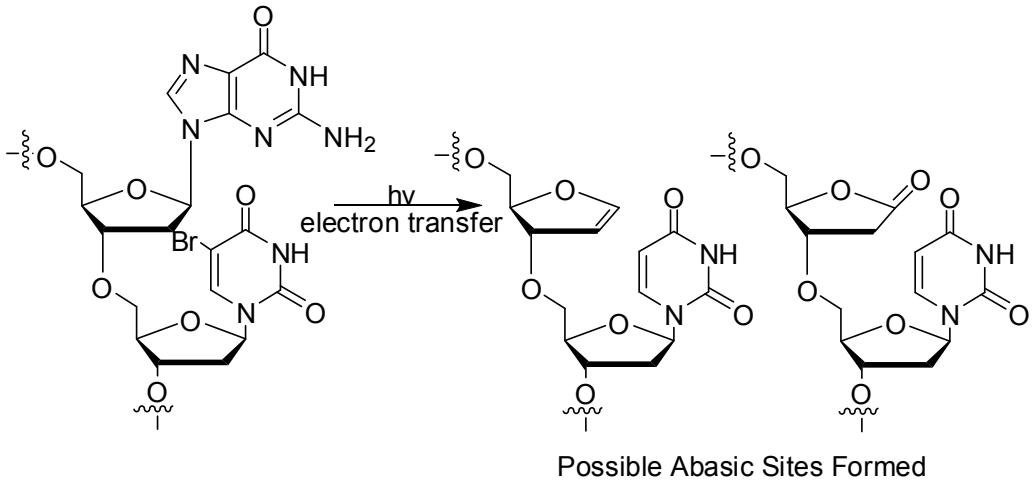

Figure 3.13: Abasic site products formed upon EET to ^{Br}U.[183-185]

The background bands in the piperidine treated sample are due to nonspecific cleavage that occurs upon treatment of the DNA with the mild base. Piperidine cleaves at a variety of DNA damage sites including 8-oxoG, abasic, ^{Br}U etc. Since this endoIV treatment only cleaves DNA upon abasic site formation which forms as a result of EET to ^{Br}U, it has the potential to decrease the number of background bands visualized on the gel. Figure 3.14 is a cartoon diagram illustrating the difference in the two detection methods.

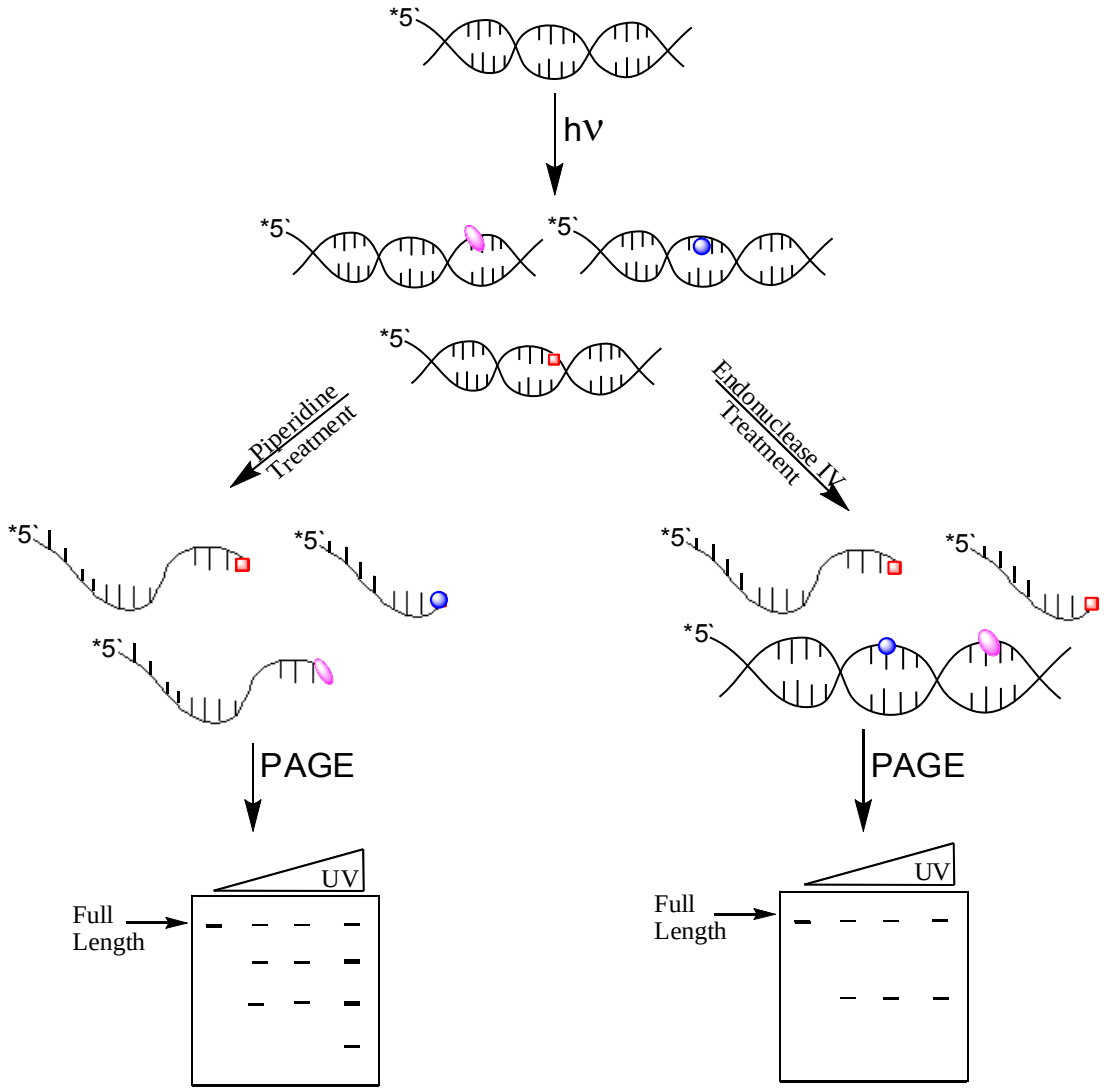

2

Figure 3.14: Comparison of cleavage bands detected by piperidine vs. endo IV treatment. The colored symbols represent sites of DNA damage, with only the red box symbolizing abasic sites.

As hypothesized, endo IV produces less background cleavage bands in comparison with piperidine treatment. Figure 3.15 is a typical PAGE gel comparing photochemical cleavage of ASF001 by piperidine and endo IV. The initial trials with endo IV were run for 1, 2, and 18 hours of incubation. Figure 3.15 illustrates that after 2 hours the cleavage reaction is not complete, which is indicated by presence of two photochemical cleavage bands. After

incubation with endo IV for 18 hours there is only one band detectable. The percent cleavage for the combination of each band in the 2 hour time point is in close agreement to the percent cleavage of the single band in the 18 hour time point (Figure II.1). This suggests that the lower band (B) is an incomplete reaction product that upon further incubation with endo IV is converted to the higher band (A). Additionally the photochemical cleavage products appear to have different mobilities, however this is due to an increased salt concentration in the endo IV samples. The increase in salt retards band migration and addition of a similar salt concentration to the piperidine samples produces the same effect (data not shown).

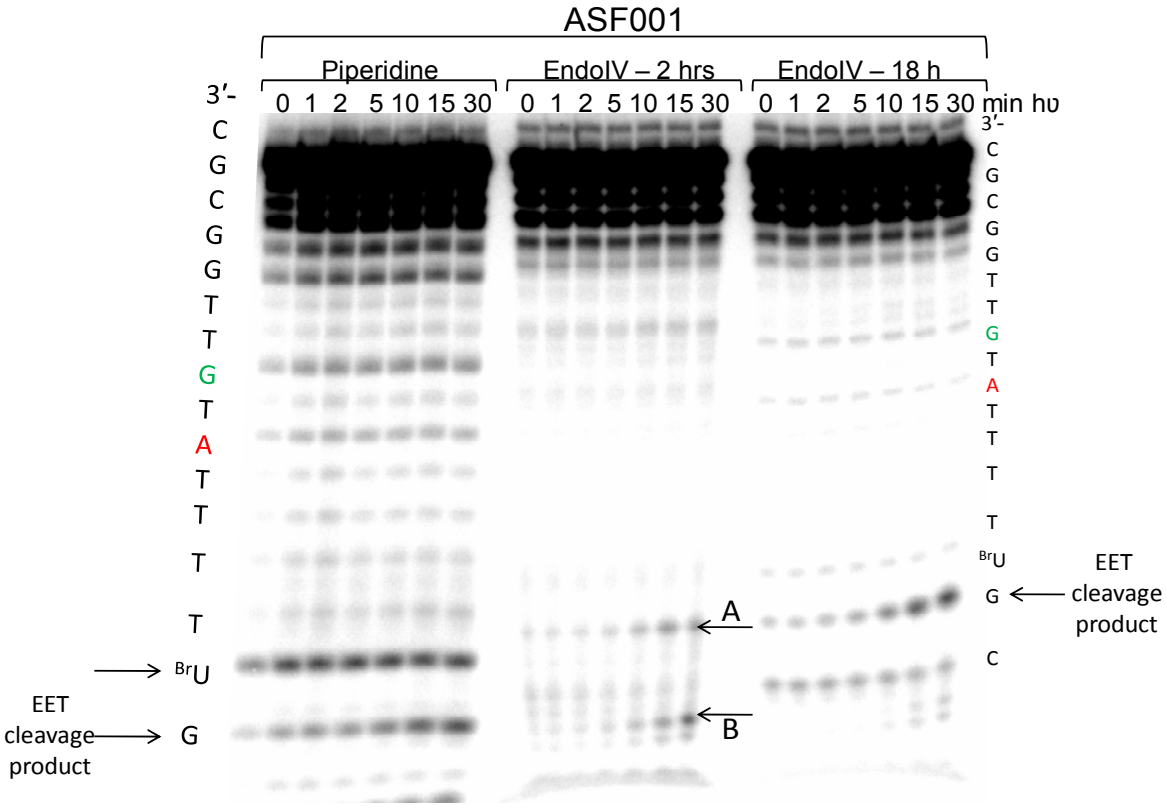

Figure 3.15: Autoradiogram of a 20 % denaturing polyacrylamide gel showing photochemical cleavage of ASF001 upon photoirradiation and treatment with either piperidine or endoIV. Lanes are normalized to 100 kdpm per lane.

Graphical analysis of the cleavage bands from Figure 3.15 shows that the total percent cleavage for all time points for piperidine vs. endoIV is similar (Figure 3.16). While it appears that the piperidine treatment gives a higher percent cleavage, the two methods of detection are virtually indiscriminable from one another if the background at zero is subtracted from the data. The fact that the percent cleavage data between endoIV and piperidine treatment are in close agreement suggests that endoIV is a complementary method for detection of EET.

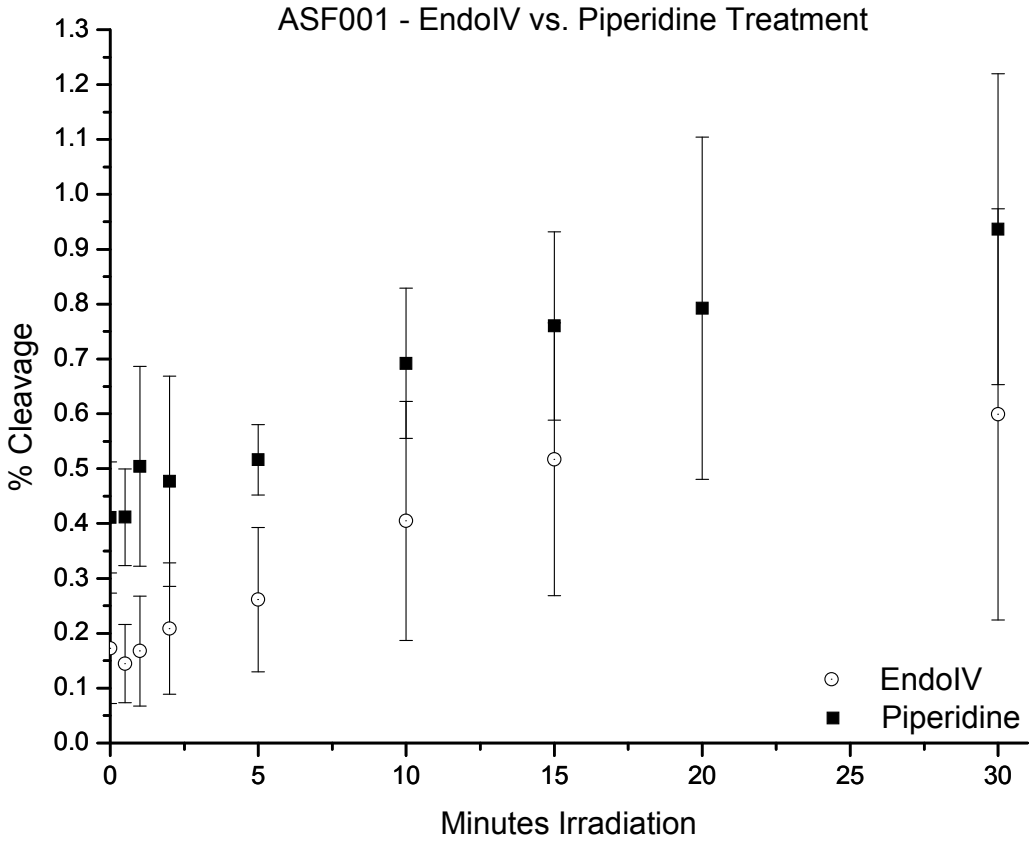

Figure 3.16: Graphical comparison of endoIV vs. piperidine cleavage methods for detection of EET in ASF001. Percent cleavage calculated from the intensity of the EET induced cleavage band relative to the total intensity. Each data point consists of 7-9 experiments at each time point and the error bars are the standard deviation of the average of each time point.

The experiments used to determine if a polaron type mechanism is operative in EET were conducted using both piperidine and endoIV cleavage methods for comparison and to ensure consistency. Additonally, each experiment was conducted under aerobic conditions and data represents an average of a minimum of three independent trials. The remainder of the DNA sequences were conjugated with TMDN, and their efficiency of EET is summarized in Table 3.3. The graphs used for determination of the data included in Table 3.3 can be found in the Appendix (Figure II.2 thru Figure II.14). The greatest percent and rate of cleavage was observed with the sequences that have 4 or more adjacent **T**'s. The greatest amount of total cleavage was observed with ASF005 which has 5 adjacent **T**'s and the **A** barrier to EET is adjacent to the ^{Br}U. ASF004 has 6 adjacent **T**'s and has the next greatest amount of total percent cleavage. ASF004 also has the highest initial rate of cleavage, which is possibly due to the sequence not having an **A** barrier to EET. While there are slight differences, the percent cleavage data of ASF001, 004, 005 and 006 are within experimental error of one another (Figure II.15). The error in the initial rates for ASF002, 003 and 101 is greater than the actual values, therefore these sequences are assumed to have little or no detectable cleavage.

Table 3.3: Comparison of percent and rates of cleavage by DNA sequence. Bases in red highlight sequence variation, G represents site of aromatic amine conjugation on complementary DNA strand and ND = not determined.

Sequence	Maximum % Cleavage (zero corrected)		Initial Cleavage Rate (percent/min)	
Aerobic hυ	**Pip**	**EndoIV**	**Pip**	**EndoIV**
^{Br}U-TTTTATG (ASF001)	0.52 ± 0.10	0.43 ± 0.14	0.031± 0.006	0.025 ± 0.019
^{Br}U-TTTATTG (ASF002)	0.15 ± 0.14	0.10 ± 0.06	0.010 ± 0.04	0.003 ± 0.016
^{Br}U-TTATTTG (ASF003)	0.22 ± 0.03	0.11 ± 0.16	0.030 ± 0.03	0.008 ± 0.042
^{Br}U-TTTTTTG (ASF004)	0.64 ± 0.45	0.44 ± 0.20	0.045 ± 0.15	0.015 ± 0.013
^{Br}U-ATTTTTG (ASF005)	0.66 ± 0.10	0.52 ± 0.03	0.028 ± 0.004	0.026 ± 0.003
^{Br}U-TTTTTAG (ASF006)	0.44 ± 0.34	ND	0.032 ± 0.014	ND
^{Br}U-TTTTGTG (ASF101)	0.09 ± 0.05	0.07 ± 0.04	0.007 ± 0.01	0.005 ± 0.003

There is little, if any, detectable cleavage seen with ASF002, 003 and 101 this suggests that a polaron type mechanism is not operative for EET. If the tract of **T**'s was acting as a polaron to stabilize an excess electron than the orientation and placement of the **T**-tract should directly affect EET. The level of EET observed for AS001, 004, 005, and 006 are all very similar and the placement of the **A** barrier does not appear to affect the total percent or the rate of cleavage. The **T**-tract in ASF002 should have stabilized an excess electron and shown an intermediate level of cleavage as compared with ASF001. Furthermore, the smaller **T**-tract of ASF003 would have shown an even smaller amount of cleavage. Since neither ASF002 nor ASF003 had any detectable cleavage it suggests that the excess electron is trapped by a mechanism other than trapping by ^{Br}U. These other mechanisms may include

back electron transfer to the AA or trapping with molecular oxygen. It was shown previously that the percent cleavage increases by 20 % when the photoirradiation is conducted under anaerobic conditions.[179] Therefore, in order to determine if quenching by molecular oxygen caused the lack of detected EET in ASF002, 003 and 101 the experiments were repeated under anaerobic conditions.

Anaerobic dpTMDN Photochemistry

The photochemistry of ASF001 was used first to directly compare the results obtained under both aerobic and anaerobic conditions. Figure 3.17 illustrates that under aerobic conditions, the amount of cleavage detectable by piperidine treatment increases by a factor of 2. This is much greater than observed previously however, the same affect was not observed with endoIV treatment. EndoIV cleavage appears to be virtually the same under both conditions (when the zero time point is taken into consideration). The increase cleavage observed by piperidine treatment, suggests that as mentioned in the introduction piperidine is less specific than EndoIV. These initial results suggest that endoIV is a more accurate method for detection of EET. The other DNA sequences that did not exhibit EET previously were then irradiated under anaerobic conditions to determine if there would be an increase in the observed cleavage for the sequences. If lack of EET in ASF002, 003 and 101 is due to trapping by molecular oxygen occurring on a

faster time scale than EET in these sequences, then EET might be more detectable if irradiation occurred under anaerobic conditions.

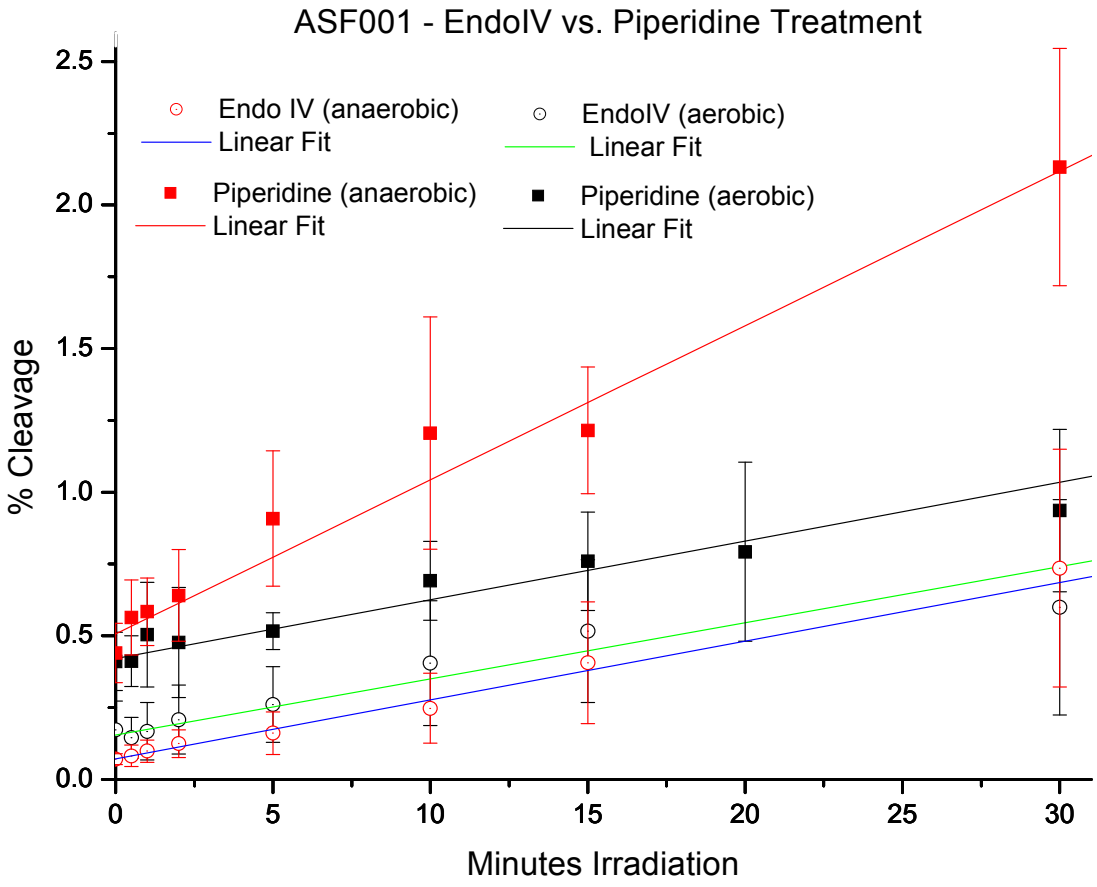

Figure 3.17: Photo-induced electron transfer from the electron donor to ^{Br}U using both endoIV and piperidine cleavage methods in aerobic and anaerobic conditions. Percent cleavage was calculated from the intensity of the photochemical cleavage band relative to the total intensity per time point. Initial rates are indicated by linear fit lines.

Table 3.4 is a compilation of the data from the anaerobic photochemistry experiments. The graphs used for determination of the data included in Table 3.3 can be found in the Appendix (Figure II.16 thru Figure II.29). With the exception of ASF001, no significant difference is observed between the total percent photochemically induced cleavage of DNA under aerobic and anaerobic conditions. Only ASF001 and ASF004 behaved

differently when irradiated under anaerobic conditions. As mentioned previously, the observed differences are only for the piperidine treated samples and not for the samples treated with endoIV. For these two sequences anaerobic conditions appear to enhance the initial rate of EET. While there was no significant difference in rates under anaerobic conditions, the error is lower in the absence of oxygen. Since the exclusion of oxygen from the experimental conditions did not enhance EET across the board, the next step question was to determine if the driving force for the initial electron injection was the limiting factor for the observed EET.

Table 3.4: Comparison of percent and rates of cleavage by DNA sequence under anaerobic conditions. Bases in red highlight sequence variation, and G represents site of aromatic amine conjugation on complementary DNA strand.

Sequence	Maximum % Cleavage (zero corrected)		Initial Cleavage Rate (percent/min)	
Anaerobic hυ	**Pip**	**EndoIV**	**Pip**	**EndoIV**
^{Br}U-TTTTATG (ASF001)	1.69 ± 0.16	0.67 ± 0.21	0.080 ± 0.033	0.020 ± 0.007
^{Br}U-TTTATTG (ASF002)	0.10 ± 0.17	0.12 ± 0.08	0.021 ± 0.014	0.004 ± 0.005
^{Br}U-TTATTTG (ASF003)	0.30 ± 0.08	0.17 ± .06	0.020 ± 0.002	0.010 ± 0.001
^{Br}U-TTTTTTG (ASF004)	0.66 ± 0.27	0.17 ± 0.02	0.116 ± 0.058	0.012 ± 0.004
^{Br}U-ATTTTTG (ASF005)	0.72 ± 0.29	0.18 ± 0.08	0.022 ± 0.01	0.020 ± 0.004
^{Br}U-TTTTTAG (ASF006)	0.31 ± 0.04	0.16 ± 0.03	0.013 ± 0.003	0.018 ± 0.001
^{Br}U-TTTTGTG (ASF101)	0.30 ± 0.12	0.07 ± 0.02	0.039 ± 0.009	0.003 ± 0.001

Developing Electron Donors of Varying Reducing Potential

Initially DAN and TMDN were chosen for EET studies because DAN is commercially available with a relatively high grade of purity and TMDN is readily synthesized from DAN. The methyl groups on TMDN were initially thought to enhance the reducing power of the AA making it a better donor for EET studies when compared to DAN. However, experimentally DAN was shown to be a much better donor for EET studies.[179] This result can now be rationalized by the steric interaction of the methyl groups on the TMDN gamma-hydrogen on the aromatic ring. These unfavorable steric interactions cause the methyl groups to be rotated out of plane from the aromatic pi system and decrease the resonance contributions from the lone pair of electrons on the nitrogens. In order to elucidate if donor efficiency was the limiting step in the EET mechanism, a series of donors with a range of methyl substitutions for EET were synthesized (Figure 3.18) by Neil Campbell in the Rokita Lab. The increasing degree of methylation on DAN derivatives was designed to provide a range of electron donating capabilities EET studies.[189] Six DAN derivatives were prepared for EET studies and in order to determine their reducing power E_{ox} values were needed.

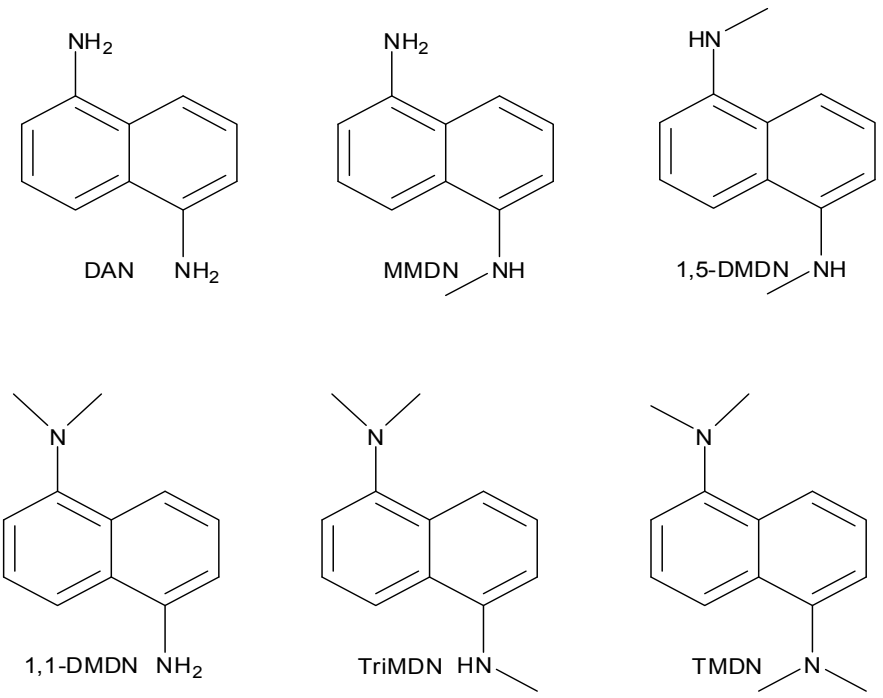

Figure 3.18: AA compounds synthesized by Neil Campbell (DAN = 1,5-diaminonapthalene, MMDAN = N1-methyl-1,5-diaminonapthalene, 1,5-DMDN = N1,N5-dimethyl-1,5-diaminonapthalene, 1,1-DMDN = N1,N1-dimethyl-1,5-diaminonapthalene, TriMDN = N1,N1,N5-trimethyl-1,5-diaminonapthalene, TMDN = N1,N1,N5,N5-tetramethyl-1,5-diaminonapthalene).

If the driving force does indeed control EET, then a correlation should be evident between the values of E_{ox}* and EET. E_{ox}*, in turn, can be determined in part by E_{ox} (Equation 3.1). Values for redox potentials of some of the DAN derivatives have been reported in the literature.[190-192] The conditions in the literature were typically conducted in organic media with a variety of electrolytes and electrodes.[190,191] Since redox potentials vary greatly depending on the solvent system, supporting electrolyte and reference electrode, voltammetry experiments were all conducted under the conditions of 10 mM sodium phosphate (pH 7.0), 100 mM sodium chloride, and < 5 % acetonitrile (used to make concentrated stock solution of the AA) to a final AA

concentration of 500 μM. This solution was chosen for its ability to dissolve the AAs and for its resemblance to biologically relevant conditions.

Equation 3.1: Conversion from reduction potentials measured by electrochemical techniques to excited state oxidation potential (E_{ox}*(Volts)), where E_{ox} is the oxidation potential of the donor (Volts), and E_{00} its excited state energy (kcal/mol).[193]

$$E_{ox} * = E_{ox} - (\frac{E_{00}}{23.06})$$

Initial trials to determine E_{ox} using cyclic voltammetry (CV) proved problematic due to polymer film formation of DAN upon the surface of the platinum electrode.[190,191,194] This polymer was not conductive under aqueous conditions therefore the reverse scan and subsequent scans showed diminishing current. In order to determine that instrumentation was not the cause of the erratic scans and polymer formation, E_{ox} determinations were repeated under the CV conditions outline in reference 190.[190] The data was successfully reproduced but an exhaustive process of cleaning the platinum electrode after each scan was necessary.

After many attempts to determine the reverse potential in aqueous media using CV, it was determined that alternating current (AC) voltammetry[180] (Army Research Labs in Adelphi, MD) could be used to determine the redox potentials of the DAN derivatives (Figure 3.19). This method gives the same information as CV, but it scans both forward and reverse potentials simultaneously. The results of all 6 compounds are illustrated in Figure 3.19. The scans from 3 – 6 trials with each compound were averaged to determine the redox potentials. The data shown is from

just one representative group of scans. The derivatives that have the possibility for steric interactions with methyl groups have lower potentials (350-389 mV) and the derivatives that have no negative steric interactions have higher potentials (208-252 mV). This data is in agreement with previous experiments conducted in the lab comparing DAN and TMDN and suggests that DAN, MMDN, and 1,5-DMDN should all behave similarly.

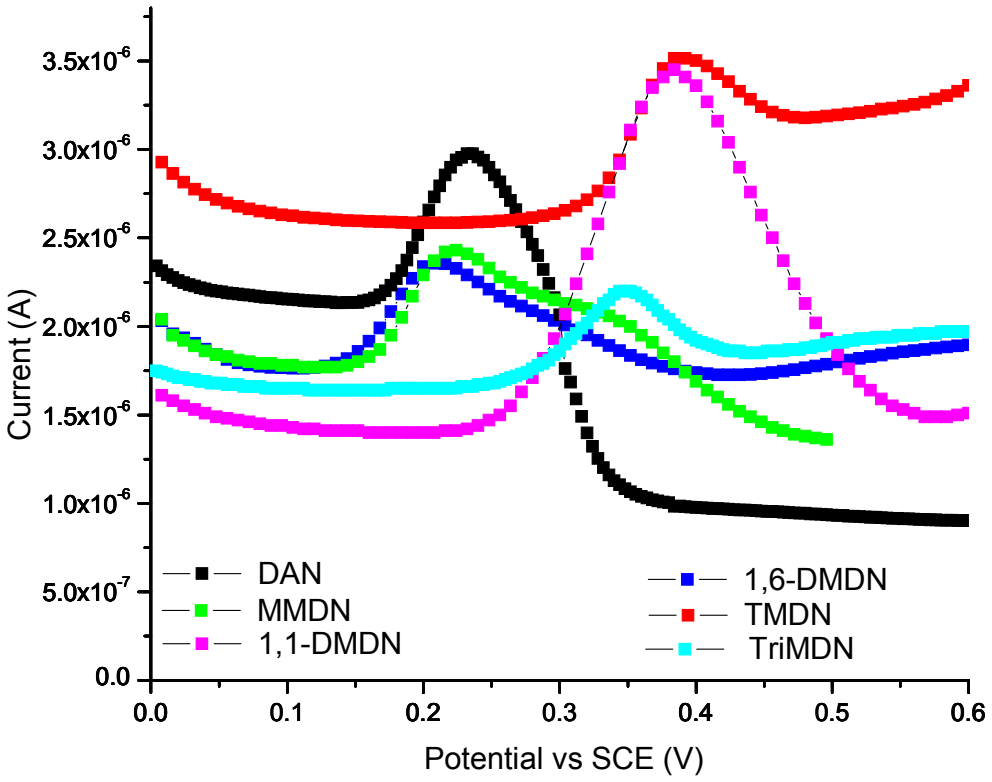

Figure 3.19: Representative composite AC voltammogram of AA compounds for determination ground state redox potentials. All experiments were conducted at ambient temperature in a three component electrode cell with a platinum working, platinum wire counter and saturated calomel reference electrode in 10 mM sodium phosphate (pH 7.0), 100 mM sodium chloride, and < 5 % acetonitrile with an AA concentration of 500 µM.

In addition to the AA derivatives, a series of aminoanthracene (AN) derivatives were also screened (Figure 3.20). AN offers a potential benefits over DAN because it has an additional conjugated aromatic ring. This

additional conjugation may increase the stability of its 1 electron oxidized species. Furthermore, the λ_{max} of 407 nm allows for direct excitation of AN without exciting the DNA.

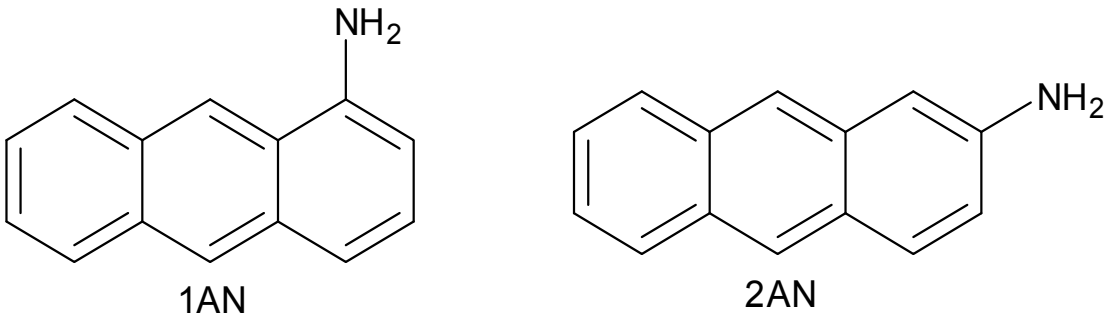

Figure 3.20: Aminoanthracene (AN) compounds.

Figure 3.21 illustrates the redox potentials of the AN compounds. These compounds are only sparingly soluble in aqueous media therefore AC voltammetry was conducted in 50 % acetonitrile solution. All other conditions remained equivalent to those used for the DAN derivatives.

The electrochemistry data combined with excitation and emission maxima (obtained from Neil Campbell (DAN derivates) and TJ Simons (AN)) were used to calculate the excited state oxidation potentials (Table 3.5). The larger negative E_{ox}* value indicates a greater reducing power. The increased conjugation in the AN derivatives does not increase the reduction potential of these compounds. In fact, the data suggests that MMDN and DAN are the best candidates for further studies on EET. Based on this data, and the availability of the starting material, DAN was chosen as the compound to test if the initial driving force was the limiting step in EET within sequences used to study contributions of polaron in transfer.

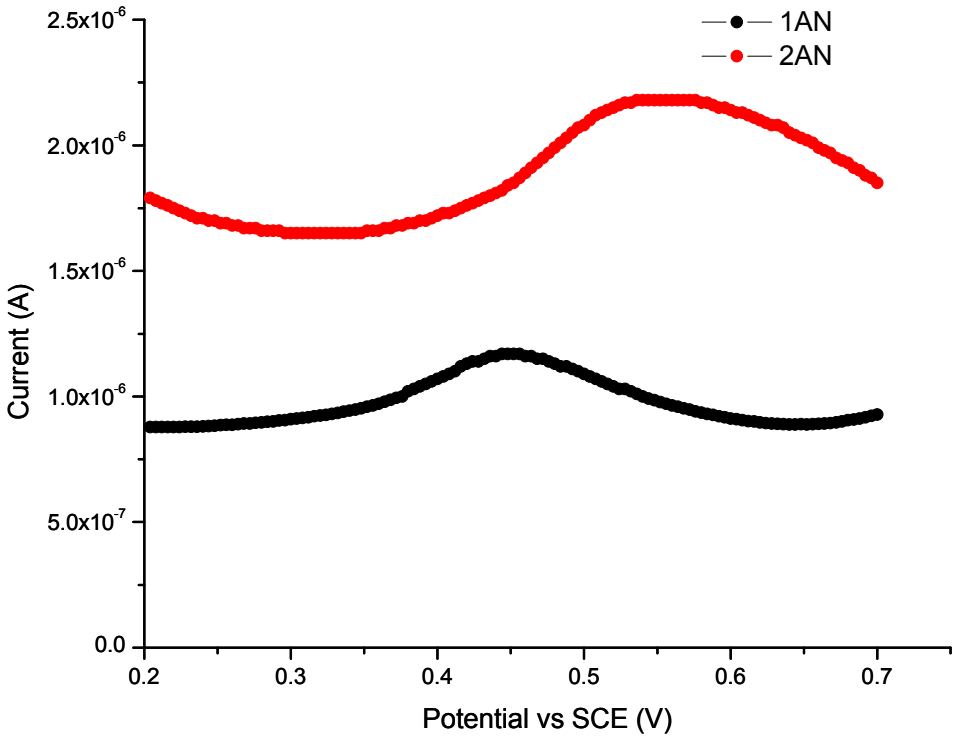

Figure 3.21: Representative composite AC voltammogram of AN derivatives for determination ground state redox potentials. All experiments were conducted at ambient temperature in a three component electrode cell with a platinum working, platinum wire counter and saturated calomel reference electrode in 10 mM sodium phosphate (pH 7.0), 100 mM sodium chloride, and 50 % acetonitrile with an AN concentration of 500 µM.

Table 3.5: Values used for determination of excited state oxidation potentials (E_{ox}*). Redox properties of the compounds studied in phosphate buffered saline *vs.*SCE. The E_{ox} is a calculated average consisting of data from no less than 3 independent experiments and the error represents the range of data obtained.

Compound	Excitation	Emission	E_{00} (kcal/mol)	E_{ox} (mV)	E_{ox}^* (V)
DAN	323	404	80.5	250±20	-3.24
MMDN	327	409	80	220±6	-3.24
N1,N5-DMDN	334	414	78.3	208±0	-3.18
N1,N1-DMDN	317	427	78.3	380±6	-3.01
TMDN	312	433	78.1	400±7	-2.99
TriMDN	323	429	76.9	350±2	-2.98
1AN	389	564	62.7	470±20	-2.25
2AN	393	506	63.4	550±5	-2.20

Effect of Increased Driving Force on EET: dpDAN Conjugate

The protected DAN (prDAN) compound was readily available as it is prepared during one of the previous steps of the synthesis of the prTMDN compound.[133] Since anhydrous conditions were not necessary for the deprotection to go to completion, hydrazine monohydrate was used instead of the anhydrous hydrazine (Figure 3.22). The reasoning for this was twofold, the first reason was that the anhydrous hydrazine is more expensive and more difficult to handle and the second reason was that the manufacturer was only offering the anhydrous version in large quantities. Since the reaction only calls for approximately 10 µL of hydrazine it was decided to attempt the deprotection with the hydrazine monohydrate. The reaction proceeded to completion with > 90 % yields and the deprotected DAN material was immediately coupled to ASF002 and ASF101.

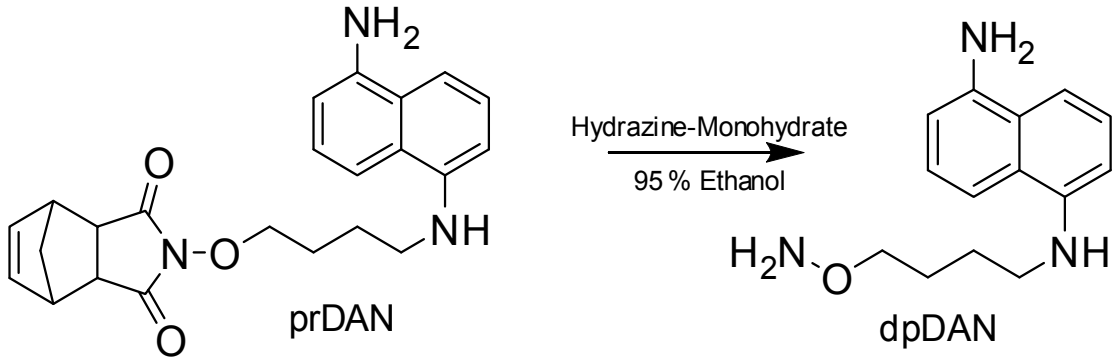

Figure 3.22: prDAN deprotection.

Preliminary EET experiments of dpDAN conjugated with DNA were conducted with ASF002 and ASF101 to determine if increasing the strength of the initial electron donor would induce EET to an observable level in these

sequences. If dpDAN is, as calculated, a better reducer than dpTMDN then it is possible that this conjugate would be able to donate an electron with enough energy to surpass the barrier inhibiting EET. In order to visualize even slight differences between the ability of dpTMDN and dpDAN to promote EET, irradiation was performed under anaerobic conditions. However, as illustrated in Figure 3.23, no visual increase in cleavage was seen in the DAN coupled DNA when compared to the TMDN coupled DNA. Figure 3.24 plots the percent cleavage in ASF002 conjugated with dpDAN vs. dpTMDN. The EET induced cleavage for dpDAN falls within experimental error of dpTMDN. These results suggest that increasing the driving force for the reaction does not affect the ability of these sequences to facilitate EET. Subsequently, more research is needed to determine if there is a factor blocking EET and if that blockage is preventing detection of EET.

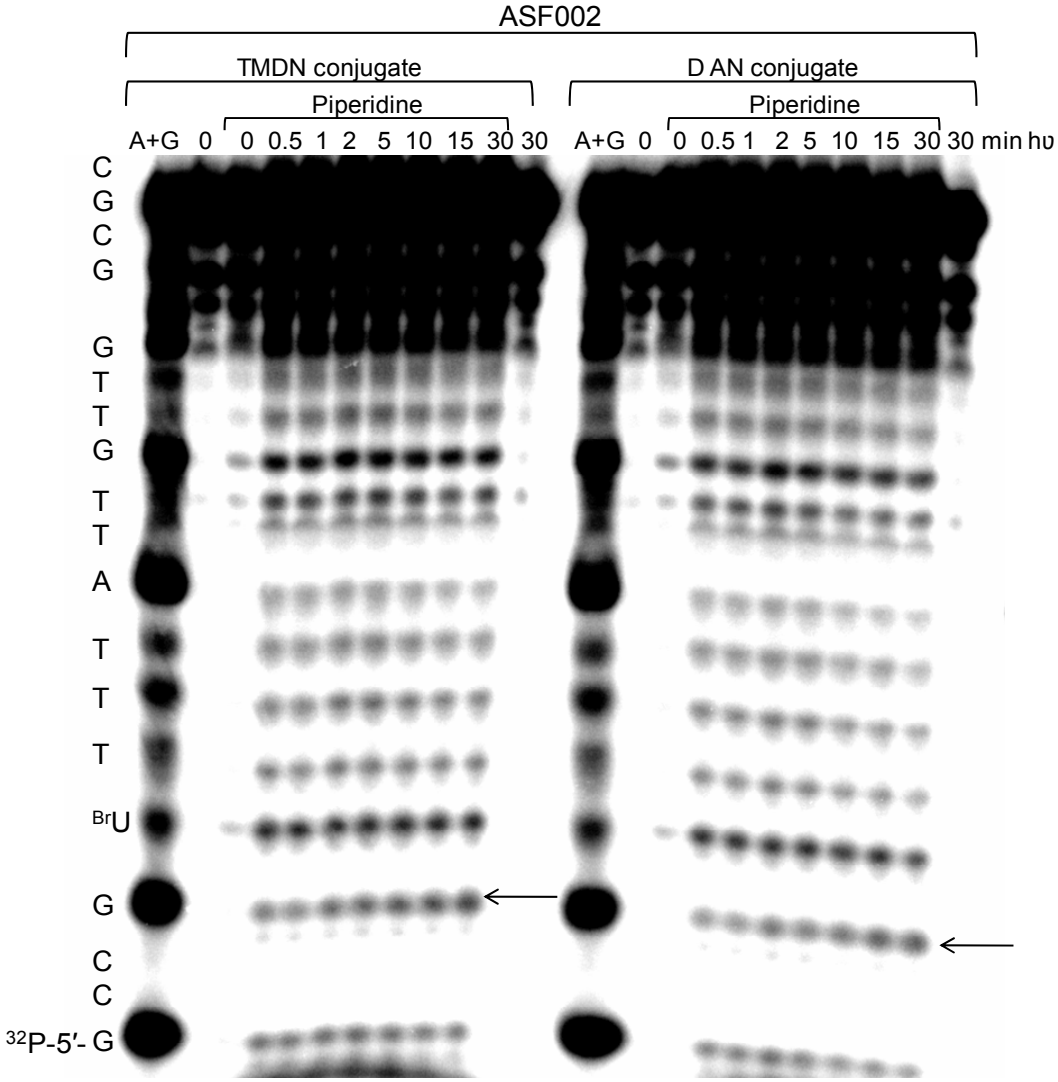

Figure 3.23: Cleavage of comparison of ASF002 conjugated with TMDN and DAN (arrow marks site of photochemical cleavage). Image was overexposed in order to illustrate site of photochemical cleavage bands.

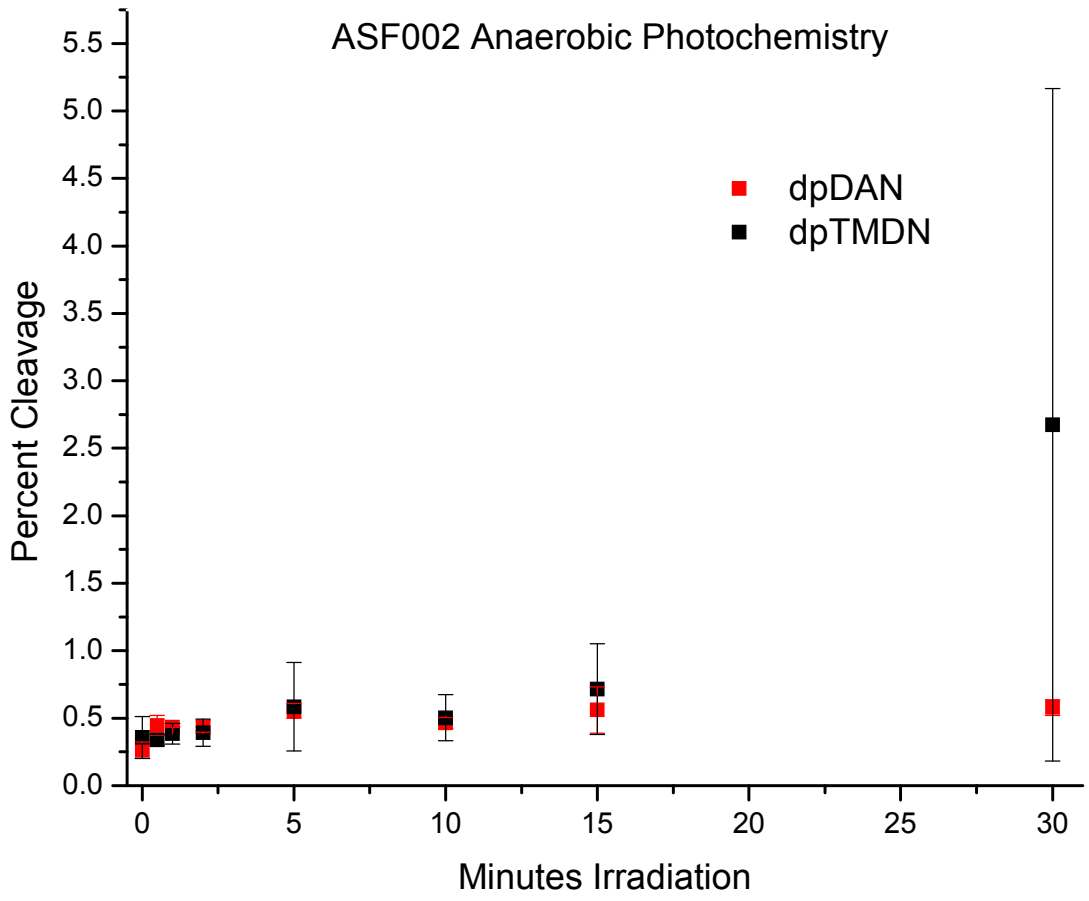

Figure 3.24: Photo-induced electron transfer from the electron donor to ^{Br}U using piperidine cleavage detection method in anaerobic conditions. Percent cleavage was calculated from the intensity of the photochemical cleavage band relative to the total intensity per time point. Each data point for dpTMDN consists of 7-9 experiments at each time point and the error bars are the standard deviation of the average of each time point.

3.4 Summary and Conclusion

Despite polaron in HT, current data on EET does not fit an equivalent model. For example, sequences which did not have an **A** barrier to EET showed a moderate amount of EET. Sequences designed that incrementally increase the **T**-tract may give insight on the maximum range of transport (Figure 3.25). Additionally, sequences that lack of observed EET may be due to charge stabilization on the adjacent **T**-tract and radical recombination as

opposed to crossing the **A** barrier (Figure 3.26). Further experiments on the sequences that facilitate EET are necessary in order to elucidate the type of mechanism and characteristics of DNA that control EET.

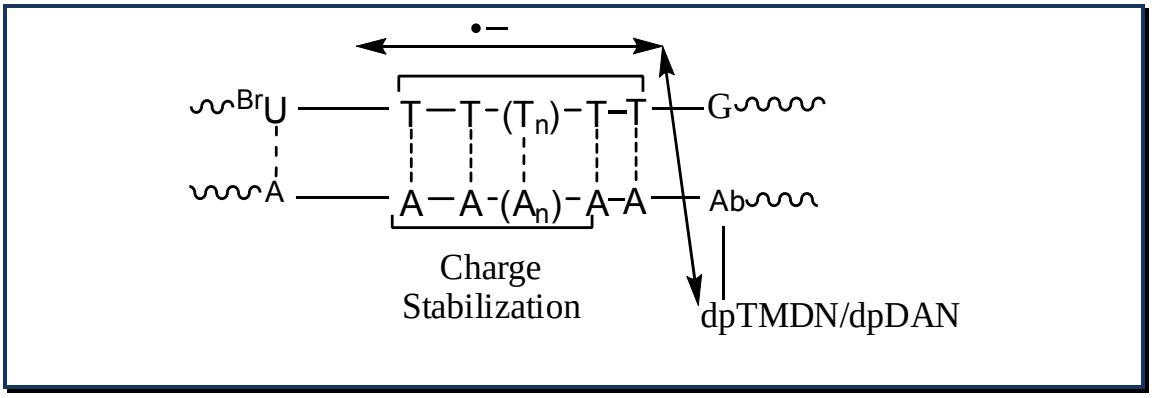

Figure 3.25: Long-range EET may be possible if barrier is removed between donor and acceptor.

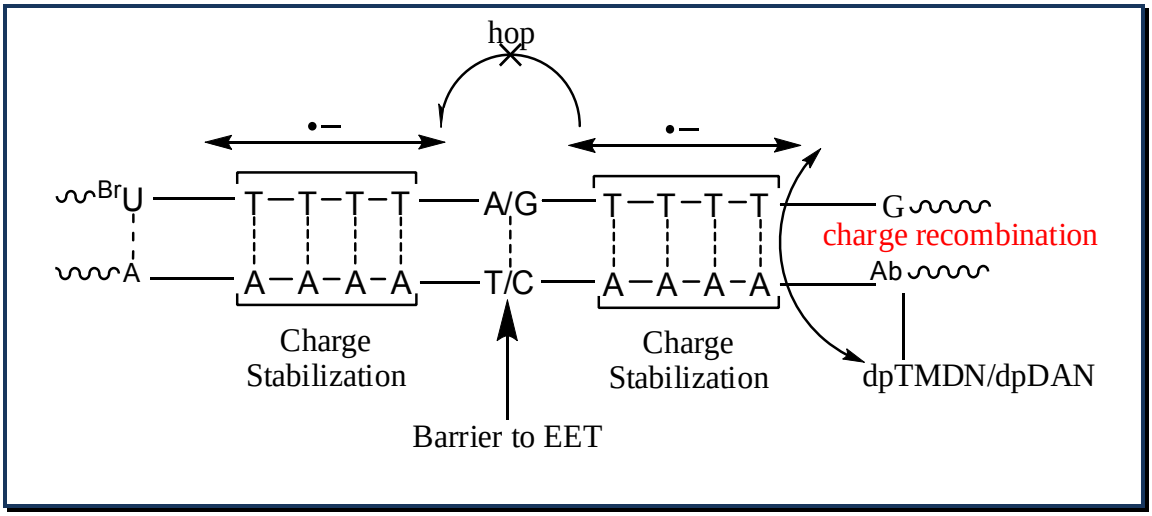

Figure 3.26: Charge recombination scheme that precludes EET to ^{Br}U. In this scheme the rate of CT across the high barrier is slower than charge recombination to the TMDN.

Chapter 4

Summary and Final Discussion

The purpose of this dissertation was to look at the variable efficiency of direct and indirect pathways affecting T^T accumulation in two biologically relevant systems.

The expected periodicity of T^T formation in the nucleosome system was used in an attempt to determine the rates of T^T redistribution and more specifically of the reversal reaction. While the rates of T^T reversion were not determined, the system did provide the minimum requirements necessary for the design of a system that will allow for study of the T^T reversion reaction. In the literature, T^T formation was modulated by using heterogenous NCP DNA and this method can be utilized for future studies.[63,66,143] Since the DNA used in these experiments is random in sequence, there is possibly a T^T at every spot with respect to the NCP. This method was not pursued initially because preliminary trials were conducted in the Rokita lab prior to the current studies and T^T modulation was not observed. Despite the experimental challenges, these experiments have already shown to give different distributions of T^T formation and this method deserves further consideration. Another method involves using DNA that is inherently bent due to sequence content.[170] As mentioned in the introduction, the distribution of T^T is structure and not protein dependent therefore the bends in these sequences should give variable rates of T^T formation.[62] Conveniently, these bending DNA sequences are studied in the lab of Professor Jason Kahn in the department of chemistry at the University of Maryland and are readily available for use. This method also does not require NCP for creating the T^T

distribution therefore nullifies any difficulties or experimental issues resulting from NCP purification or reconstitution efficiency. Despite the fact that the reversibility of T^T was not determined using the NCP system, these experiments described are an optimal place to start new research on the rates of T^T reversibility.

The second system was a model system that was used to determine the intrinsic factors that could influence EET. This system was used to focus on the effect of sequence on EET and more specifically, studies were conducted to determine if a polaron-type mechanism was operative for EET. Seven DNA sequences were screened for their ability to promote EET. These sequences were static in length and distance between the donor (dpTMDN) and acceptor (^{Br}U) yet they differed in the intervening DNA sequence. Different size **T**-tracts were used to possibly stabilize an excess electron and to determine if a polaron-type mechanism was operative. Initial trials were conducted under aerobic conditions with two complementary methods of detection. These early studies indicated a lack of detectable EET in majority of the sequences and led to further studies under anaerobic conditions in order to determine if lack of detection was due to molecular oxygen quenching the excess electron. While the error was lower under anaerobic conditions, there was little observable difference in comparing initial rates and total percent cleavage in aerobic vs. anaerobic conditions. The next step was to determine if the initial electron donor was the limiting step in the EET mechanism. If driving force did play a role in EET, then a

correlation would have been evident between E_{ox}* and EET. In order to determine E_{ox}* the values of E_{ox} for a variety of AA's were determined using AC voltammetry. The E_{ox}* values suggested that dpDAN would be a stronger donor for EET studies. Two of the sequences used in the previous studies were screened for their ability to promote EET while conjugated to dpDAN. However these initial studies suggest that increasing the driving force for the reaction does not affect the ability of these sequences to promote EET. While current studies suggest that a polaron-type mechanism is not operative in EET, more studies are necessary in order to determine what is preventing EET in the model system and sequences used.

Appendix I

Supporting Information for Chapter 2

Figure I.1 illustrates that formation of T^T decreases after 30 minutes, suggesting that there are multiple sites of DNA damage thus causing a decrease in the detectable amount of accumulated T^T. Also T^T levels off between 10 to 30 minutes suggesting a photostationary state of formation and reversion of T^T between these time points

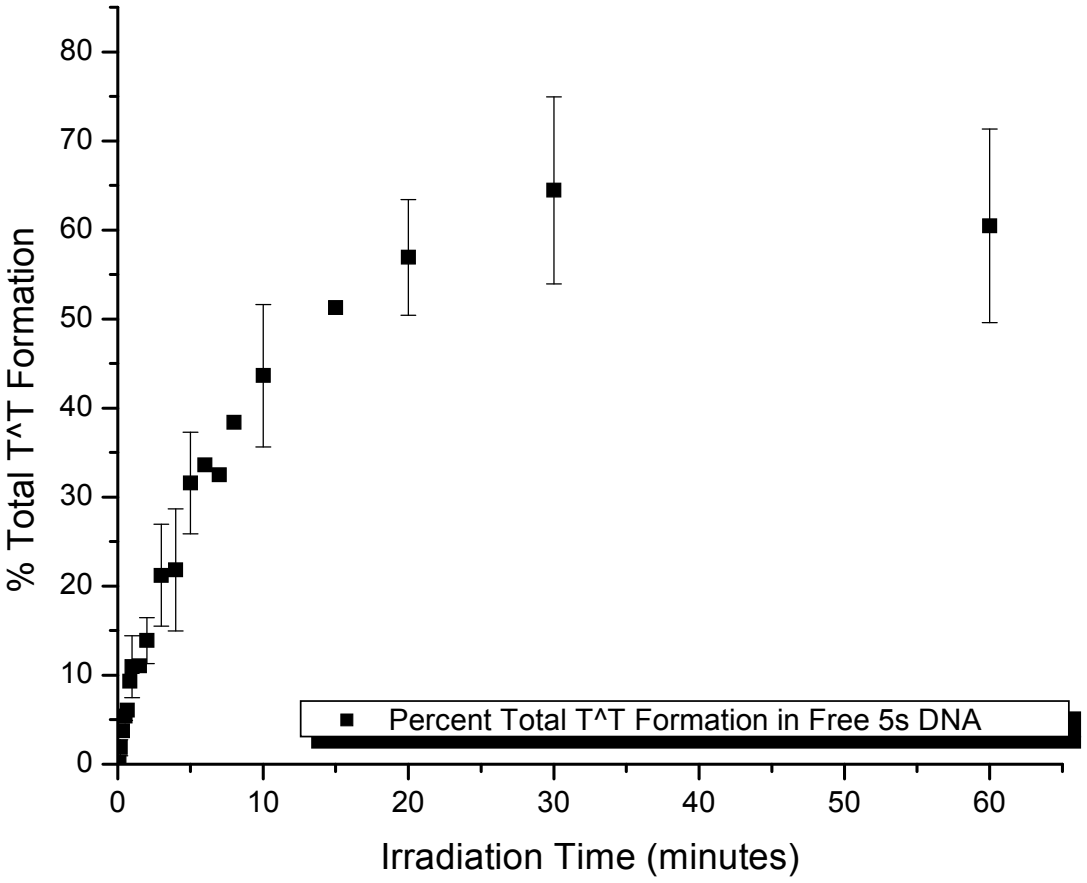

Figure I.1: Total T^T formation in free 5s DNA. Yields for percent cleavage were calculated from the total intensity of T^T with respect to the total intensity per sample as determined by 8 % denaturing gel electrophoresis. Each time point represents an average value from no less than 3 independent experiments and the indicated uncertainty represents the standard deviation from the average.

Maxam-Gilbert sequencing (as described in reference)[145] was used to correlate T^T cleavage bands on gel with DNA sequence. Figure I.2 is an

example of sequencing that is specific for **A** and **G** nucleotides. Figure I.3 is an example of sequencing that is specific for **T** nucleotides.

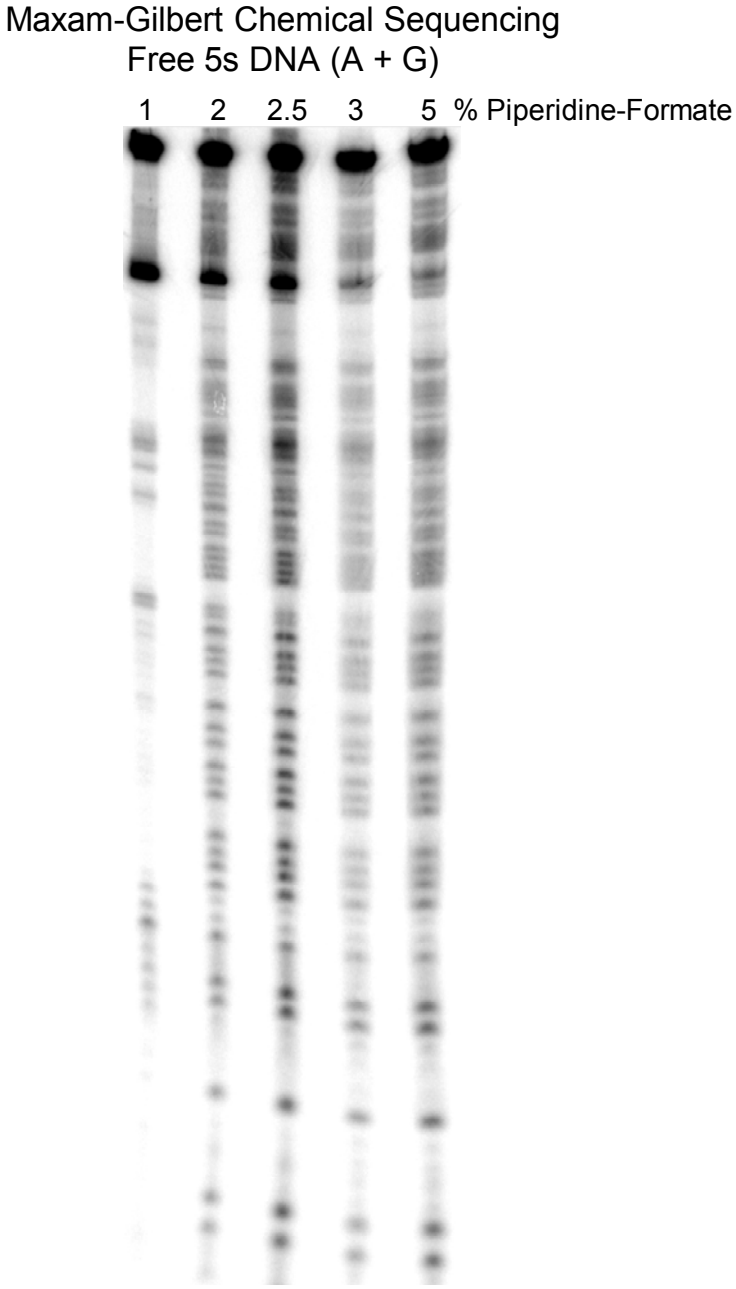

Figure I.2: PAGE gel (8 % denaturing) illustrating chemical sequencing specific for A and G of 5s DNA. Each lane indicates different amounts of 1.0 M piperidine-formate solution (pH 2.0) incubated with the DNA for 10 minutes at 42 °C.

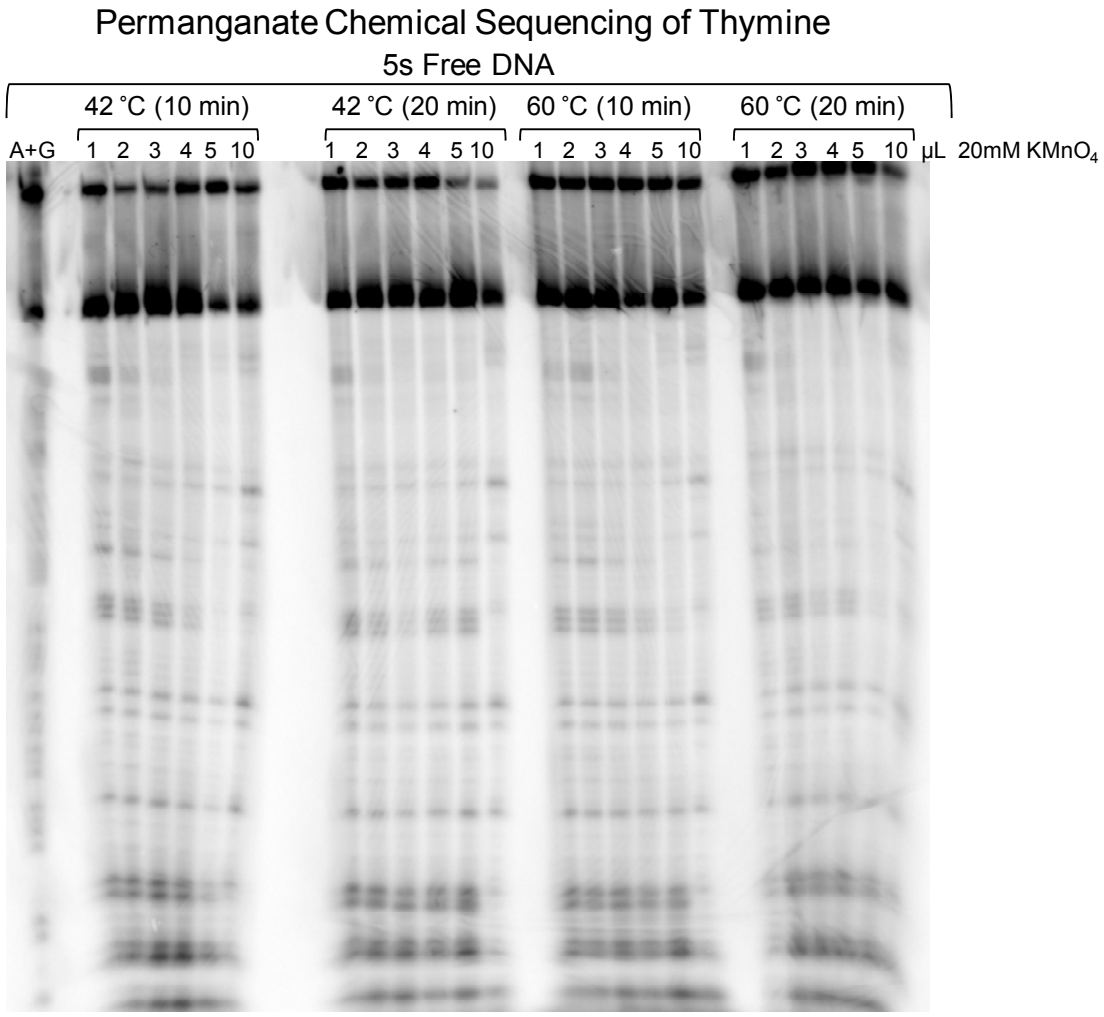

Figure I.3: Denaturing PAGE gel (8 %) illustrating permanganate chemical sequencing specific for T with 5s DNA. Total solution volume was kept constant at 40 µL and permanganate concentration was varied from 500 µM to 5 mM using increasing volumes of 20 mM permanganate. Incubation time and temperature were also varied in order to determine the conditions necessary for reaction at T residues.

Example of one secondary structure of 5s DNA as calculated by MFold (Figure I.4).[159] The structure is fairly stable with a negative ΔG of 31 kcal/mol and a melting temperature of 70 °C. Attempts at denaturation of 5s DNA secondary structure during denaturing PAGE were unsuccessful.

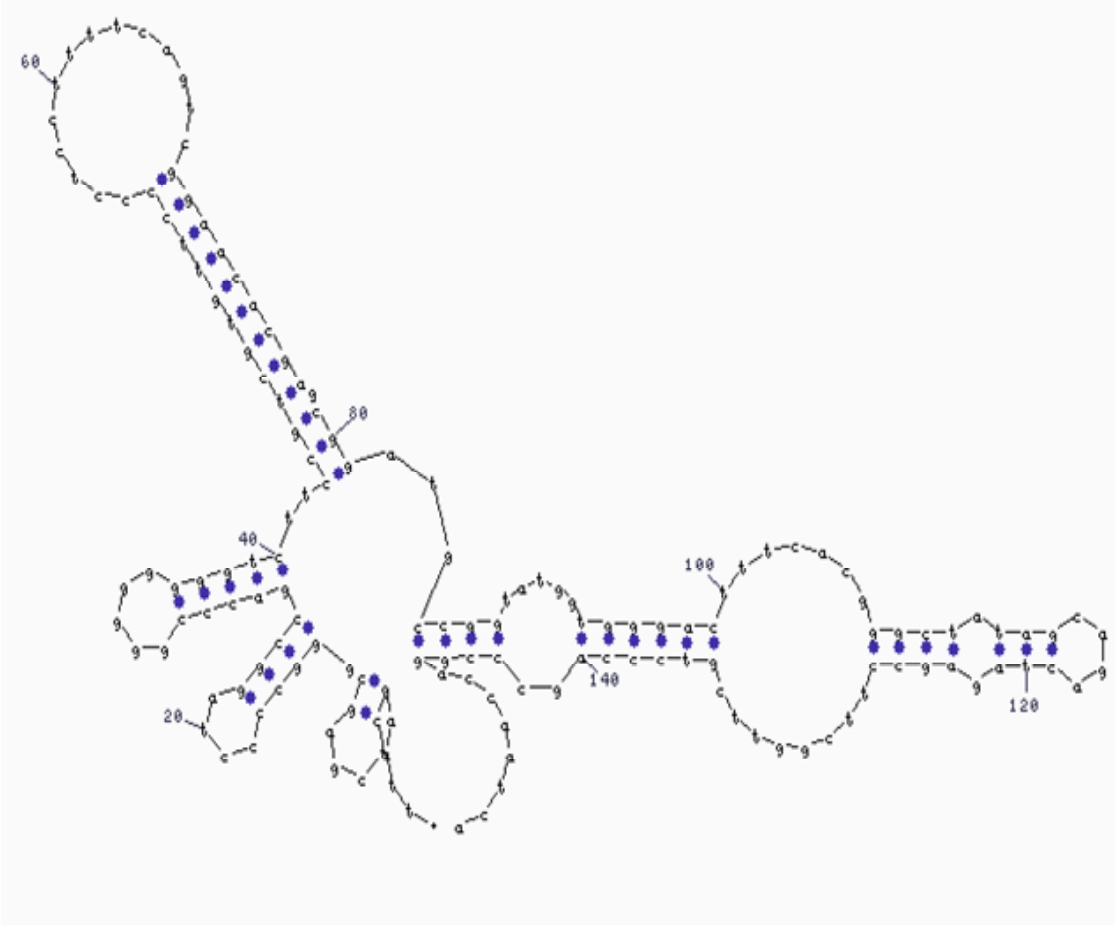

Figure I.4: Secondary structure of 5s DNA as calculated by MFold.[159]

In an attempt to denature secondary structure (example shown in Figure I.4) sequential gel loading of free 5s DNA was attempted. Figure I.5 is a representative denaturing PAGE gel illustrating the results from the sequential gel loading technique.

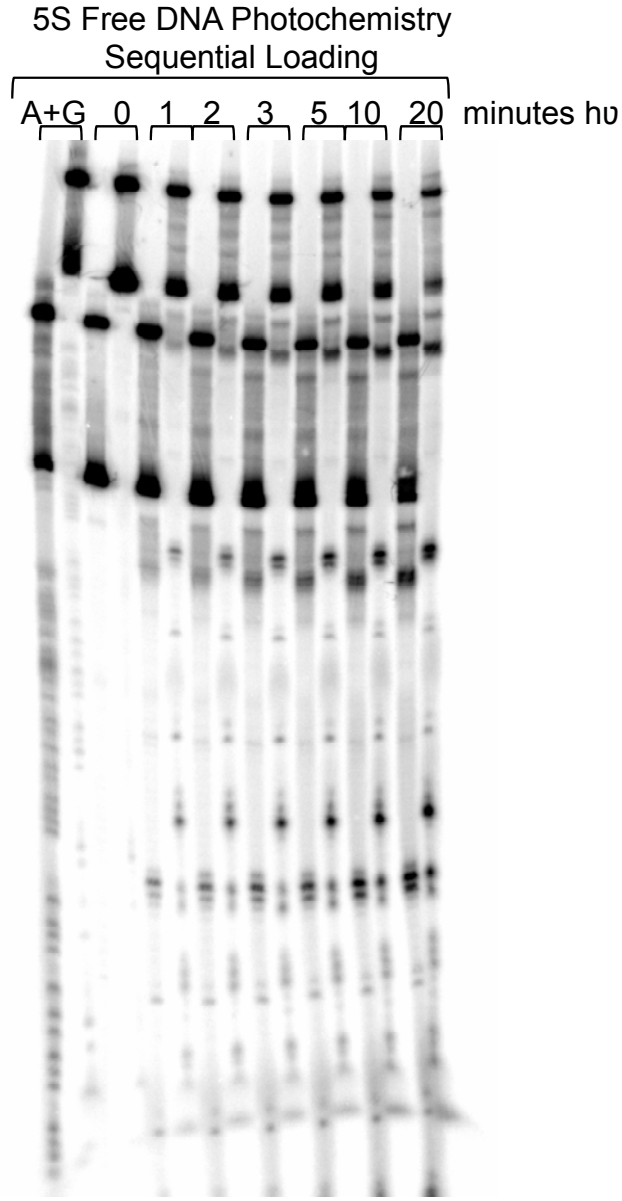

Figure I.5: Denaturing PAGE gel (8 %) illustrating sequential loading of 5s free DNA. Initial samples were loaded and gel was run at 65 W for 30 minutes before second samples were loaded and run at 65 W for 1.5 hours. Prior to PAGE, photoirradiated samples were incubated with endoV 18 hours in order to induce cleavage of T^T.

T4 DNA polymerase (T4 pol) was used as a complementary method for detection of T^T. The graphs below compare the percent cleavage as detected by endoV and T4 pol. The majority of the cleavage detected is within experimental error of the experiment. It is not evident what causes the slight differences in observed cleavage of T^T 3, 7 and 8. The T4 pol reaction was only conducted once, therefore it is not clear if these differences are significant or if they would fall within experimental error after many trials were averaged.

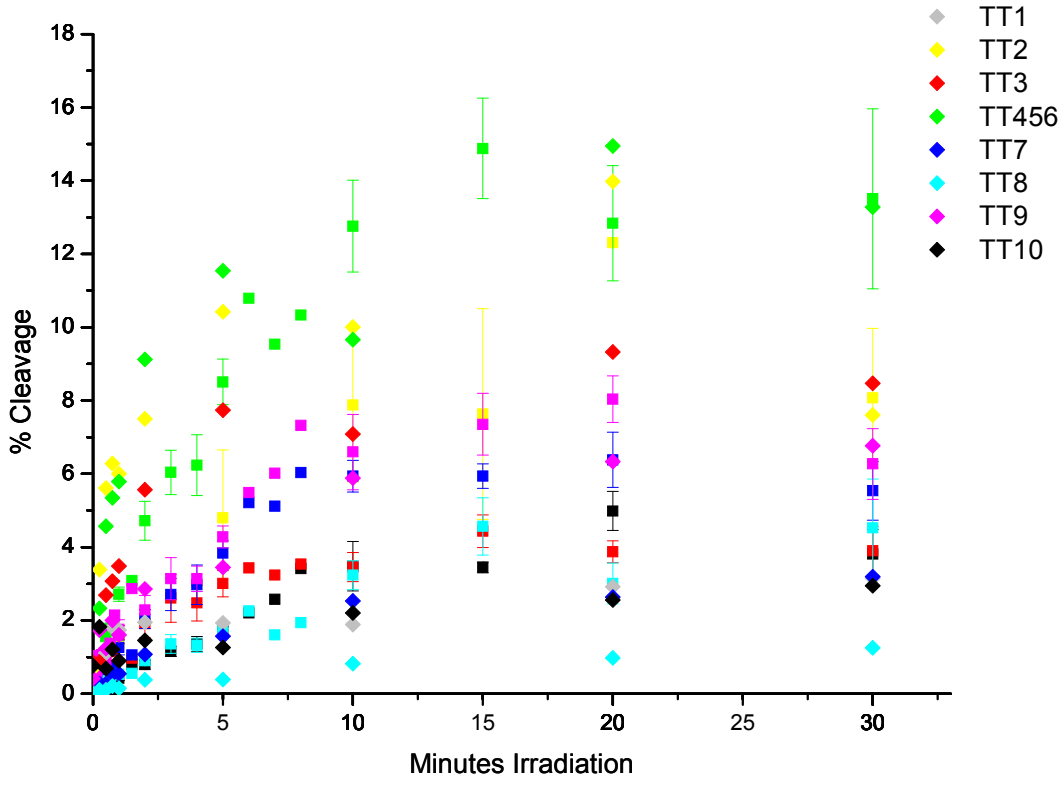

Figure I.6: Graphical comparison of T^T cleavage methods, squares represent cleavage by endo V and diamonds represent cleavage by T4 pol.

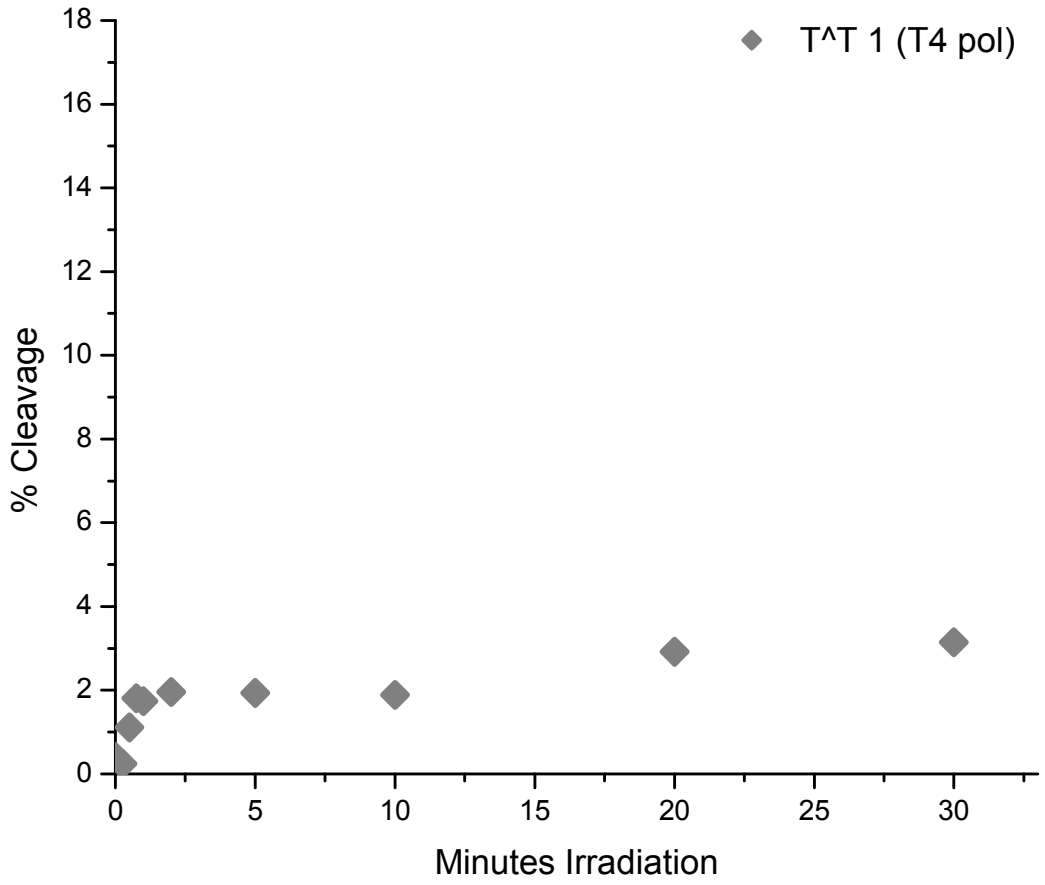

Figure I.7: Graphical representation T4 pol (diamond) treatment method for detection of T^T 1 formation in free 5s DNA. Percent cleavage calculated from the intensity of the T^T induced cleavage band relative to the total intensity per sample. The T4 pol data points represent one experimental trial.

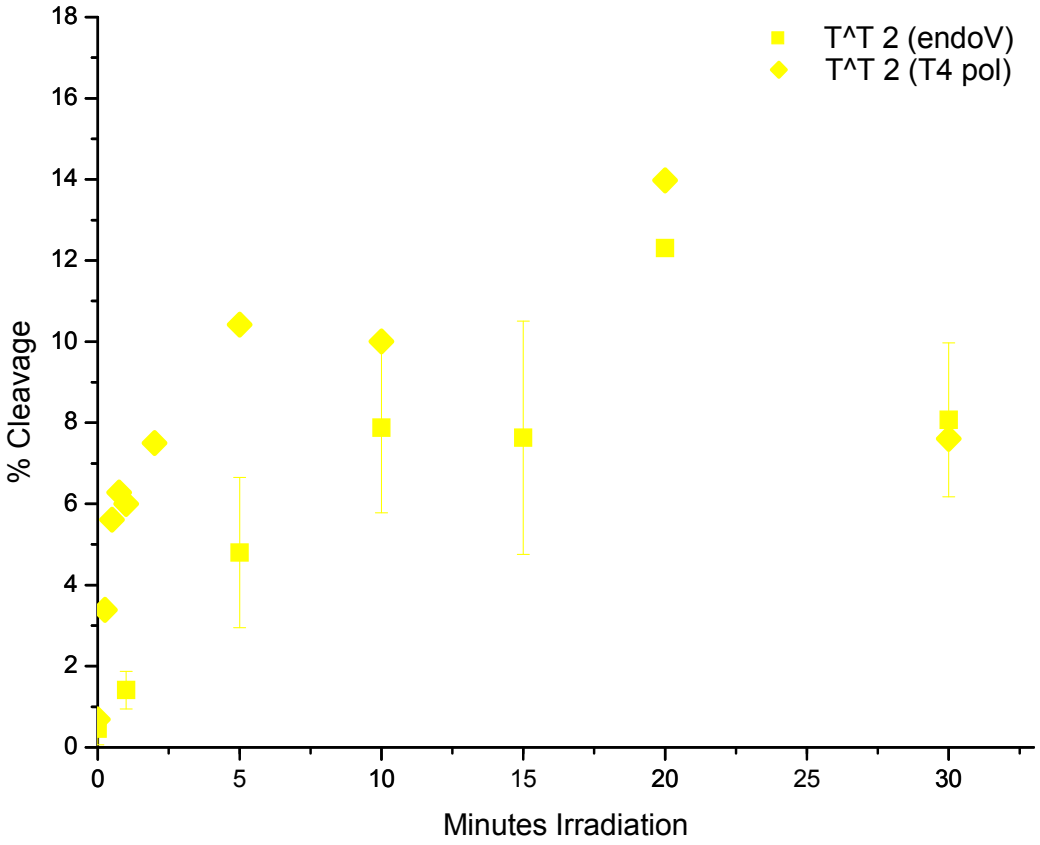

Figure I.8: Graphical comparison of endo V (square) vs. T4 pol (diamond) methods for detection of T^T 2 formation in free 5s DNA. Percent cleavage calculated from the intensity of the T^T induced cleavage band relative to the total intensity per sample. The endo V data points consist of a minimum of three independent experiments at each time point and the error bars are the standard deviation of the average of each time point. The T4 pol data points represent one experimental trial.

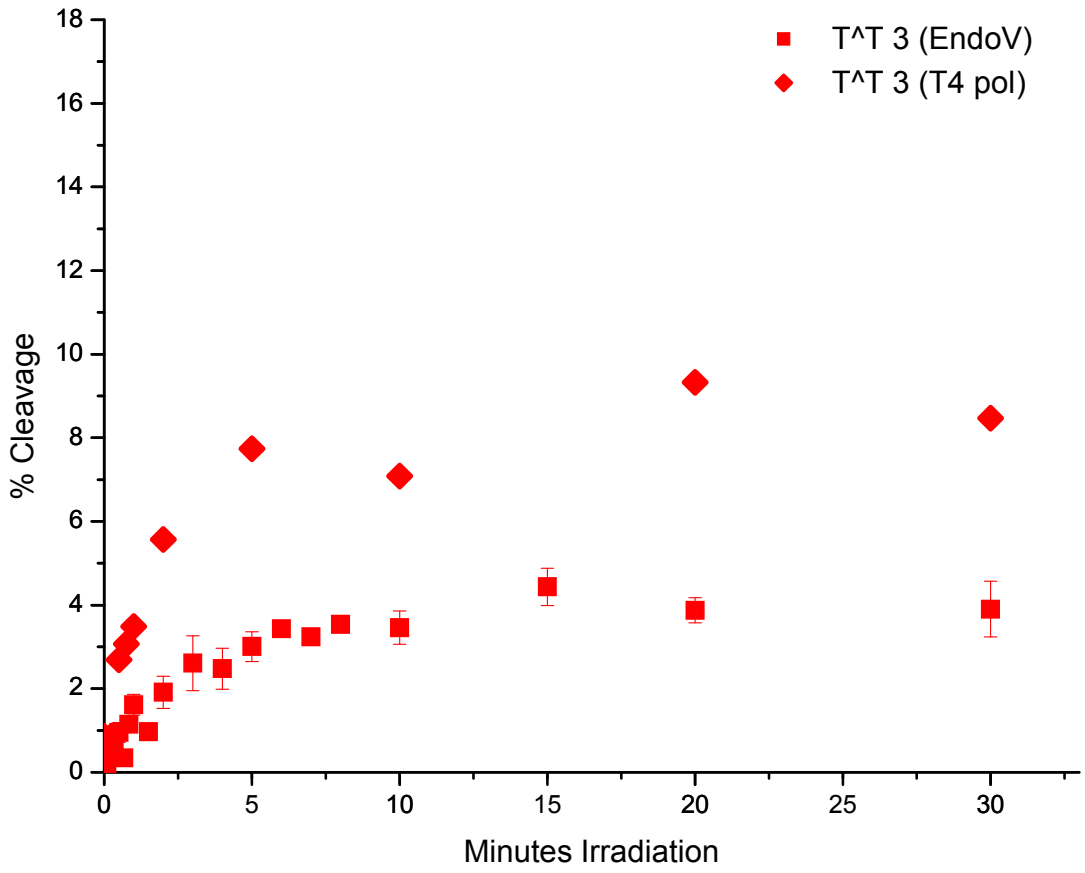

Figure I.9: Graphical comparison of endo V (square) vs. T4 pol (diamond) cleavage methods for detection of T^T 3 formation in free 5s DNA. Percent cleavage calculated from the intensity of the T^T induced cleavage band relative to the total intensity per sample. The endo V data points consist of a minimum of three independent experiments at each time point and the error bars are the standard deviation of the average of each time point. The T4 pol data points represent one experimental trial.

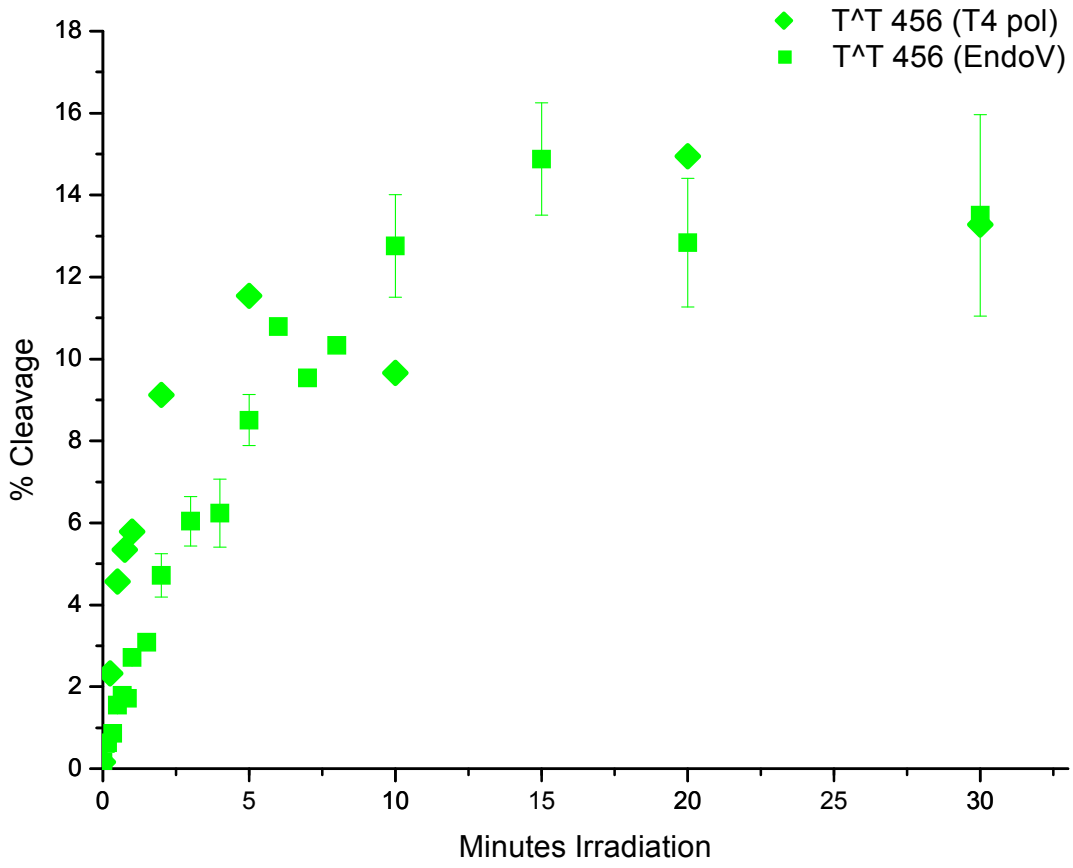

Figure I.10: Graphical comparison of endo V (square) vs. T4 pol (diamond) cleavage methods for detection of T^T 456 formation in free 5s DNA. Percent cleavage calculated from the intensity of the EET T^T induced cleavage band relative to the total intensity per sample. The endo V data points consist of a minimum of three independent experiments at each time point and the error bars are the standard deviation of the average of each time point. The T4 pol data points represent one experimental trial.

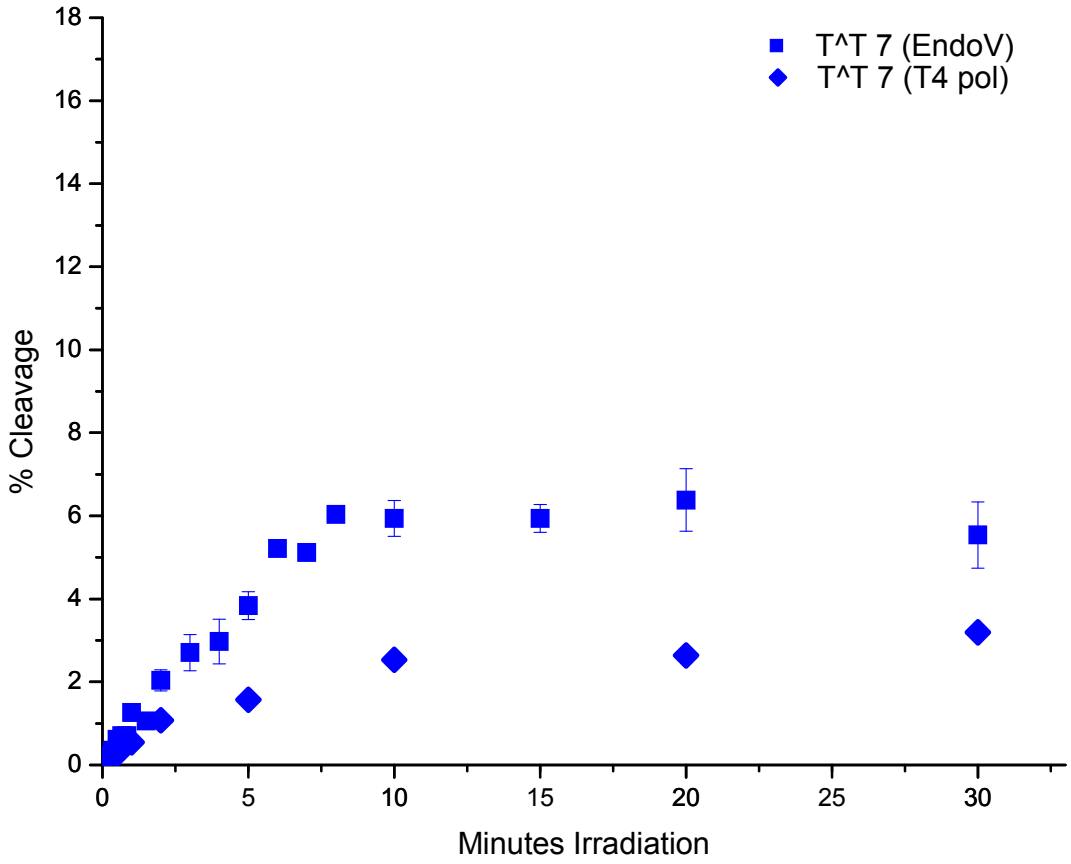

Figure I.11: Graphical comparison of endo V (square) vs. T4 pol (diamond) methods for detection of T^T 7 formation in free 5s DNA. Percent cleavage calculated from the intensity of the T^T induced cleavage band relative to the total intensity per sample. The endo V data points consist of a minimum of three independent experiments at each time point and the error bars are the standard deviation of the average of each time point. The T4 pol data points represent one experimental trial.

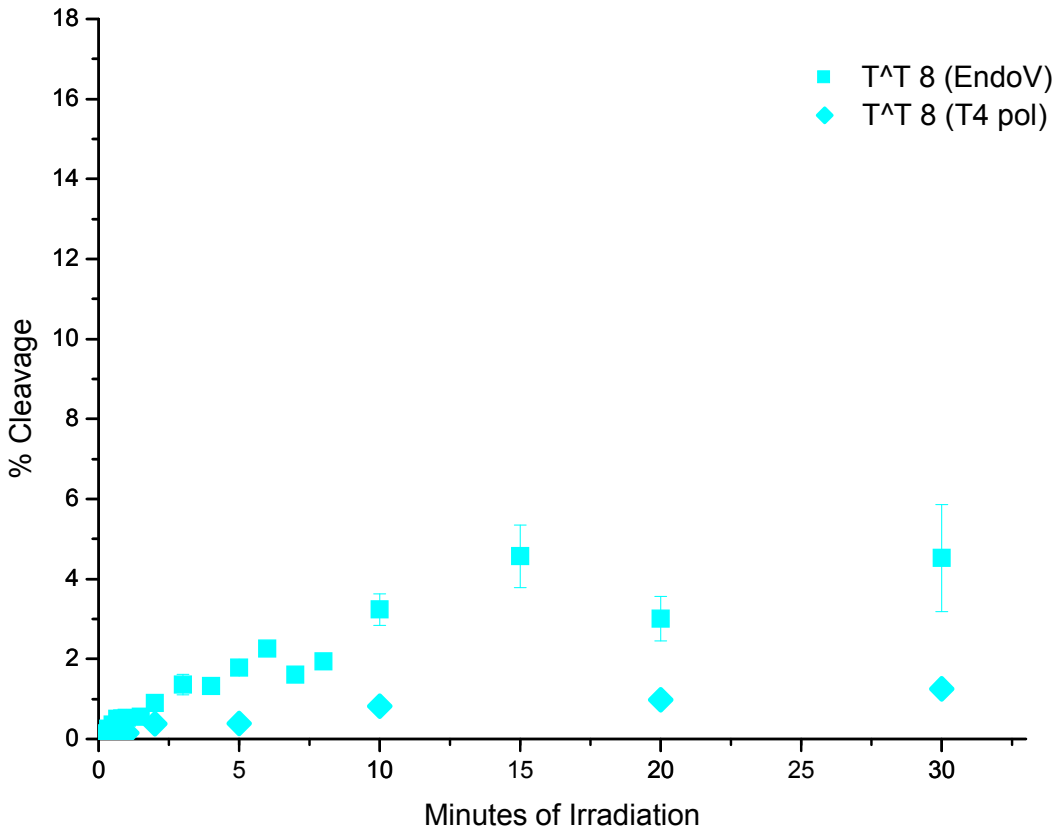

Figure I.12: Graphical comparison of endo V (square) vs. T4 pol (diamond) cleavage methods for detection of T^T 8 formation in free 5s DNA. Percent cleavage calculated from the intensity of the T^T induced cleavage band relative to the total intensity per sample. The endo V data points consist of a minimum of three independent experiments at each time point and the error bars are the standard deviation of the average of each time point. The T4 pol data points represent one experimental trial.

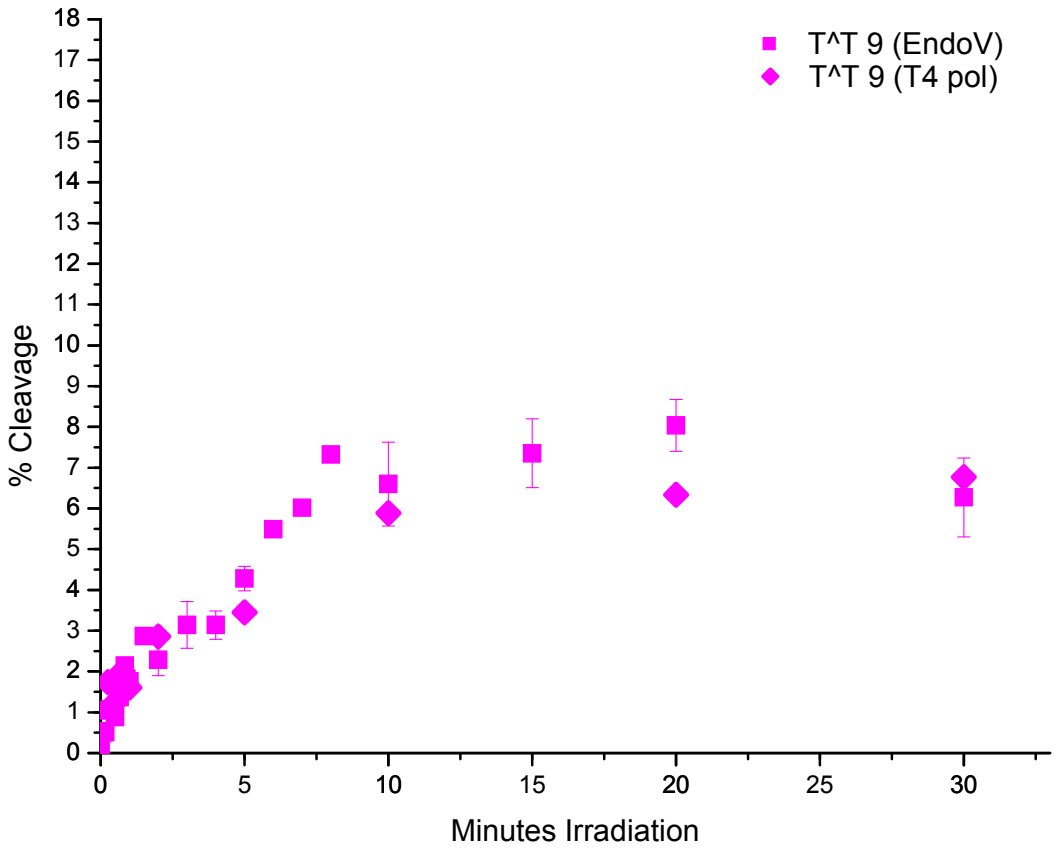

Figure I.13: Graphical comparison of endo V (square) vs. T4 pol (diamond) cleavage methods for detection of T^T 9 formation in free 5s DNA. Percent cleavage calculated from the intensity of the T^T induced cleavage band relative to the total intensity per sample. The endo V data points consist of a minimum of three independent experiments at each time point and the error bars are the standard deviation of the average of each time point. The T4 pol data points represent one experimental trial.

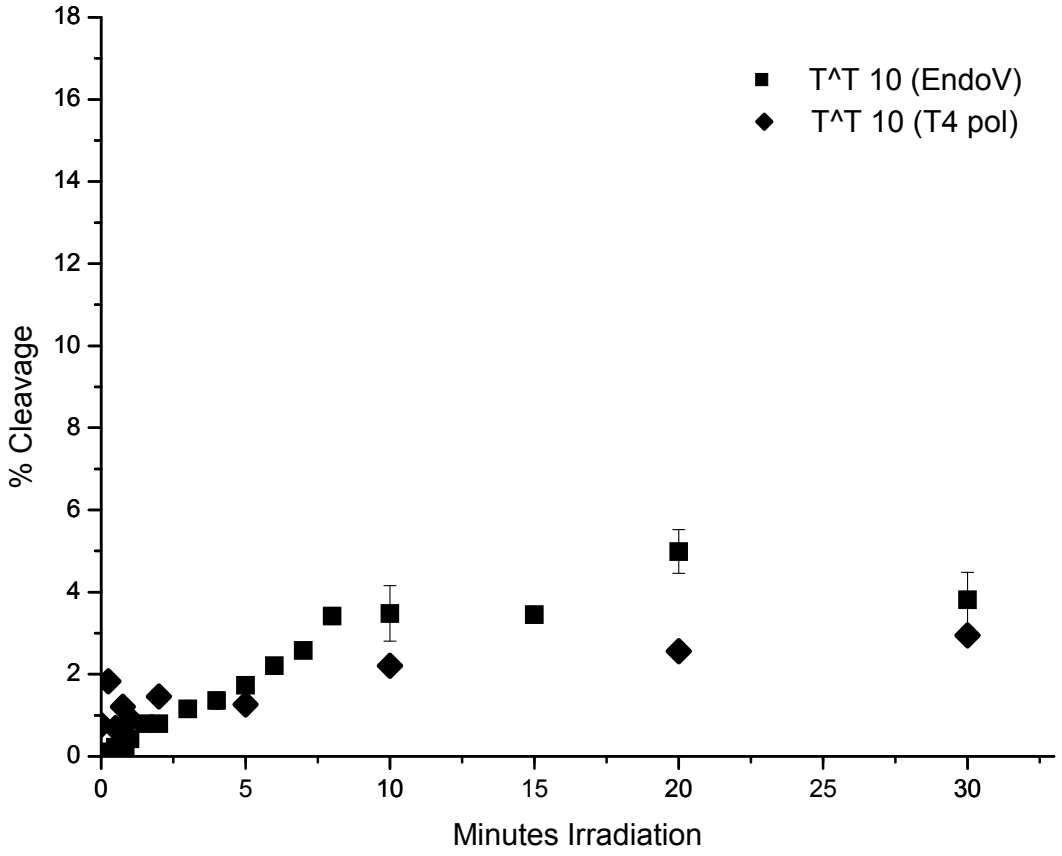

Figure 1.14: Graphical comparison of endo V vs. T4 pol cleavage methods for detection of T^T 10 formation in free 5s DNA. Percent cleavage calculated from the intensity of the T^T induced cleavage band relative to the total intensity per sample. The endo V data points consist of a minimum of three independent experiments at each time point and the error bars are the standard deviation of the average of each time point. The T4 pol data points represent one experimental trial.

In order to determine that excess of NCP in solution did not affect the accumulation of T^T in free 5s DNA a control experiment was conducted under the same conditions as free 5s DNA except an excess of nucleosomes (1:1000) was present during the photoirradiation. Figure I.15 is a representative denaturing PAGE gel of this control experiment.

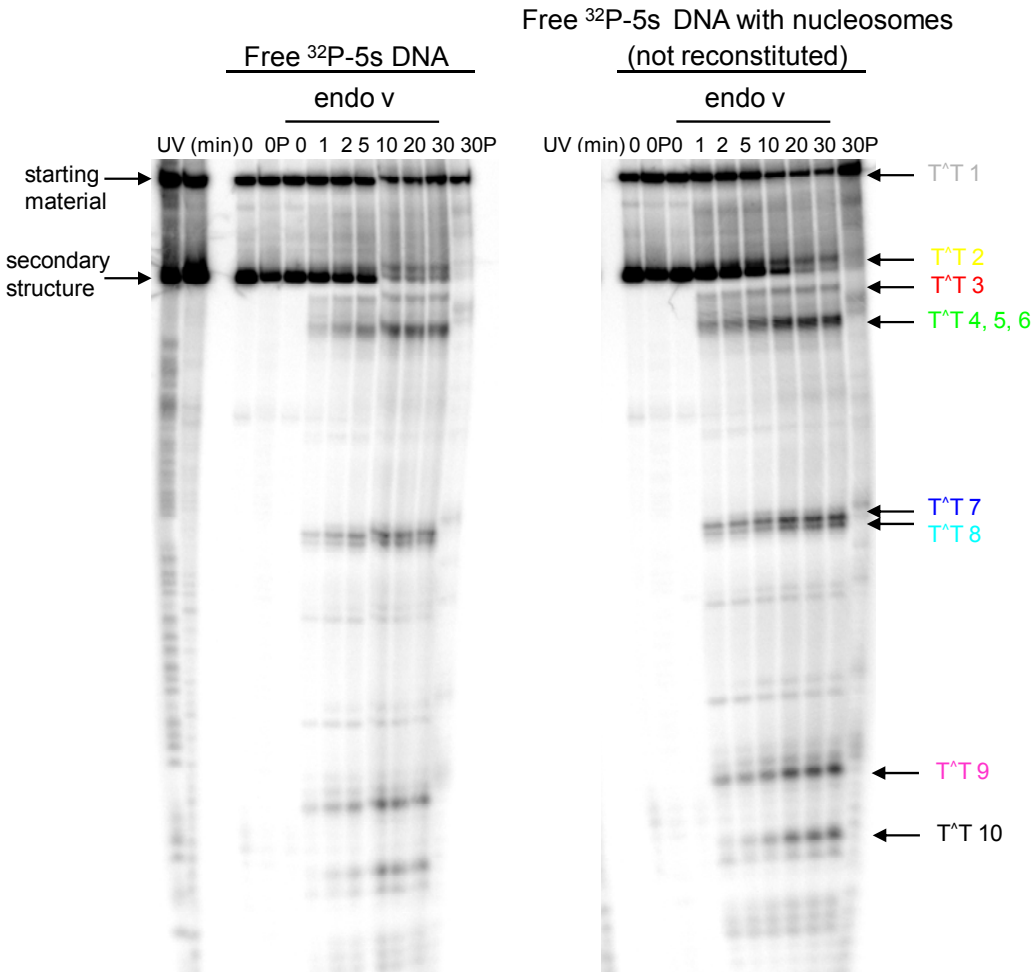

Figure I.15: Denaturing PAGE (8%) with free 5s DNA and free 5s DNA with 1000 mole excess of NCP in solution were run in tandem. Prior to electrophoresis, samples were incubated for 18 hours with endoV for T^T cleavage. Samples labeled "P" were treated with piperidine as opposed to endoV.

Percent formation of each individual T^T was determined for free and NCP reconstituted 5s DNA. No difference between the rates of T^T formation was detected in comparing free vs. NCP reconstituted 5s DNA. This data is illustrated in Figures I.16 thru I.22.

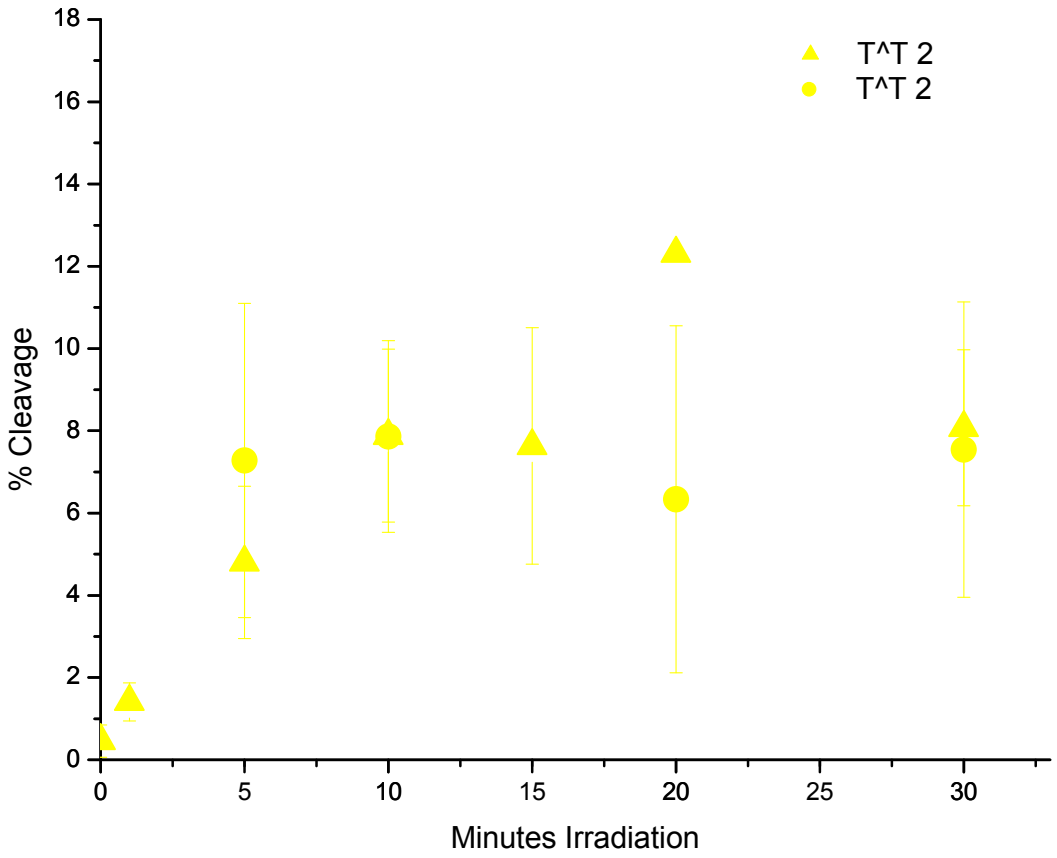

Figure I.16: Percent T^T 2 formation in free (triangles) vs. NCP reconstituted (circles) 5s DNA. Percent cleavage calculated from the intensity of the T^T induced cleavage band relative to the total intensity per sample. The data points consist of a minimum of three independent experiments at each time point and the error bars are the standard deviation of the average of each time point.

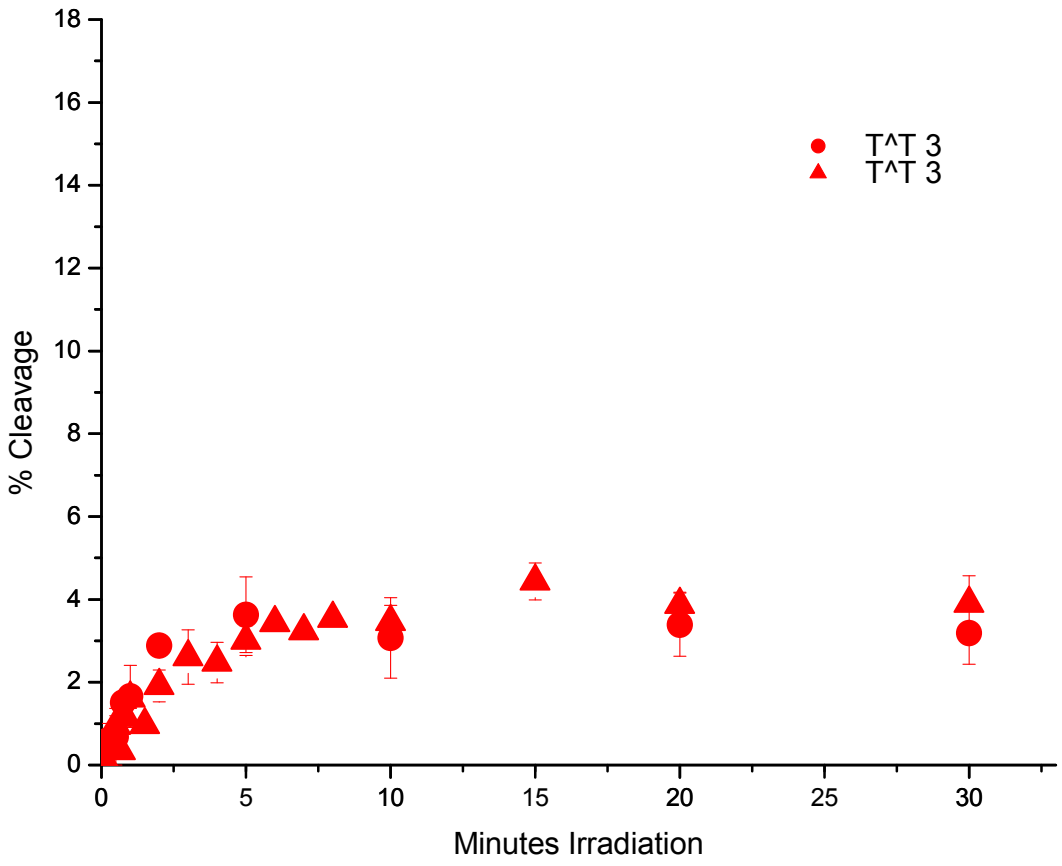

Figure I.17: Percent T^T 3 formation in free (triangles) vs. NCP reconstituted (circles) 5s DNA. Percent cleavage calculated from the intensity of the T^T induced cleavage band relative to the total intensity per sample. The data points consist of a minimum of three independent experiments at each time point and the error bars are the standard deviation of the average of each time point.

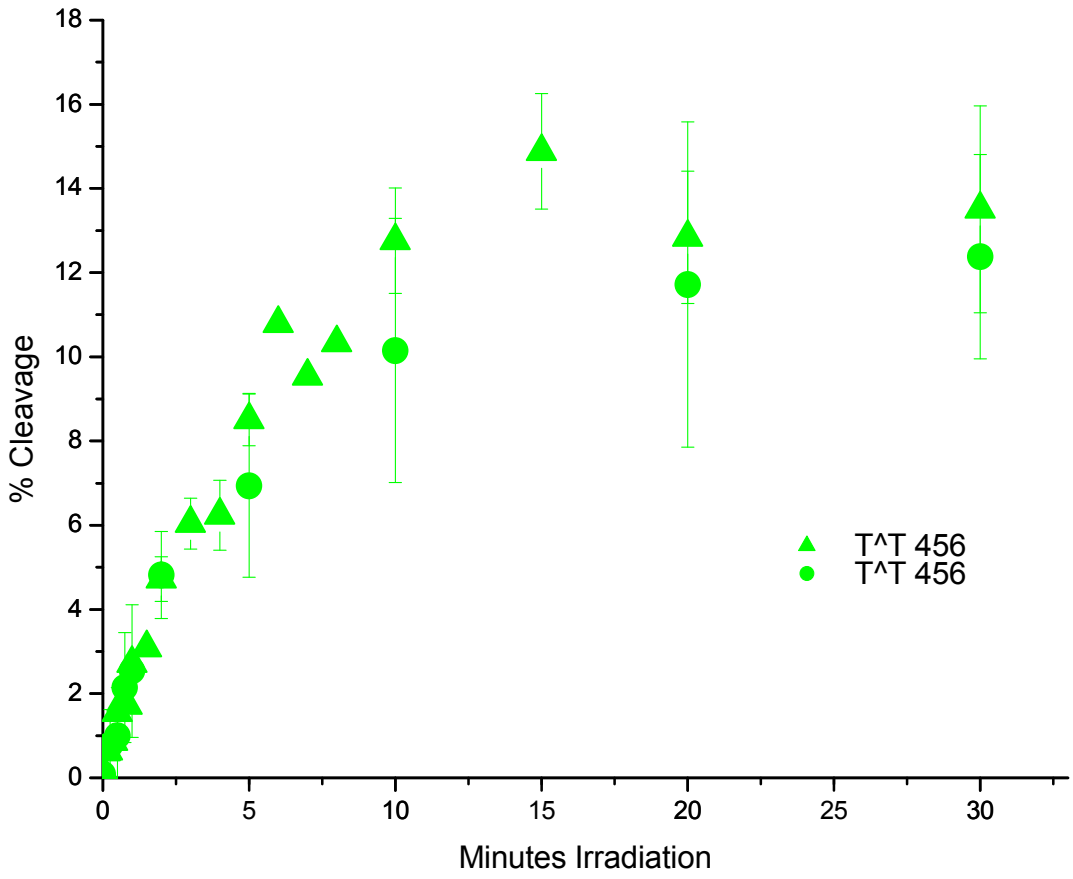

Figure I.18: Percent T^T 456 formation in free (triangles) vs. NCP reconstituted (circles) 5s DNA. Percent cleavage calculated from the intensity of the T^T induced cleavage band relative to the total intensity per sample. The data points consist of a minimum of three independent experiments at each time point and the error bars are the standard deviation of the average of each time point.

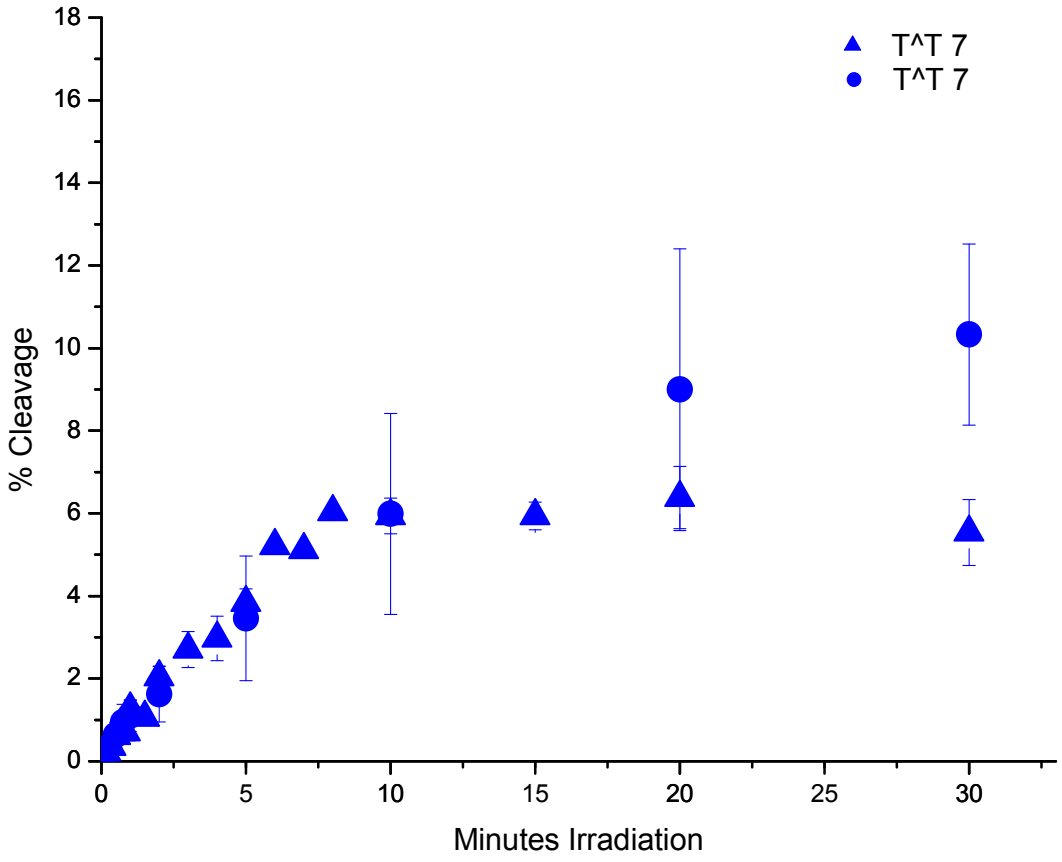

Figure I.19: Percent T^T 7 formation in free (triangles) vs. NCP reconstituted (circles) 5s DNA. Percent cleavage calculated from the intensity of the T^T induced cleavage band relative to the total intensity per sample. The data points consist of a minimum of three independent experiments at each time point and the error bars are the standard deviation of the average of each time point.

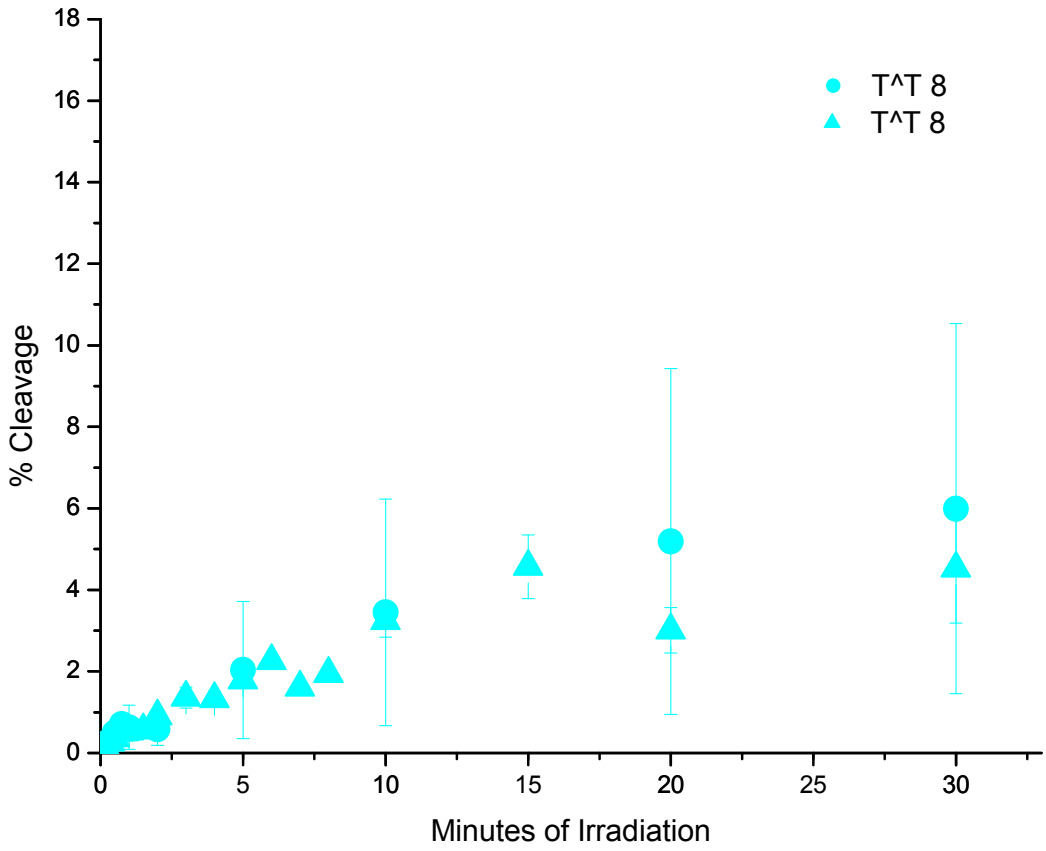

Figure I.20: Percent T^T 8 formation in free (triangles) vs. NCP reconstituted (circles) 5s DNA. Percent cleavage calculated from the intensity of the T^T induced cleavage band relative to the total intensity per sample. The data points consist of a minimum of three independent experiments at each time point and the error bars are the standard deviation of the average of each time point.

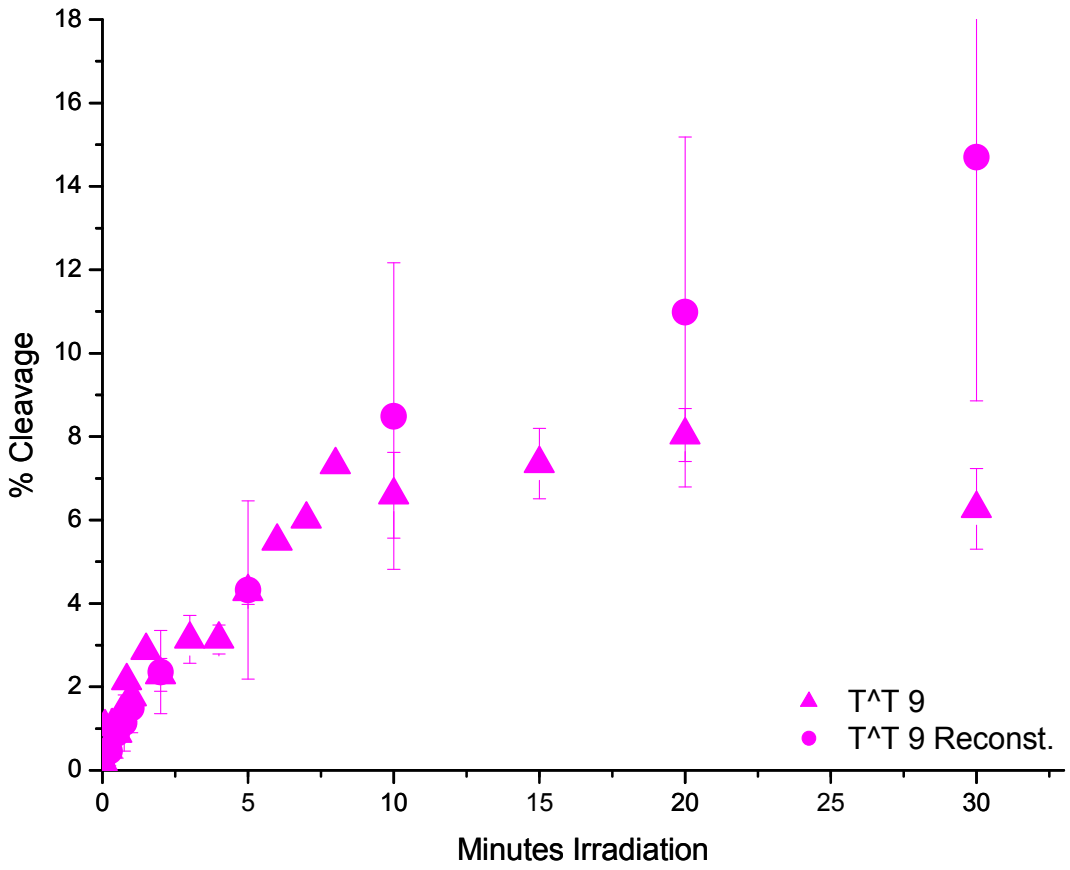

Figure I.21: Percent T^T 9 formation in free (triangles) vs. NCP reconstituted (circles) 5s DNA. Percent cleavage calculated from the intensity of the T^T induced cleavage band relative to the total intensity per sample. The data points consist of a minimum of three independent experiments at each time point and the error bars are the standard deviation of the average of each time point.

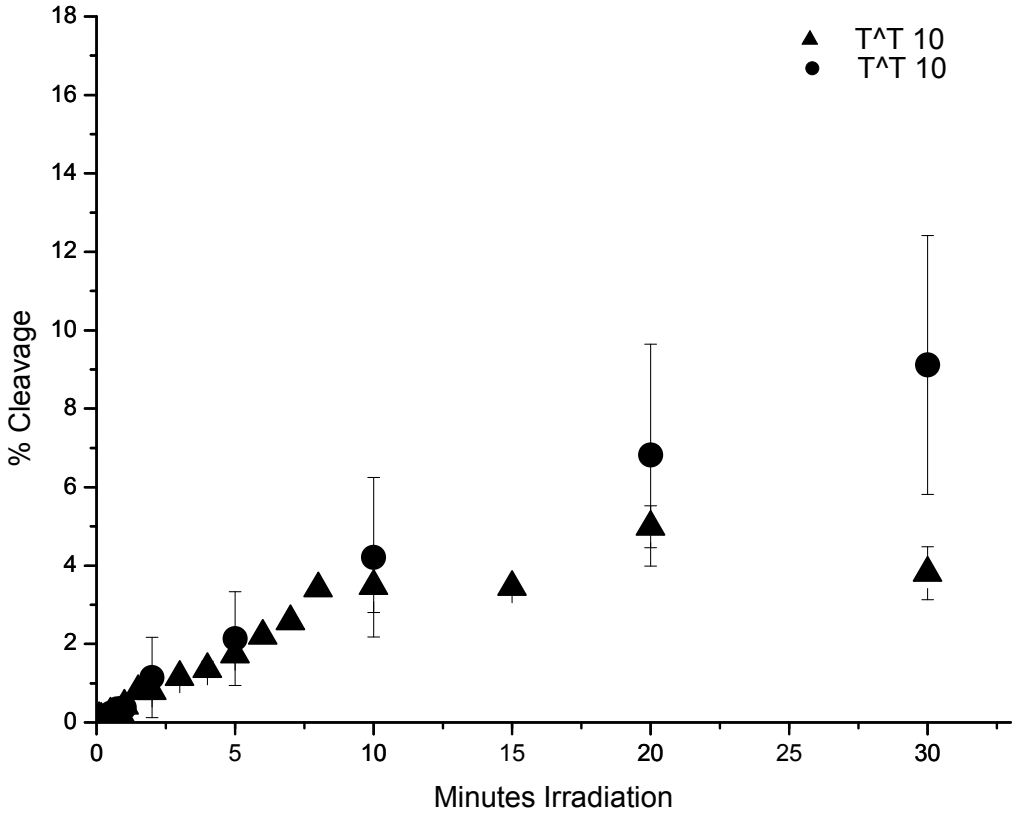

Figure I.22: Percent T^T 10 formation in free (triangles) vs. NCP reconstituted (circles) 5s DNA. Percent cleavage calculated from the intensity of the T^T induced cleavage band relative to the total intensity per sample. The data points consist of a minimum of three independent experiments at each time point and the error bars are the standard deviation of the average of each time point.

The W601 sequence was obtained from the lab of J. Widom in the form of an insert in the pGEM-3z vector (Figure I.23). PCR directly from the plasmid using radioactive primers was used to obtain the 147 W601 NPS for T^T studies.

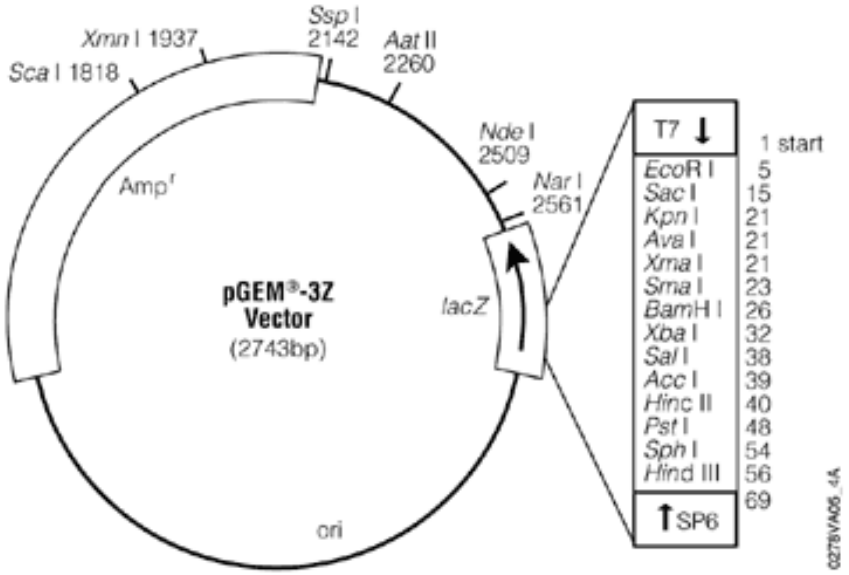

Figure I.23: pGEM-3z vector diagram as obtained from www.promega.com.

Prior to photochemistry with NCP reconstituted W601, it was necessary to illustrate that the NCP remained intact during the experimental conditions of the photochemistry reaction. Figure I.24 illustrates that even after 30 minutes of irradiation the NCP remains intact and no degradation was observed.

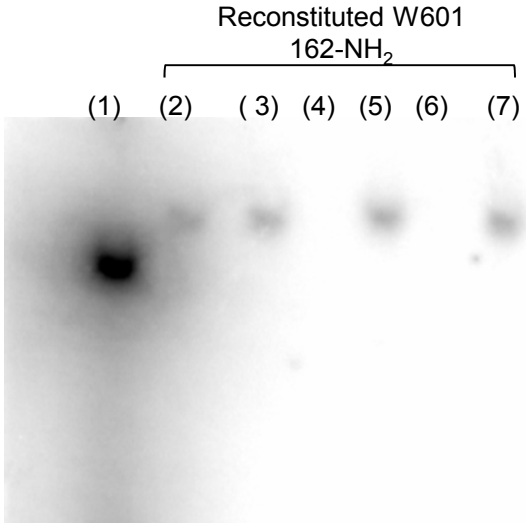

Figure I.24: Native 8 % PAGE gel analysis of W601 after photoirradiation. (Lane 1) free W601, (Lane 2) 0 minutes irradiation, (Lane 3) 30 seconds irradiation, (Lane 4) blank, (Lane 5) 2 minutes irradiation, (Lane 6) blank, (Lane 7) 30 minutes irradiation.

Appendix II

Supporting Information for Chapter 3

Endonuclease IV (endoIV) treatment was used in addition to piperidine treatment for detection of photochemical cleavage induced by EET. This method was employed in order to reduce the number of background cleavage bands on autoradiograms. Initial experiments with EndoIV were conducted at three different incubation times to determine the optimal time for full detection of cleavage. As mentioned in Chapter 3, the one hour and 2 hour time points had two photochemical cleavage band, whereas the 18 hour time point only had one. Figure II.1 illustrates that there is little difference between the total cleavage when the two bands in the one and two hour incubations are combined they total the one band detected in the 18 hour treatment.

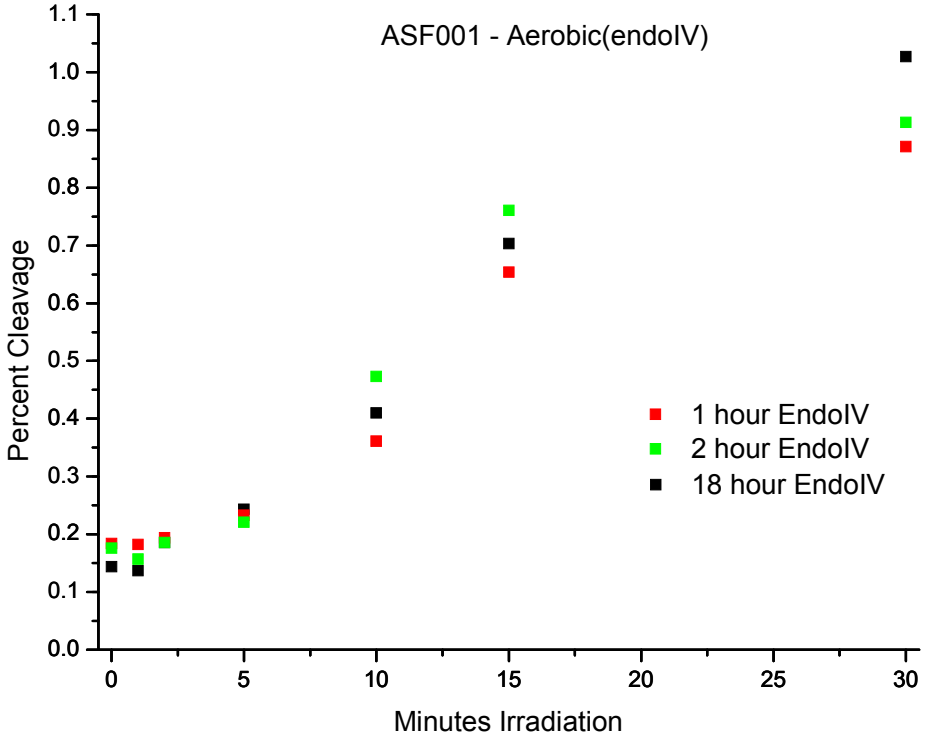

Figure II.1: Varying incubation time with endoIV does not increase total observed cleavage in ASF001. Percent cleavage calculated from the intensity of the EET induced cleavage band relative to the total intensity per sample.

Initial rates were determined for all seven DNA sequences under aerobic conditions with both piperidine and endoIV treatment (Figure II.2 through Figure II.14). Cleavage was linear up to 10 minutes therefore only data points from 0 – 10 minutes were used for initial rate determination. Data points represent a minimum of 3 trials per time point and percent cleavage was calculated relative to the total intensities of each lane with error bars representing the standard deviation from the mean.

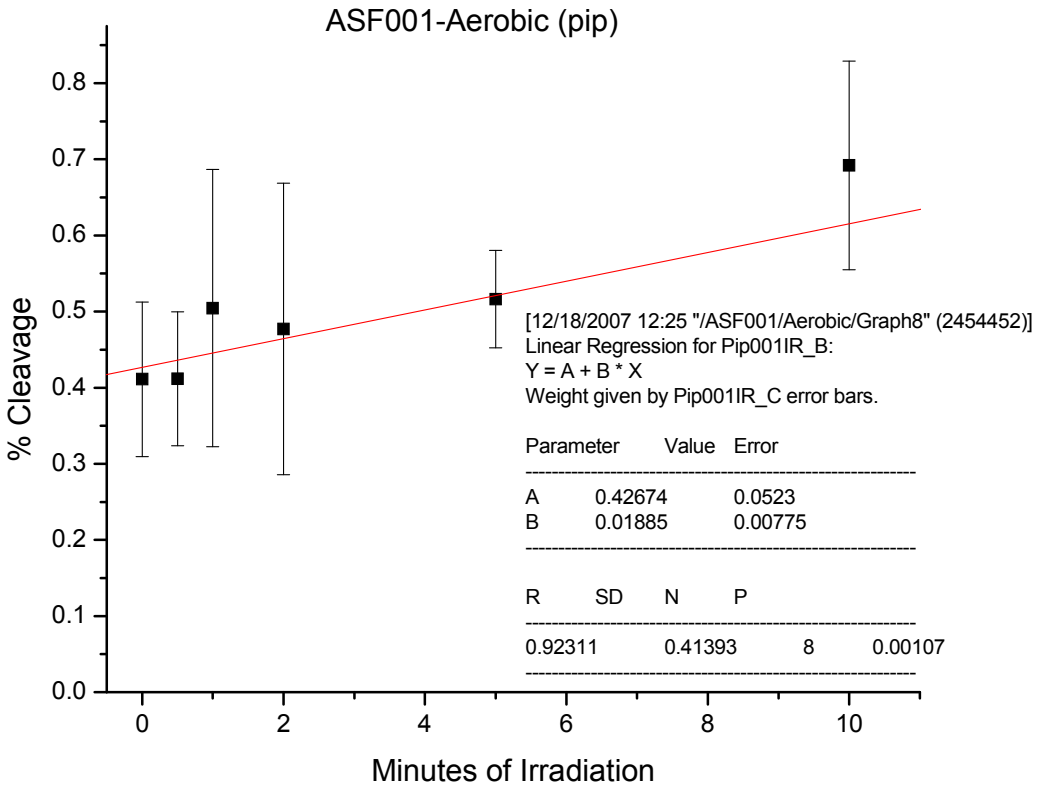

Figure II.2: Initial rate determination of EET in ASF001 as detected by piperidine treatment under aerobic conditions. Percent cleavage calculated from the intensity of the EET induced cleavage band relative to the total intensity per sample. The data points represent an average of a minimum of three independent experiments at each time point and the error bars are the standard deviation of the average of each time point.

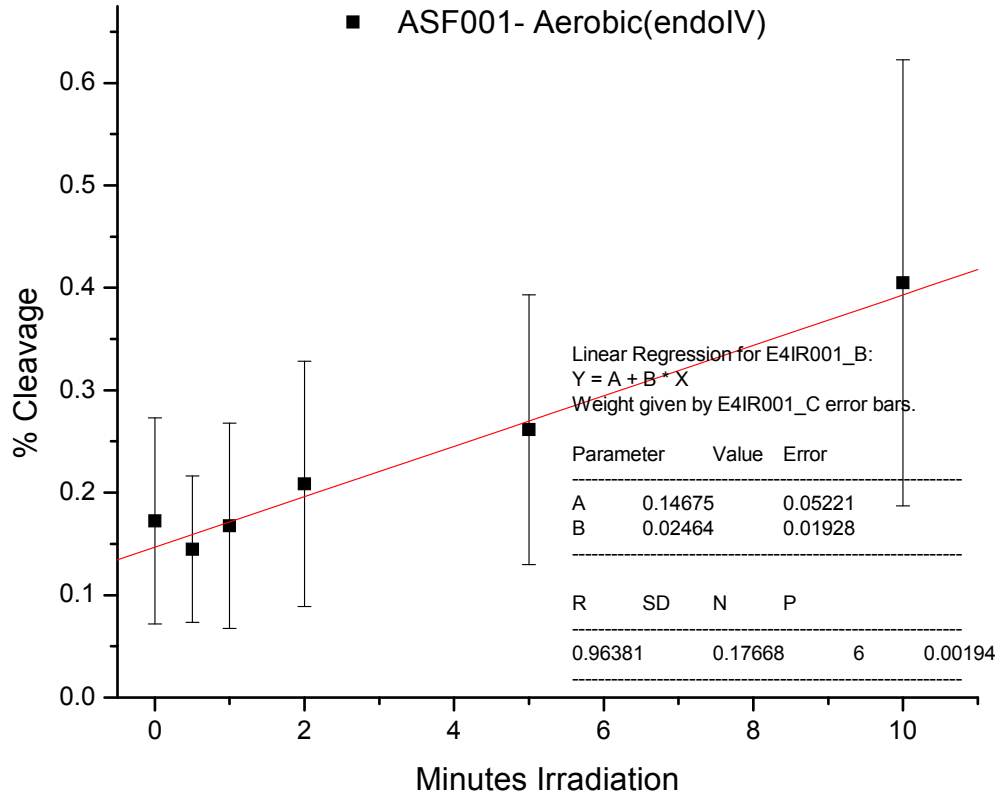

Figure II.3: Initial rate determination of EET in ASF001 as detected by endoIV treatment under aerobic conditions. Percent cleavage calculated from the intensity of the EET induced cleavage band relative to the total intensity per sample. The data points represent an average of a minimum of three independent experiments at each time point and the error bars are the standard deviation of the average of each time point.

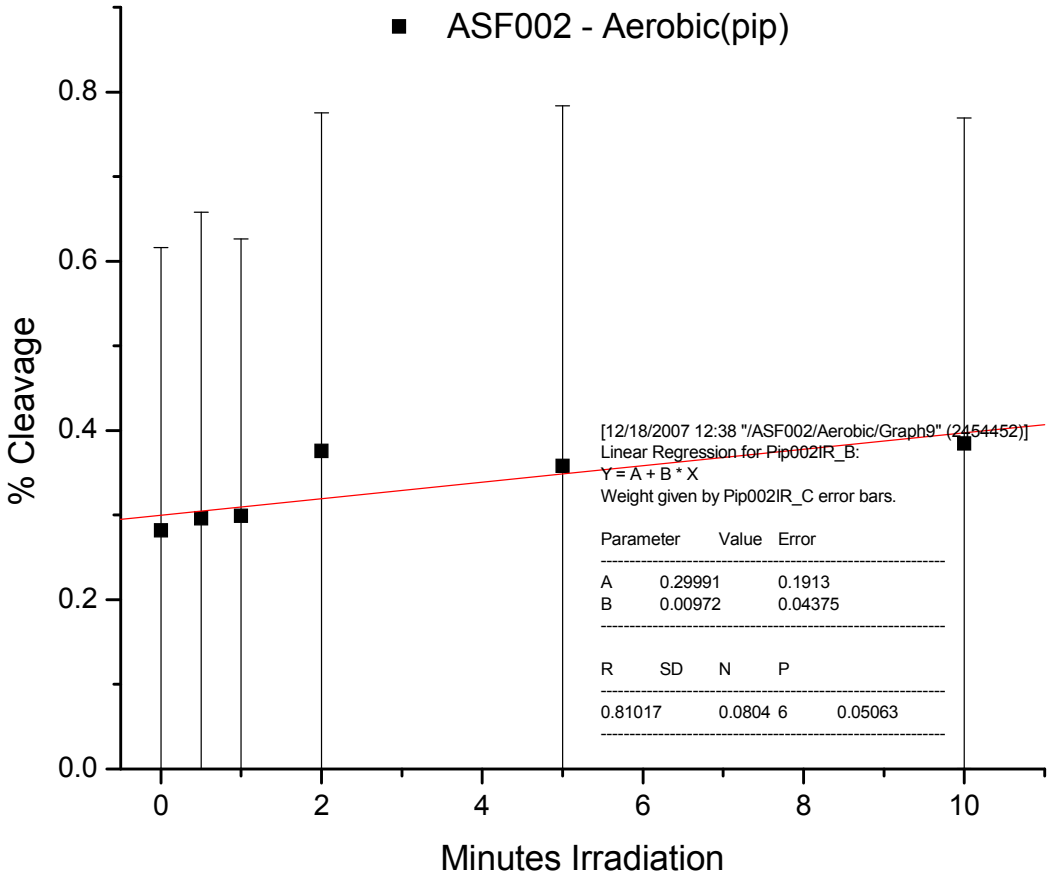

Figure II.4: Initial rate determination of EET in ASF002 as detected by piperidine treatment under aerobic conditions. Percent cleavage calculated from the intensity of the EET induced cleavage band relative to the total intensity per sample. The data points represent an average of a minimum of three independent experiments at each time point and the error bars are the standard deviation of the average of each time point.

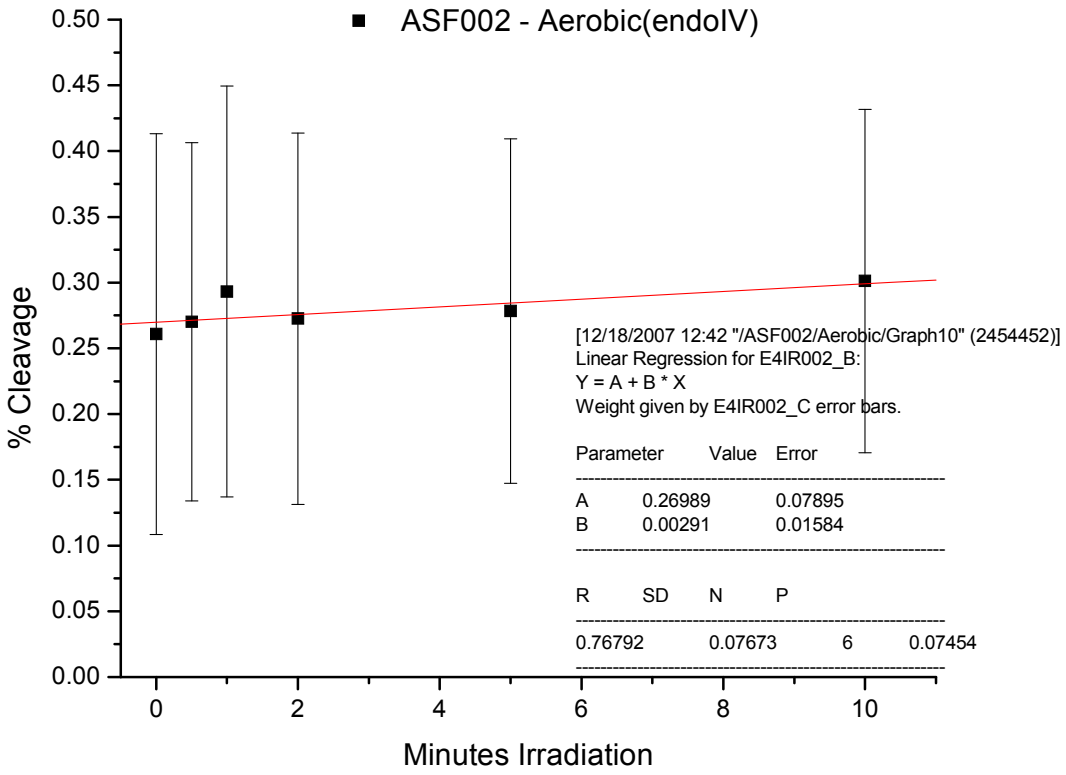

Figure II.5: Initial rate determination of EET in ASF002 as detected by endoIV treatment under aerobic conditions. Percent cleavage calculated from the intensity of the EET induced cleavage band relative to the total intensity per sample. The data points represent an average of a minimum of three independent experiments at each time point and the error bars are the standard deviation of the average of each time point.

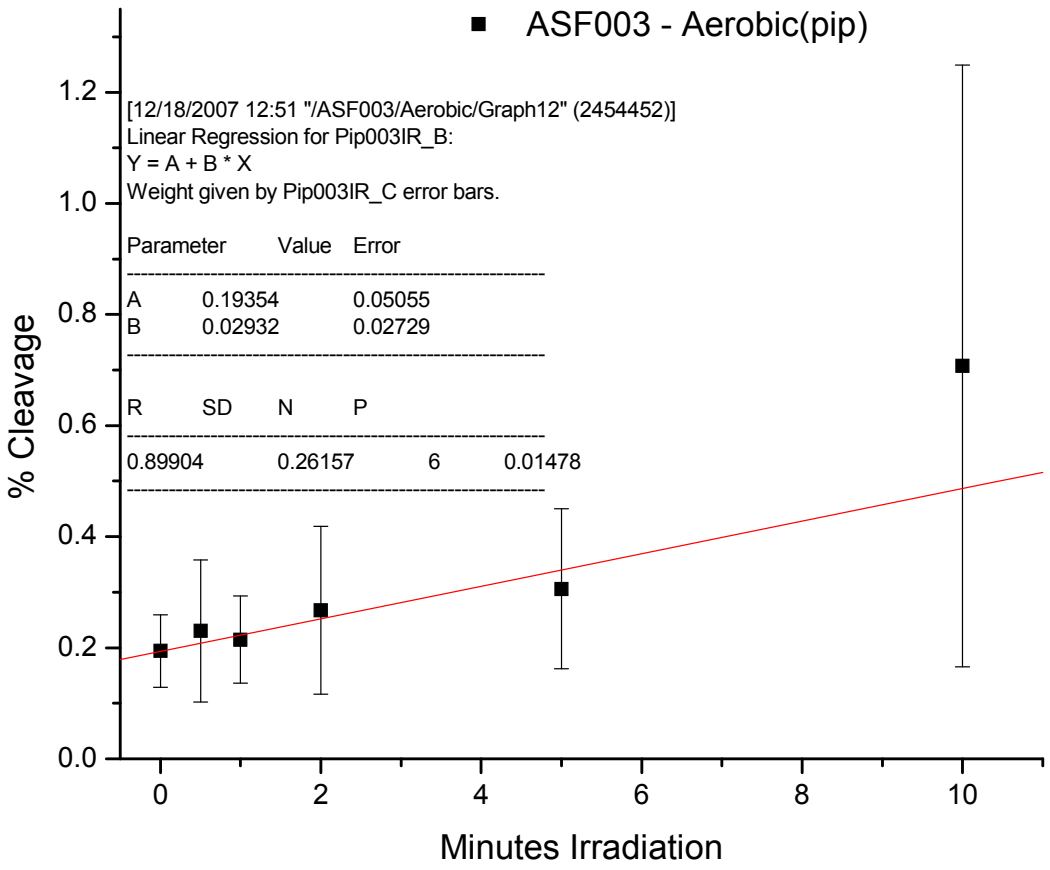

Figure II.6: Initial rate determination of EET in ASF003 as detected by piperidine treatment under aerobic conditions. Percent cleavage calculated from the intensity of the EET induced cleavage band relative to the total intensity per sample. The data points represent an average of a minimum of three independent experiments at each time point and the error bars are the standard deviation of the average of each time point.

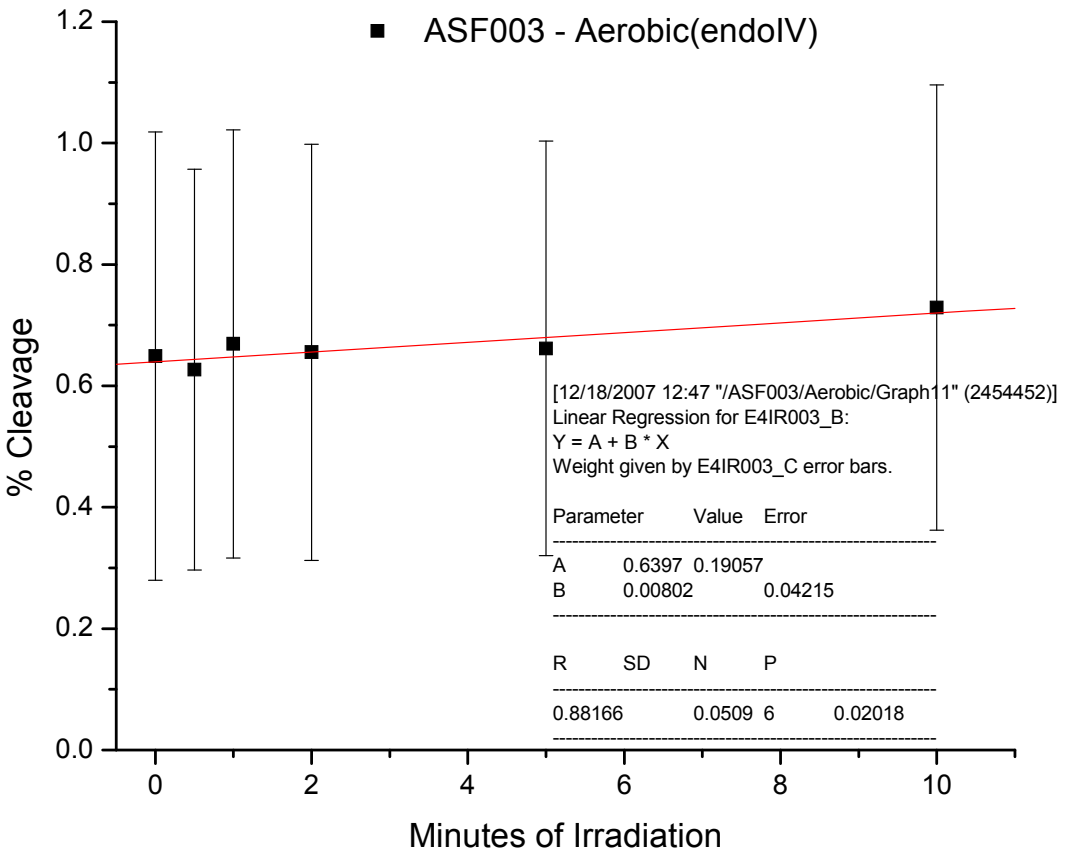

Figure II.7: Initial rate determination of EET in ASF003 as detected by endoIV treatment under aerobic conditions. Percent cleavage calculated from the intensity of the EET induced cleavage band relative to the total intensity per sample. The data points represent an average of a minimum of three independent experiments at each time point and the error bars are the standard deviation of the average of each time point.

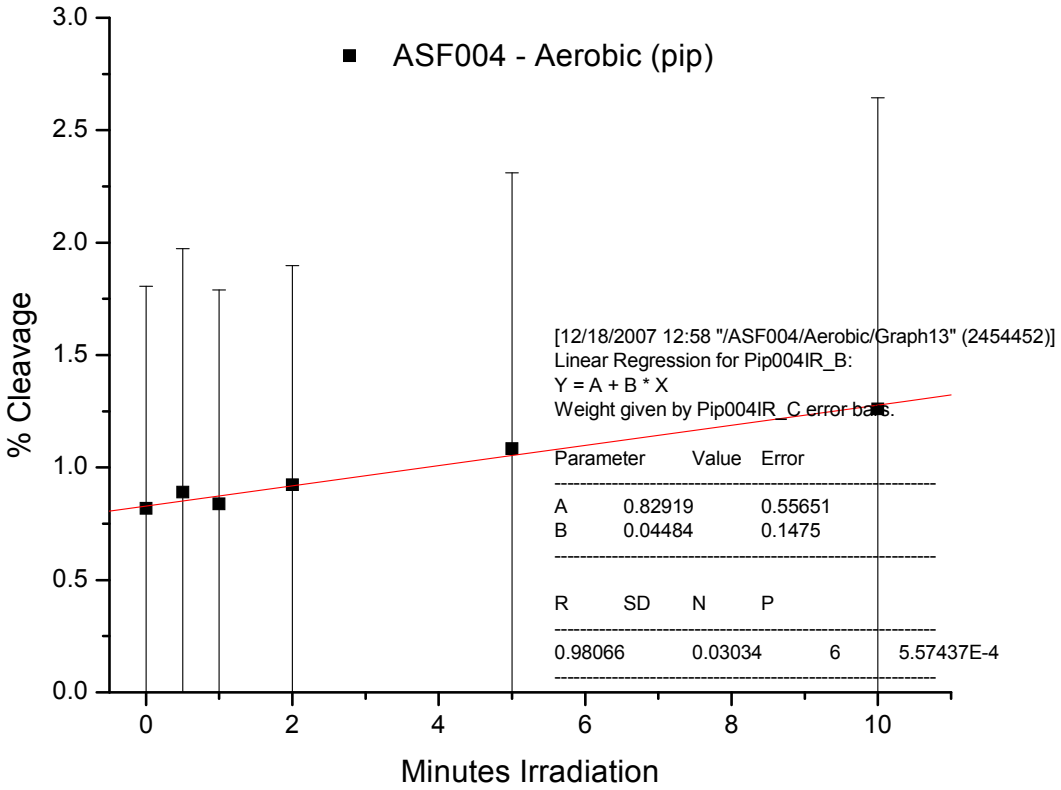

Figure II.8: Initial rate determination of EET in ASF004 as detected by piperidine treatment under aerobic conditions. Percent cleavage calculated from the intensity of the EET induced cleavage band relative to the total intensity per sample. The data points represent an average of a minimum of three independent experiments at each time point and the error bars are the standard deviation of the average of each time point.

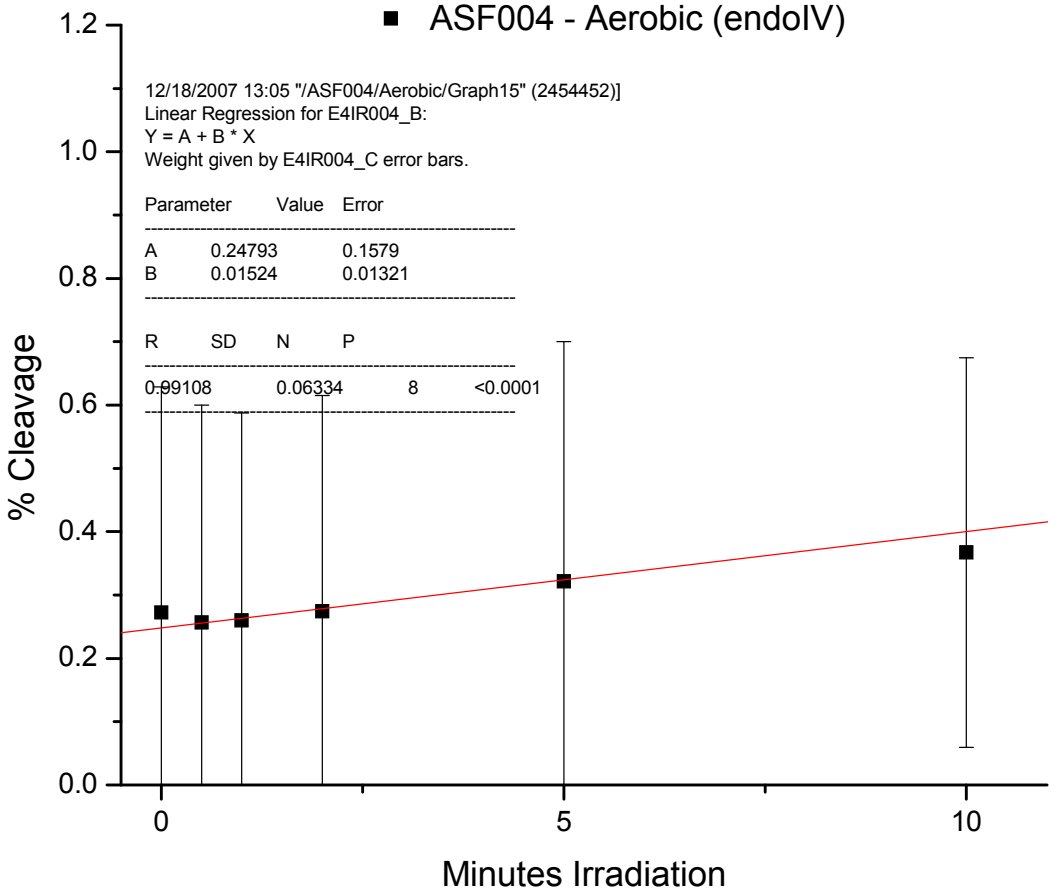

Figure II.9: Initial rate determination of EET in ASF004 as detected by endoIV treatment under aerobic conditions. Percent cleavage calculated from the intensity of the EET induced cleavage band relative to the total intensity per sample. The data points represent an average of a minimum of three independent experiments at each time point and the error bars are the standard deviation of the average of each time point.

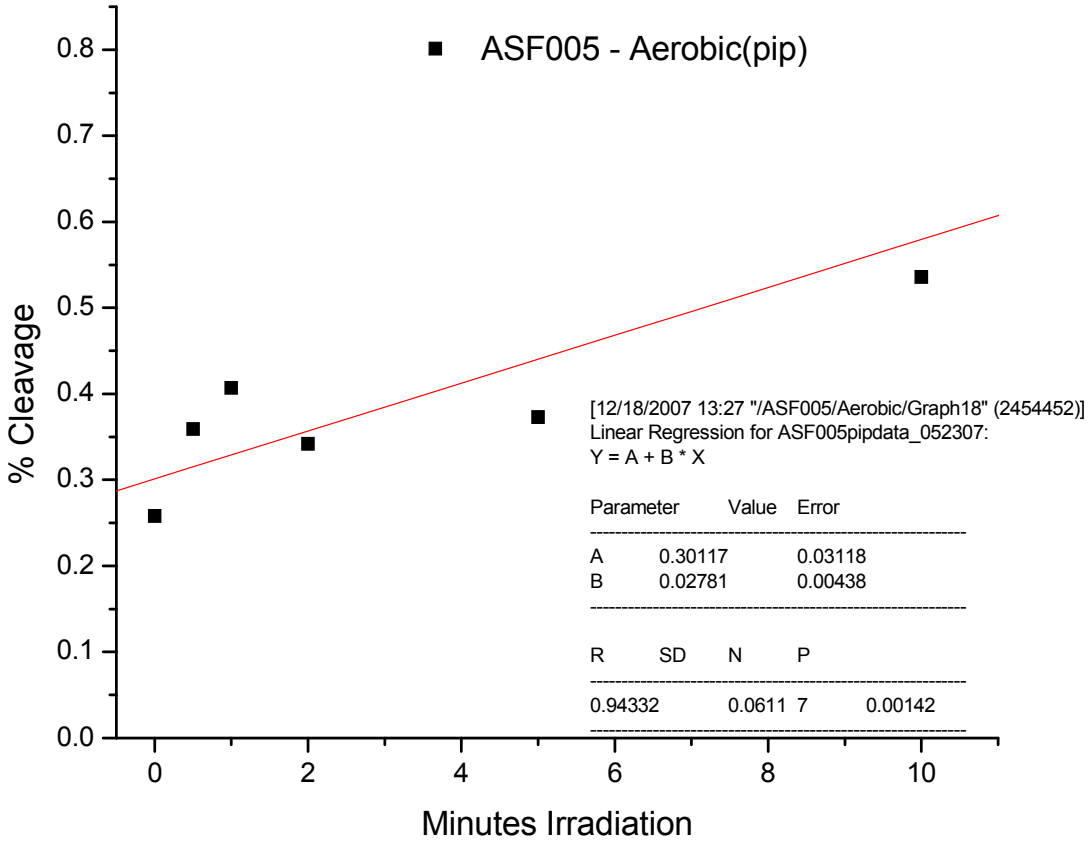

Figure II.10: Initial rate determination of EET in ASF005 as detected by piperidine treatment under aerobic conditions. Percent cleavage calculated from the intensity of the EET induced cleavage band relative to the total intensity per sample. The data points represent an average of a minimum of three independent experiments at each time point and the error bars are the standard deviation of the average of each time point.

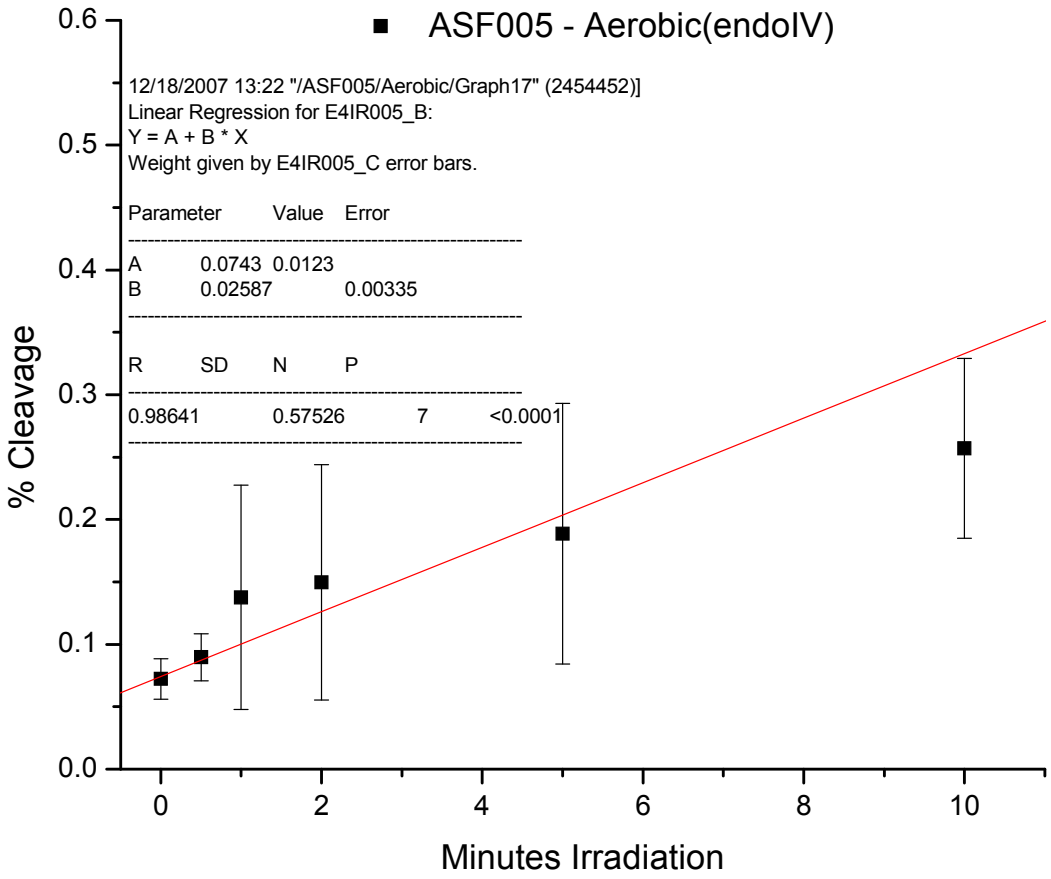

Figure II.11: Initial rate determination of EET in ASF005 as detected by endoIV treatment under aerobic conditions. Percent cleavage calculated from the intensity of the EET induced cleavage band relative to the total intensity per sample. The data points represent an average of a minimum of three independent experiments at each time point and the error bars are the standard deviation of the average of each time point.

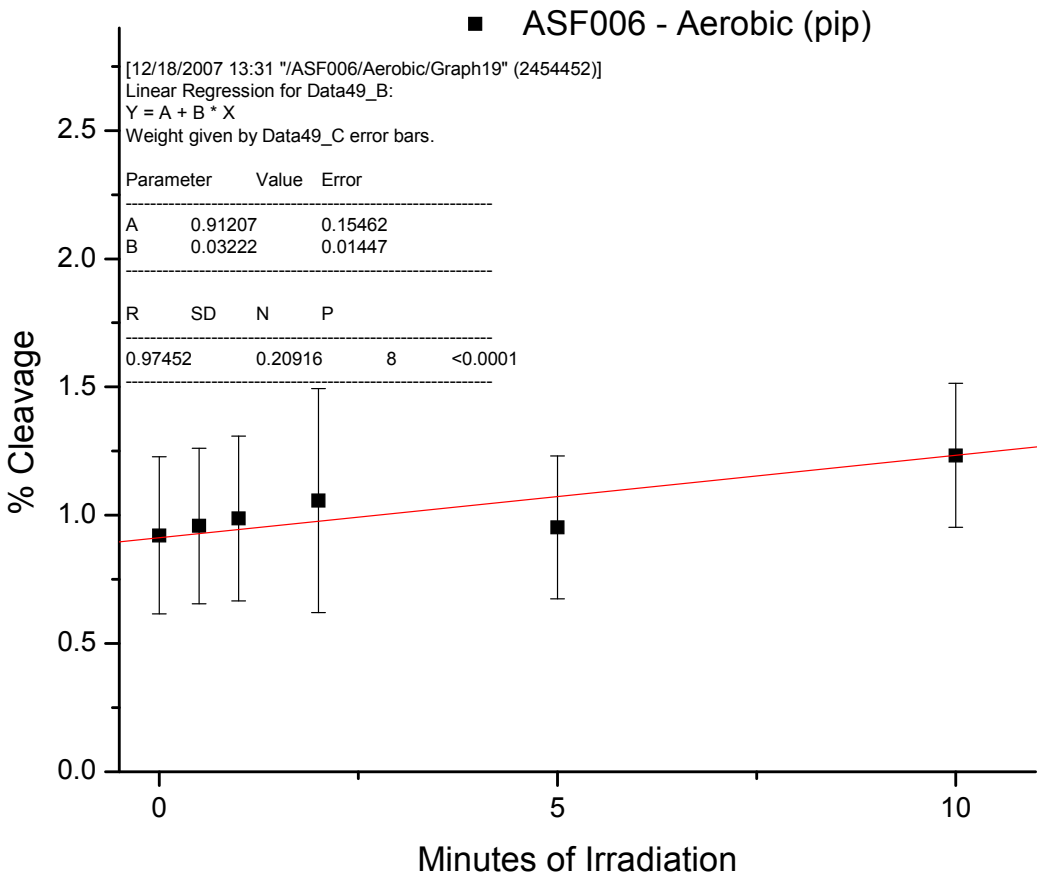

Figure II.12: Initial rate determination of EET in ASF006 as detected by piperidine treatment under aerobic conditions. Percent cleavage calculated from the intensity of the EET induced cleavage band relative to the total intensity per sample. The data points represent an average of a minimum of three independent experiments at each time point and the error bars are the standard deviation of the average of each time point.

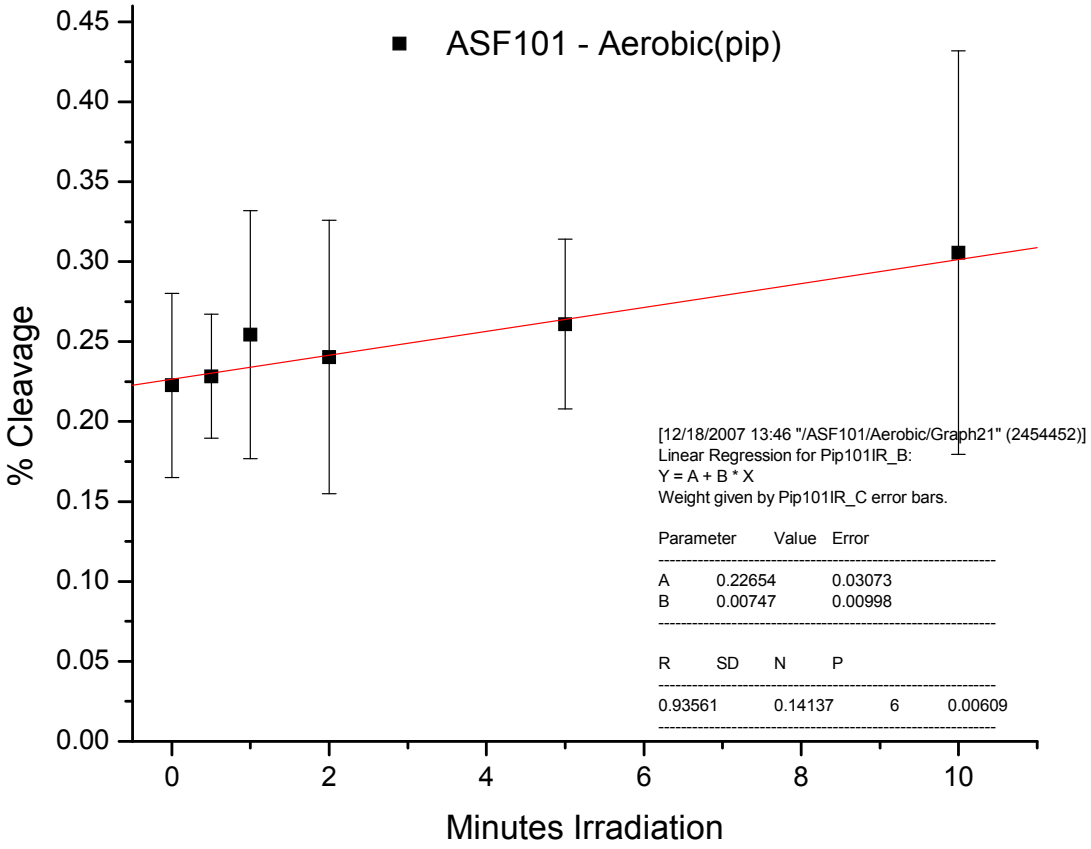

Figure II.13: Initial rate determination of EET in ASF101 as detected by piperidine treatment under aerobic conditions. Percent cleavage calculated from the intensity of the EET induced cleavage band relative to the total intensity per sample. The data points represent an average of a minimum of three independent experiments at each time point and the error bars are the standard deviation of the average of each time point.

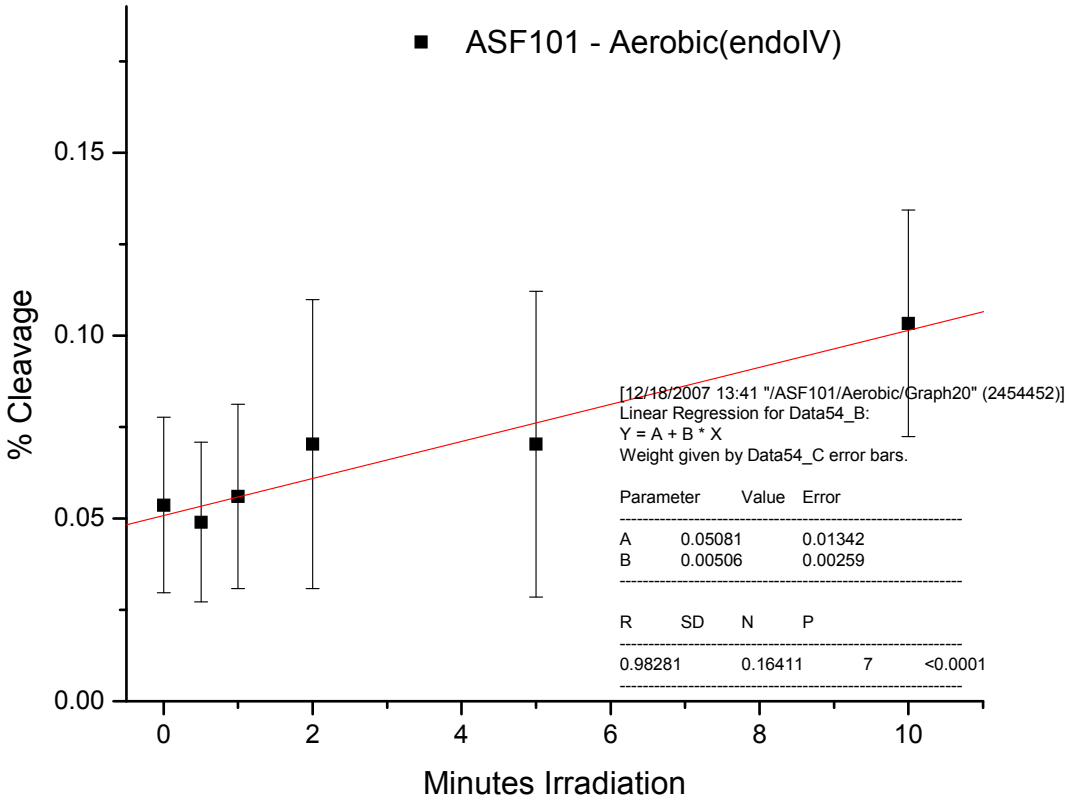

Figure II.14: Initial rate determination of EET in ASF101 as detected by endoIV treatment under aerobic conditions. Percent cleavage calculated from the intensity of the EET induced cleavage band relative to the total intensity per sample. The data points represent an average of a minimum of three independent experiments at each time point and the error bars are the standard deviation of the average of each time point.

While the absolute numbers for the total percent cleavage of ASF001, 004, 005, and 006 appear to vary, Figure II.15 illustrates that when the error bars are taken into consideration there is no discernable difference between the values. Data points represent a minimum of 3 trials per time point and percent cleavage was calculated relative to the total intensities of each lane with error bars representing the standard deviation from the mean. Additionally, with the zero time point subtracted the difference between ASF004/006 and ASF001/005 becomes even less significant.

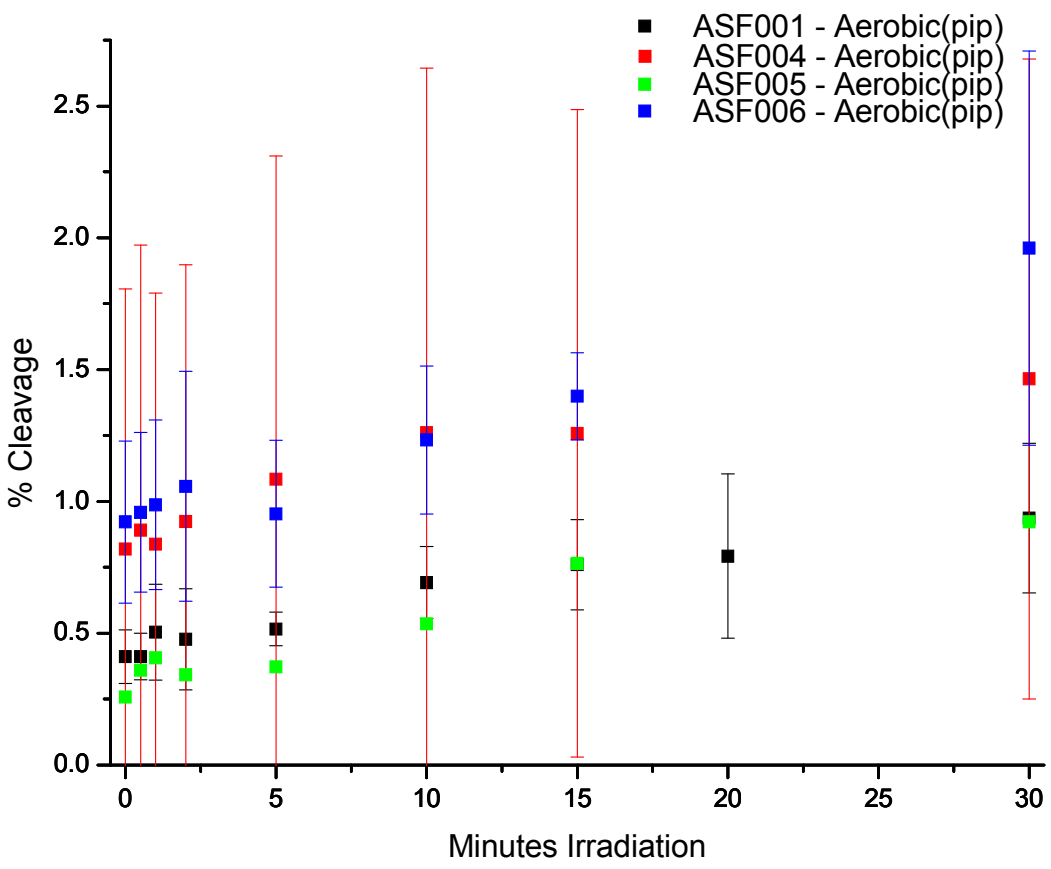

Figure II.15: Comparison of photochemically induced cleavage by EET as detected by piperidine treatment under aerobic conditions. Percent cleavage calculated from the intensity of the EET induced cleavage band relative to the total intensity per sample. The data points represent an average of a minimum of three independent experiments at each time point and the error bars are the standard deviation of the average of each time point.

Initial rates were determined for all seven DNA sequences under anaerobic conditions with both piperidine and endoIV treatment (Figure II.16 through Figure II.29). Cleavage was linear up to 10 minutes therefore only data points from 0 – 10 minutes were used for initial rate determination with the exception of ASF004 which was only linear to 5 minutes. Data points represent a minimum of 3 trials per time point and percent cleavage was calculated relative to the total intensities of each lane with error bars representing the standard deviation from the mean.

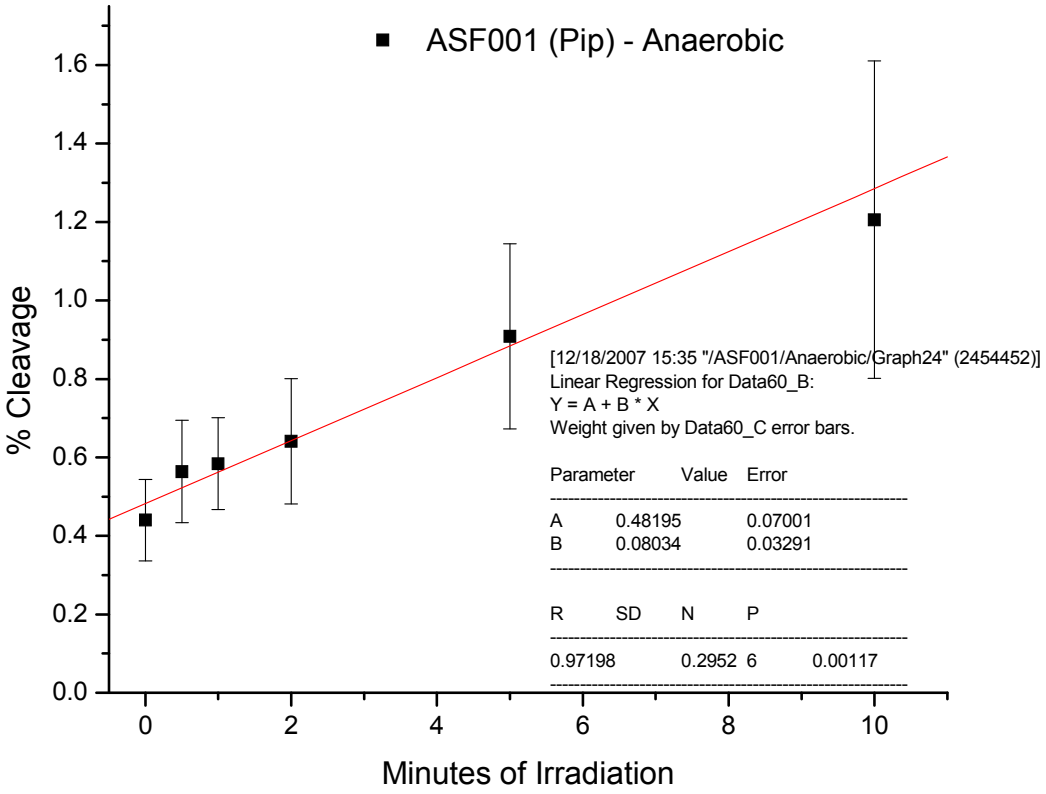

Figure II.16: Initial rate determination of EET in ASF001 as detected by piperidine treatment under anaerobic conditions. Percent cleavage calculated from the intensity of the EET induced cleavage band relative to the total intensity per sample. The data points represent an average of a minimum of three independent experiments at each time point and the error bars are the standard deviation of the average of each time point.

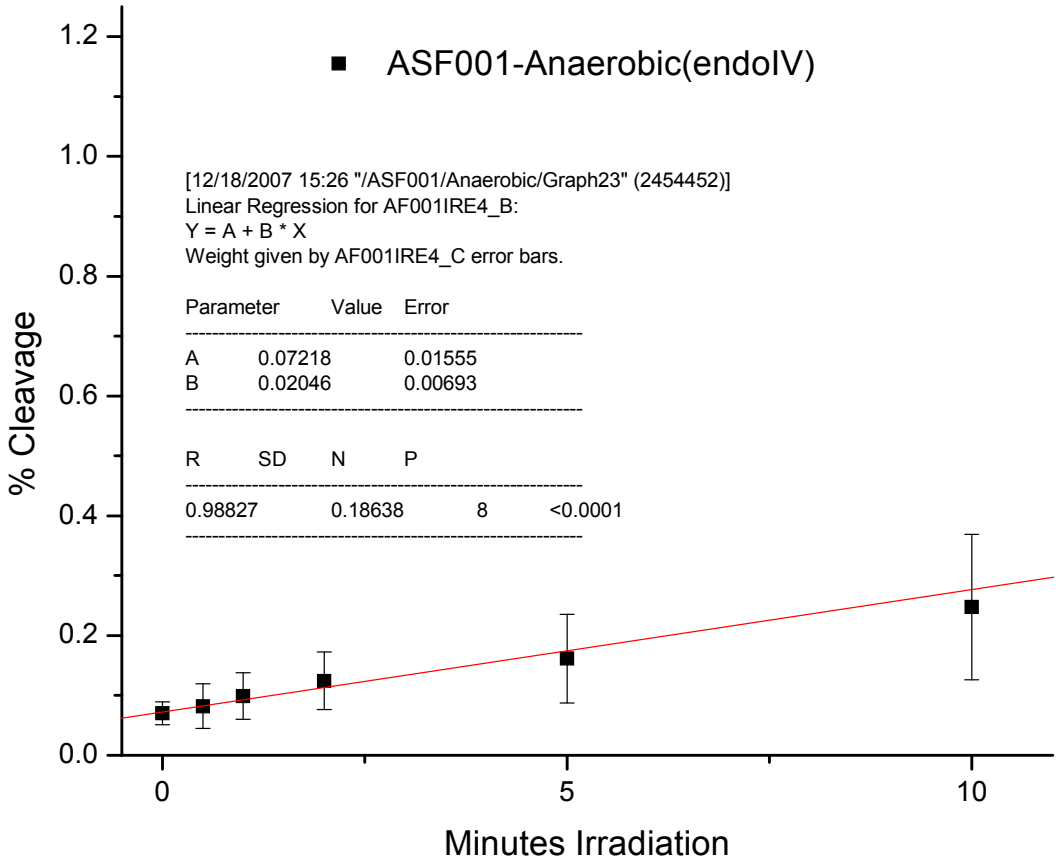

Figure II.17: Initial rate determination of EET in ASF001 as detected by endoIV treatment under anaerobic conditions. Percent cleavage calculated from the intensity of the EET induced cleavage band relative to the total intensity per sample. The data points represent an average of a minimum of three independent experiments at each time point and the error bars are the standard deviation of the average of each time point.

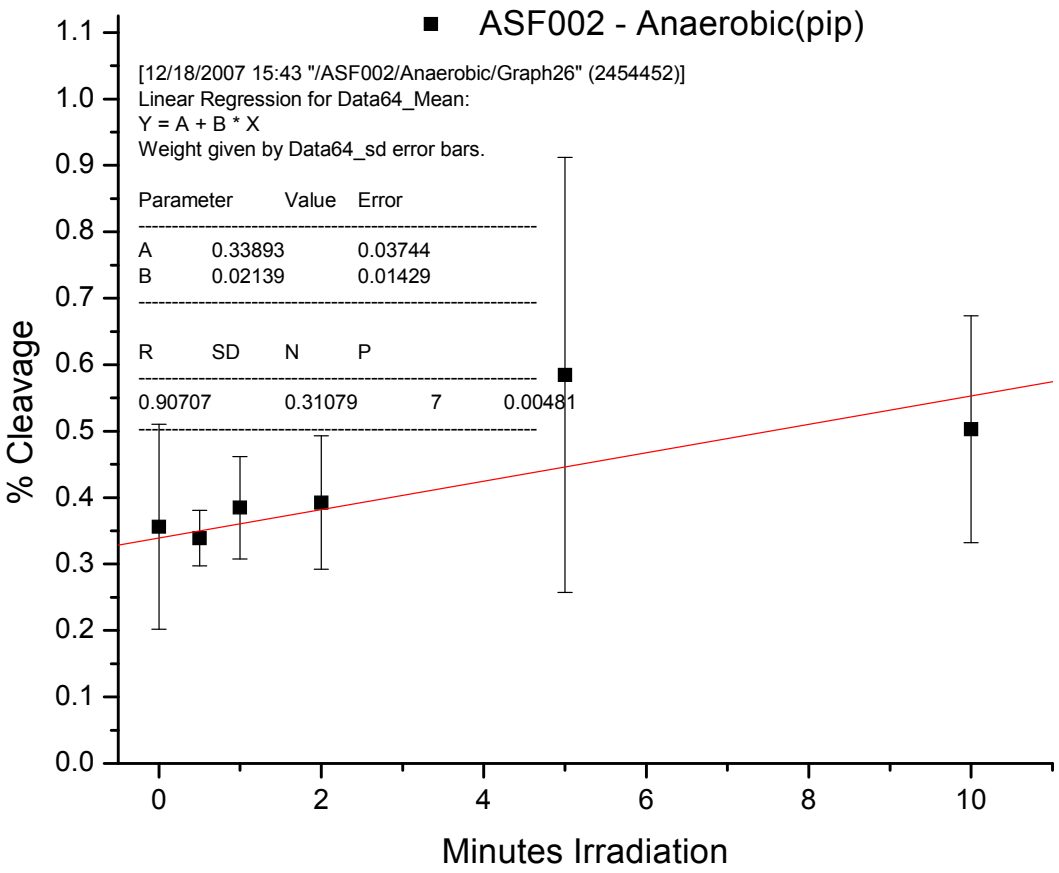

Figure II.18: Initial rate determination of EET in ASF002 as detected by piperidine treatment under anaerobic conditions. Percent cleavage calculated from the intensity of the EET induced cleavage band relative to the total intensity per sample. The data points represent an average of a minimum of three independent experiments at each time point and the error bars are the standard deviation of the average of each time point.

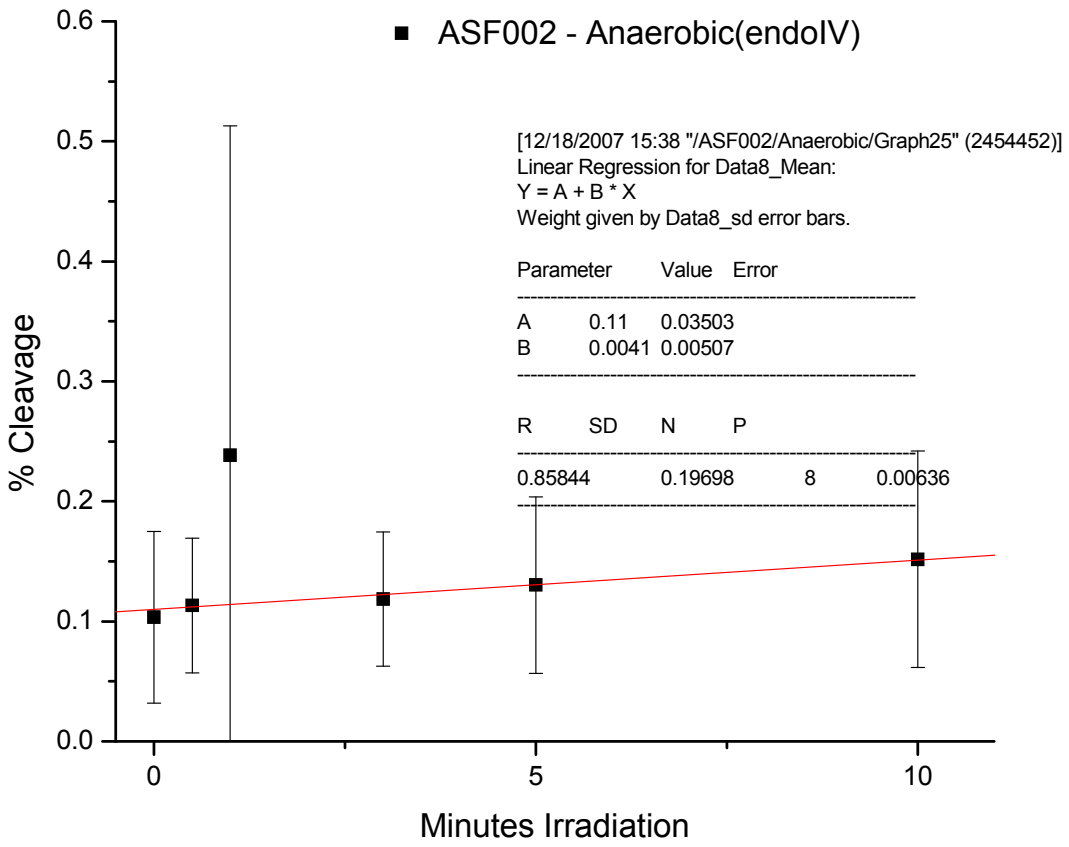

Figure II.19 Initial rate determination of EET in ASF002 as detected by endoV treatment under anaerobic conditions. Percent cleavage calculated from the intensity of the EET induced cleavage band relative to the total intensity per sample. The data points represent an average of a minimum of three independent experiments at each time point and the error bars are the standard deviation of the average of each time point.

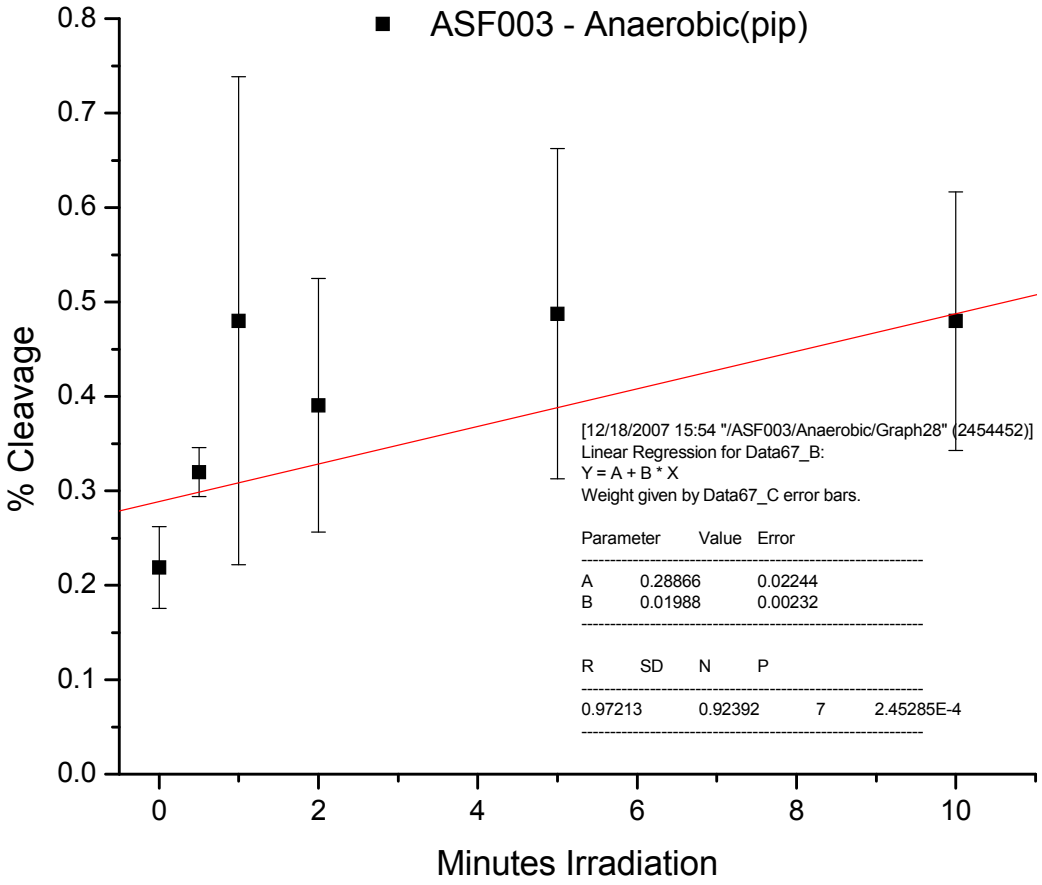

Figure II.20: Initial rate determination of EET in ASF003 as detected by piperidine treatment under anaerobic conditions. Percent cleavage calculated from the intensity of the EET induced cleavage band relative to the total intensity per sample. The data points represent an average of a minimum of three independent experiments at each time point and the error bars are the standard deviation of the average of each time point.

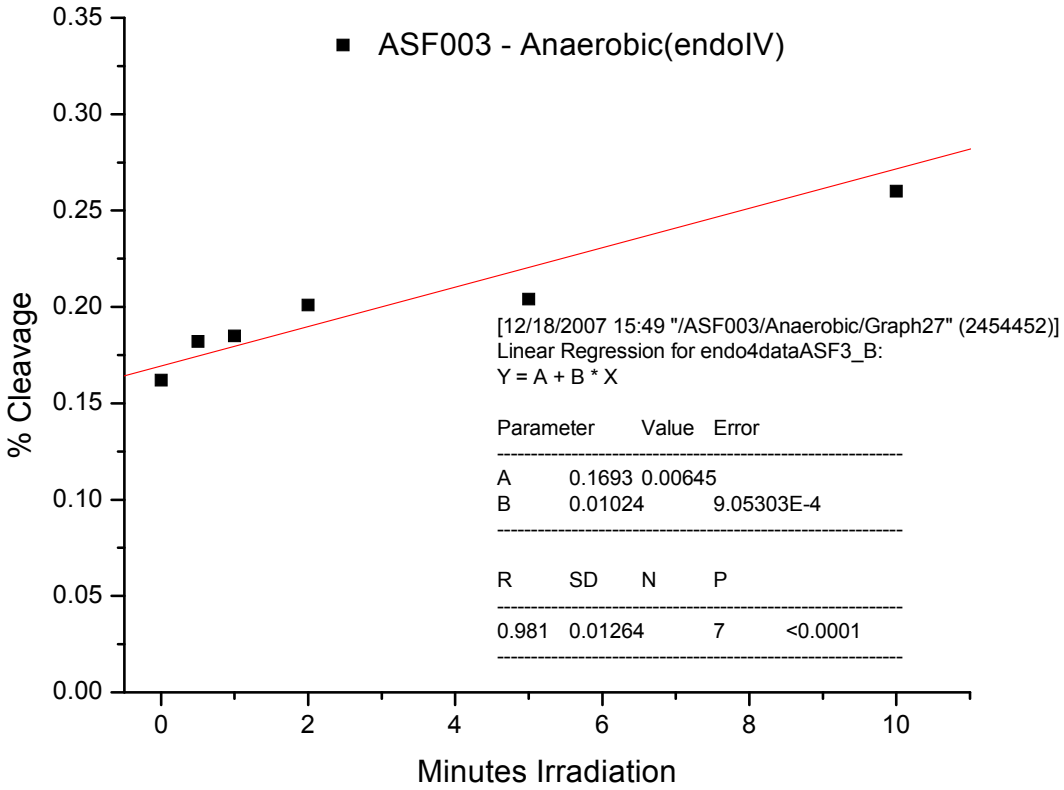

Figure II.11: Initial rate determination of EET in ASF003 as detected by endoIV treatment under anaerobic conditions. Percent cleavage calculated from the intensity of the EET induced cleavage band relative to the total intensity per sample. The data points represent an average of a minimum of three independent experiments at each time point and the error bars are the standard deviation of the average of each time point.

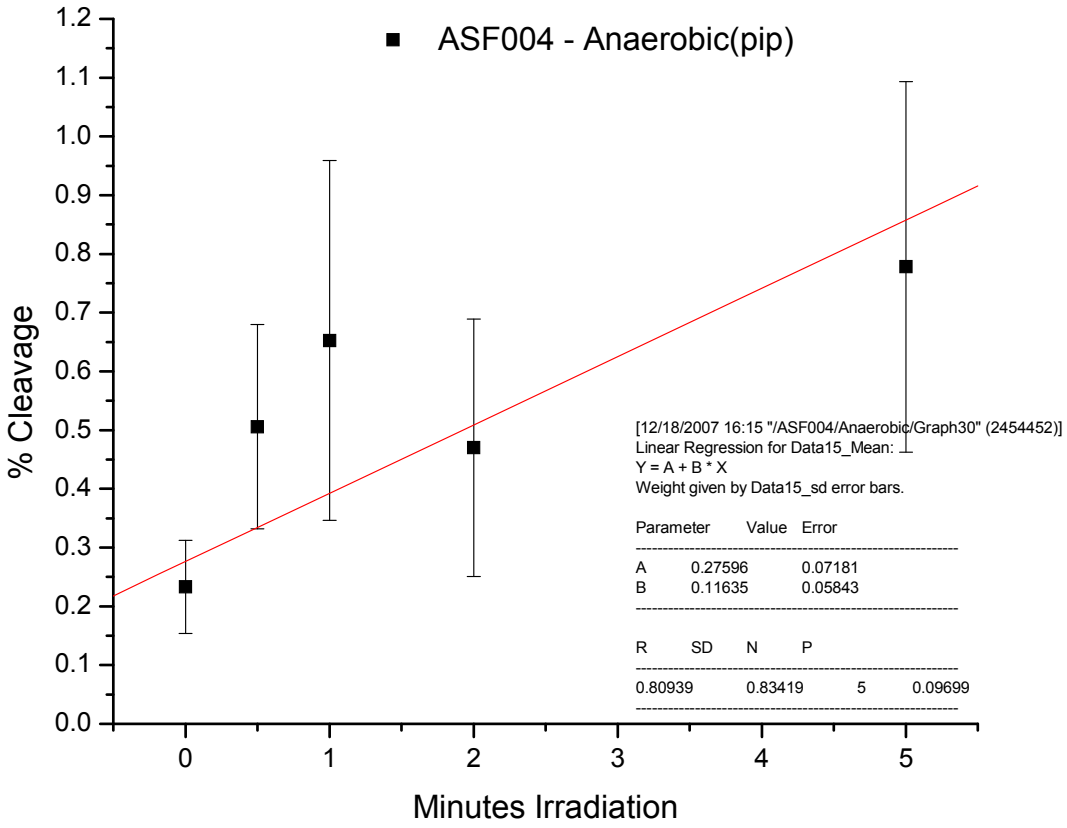

Figure II.22: Initial rate determination of EET in ASF004 as detected by piperidine treatment under anaerobic conditions. Percent cleavage calculated from the intensity of the EET induced cleavage band relative to the total intensity per sample. The data points represent an average of a minimum of three independent experiments at each time point and the error bars are the standard deviation of the average of each time point.

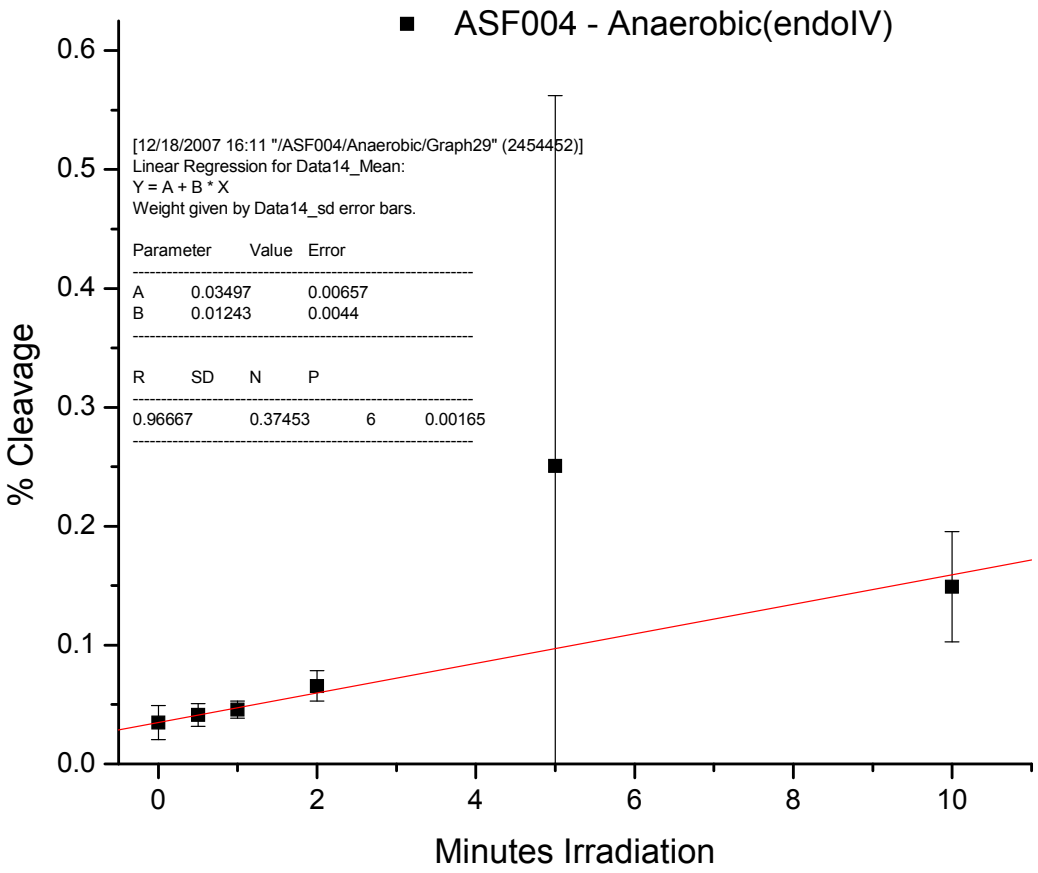

Figure II.23: Initial rate determination of EET in ASF004 as detected by endoIV treatment under anaerobic conditions. Percent cleavage calculated from the intensity of the EET induced cleavage band relative to the total intensity per sample. The data points represent an average of a minimum of three independent experiments at each time point and the error bars are the standard deviation of the average of each time point.

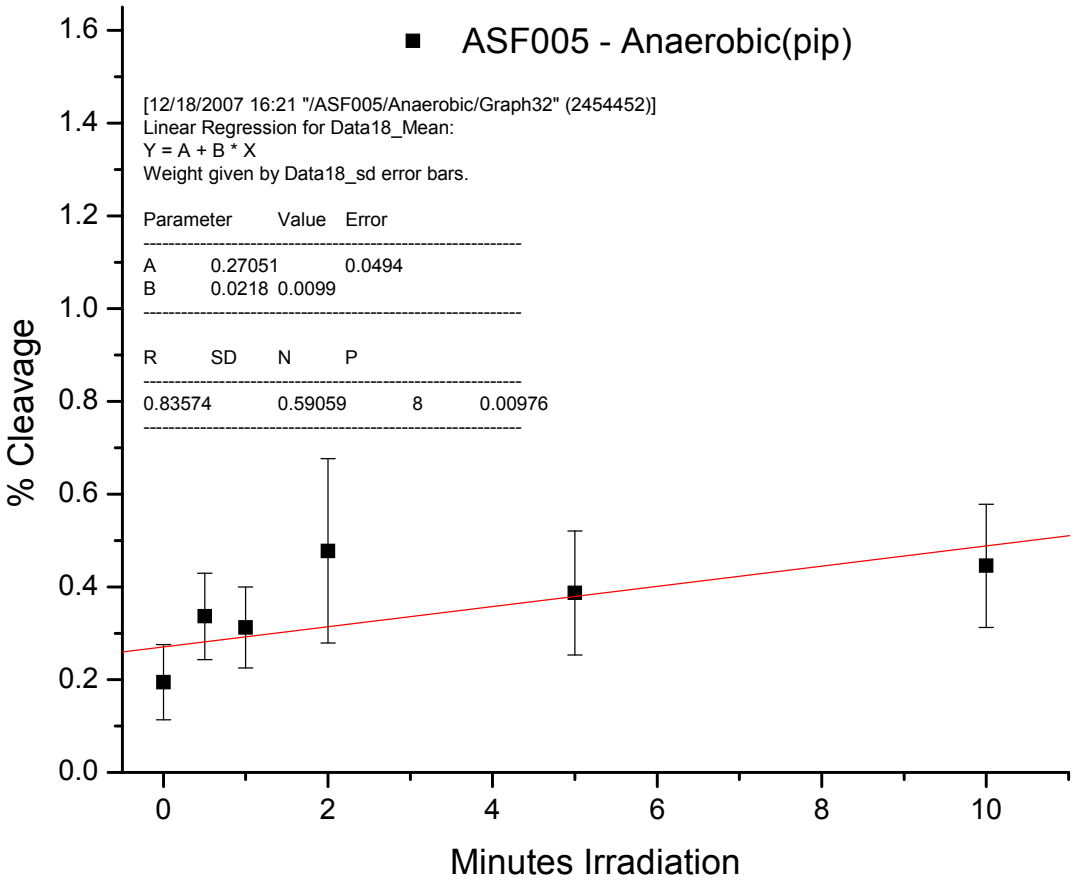

Figure II.24: Initial rate determination of EET in ASF005 as detected by piperidine treatment under anaerobic conditions. Percent cleavage calculated from the intensity of the EET induced cleavage band relative to the total intensity per sample. The data points represent an average of a minimum of three independent experiments at each time point and the error bars are the standard deviation of the average of each time point.

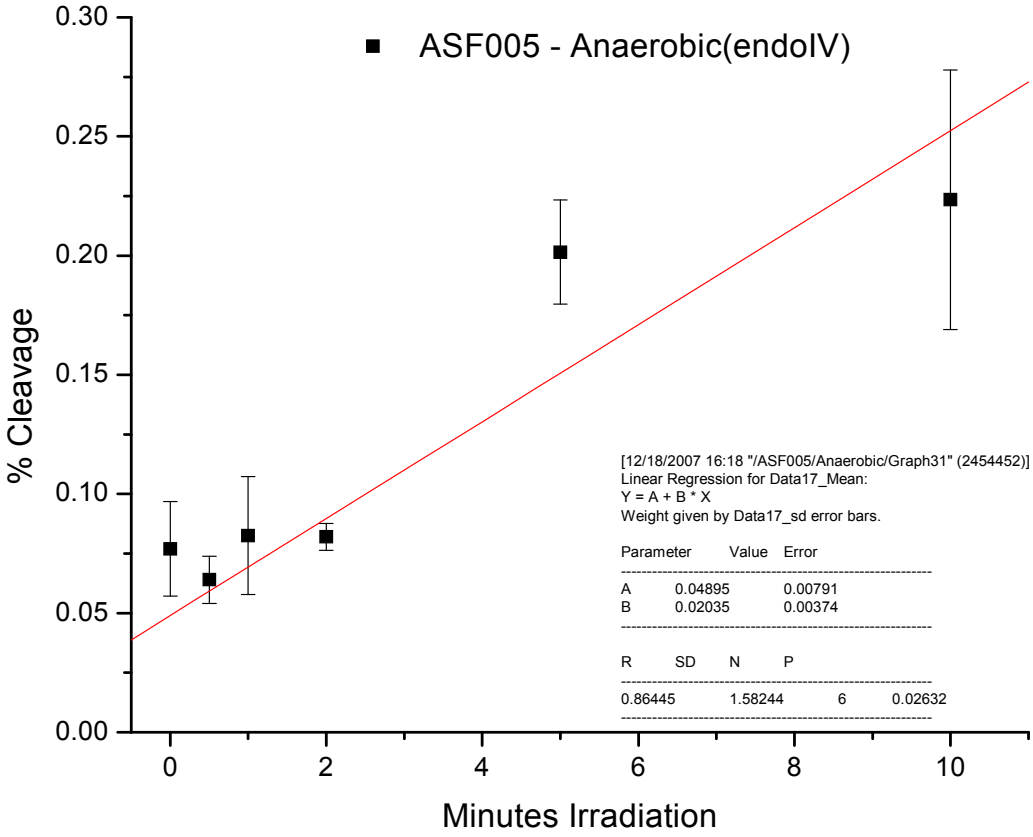

Figure II.25: Initial rate determination of EET in ASF005 as detected by endoIV treatment under anaerobic conditions. Percent cleavage calculated from the intensity of the EET induced cleavage band relative to the total intensity per sample. The data points represent an average of a minimum of three independent experiments at each time point and the error bars are the standard deviation of the average of each time point.

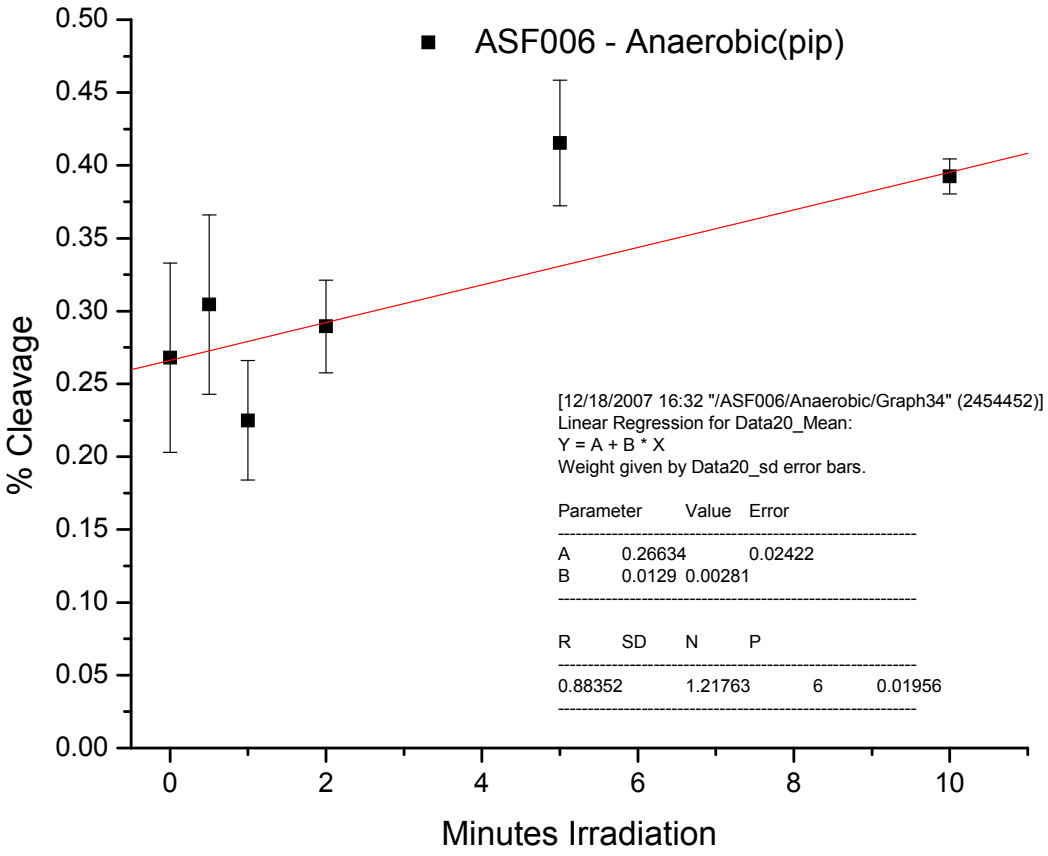

Figure II.26: Initial rate determination of EET in ASF006 as detected by piperidine treatment under anaerobic conditions. Percent cleavage calculated from the intensity of the EET induced cleavage band relative to the total intensity per sample. The data points represent an average of a minimum of three independent experiments at each time point and the error bars are the standard deviation of the average of each time point.

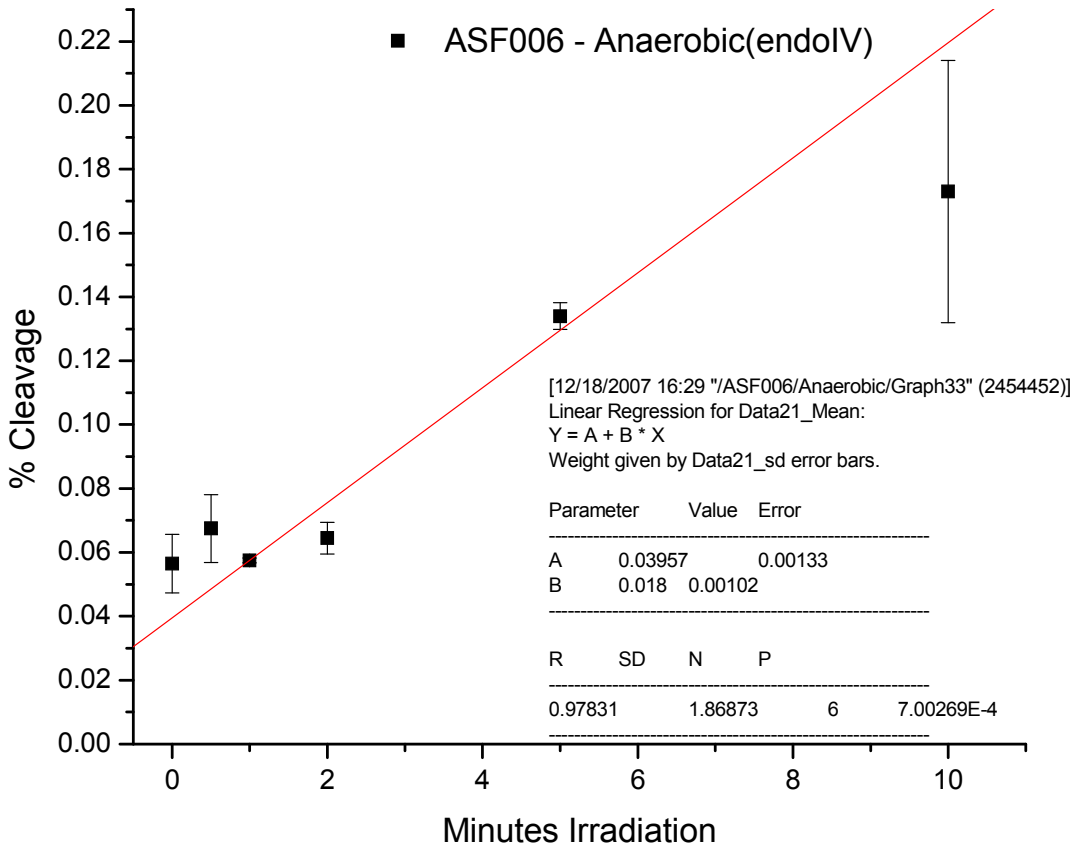

Figure II.27: Initial rate determination of EET in ASF006 as detected by endoIV treatment under anaerobic conditions. Percent cleavage calculated from the intensity of the EET induced cleavage band relative to the total intensity per sample. The data points represent an average of a minimum of three independent experiments at each time point and the error bars are the standard deviation of the average of each time point.

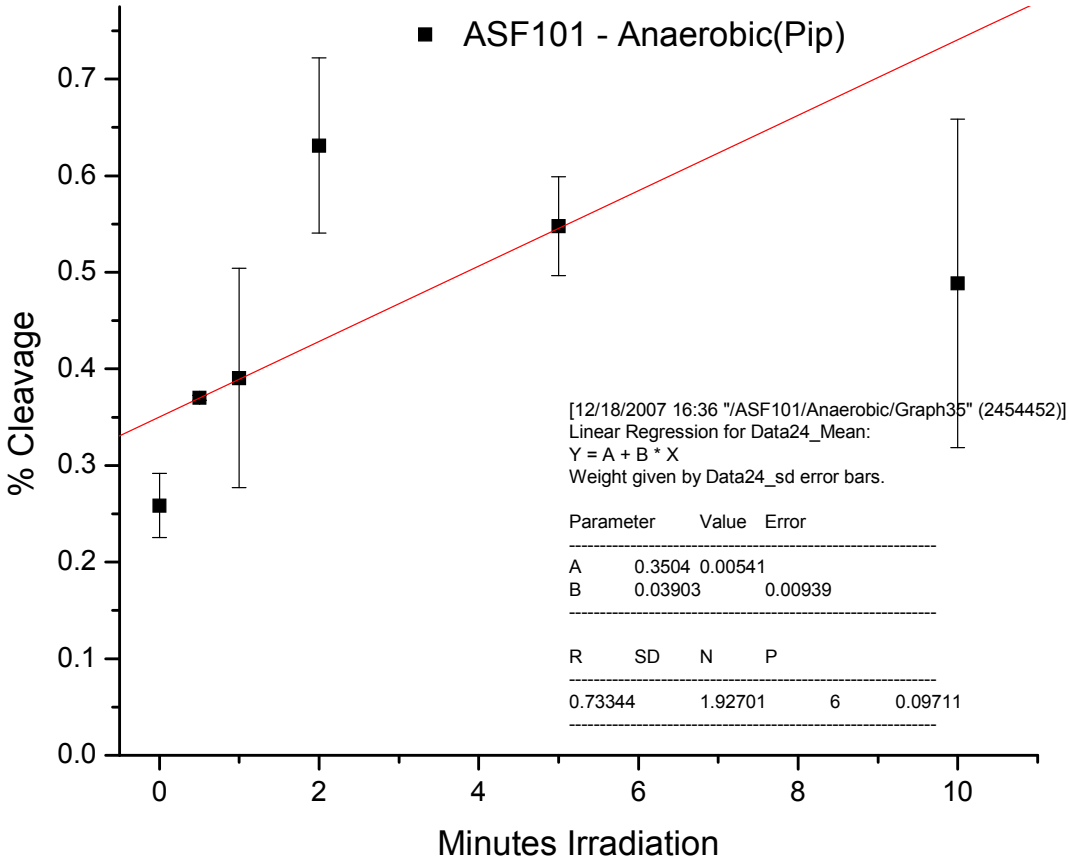

Figure II.28: Initial rate determination of EET in ASF101 as detected by piperidine treatment under anaerobic conditions. Percent cleavage calculated from the intensity of the EET induced cleavage band relative to the total intensity per sample. The data points represent an average of a minimum of three independent experiments at each time point and the error bars are the standard deviation of the average of each time point.

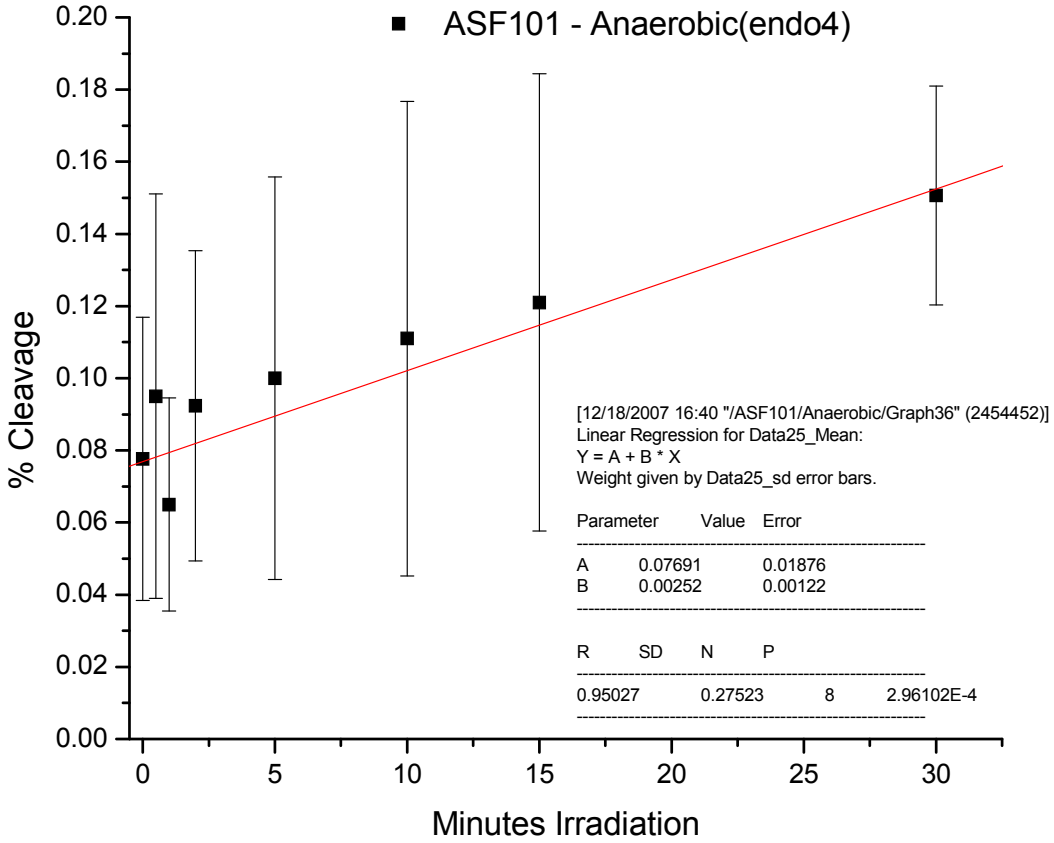

Figure II.29: Initial rate determination of EET in ASF101 as detected by endoIV treatment under anaerobic conditions. Percent cleavage calculated from the intensity of the EET induced cleavage band relative to the total intensity per sample. The data points represent an average of a minimum of three independent experiments at each time point and the error bars are the standard deviation of the average of each time point.

Bibliography

1. Lodish, H.; Berk, A.; Zipursky, S.L.; Matsudaira, P.; Baltimore, D.; Darnell, J., *Molecular Cell Biology*. 4th ed.; W. H. Freeman and Company: New York, New York, 2000.

2. Downes, A.; Blunt, T.P., Researches on the effect of light upon bacteria and other organisms. *Proceedings of the Royal Society of Medicine* **1877,** 26, 488.

3. Gates, F.L., On nuclear derivates and the lethal action of ultraviolet light. *Science* **1928,** 68, 479-480.

4. Chart of the Electromagnetic Spectrum. www.sura.org

5. Taylor, J.S., Unraveling the molecular pathway from sunlight to skin cancer. *Acc. Chem. Res.* **1994,** 27, 76-82.

6. Urbach, F., Potential effects of altered solar ultraviolet radiation on human skin cancer. *Photochem. Photobiol.* **1989,** 50, 507-513.

7. Peak, M.J.; Peak, J.G.; Moehring, M.P.; Webb, R.W., Ultraviolet action spectra for DNA dimer induction, lethality and mutagenesis in *Escherichia coli*: With emphasis on the UVB region. *Photochem. Photobiol.* **1984,** 40, 613-620.

8. Caldwell, M.; Camp, L.B.; Warner, C.W.; Flint, S.D., Action spectra and their key role in assessing biological consequences of solar UV-B radiation change. In *Stratospheric Ozone Reduction, Solar Ultraviolet Radiation and Plant Life*, Worrest, R.C.; Caldwell, M., Eds. Springer Berlin, 1984; Vol. 8, pp 87-112.

9. Bykov, V.J.; Hemminki, K., Assay of different photoproducts after UV A, B, and C irradiation of DNA and human skin explants. *Carcinogenesis* **1996,** 17, 1949-1955.

10. Taylor, J.S., DNA, sunlight, and skin cancer. *J. Chem. Educ.* **1990,** 67, 835-841.

11. Stolarski, R.; Bokjov, R.; Bishop, L.; Zerefos, C.; Staehelin, J.; Zawodny, J., Measured trends in stratospheric ozone *Science* **1992,** 256, 342-349.

12. Van Der Leun, J.C., Ozone depletion and skin cancer. *J. Photochem. Photobiol., A* **1988,** 1, 493.

13. Norval, M.; Cullen, A.P.; De Gruijl, F.R.; Longstreth, J.; Takizawa, Y.; Lucas, R.M.; Noonan, F.P.; Van Der Leun, J.C., The effects on human health from stratospheric ozone depletion and its interactions with climate change. *Photochem. Photobiol. Sci.* **2007,** 6, 232-251.

14. Van Der Leun, J.C., UV radiation from sunlight: summary, conclusions and recommendations. *J. Photochem. Photobiol., B* **1996,** 35, 237-244.

15. Patrick, M.H., Studies on thymine-derived UV photoproducts in DNA--I. Formation and biological role of pyrimidine adducts in DNA. *J. Photochem. Photobiol.* **1977,** 25, 357-372.

16. Johns, H.E.; Pearson, M.L.; Leblanc, J.C.; Helleiner, C.W., The ultraviolet photochemistry of thymidylyl-(3' - 5')thymidine. *J. Mol. Biol.* **1964,** 9, 503-524.

17. Frederico, L.A.; Kunkel, T.A.; Shaw, B.R., A sensitive genetic assay for the detection of cytosine deamination: determination of rate constants and the activation energy. *Biochemistry* **1990,** 29, 2532-2537.

18. Bloomfield, V.A.; Crothers, D.M.; Tinoco, I., *Nucleic Acids: Structures, Properties, and Functions*. University Science Books: Sausalito, 2000; p 794.

19. Inaki, Y., Reversible Photodimerization of Pyrimidine Bases. In *CRC Handbook of Organic Photochemistry and Photobiology*, Second ed.; Horspool, W.; Lenci, F., Eds. CRC Press: Washington, DC, 2004; pp **104**-**10**1 - **104**-**1**33.

20. Friedberg, E., *DNA Repair*. W.H.Freeman and Company: New York, 1985.

21. Taubes, G., Double helix chemistry at a distance--but how? *Science* **1997,** 275.

22. Taylor, J.S.; Brockie, I.R., Synthesis of a trans-syn thymine dimer building block, solid phase synthesis of CGTAT(t,s)TATGC. *Nucleic Acids Res.* **1988,** 16, 5123-5137.

23. Berg, J.M.; Tymoczko, J.L.; Stryer, L., *Biochemistry*. 5 ed.; W.H. Freeman and Company: New York, 2002; p 974.

24. Wang, S.Y., Photochemical reactions in frozen solutions. *Nature* **1961,** 190, 690-694.

25. Setlow, R.R.; Carrier, W.L., The disappearance of thymine dimers from DNA: An error-correcting mechanism. *Proc. Natl. Acad. Sci.* **1964,** 51, 226-231.

26. Sancar, A.; Lindsey-Boltz, L.A.; Ünsal-Kaçmaz, K.; Linn, S., Molecular mechanisms of mammalian DNA repair and the DNA damage checkpoints. *Annu. Rev. Biochem.* **2004,** 73, 39-85.

27. Kunkel, T.A.; Erie, D.A., DNA mismatch repair. *Annu. Rev. Biochem.* **2005,** 74, 681-710.

28. Sancar, A.; Tang, M., Nucleotide excision repair. *Photochem. Photobiol.* **1993,** 57, 905-921.

29. Krokan, H.E.; Standal, R.; Slupphaug, G., DNA glycosylases in the base excision repair of DNA. *Biochem. J.* **1997,** 325, 1-16.

30. Thompson, L.H., Nucleotide excision repair. In *DNA damage and repair: DNA repair in higher eukaryotes*, Nickoloff, J.A.; Hoekstra, M.F., Eds. Humana Press: Totowa, NJ, 1998; Vol. 2, pp 335-393.

31. Cleaver, J.E., Defective repair replication of DNA in Xeroderma Pigmentosum. *Nature* **1968,** 218, 652-656.

32. Berneburg, M.; Lehmann, A.R., Xeroderma pigmentosum and related disorders: defects in DNA repair and transcription. *Advances in Genetics* **2001,** 43, 71-102.

33. Kraemer, K.H.; Levy, D.D.; Parris, C.N.; Gozukara, E.M.; Moriwaki, S.; Adelberg, S.; Seidman, M.M., Xeroderma Pigmentosum and related disorders: examining the linkage between defective DNA repair and cancer. *The Journal of Investigative Dermatology* **1994,** 103, 96-101.

34. Lee, J.A., The relationship between malignant melanoma of skin and exposure to sunlight. *Photochem. Photobiol.* **1989,** 50, 493-496.

35. Setlow, R.R., Repair-deficient human disorders and cancer. *Nature* **1978,** 271, 713-717.

36. Prakash, S.; Johnson, R.E.; Prakash, L., Eukaryotic translesion synthesis DNA polymerases: Specificity of structure and function. *Annu. Rev. Biochem.* **2005,** 74, 317-353.

37. Weaver, R.F., *Molecular Biology*. 2nd ed.; McGraw Hill: Boston, 2002; p 668-679.

38. Kow, Y.W., Repair of deaminated bases in DNA. *Free Radical Biology and Medicine* **2002,** 33, 886-893.

39. Mu, D.; Hsu, D.; Sancar, A., Reaction mechanism of human DNA repair excision nuclease. *J. Biol. Chem.* **1996,** 271, 8285-8294.

40. Sancar, A.; Hearst, J., Molecular matchmakers. *Science* **1993,** 259, 1415-1420.

41. Heelis, P.F.; Hartman, R.F.; Rose, S.D., Photoenzymatic repair of UV-damaged DNA: A chemist's perspective. *Chem. Soc. Rev.* **1995,** 24, 289 - 297.

42. Sancar, A., Structure and function of DNA photolyase. *Biochemistry* **1994,** 33, 2-9.

43. Kim, S.T.; Sancar, A., Photochemistry, photophysics, and mechanism of pyrimidine dimer repair by DNA photolyase. *Photochem. Photobiol.* **1993,** 57, 895-904.

44. Komori, H.; Masui, R.; Kuramitsu, S.; Yokoyama, S.; Shibata, T.; Inoue, Y.; Miki, K., Crystal structure of thermostable DNA photolyase: Pyrimidine-dimer recognition mechanism. *Proc. Natl. Acad. Sci.* **2001,** 98, 13560-13565.

45. Mees, A.; Klar, T.; Gnau, P.; Hennecke, U.; Eker, A.P.M.; Carell, T.; Essen, L.-O., Crystal Structure of a Photolyase Bound to a CPD-Like DNA Lesion After in Situ Repair. *Science* **2004,** 306, 1789-1793.

46. Park, H.W.; Kim, S.T.; Sancar, A.; Deisenhofer, J., Crystal structure of DNA photolyase from *Escherichia coli*. *Science* **1995,** 268, 1866-1872.

47. Tamada, T.; Kitadokoro, K.; Higuchi, Y.; Inaka, K.; Yasui, A.; De Ruiter, P.E.; Eker, A.P.M.; Miki, K., Crystal structure of DNA photolyase from *Anacystis nidulans*. *Nat. Struct. Mol. Biol.* **1997,** 4, 887-891.

48. Li, J.; Uchida, T.; Todo, T.; Kitagawa, T., Similarities and differences between cyclobutane pyrimidine dimer photolyase and (6-4) photolyase as revealed by resonance raman spectroscopy: Electron transfer from the FAD cofactor to ultraviolet-damaged DNA. *J. Biol. Chem.* **2006,** 281, 25551-25559.

49. Holman, M.R.; Ito, T.; Rokita, S.E., Self-repair of thymine dimer in duplex DNA. *J. Am. Chem. Soc.* **2007,** 129, 6-7.

50. Dandliker, P.J.; Holmlin, R.E.; Barton, J.K., Oxidative thymine dimer repair in the DNA helix. *Science* **1997,** 275, 1465-1468.

51. Derosa, M.C.; Sancar, A.; Barton, J.K., Electrically monitoring DNA repair by photolyase. *Proc. Natl. Acad. Sci.* **2005,** 102, 10788-10792.

52. Yeh, S.R.; Falvey, D.E., Model studies of DNA photorepair: energetic requirements for the radical anion mechanism determined by fluorescence quenching. *J. Am. Chem. Soc.* **1992,** 114, 7313-7314.

53. Scannell, M.P.; Fenick, D.J.; Yeh, S.R.; Falvey, D.E., Model studies of DNA photorepair: Reduction potentials of thymine and cytosine cyclobutane dimers measured by fluorescence quenching. *J. Am. Chem. Soc.* **1997,** 119, 1971-1977.

54. Brash, D.E.; Seetharam, S.; Kraemer, K.H.; Seidman, M.M.; Bredberg, A., Photoproduct frequency is not the major determinant of UV base substitution hot spots or cold spots in human cells. *Proc. Natl. Acad. Sci.* **1987,** 84, 3782-3786.

55. Svoboda, D.L.; Smith, C.A.; Taylor, J.S.; Sancar, A., Effects of sequence, adduct type, and opposing lesions on the binding and repair of ultraviolet photodamage by DNA photolyase and (A)BC exinuclease. *J. Biol. Chem.* **1993,** 1993, 10694-10700.

56. Haseltine, W.A.; Gordon, L.K.; Lindan, C.P.; Grafstrom, R.H.; Shaper, N.L.; Grossman, L., Cleavage of pyrimidine dimers in specific DNA sequences by a pyrimidine dimer DNA-glycosylase of *M. luteus*. *Nature* **1980,** 285, 634-639.

57. Sage, E., Distribution and repair of photolesions in DNA: Genetic consequences and the role of sequence context. *Photochem. Photobiol.* **1993,** 57, 163-174.

58. Lippke, J.A.; Gordon, L.K.; Brash, D.E.; Haseltine, W.A., Distribution of UV light-induced damage in a defined sequence of human DNA: Detectin of alkaline-sensitive lesions at pyrimidine nucleoside-cytidine sequences. *Proc. Natl. Acad. Sci.* **1981,** 78, 3388-3392.

59. Gale, J.M.; Smerdon, M.J., UV induced (6-4) photoproducts are distributed differently than cyclobutane dimers in nucleosomes. *Photochem. Photobiol.* **1990,** 51, 411-417.

60. Meijer, M.; Smerdon, M.J., Accessing DNA damage in chromatin: Insights from transcription. *BioEssays* **1999,** 21, 596-603.

61. Smerdon, M.J., *DNA excision repair at the nucleosome level of chromatin*. Plenum Press: New York, 1989.

62. Pehrson, J.R.; Cohen, L.H., Effects of DNA looping on pyrimidine dimer formation. *Nucleic Acids Res.* **1992,** 20, 1321-1324.

63. Brown, D.W.; Libertini, L.J.; Suquet, C.; Small, E.W.; Smerdon, M.J., Unfolding of Nucleosome Cores Dramatically Changes the Distribution of Ultraviolet Photoproducts in DNA. *Biochemistry* **1993,** 32, 10528-10531.

64. Liu, X.; Mann, D.B.; Suquet, C.; Springer, D.L.; Smerdon, M.J., Ultraviolet damage and nucleosome folding of the 5S ribosomal RNA gene. *Biochemistry* **2000,** 39, 557-566.

65. Mann, D.B.; Springer, D.L.; Smerdon, M.J., DNA damage can alter the stability of nucleosomes: effects are dependent on damage type. *Proc. Natl. Acad. Sci.* **1997,** 94, 2215-2220.

66. Pehrson, J.R., Thymine dimer formation as a probe of the path of DNA in and between nucleosomes in intact chromatin. *Proc. Natl. Acad. Sci.* **1989,** 86, 9149-9153.

67. Mitchell, D.L.; Clarkson, J.M.; Chao, C.C.; Rosenstein, B.S., Repair of cyclobutane dimers and (6-4) photoproducts in ICR 2A frog cells. *Photochem. Photobiol.* **1986,** 43, 595-597.

68. Mitchell, D.L.; Nguyen, T.D.; Cleaver, J.E., Nonrandom induction of pyrimidine-pyrimidone (6-4) photoproducts in ultraviolet-irradiated human chromatin. *J. Biol. Chem.* **1990,** 265, 5353-5356.

69. Myles, G.M.; Van Houten, B.; Sancar, A., Utilization of DNA photolyase, pyrimidine dimer endonuclease, and alkali hydrolysis in the analysis of aberrant ABC exinuclease incisions adjacent to UV-induced DNA photoproducts. *Nucleic Acids Res.* **1987,** 15, 1227-1243.

70. Rinaldy, A.; Bellew, T.; Egli, E.; Lloyd, R.S., Increased UV resistance in Xeroderma Pigmentosum group A cells after transformation with a

human genomic DNA clone. *Proc. Natl. Acad. Sci.* **1990,** 87, 6818-6822.

71. Taylor, J.S., DNA, light, and dewar pyrimidones: The structure and biological significance of TpT3. *J. Am. Chem. Soc.* **1987,** 209, 2834-2835.

72. Thompson, L.H.; Mitchell, D.L.; Regan, J.D.; Bouffler, S.D.; Stewart, S.A.; Carrier, W.L.; Nairn, R.S.; Johnson, R.T., CHO mutant UV61 removes (6-4) photoproducts in DNA. *Mutagenesis* **1989,** 4.

73. Szymkowski, D.E.; Lawrence, C.W.; Wood, R.D., Repair by human cell extracts of single (6-4) and cyclobutane thymine-thymine photoproducts in DNA. *Proceedings of the National Academy of Sciences of the United States of America* **1993,** 90, 9823-9827.

74. Ye, N.; Bianchi, M.S.; Bianchi, N.O.; Holmquist, G.P., Adaptive enhancement and kinetics of nucleotide excision repair in humans. *Mutat. Res.* **1999,** 435, 43-61.

75. Tornaletti, S.; Pfeifer, G.P., UV damage and repair mechanisms in mammalian cells. *BioEssays* **1996,** 18, 221-228.

76. Vogelstein, B., Cancer: A deadly inheritance. *Nature* **1990,** 348, 681-682.

77. Hauswirth, W.; Wang, S.Y., Excited state process and solution conformation of dipyrimidine adducts. *Photochem. Photobiol.* **1977,** 25, 161-166.

78. Pouwels, P.J.; Hartman, R.F.; Rose, S.D.; Kaptein, R., Photo-CIDNP study of pyrimidine dimer splitting I/II: Reactions involving pyrimidine radical cation/anion intermediates. *Photochem. Photobiol.* **1995,** 61, 575-583.

79. Dandliker, P.J.; Nunez, M.E.; Barton, J.K., Oxidative charge transfer to repair thymine dimers and damage guanine bases in DNA assemblies containing tethered metallointercalators. *Biochemistry* **1998,** 37, 6491-6502.

80. Moysan, A.; Viary, A.; Vigny, P.; Voituriez, L.; Cadet, J.; Moustacchi, E.; Sage, E., Formation of cyclobutane thymine dimers photosensitized by pyridopsoralens: quantitative and qualitative distribution within DNA. *Biochemistry* **1991,** 30, 7080-7088.

81. Lamola, A.A., Triplet photosensitization and the photobiology of thymine dimers in DNA. *Pure Appl. Chem.* **1970,** 24, 599-610.

82. Wang, C.I.; Taylor, J.S., Site-specific effect of thymine dimer formation on dAn.cntdot.dTn tract bending and its biological implications. *Proc. Natl. Acad. Sci.* **1991,** 88, 9072-9076.

83. Holman, M.R. Determinants of UV-induced cyclobutane pyrimidine dimer hot spots in DNA. PhD, University of College Park, Maryland, College Park, 2000.

84. Eley, D.D.; Spivey, D.I., Semiconductivity of organic substances. Nucleic acid in the dry state. *Transactions of the Faraday Society* **1962,** 58, 411-415.

85. Whitesides, G.M.; Grzybowski, B., Self Assembly at All Scales. *Science* **2002,** 295.

86. Condon, A., Designed DNA molecules: Principles and applications of molecular nanotechnology. *Nature Reviews Genetics* **2006,** 7, 565-575.

87. Eijkel, J.C.T.; Van Den Berg, A., The promise of nanotechnology for separation devices - from a top-down approah to nature-inspired separation devices. *Electrophoresis* **2006,** 27, 677-685.

88. Berlin, Y.A.; Burin, A.L.; Ratner, M.A., Charge hopping in DNA. *J. Am. Chem. Soc.* **2001,** 123, 260-268.

89. Fink, H.W.; Schonenberger, C., Electrical conduction through DNA molecules. *Nature* **1999,** 398, 407-410.

90. Van Zalinge, H.; Schiffrin, D.J.; Bates, A.D.; Starikov, E.B.; Wenzel, W.; Nichols, R.J., Variable-temperature measurements of the single-

moleucle conductance of double-stranded DNA. *Angew. Chem., Int. Ed.* **2006,** 45, 5499-5502.

91. Drummond, T.G.; Hill, M.G.; Barton, J.K., Electrochemical DNA sensors. *Nat. Biotechnol.* **2003,** 21, 1192-1199.

92. Tarlov, M.J.; Steel, A.B., DNA-based sensors. *Surfactant Science Series* **2003,** 111, 545-608.

93. Gu, Q.; Cheng, C.; Gonela, R.; Suryanarayanan, S.; Anabathula, S.; Dai, K.; Haynie, D.T., DNA Nanowire fabrication. *Nanotechnology* **2006,** 17, 14-25.

94. Turro, N.J.; Barton, J.K., Paradigms, supermolecules, electron transfer and chemistry at a distance. What's the problem? The science or the paradigm? *J. Biol. Inorg. Chem.* **1998,** 3, 201-209.

95. Porath, D.; Cuniberti, G.; Di Felice, R., Charge transport in DNA-based devices. *Top. Curr. Chem.* **2004,** 237, 183-227.

96. Grinstaff, M.W., How do charges travel through DNA? - An update on a current debate. *Angew. Chem.* **1999,** 38, 3629-3635.

97. Wagenknecht, H.A., Synthetic oligonucleotide modifications for the investigation of charge transfer and migration processes in DNA. *Curr. Org. Chem.* **2004,** 8, 251-266.

98. Seeman, N.C., The challenge of structural control on the nanoscale bottom-up self-assembly of nucleic acids in 3D. *Int. J. Nanotechnol.* **2005,** 2, 348-370.

99. Wagenknecht, H.A., Electron transfer processes in DNA: mechanisms, biological relevance, and applications in DNA analytics. *Nat. Prod. Rep.* **2006,** 23, 973-1006.

100. Lewis, F.D.; Wasielewski, M.R., Dynamics and equilibrium for single step hole transport processes in duplex DNA. *Topics Curr. Chem.* **2004,** 236, 45-65.

101. Lewis, F.D.; Zhu, H.; Daublain, P.; Fiebig, T.; Raytchev, M.; Wang, Q.; Shafirovich, V., Crossover from superexchange to hopping as the mechanism for photoinduced electron charge transfer in DNA hairpin conjugates. *J. Am. Chem. Soc.* **2006,** 128, 791-800.

102. Bixon, M.; Jortner, J., Long-range and very long-range charge transport in DNA. *Chem. Phys.* **2002,** 281, 393-408.

103. Jortner, J.; Bixon, M.; Voityuk, A.A.; Roesch, N., Superexchange mediated charge hopping in DNA. *J. Phys. Chem. A* **2002,** 106, 7599-7606.

104. Liu, C.-S.; Schuster, G.B., Base sequence effects in radical cation migration in duplex DNA: Support for the polaron-like hopping model. *J. Am. Chem. Soc.* **2003,** 125, 6098-6102.

105. Conwell, E.M., Polarons and transport in DNA. *Top. Curr. Chem.* **2004,** 2004, 73-101.

106. Conwell, E.M., Charge transport in DNA in solution: The role of polarons. *Proc. Natl. Acad. Sci.* **2005,** 102, 8795-8799.

107. Ly, D.; Sanii, L.; Schuster, G.B., Mechanism of charge transport in DNA: Internally-linked anthraquinone conjugates support phonon-assisted polaron hopping. *J. Am. Chem. Soc.* **1999,** 121, 9400-9410.

108. Lewis, F.D., Distance-dependent electron transfer in DNA hairpins. *Science* **1997,** 277, 673-676.

109. Lewis, F.D., Dynamics of photoinduced charge separation and charge recombination in synthetic DNA hairpins with stilbenedicarboxamide linkers. *J. Am. Chem. Soc.* **2000,** 122, 2889-2902.

110. Harriman, A., Electron tunneling in DNA. *Angew. Chem. Int. Ed.* **1999,** 38, 945-949.

111. Fukui, K., Distance dependence of electron transfer in acridine-intercalated DNA. *J. Photochem. Photobiol. B* **1999,** 50, 18-27.

112. Schuster, G.B., Long-range charge transfer in DNA: Transient structural distortions control the distance dependence. *Acc. Chem. Res.* **2000,** 33, 253-260.

113. Basko, D.M.; Conwell, E.M., Self-trapping versus trapping: Application to hole transport in DNA. *Phys. Rev. E: Stat., Nonlinear, Soft Matter Phys.* **2002,** 65, 061902/061901-061902/061907.

114. Henderson, P.T.; Jones, D.; Hampikian, G.; Kan, Y.; Schuster, G.B., Long-distance charge transport in duplex DNA: The phonon-assisted polaron-like hopping mechanism *Proc. Natl. Acad. Sci.* **1999,** 96, 8353 - 8358.

115. Kino, K.; Saito, I.; Sugiyama, H., Product analysis of GG-specific photooxidation of DNA via electron transfer: 2-aminoimidazolone as a major guanine oxidation product. *J. Am. Chem. Soc.* **1998,** 120, 7373-7374.

116. Saito, I.; Nakamura, T.; Nakatani, K.; Yoshioka, Y.; Yamaguchi, K.; Sugiyama, H., Mapping of the hot spots for DNA damage by one-electron oxidation: Efficacy of GG doublets and GGG triplets as a trap in long-range hole migration. *J. Am. Chem. Soc.* **1998,** 120, 12686-12687.

117. Crespo-Hernandez, C.E.; Close, D.M.; Gorb, L.; Leszczynski, J., Determination of redox potentials for the watson-crick base pairs, DNA nucleosides, and relevant nucleoside analogues. *J. Phys. Chem. B* **2007,** 111, 5386-5395.

118. Wagenknecht, H.A., *Charge transfer in DNA: From mechanism to application*. Wiley-VCH: Weinheim, 2005; p 229.

119. Giese, B., Long-distance electron transfer through DNA. *Annu. Rev. Biochem.* **2002,** 71, 51-70.

120. Joy, A.; Schuster, G.B., Long-range radical cation migration in DNA: Investigation of the mechanism. *Chem. Commun.* **2005**, 2778-2784.

121. Nunez, M.E.; Barton, J.K., Probing DNA charge transport with metallointercalators. *Curr. Opin. Chem. Biol.* **2000,** 4, 199-206.

122. Lewis, F.D.; Letsinger, R.L.; Wasielewski, M.R., Dynamics of photoinduced charge transfer and hole transport in synthetic DNA hairpins. *Acc. Chem. Res.* **2001,** 34, 159-170.

123. Reynisson, J.; Schuster, G.B.; Howerton, S.B.; Williams, L.D.; Barnett, R.N.; Cleveland, C.L.; Landman, U.; Harrit, N.; Chaires, J.B., Intercalation of trioxatriangulenium ion in DNA: Binding, electron transfer, x-ray crystallography, and electronic structure. *J. Am. Chem. Soc.* **2003,** 125, 2072-2083.

124. Dotse, A.K.; Boone, E.K.; Schuster, G.B., Remote cis-syn-thymine [2 + 2] dimers are not repaired by radical cations migrating in duplex DNA. *J. Am. Chem. Soc.* **2000,** 122, 6825-6833.

125. Clever, G.H.; Kaul, C.; Carell, T., DNA-Metal Base Pairs. *Angew. Chem.* **2007,** 46, 6226-6236.

126. Liu, T.; Barton, J.K., DNA electrochemistry through the base pairs not the sugar-phosphate backbone. *J. Am. Chem. Soc.* **2005,** 127, 10160-10161.

127. Zeglis, B.M.; Barton, J.K., A mismatch-selective bifunctional rhodium-oregon green conjugate: A flurorescent probe for mismatched DNA. *J. Am. Chem. Soc.* **2006,** 128, 5654-5655.

128. Amann, N.; Pandurski, E.; Fiebig, T.; Wagenknecht, H.-A., A model nucleoside for electron injection into DNA: 5-pyrenyl-2'-deoxyribose. *Angew. Chem.* **2002,** 41, 2978-2980.

129. Amann, N.; Pandurski, E.; Fiebig, T.; Wagenknecht, H.A., Electron injection into DNA: Synthesis and spectroscopic properties of pyrenyl-modified oligonucleotides. *Chem.--Eur. J.* **2002,** 8, 4877-4883.

130. Ito, T.; Rokita, S.E., Criteria for efficient transport of excess electrons in DNA. *Angew. Chem.* **2004,** 43, 1839-1842.

131. Schwogler, A.; Burgdorf, L.T.; Carell, T., Self-repairing DNA based on a reductive electron transfer through the base stack. *Angew. Chem.* **2000,** 39, 3918-3920.

132. Behrens, C.; Burgdorf, L.T.; Schwogler, A.; Carell, T., Weak distance dependence of excess electron transfer in DNA. *Angew. Chem.* **2002,** 41, 1763-1766.

133. Ito, T.; Rokita, S.E., Excess electron transfer from an internally conjugated aromatic amine to 5-bromo-2'-deoxyuridine in DNA. *J. Am. Chem. Soc.* **2003,** 128, 11480-11481.

134. Seidel, C.A.M.; Schulz, A.; Sauer, M.H.M., Nucleobase-specific quenching of fluorescent dyes. 1. Nucleobase one-electron redox potentials and their correlation with static and dynamic quenching efficiencies. *J. Phys. Chem.* **1996,** 100, 5541-5553.

135. Behrens, C.; Ober, M.; Carell, T., Excess electron transfer in flavin-capped DNA-hairpins. *Eur. J. Org. Chem.* **2002**, 3281-3289.

136. Kawanishi, S.; Takada, T.; Nagai, T.; Cai, X.; Sugimoto, A.; Fujisuka, M.; Majima, T., Long-lived charge-separated state leading to DNA damage through hole transfer. *J. Am. Chem. Soc.* **2003,** 125, 16198-16199.

137. Rivera, E.; Schuler, R.H., Intermediates in the reduction of 5-halouracils by e_{aq}^{-1}. *J. Phys. Chem.* **1983,** 87, 3966.

138. Griffiths, J.F.; Miller, J.H.; Suzuki, J.H.; Lewontin, R.C.; Gelbart, W.M., *An Introduction to Genetic Analysis*. 6th ed.; W.H. Freeman: New York, 1996.

139. Hartl, D.; Jones, E., *The Structure of Eukaryotic Chromasomes*. 4th ed.; Jones and Bartlett: Sudbury, 1998.

140. Luger, K.; Mader, A.W.; Richmond, R.K.; Sargent, D.F.; Richmond, T.J., Crystal structure of the nucleosome core particle at 2.8Å resolution. *Nature* **1997,** 389, 251-260.

141. Richmond, T.J.; Davey, C.A., The structure of DNA in the nucleosome core. *Nature* **2003,** 423, 145-150.

142. Wheeler, R. Schematic representation of the assembly of the core histones into the nucleosome www.wikipedia.org

143. Gale, J.M.; Nissen, K.A.; Smerdon, M.J., UV-induced formation of pyrimidine dimers in nucleosome core DNA is strongly modulated with a period of 10.3 bases. *Proc. Natl. Acad. Sci.* **1987,** 84, 6644-6648.

144. Ghosh, M. Carcinogenic metal-mediated oxidation of proteins and DNA. University of Maryland, College Park, 1998.

145. Ausebel, F.M.; Brent, R.; Kingston, R.E.; Moore, D.D.; Seidman, J.G.; Smith, J.A.; Struhl, K., *Short Protocols in Molecular Biology*. 5th ed.; Wiley: New York, 2002.

146. Millard, J.T.; Wilkes, E.E., cis- and trans-diamminedichloroplatinum(II) interstrand cross-linking of a defined sequence nucleosomal core particle. *Biochemistry* **2000,** 39, 16046-16055.

147. Oriel-Instruments, The Book of Photon Tools. In www.newport.com: Stratford, 2007.

148. Ausio, J.; Dong, F.; Van Holde, K.E., Use of selectively trypsinized nucleosome core particles to analyze the role of histone tails in the stabilization of the nucleosome. *J. Mol. Biol.* **1989,** 206, 451-463.

149. Libertini, L.J.; Small, E.W., Salt-induced transitions of chromatin core particles studied by tyrosine fluorescence anisotropy. *Nucleic Acids Res.* **1980,** 8.

150. Ausubel, F.M.; Brent, R.; Kingston, R.E.; Moore, D.D.; Seidman, J.G.; Smith, J.A.; Struhl, K., *Short Protocols in Molecular Biology*. 5th ed.; Wiley: New York, 2002.

151. Portugal, J., Drug interaction with nucleosome and chromatin. *Methods Enzymol.* **2001,** 340, 503-518.

152. Miller, J.H.; Swenberg, C.E., Radical yields in DNA exposed to ionizing-radiation - Role of energy and charge-transfer. *Can. J. Phys.* **1990,** 68, 962-966.

153. Luger, K.; Rechsteiner, T.J.; Richmond, T.J., Chromatin Protocols. In *Methods in Enzymology: Chromatin*, Wassarman, P.M.; Wolffe, A.P., Eds. Academic Press: Burlington, 1999; Vol. 304, pp 3-19.

154. Lorch, Y.; Lapointe, J.; Kornberg, R.D., On the displacement of histones from DNA by transcription. *Cell* **1988,** 55, 743-744.

155. Rhodes, D., Structural analysis of a triple complex between the histone octamer, a Xenopus gene for 5S RNA and transcription factor IIIA. . *EMBO J.* **1985,** 4, 3473-3482.

156. Pruss, D.; Wolffe, A.P., Histone-DNA contacts in a nucleosome containing a *Xenopus* 5s rRNA gene. *Biochemistry* **1993,** 32, 6810-6814.

157. Hayes, J.J.; Tullius, T.D.; Wolffe, A.P., The structure of DNA in a nucleosome. *Proc. Natl. Acad. Sci. U. S. A.* **1990,** 87, 7405-7409.

158. Burrows, C.J.; Muller, J.G., Oxidative nucleobase modifications leading to strand scission. *Chem. Rev.* **1998,** 98, 1109-1151.

159. Zucker, M., Mfold web server for nucleic acid folding and hybridization prediction. *Nucleic Acids Res.* **2003,** 31.

160. Barciszewska, M.Z.; Szymanski, M.; Erdmann, V.A.; Barciszewski, J., Structure and functions of 5s rRNA. *Acta Biochim. Pol.* **2001,** 48, 191-198.

161. Tabor, S.; Struhl, K., DNA-Dependent DNA Polymerases. In *Current Protocols in Molecular Biology*, Ausebel, F.M.; Brent, R.; Kingston, R.E.; Moore, D.D.; Seidman, J.G.; Smith, J.A.; Struhl, K., Eds. 1989; pp 3.5.10-13.15.12.

162. Rhodes, D.; Laskey, R.A., Assembly of nucleosomes and chromatin *in vitro*. *Methods Enzymol.* **1989,** 170, 575-585.

163. Stein, A., Reconstitution of chromatin from purified components. *Methods Enzymol.* **1989,** 170, 585-603.

164. O'neill, L.P.; Turner, B.M., Immunoprecipitation of native chromatin: NChIP. *Methods* **2003,** 31, 76-82.

165. Alexander, M.; Heppel, L.A.; Hurwitz, J., The purification and properties of micrococcal nuclease. *J. Biol. Chem.* **1961,** 236, 3014-3019.

166. Ohsaka, A.; Mukai, J.-I.; Laskowski, M., The use of purified micrococcal nuclease in identifying the nucleotide terminus bearing a free 5'-monophosphate. *J. Biol. Chem.* **1964,** 239, 3498-3504.

167. Lowary, P.T.; Widom, J., New DNA sequence rules for high affinity binding to histone octamer and sequence-directed nucleosome positioning. *J. Mol. Biol.* **1998,** 276, 19-42.

168. Thastrom, A.; Bingham, L.M.; Widom, J., Nucleosomal locations of dominant DNA sequence motifs for histone-DNA interactions and nucleosome positioning. *J. Mol. Biol.* **2004,** 338, 695-709.

169. Thastrom, A.; Lowary, P.T.; Widlund, H.R.; Cao, H.; Kubista, M.; Widom, J., Sequence motifs and free energies of selected natural and non-natural nucleosome positioning DNA sequences. *J. Mol. Biol.* **1999,** 288, 213-229.

170. Morgan, M.A.; Okamoto, K.; Kahn, J.D.; English, D.S., Single-molecule spectroscopic determination of lac repressor-DNA loop conformation. *Biophys. J.* **2005,** 89, 2588-2596.

171. Jortner, J.; Bixon, M.; Langenbacher, T.; Michel-Beyerle, M.E., Charge transfer and transport in DNA. *Proc. Natl. Acad. Sci.* **1998,** 95, 12759-12765.

172. Meggers, E.; Michel-Beyerle, M.E.; Giese, B., Sequence dependent long range hole transport in DNA. *J. Am. Chem. Soc.* **1998,** 120, 12950-12955.

173. Bixon, M.; Giese, B.; Wessely, S.; Langenbacher, T.; Michel-Beyerle, M.E.; Jortner, J., Long-range charge hopping in DNA. *Proc. Natl. Acad. Sci.* **1999,** 96, 11713-11716.

174. Bixon, M.; Jortner, J., Energetic control and kinetics of hole migration in DNA. *J. Phys. Chem. B* **2000,** 104, 3906-3913.

175. Giese, B., Electron transfer in DNA. *Curr. Opin. Chem. Biol.* **2002,** 6, 612-618.

176. Meggers, E.; Giese, B., Hole transport between G bases in DNA. *Nucleosides Nucleotides* **1999,** 18, 1317-1318.

177. Giese, B., Long distance charge transport in DNA: The hopping mechanism. *Acc. Chem. Res.* **2000,** 33, 631-636.

178. Liu, C.-S.; Hernandez, R.; Schuster, G.B., Mechanism for radical cation transport in duplex DNA oligonucleotides. *J. Am. Chem. Soc.* **2004,** 126, 2877-2884.

179. Ito, T.; Rokita, S.E., Reductive Electron Injection into Duplex DNA by Aromatic Amines. *J. Am. Chem. Soc.* **2004,** 126, 15552-15559.

180. Bard, A.J.; Faulkner, L., R., *Electrochemical Methods: Fundamentals and Applications*. John Wiley & Sons, Inc.: New York, 2001; p 856.

181. Amlaiky, N.; Leclerc, G.; Carpy, A., Unusual reaction of N-hydroxypthalimido ethers leading to oxygen-nitrogen heterocycles. *J. Org. Chem.* **1982,** 47, 517-523.

182. Nazarpack-Kandlousy, N.; Zweigenbaum, J.; Henion, J.; Eliseev, A.V., Synthesis and characterization of a mixture-based library of oxime ethers based on a common aromatic scaffold. *J. Comb. Chem.* **1999,** 1, 199-206.

183. Griggs, G.W., Selective breakage of DNA alongside 5-bromodoxyuridine nucleotide residues by high-temperature hydrolysis. *Nucleic Acids Res.* **1977,** 4, 969-987.

184. Cook, G.P.; Greenberg, M.M., A novel mechanism for the formation of direct strand beaks upon anaerobic photolysis of duplex DNA containing 5-bromodeoxyuridine. *J. Am. Chem. Soc.* **1996,** 118, 10025-10030.

185. Watanabe, T.; Bando, T.; Xu, Y.; Tashiro, R.; Sugiyama, H., Efficient generation of 2'-deoxyuridin-5-yl at 5'-(G/C)AAXUXU-3' (X = Br, I) sequences in duplex DNA under UV irradiation. *J. Am. Chem. Soc.* **2005,** 127, 44-45.

186. Bailly, V.; Verly, W.G., The multiple activities of Escherichia coli endonuclease IV and the extreme lability of 5'-terminal base-free deoxyribose 5-phosphates. *Biochem. J.* **1989,** 259, 761-768.

187. Ramotar, D., The apurinic–apyrimidinic endonuclease IV family of DNA repair enzymes. *Biochem. Cell Biol.* **1997,** 75, 327-336.

188. Pham, M.-C.; Oulahyane, M.; Mostefai, M.; Chehimi, M.M., Multiple internal reflection FT-IR spectroscopy (MIRFTIRS) study of the electrochemical synthesis and the redox process of poly(1,5-diaminonaphthalene). *Synth. Met.* **1998,** 93, 89-96.

189. Campbell, N., University of Maryland, College Park: College Park, Private Communications, 2007.

190. Abdel-Azzem, M., Electrooxidative oligomerization of 1,5-diaminonapthalene in acetonitrile medium. *J. Electroanal. Chem.* **1996,** 417, 163-173.

191. Abdel-Azzem, M.; Yousef, U.S.; Pierre, G., A cyclic voltammetric and coulometric study of a modified electrode prepared by electrooxidative polymerization of 1,5-diaminonapthalene in aqueous acidic medium. *Eur. Polym. J.* **1998,** 34, 819-826.

192. Pysh, E.S.; Yang, N.C., Polarographic oxidation potentials of aromatic compounds. *J. Am. Chem. Soc.* **1963,** 85, 2124-2130.

193. Turro, N.J., *Modern Molecular Photochemistry*. University Science Books: Sausalito, 1991; p 644.

194. Yousef, U.S.; Abdel-Azzem, M., A cyclic voltammetric and coulometric study of a modified electrode prepared by electrooxidative polymerization of nickel complex of 1,5-diaminonapthalene in acetonitrile. *Pol. J. Chem.* **1998,** 72, 2583-2596.